Terms and Conditions of Use of Digitised Theses from Trinity College Library Dublin

Copyright statement

All material supplied by Trinity College Library is protected by copyright (under the Copyright and Related Rights Act, 2000 as amended) and other relevant Intellectual Property Rights. By accessing and using a Digitised Thesis from Trinity College Library you acknowledge that all Intellectual Property Rights in any Works supplied are the sole and exclusive property of the copyright and/or other IPR holder. Specific copyright holders may not be explicitly identified. Use of materials from other sources within a thesis should not be construed as a claim over them.

A non-exclusive, non-transferable licence is hereby granted to those using or reproducing, in whole or in part, the material for valid purposes, providing the copyright owners are acknowledged using the normal conventions. Where specific permission to use material is required, this is identified and such permission must be sought from the copyright holder or agency cited.

Liability statement

By using a Digitised Thesis, I accept that Trinity College Dublin bears no legal responsibility for the accuracy, legality or comprehensiveness of materials contained within the thesis, and that Trinity College Dublin accepts no liability for indirect, consequential, or incidental, damages or losses arising from use of the thesis for whatever reason. Information located in a thesis may be subject to specific use constraints, details of which may not be explicitly described. It is the responsibility of potential and actual users to be aware of such constraints and to abide by them. By making use of material from a digitised thesis, you accept these copyright and disclaimer provisions. Where it is brought to the attention of Trinity College Library that there may be a breach of copyright or other restraint, it is the policy to withdraw or take down access to a thesis while the issue is being resolved.

Access Agreement

By using a Digitised Thesis from Trinity College Library you are bound by the following Terms & Conditions. Please read them carefully.

I have read and I understand the following statement: All material supplied via a Digitised Thesis from Trinity College Library is protected by copyright and other intellectual property rights, and duplication or sale of all or part of any of a thesis is not permitted, except that material may be duplicated by you for your research use or for educational purposes in electronic or print form providing the copyright owners are acknowledged using the normal conventions. You must obtain permission for any other use. Electronic or print copies may not be offered, whether for sale or otherwise to anyone. This copy has been supplied on the understanding that it is copyright material and that no quotation from the thesis may be published without proper acknowledgement.

Fiat Lux:

The Synthesis and Manipulation of Molecular Scaffolds for Photodynamic Therapy and Light-harvesting Arrays.

Submitted by

Luke Rogers

B.A. (Mod.) Medicinal Chemistry

Trinity College Dublin, Ireland

A thesis submitted to the University of Dublin, Trinity College for the degree of

Doctor of Philosophy

University of Dublin, Trinity College *December 2014*

Declaration

I declare that this thesis has not been submitted as an exercise for a degree at this or any other university and it is entirely my own work.

I agree to deposit this thesis in the University's open access institutional repository or allow the library to do so on my behalf, subject to Irish Copyright Legislation and Trinity College Library conditions of use and acknowledgement.

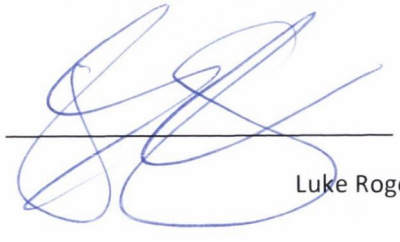

Luke Rogers

Summary

Molecular scaffolds are an emerging paradigm that offers chemists the use of preformed chemical structures that can be manipulated structurally and synthetically for use in a plethora of applications. The goal of the research discussed herein was to develop new methodologies for the synthesis and manipulation of either new or preformed molecular scaffolds for PDT and light-harvesting technologies. It was hoped to implement techniques and synthetic strategies previously developed in house in the Senge lab, in concert with the development of new pathways for the installation of biologically and photophysically interesting molecules.

To investigate these new pathways and methodologies the project was divided into two disparate sections:

- The use of a preformed photosensitizer scaffold in functionalization reactions as a demonstrative example of simple porphyrin desymmetrization, with subsequent evaluation of synthesized porphyrins in photodynamic therapy studies.
- The use of molecular scaffolds for the synthesis of larger, more complex systems, i.e. for the construction of complex multi-porphyrin arrays.

By controlling the number of equivalents, one can functionalize the periphery of *m*-THPP and *m*-THPC, two known photosensitizers in a controlled manner and obtain monofunctionalized porphyrin and chlorin derivatives in high yields and few synthetic steps. This methodology can be used to install practical synthetic handles that allow for the introduction of biologically pertinent groups. As such a library of porphyrin bile acid adducts was synthesized through the copper(I) catalyzed click reaction using a preinstalled propargyl group present on the photosensitizer scaffold. This library of highly soluble PS were readily up taken and accumulated within the cytoplasm of the cell. Unfortunately, they did not exhibit any photocytotoxicity which has been attributed to the presence of the triazole ring.

This methodology was then applied to a library of suitable benzyl coupling partners. A library of monosubstituted m-THPP derivatives was successfully prepared through a number of simple reactions pathways. By using historic phenolic chemistry, compounds were synthesized through nucleophilic substitution, esterification, and OH activation reactions. This chemistry was updated for porphyrins by using the recently discovered Chan–Lam copper-catalyzed coupling of a heteroatom with a boronic acid. This allowed for the synthesis of some simple, unsymmetrical porphyrin systems.

In an effort to improve post-treatment tumor regrowth due to the upregulation of proinflammatory molecules in the tumor microenvironment, a series of non-steroidal anti-inflammatories were conjugated to the Temoporfin scaffold through a modified Steglich reaction. By monitoring the reaction equivalents and time, it is possible to control the degree of

substitution and thus produce mono- to tetrafunctionalized "iChlorins" in reasonable yields and few synthetic steps. All conjugates successfully entered into the cells and whilst no cytotoxicity was observed, due to positive results observed in $^1O_2$ production assays, it is believed that longer irradiation times may be able to improve the cytotoxicity of the conjugates and therefore the efficacy of the treatment.

Finally, to investigate the use of molecular scaffolds as synthetic building blocks for the construction of light-harvesting arrays, triptycene was selected as a readily available rigid scaffold that is susceptible to further functionalization. A library of hexasubstituted triptycene building blocks were synthesized through the use of transition metal catalyzed cross coupling reactions i.e., Suzuki and Sonogashira couplings. All building blocks contained distal functional groups that allow for further functionalization reactions to occur. These highly substituted derivatives may be implemented as synthetic scaffolds in future reactions for applications such as metal-organic frameworks, light-harvesting arrays and drug-delivery vehicle.

Finally, a plethora of coupling conditions and pathways were attempted for the synthesis of a hexaporphyrin array. These involved both cross coupling reactions and also more historic esterification and nucleophilic substitution chemistry. Whilst there were some positive spectroscopic results throughout the project, to this date we have not been able to purify and isolate the array and subject it to photophysical measurements.

Publications

Rogers, L.; Majer, F.; Sergeeva, N. N.; Paszko, E.; Gilmer, J. F.; Senge, M. O. "Synthesis and biological evaluation of Foscan® bile acid conjugates to target esophageal cancer cells" *Bioorg. Med. Chem. Let.* **2013**, *23*, 2495-2499.

Reddy, M. H. V.; Al-Shammari, R. M.; Al-Attar, N.; Rogers, L.; Lopez, S.; Forster, R. J.; Senge, M. O.; Keyes, T. E.; Rice, "Fractal structures in n-phenyl-porphyrin J-aggregate films" *J. H. Mater. Chem. Phys.* **2014**, *143,* 963-968.

Harsha V. R., M.; Al-Shammari, R. M.; Al-Attar, N.; Kennedy, E.; Rogers, L.; Lopez, S.; Senge, M. O.; Keyes, T. E.; Rice, J. H. "Micro- or nanorod and nanosphere structures derived from a series of phenyl-porphyrins" *Phys. Chem. Chem. Phys.* **2014**, *16*, 4386-4393.

Rogers, L.; Burke-Murphy, E.; Senge, M. O. "Simple Porphyrin Desymmetrization: 5,10,15,20-Tetrakis(3-hydroxyphenyl)porphyrin (*m*THPP) as a Gateway Molecule for Peripheral Functionalization" *Eur. J. Org. Chem.* **2014**, 4283-4294.

Rogers, L.; Senge, M. O. "The Translocator Protein (TSPO, 18kDa) as a Potential Molecular Target for Improved Treatment Efficacy in Photodynamic Therapy" *Future Med. Chem.* **2014**, *6*, 775-792.

Rogers, L.; Moylan, C.; Davis, M.; Eckhardt, H. G.; Ryan, A. A.; Shaker, Y. M.; Senge, M. O. "Hexasubstituted triptycene synthons as molecular scaffold building blocks" *Submitted J. Org. Chem.* ***2014.***

Rogers, L; Senge, M. O. "Lead Structures for Applications in Photodynamic Therapy. 6. **iChlorins**: Temoporfin anti-inflammatory conjugates to target the esophageal tumor microenvironment for *in vitro* PDT" *Submitted PLOS ONE* ***2014.***

Conference Abstracts

Plunkett, S.; Rogers, L.; Moylan, C.; Senge, M. O. Synthesis of ABCD Porphyrins" in *Porphyrins and Porphyrias (Tetrapyrrole Discussion Group meeting)* Cardiff, Wales, 10-14 April **2011.**

Rogers, L.; Ryan, A.; Senge, M. O. "Synthetic strategies for unsymmetrical porphyrins and porphyrin arrays for QSAR studies in photodynamic therapy" *14th Congress of the European Society for Photobiology.*, Geneva, Switzerland, 01st – 06th September **2011**.

Rogers, L.; Ryan, A.; Senge, M. O. "Synthetic strategies for unsymmetrical porphyrins and porphyrin arrays for QSAR studies in photodynamic therapy" *TCD Medical School Tercentenary Symposium.* TBSI, Trinity College Dublin, Dublin, Ireland. 04th November **2011**.

Rogers, L.; Majer, F.; Gilmer, J.; Senge, M. O. "Synthesis of Porphyrin Bile acid Conjugates for use in Photodynamic Therapy" *CSCB, Conference on Recent Advances in Synthesis and Chemical Biology, UCD,* Dublin, Ireland 9th December **2011**.

Rogers, L.; Majer, F.; Gilmer, J.; Sergeeva, N. N.; Paszko, E.; Senge, M. O. "Synthesis of Porphyrin Conjugates for use in Photodynamic Therapy" *7th International Conference on Porphyrins and Phthalocyanines,* Jeju Island, S. Korea, 1-7 July **2012**.

Vaz, G.; Rogers, L.; Senge, M. O. "Research and Development of New Photosensitizers: A High Content Approach" *7th International Conference on Porphyrins and Phthalocyanines,* Jeju Island, S. Korea, 1-7 July **2012**.

Rogers, L.; Majer, F.; Gilmer, J.; Sergeeva, N. N.; Paszko, E.; Senge, M. O. "Synthesis of Temoporfin Conjugates for use in Photodynamic Therapy" *15th Institute of Molecular Medicine Conference,* IMM, St. James' Hospital, Dublin, Ireland, 9th November **2012**.

Haughey, A.; Rogers, Majer, F.; Gilmer, J.; Sergeeva, N. N.; Paszko, E.; Senge, M. O. "Synthesis of Porphyrin Conjugates for use in Photodynamic Therapy" *16th Institute of Molecular Medicine Conference,* IMM, St. James' Hospital, Dublin, Ireland, 8th November **2013**.

Acknowledgements

First and foremost, I would like to thank Prof. Mathias Senge for giving me the opportunity to work within his research group. For the guidance, encouragement and support which he has provided over the past four years. Also, thanks to Science Foundation Ireland for providing their financial support for this research.

I would like to extend my gratitude to all past members of the Senge group, in particular Dr. Mia Davis, Tech Support (Dr. Stuart Mac Gowan) and all the visiting students under my supervision who helped in the development of these projects. To all the current members of the group, especially Dr. Aoife Ryan, Claire Moylan and Shane Plunkett for making the PhD experience fun, enjoyable and bearable. Thank you to Dr. Natalia Sergeeva, Dr. Gisela Vaz and Dr. Edyta Paszko for conducting the biological evaluations and enduring my unrelenting optimism that every batch of compounds would finally be the ones to work.

To Dr. Aoife Ryan and Shane Plunkett for the coffee breaks, nights out, proof reading and Monday morning analysis of the weekend's sport. Thanks to Dr. Ferenc Majer, under the supervision of Prof. John Gilmer, TCD for his work on the bile acids used for the conjugates work and Claire Moylan for her work and brainstorming sessions on the triptycene project.

To all the technical and administrative staff in the chemistry department, particularly to Dr. John O'Brien and Dr. Manuel Reuther for the countless NMR analysis and to Dr. Martin Feeney and Dr. Gary Hessman for HRMS measurements.

Finally, I would like to thank my family and friends. To my family, for their unwavering support and love throughout the four years, I am eternally in their debt. To my housemates, past and present, thank you for your time, patience and numerous warm meals after late nights in the lab/office. To Daithi, for your emotional support even though you deserted me for Canada, to Djemba Djemba, for always playing the devils advocate and keeping me on my toes. Proinsios, for funding my PhD through the money I won off you in our golf games and Ronan, for your world famous pasta dish. My extreme gratitude must also go to Shaun for the countless games of golf that took my mind of the PhD when things weren't going too well.

Finally, to Rachael, my girlfriend, my Pooh, thank you for your encouragement, love and understanding. You have been there for me all the way, through the highs and lows, you have helped me with everything. You are the push I need when things were tough and the extra bonus when things were going well, for that, thank you.

Table of Contents

Abbreviations

acac	acetylacetonate
AcOH	glacial acetic acid
BChl	bacteriochlorophyll
Bu	butyl
calcd	calculated
COSY	correlation spectroscopy
d	doublet
DABCO	1,4-diazabicyclo[1]octane
dba	dibenzylideneacetone
dd	double doublet
DCE	1,2-dichloroethane
DDQ	2,3-dichloro-5,6-dicyanobenzoquinone
DME	dimethoxyethane
DMF	*N,N*'-dimethylformamide
DPM	dipyrromethane
EAS	electrophilic aromatic substitution
equiv	equivalents
ESI	electrospray ionisation
GM	Goeppert Mayer
Hex	hexyl
HOMO	highest occupied molecular orbital
HpD	haematoporphyrin derivative
HRMS	high resolution mass spectrometry
IR	infrared
LH2	light harvesting complex II
LUMO	lowest unoccupied molecular orbital
m	multiplet
mp	melting point
MALDI	matrix assisted laser desorption ionisation
Me	methyl
MeOH	methanol
MW	microwave
m/z	mass-to-charge ratio
NBS	*N*-bromosuccinimide

NIR	near infrared
NLO	non-linear optics
NMR	nuclear magnetic resonance
NOESY	nuclear overhauer effect spectroscopy
OAc	acetate
OELD	organic electroluminescent device
OEP	2,3,7,8,12,17,18-octaethylporphyrin
OLED	organic light emitting diode
OTf	triflate
PFO	polyfluorene
PhLi	phenyllithium
PhOLED	phosphorescent organic light emitting diode
PIFA	phenyliodine(bis-trifluoroacetate)
PPh_3	triphenylphosphine
ppm	parts per million
PVK	poly(N-vinylvarbazole)
q	quartet
RC	reaction centre
R_f	retention factor
rt	room temperature
s	singlet
t	triplet
TEA	triethylamine
TFA	trifluoroacetic acid
THF	tetrahydrofuran
TLC	thin layer chromatography
TOCSY	total correlation spectroscopy
tol	tolyl
2PA	two-photon absorption
TPP	5,10,15,20-tetraphenylporphyrin
UV	ultraviolet
vis	visible
v/v	volume to volume

Chapter 1:

Introduction

1.1 Introduction

1.1.1 Scaffolds in Chemistry

Historically, within the field of chemistry, the expression scaffold has been employed as a term describing the core structure of a molecule; with the textbook definition of a molecular scaffold especially within the field of drug design describing them as "a fixed part of a molecule upon which functional groups may be attached or substituted" [2]. However, in recent times, chemists have pushed the boundaries of this term to include the use of natural or synthetic organic molecules as scaffolds to complement the construction of larger chemical frameworks (Figure 1.1) [3]. Whilst the differences between the uses of the term for both instances are subtle, the two are in no means mutually exclusive, with many organic scaffolds, e.g., tetrapyrroles, being used as scaffolds in the construction of nanomaterials or three-dimensional constructs, e.g., porphyrin arrays [4-6].

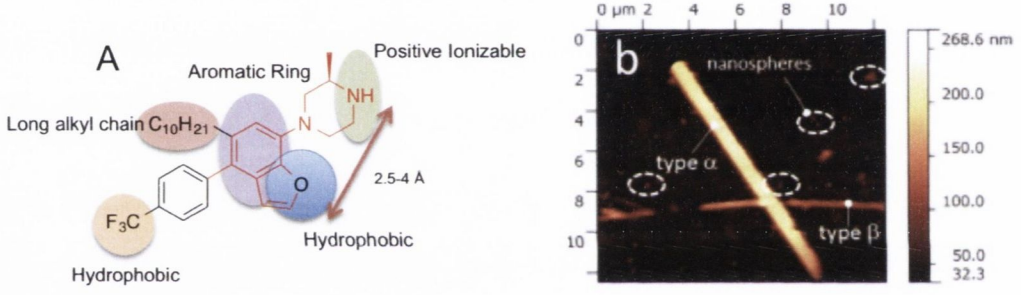

Figure 1.1. Demonstrative examples of chemical scaffolds. A) A hypothetical pharmacophore required for activity. B) Polymerized *n*-phenylporphyrins for the construction of nanorods [7,8].

1.1.1.1 Applications

Chemical scaffolds occur in all fields of chemistry, however, they are of fundamental importance in the field of drug design. Typically a medicinal chemist will find a lead molecule for the ailment that they are investigating by using experimental data from *in vitro* or *ab initio* studies and they will then put forward a core chemical scaffold, i.e., a pharmacophore needed for activity (Figure 1.2) [9-11]. This lead compound represents a scaffold, upon which modifications and fine-tunings of its properties can be made as to enhance its biological proficiency. From here a library of derivatives will be synthesized and tested for their biological activity.

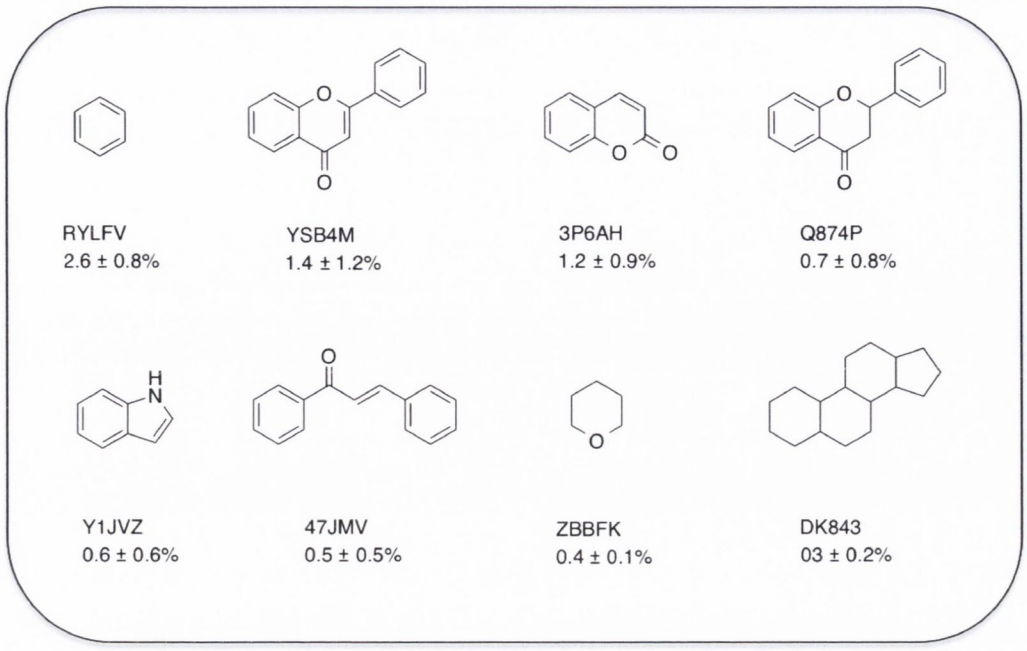

Figure 1.2. Most common scaffolds in all natural products databases in the public domain[1] [2].

Conversely, since their discovery and subsequent implementation into planned syntheses, molecular scaffolds have become of fundamental importance in the construction of model systems for biological and photophysical studies. Porphyrin and triptycene embody these attributes of rigidity and variability as they allow chemists to build large supermolecular systems around them, whilst utilizing their innate chemical properties, e.g. the synthesis of triptycene-helicane conjugates for the investigation into synthetic molecular machinery [12,13]. Whilst there are extensive examples of both uses of scaffolds in the literature for a myriad of applications, for the purpose of this research, it was deemed appropriate to focus on one particular medicinal application, i.e., photodynamic therapy (PDT), where the use of a scaffold or pharmacophore could prove instrumental; and examples of a molecular scaffold used for the synthesis of larger, more complex systems, i.e., the use of triptycene and porphyrin as scaffolds to aid the construction of complex multi-porphyrin arrays for use as light-harvesting antennae systems (Figure 1.3).

[1] Scaffolds shown are present in at least four natural products databases with an average frequency of at least 0.3%.

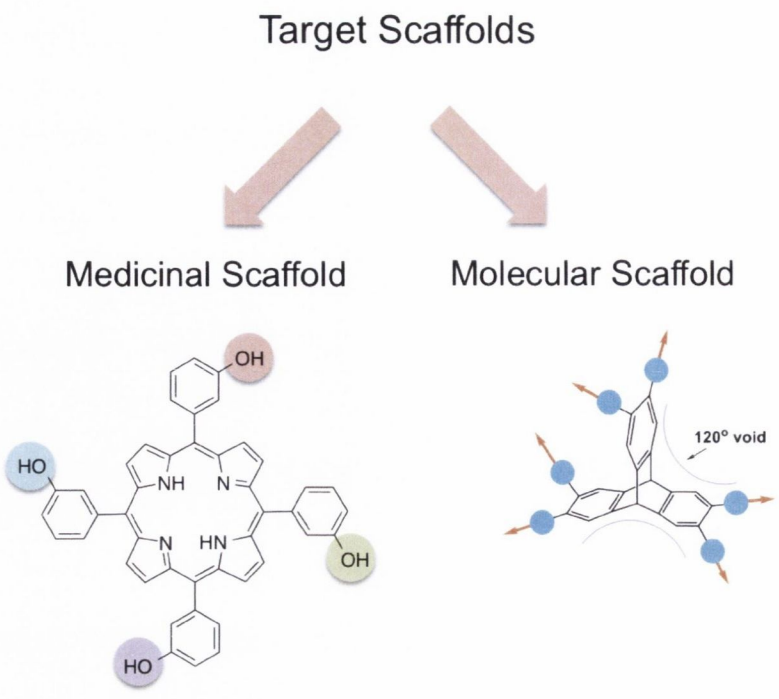

Figure 1.3. Compounds chosen for investigation into their potential as medicinal and structural scaffolds.

1.2 Medicinal Scaffolds- Porphyrins & PDT

1.2.1 Porphyrin based Pharmacophores for PDT

Porphyrins are a ubiquitous class of compound found in nature that are of critical importance to a large array of fundamental biological processes. Their applications are limited only by the imagination, summed up best by the recently published 35 volume 'Handbook of Porphyrin science', a body of work that encompasses academic advances across all disciplines in the field of porphyrin science. From light-harvesting arrays to molecular sensors and porphyrins in catalysis to non-linear optics, porphyrins have truly been implemented in a plethora of applications. However, their medicinal applications have intrigued academics for millennia, from their use in photomedicine by the ancient Egyptians to a group of diseases that gave root to vampire lore [14].

The major mainstream success of porphyrins as medicinal scaffolds has come in the field of photodynamic therapy, a relatively new treatment modality for a range of cancers and sufferers of Acne vulgaris. One of the main reasons contributing to this success is the versatility offered to researchers by the tetrapyrrole scaffold. There are three chemically distinct regions that have varying degrees of reactivity and thus, varying ability to undergo specific types of reactions (Figure 1.4). Accordingly, researchers can implement this discrepancy in reactivity to impart selectivity in their functionalization of the porphyrin scaffold and therefore generate large libraries of diverse tetrapyrroles to be screened for their potential as photosensitizers.

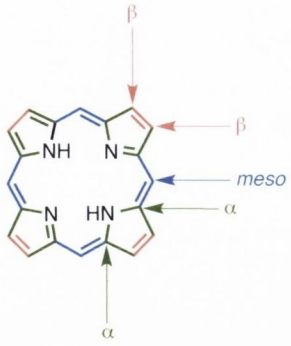

Figure 1.4. Diagrammatic representation of the different chemical regions present in the tetrapyrrole scaffold.

1.2.2 Esophageal Cancer

Esophageal cancer is a potent form of cancer with five-year survival rates as low as 17 % [15]. This is due to the fact that patients typically present with symptoms at quite a late stage of the disease, as there is currently no diagnostic marker and treatment is usually restricted to surgical or chemotherapeutic palliative care. Recently, gastro-esophageal reflux disease (GERD) has been shown to be concomitant with the development of Barrett's metaplasia and associated molecular markers of inflammation, which have been shown to support transformation, initiation and progression of tumor development [16,17]. However, there is no guarantee that a patient suffering from GERD will progress to Barrett's metaplasia and likewise, a patient presenting with Barrett's may never progress to the extremely fatal adenocarcinoma. This inability to predict disease progression has hampered research into esophageal cancer treatments and it is truly imperative that research into the mechanisms of the disease state continues.

1.2.2.1 Current Treatments Available to Patients

Current treatment modalities for esophageal cancer mainly revolve around surgical and chemotherapeutic options, which both have significant drawbacks. Whilst surgery allows for the complete removal of the tumor from the patient, it is invasive, expensive and limited by the type of patient capable of undergoing a surgical procedure. Similarly, chemotherapy or radiation therapy can induce a deregulation in the immune system of the patient, leaving them potentially immunocompromised and therefore susceptible to various immune disorders [18].

1.2.3 Photodynamic Therapy

1.2.3.1 An Introduction to PDT

Whilst wide scale acceptance of PDT has been slow, it continues to gain traction by practitioners due to the many positives associated with this type of treatment and positive case studies conducted [19]. With respect to clinical implementation, it is difficult for practitioners to ignore PDT as the treatment offers a relatively simplistic methodology. It is a three-component treatment modality involving a photosensitizer (drug), light of an appropriate wavelength and tissue oxygen. The photosensitizer is administered to the site of treatment; the PS is allowed a specified time-period to allow for maximum accumulation in the target tissue, and subsequent irradiation of the region with light produces a photodynamic effect (Figure 1.6). Thus, it is an outpatient, non-invasive procedure that is cost-effective in comparison to other methodologies and contains minimal side effects.

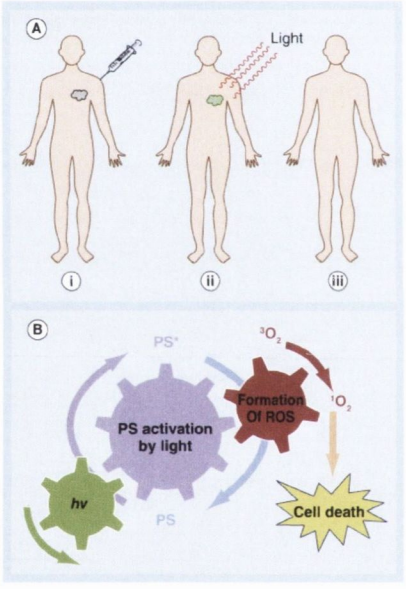

Figure 1.6. Photodynamic therapy treatment. (A) (i) PS is injected into the body; (ii) the PS is allowed accumulate at the tumor site before irradiation with light, and (iii) selective destruction of tumor. (B) Chemically this method is based on the formation of singlet oxygen and other ROS.

1.2.3.2 Timeline of PDT Development

Despite the therapeutic properties of light having been known for thousands of years, i.e., the ancient Egyptians, Indians and Chinese used light to treat a variety of diseases, it was not until the 1900s that researchers observed that a combination of light and certain chemicals could induce cell death [20]. Later experiments that tested different combinations of reagents and light led to the development of what one now calls Photodynamic Therapy (PDT). However, it was not until the 1960s that Lipson *et al.* initiated the modern era of PDT in the Mayo clinic [21,22] using a 'haematoporphyrin derivative' (HPD) developed by Samuel Schwartz (Figure 1.7) [23]. This HPD was prepared by treating haematoporphyrin with acetic and sulfuric acids,

filtering and then neutralizing the product with sodium acetate. Lipson and Baldes were successful in demonstrating this compound's ability to localize in tumors and emit fluorescence. They were also able to administer significantly smaller therapeutic doses of HPD in comparison to haematoporphyrin and therefore this HPD held promise as a diagnostic tool [24].

The next major development came in 1972 when Diamond and colleagues hypothesized that the combination of the tumor-localizing and tumor-phototoxic properties of porphyrins might be exploited to kill cancer cells [25]. The *in vivo* results from the subsequent studies showed that PDT delayed the growth of rat-implanted gliomas with tumor growth suppressed for 10-20 days. Unfortunately, viable areas from deeper regions of the tumor began re-growing, which showed one of the immediate drawbacks of PDT, i.e., the treatment was limited by the depth of light penetration. Dougherty *et al.* provided a significant breakthrough in PDT efficacy when they reported the complete eradication of mammary tumor growth in mice using HPD and red light in 1975 [26]. This discovery came in the same year Kelly and co-workers achieved similar tumor eradication using HPD and light activation in mice with bladder carcinoma [27].

Both these positive results paved the way for the first clinical trial to be initiated with HPD as the photosensitizer and conducted on patients suffering from bladder cancer [28]. Subsequent patient trials conducted by a variety of different researchers for a range of tumors followed and their success allowed for the regulatory approval of HPD for patients with breast [29-31], gynaecological tumors [32-34], intraocular tumors [35-37], brain tumors [38,39], head and neck tumors [40,41], colorectal cancer [42], cutaneous malignancies, [43,44] pancreatic cancer, [45] who had early-stage cancers that were inoperable, due to other complications.

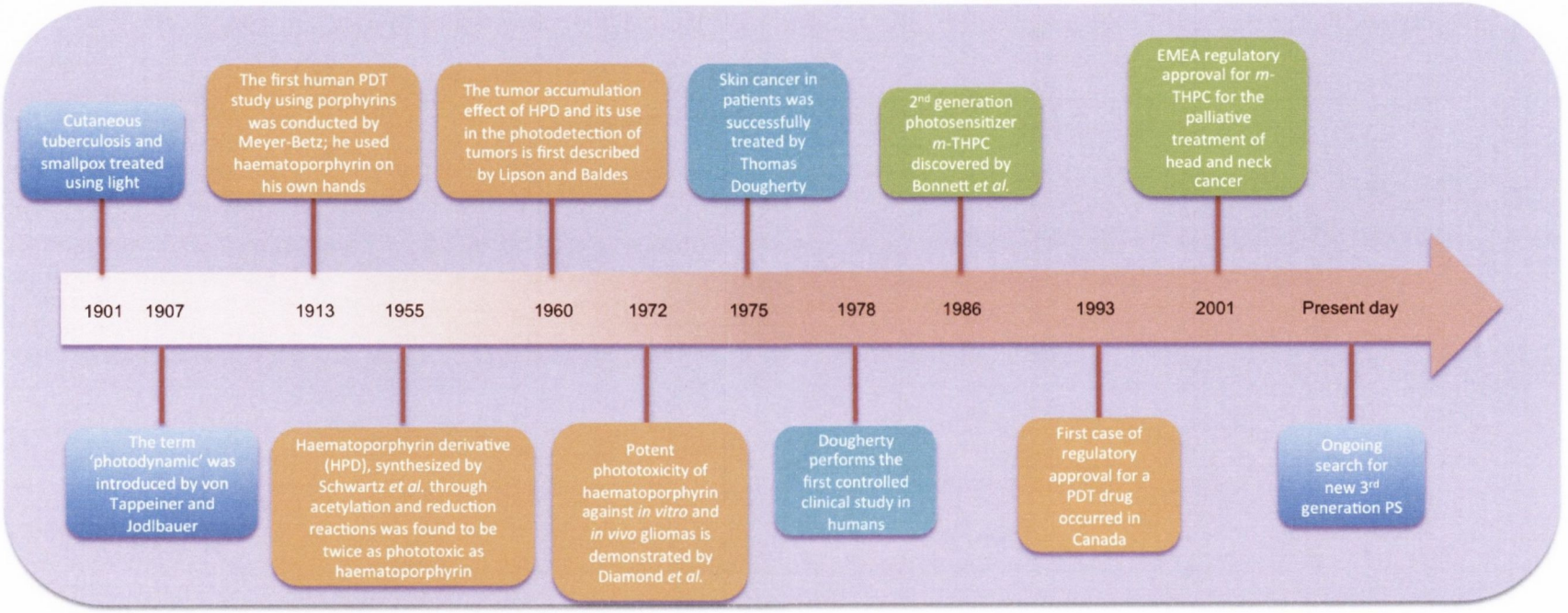

Figure 1.7. Timeline of key events in the progression of medicinal PDT, (Modified from [46]).

1.2.3.3 Mechanism of PS Uptake & Localization

The first logical parameter to consider when investigating the mechanisms at work during a course of PDT treatment would be the 'selective' uptake and localization of the photosensitizer in the tumors. Certain characteristics of hyperproliferative tissues, e.g., tumors, aid the accumulation of the photosensitizer within them [47-51]. Examples of these properties are: the high-incidence of LDL-receptors in the cell membranes, the low pH level of the interstitial fluid caused by the increased rate of glycolysis and the decreased supply of $^3O_2$ to the tissue. Additionally, the capillaries present in cancerous tumors are uncharacteristically permeable which facilitates the transition of the photosensitizer from the blood into the large interstitial space of the tumor [52].

These factors account for the preferential accumulation of photosensitizers in cancerous cells, however, it does not fully explain why the photosensitizer is retained by such an extent in the tumor. Porphyrin accumulation in tumors can largely be attributed to poor lymphatic drainage, due to the underdevelopment of the lymphatic system or lymphatic obstruction [49]. As photosensitizers bind to serum proteins, mechanisms such as enhanced tumor vasculature permeability and hypervascularity, which are the main reasons for the accumulation of proteins and macromolecules in tumors, may have a profound effect on the preferential localization of these photosensitizers.

Research conducted by Henderson *et al.* and Pandey *et al.* has demonstrated a strong correlation between PS uptake and hydrophobicity using a series of alkyl ether derivatives of pyropheophorbide a (a chlorophyll-a derivative) [53,54]. They both found that the most hydrophobic dodecyl ether derivative accumulated mainly in the tumor compared with photosensitizers with high partition coefficient values, which induced sensitizer insolubility and thus prevents PS circulation. These results correlated with data obtained previously by Moan *et al.* with a series of diether hematoporphyrin derivatives which saw the retention of the PSs in cells increase as polarity decreased [55].

Tumor cells maintain high levels of aerobic glycolysis to meet their energy needs [56]. This occurrence results in the elevated production of lactic acid and therefore a lower pH for the interstitial fluid of malignant tissue [57]. Thomas and Girotti provided the first evidence for a theory by Moan *et al.*, i.e., that the decreased pH of malignant cells might result in a high retention of porphyrins [58]. Their experiments demonstrated that glucose administration prior to PDT treatment resulted in a decrease in tumor pH and consequently greater accumulation of HpD in tumor cells and increased efficacy of the treatment. Similar results have subsequently been reported for the second-generation PS *m*-THPC by Moan and Ma [59].

1.2.3.4 PDT Induced Effects in Tumors

With a clearer understanding of why the PS is retained preferentially in the tumor tissue, it is now necessary to discuss the effect a course of PDT treatment has on the targeted tumor. It is now understood after thirty years of research that PDT can mediate tumor destruction through three distinct mechanisms. These are as follows:

- Photodamage
- Vascular Damage
- Immune Response

The first mechanism involves direct tumor killing through the ROS (reactive oxygen species) generated during PDT. Photodamage caused by PDT has been shown to reduce clongenic tumor cells *in vivo* [[60]]. Unfortunately, complete tumor eradication is not always achieved through this pathway alone for a number of reasons, one of which being the non-homogenous distribution of the photosensitizer throughout the tumor. It would also appear that the distance of tumor cells from the vascular supply could significantly reduce PDT efficacy. PS accumulation and tumor killing was shown by Korbelik *et al.* to be directly affected by the distance of tumor cells to the vascular supply [61].

Similar to distance to tumor vasculature, availability of oxygen within the target tissue can directly limit the efficacy of a course of PDT treatment. This shortage of oxygen can arise from the photochemical consumption of oxygen during the PDT process or from the proximate effects of PDT on the tumor vasculature. To overcome this problem, researchers discovered that one can lower the fluence rate as to reduce the oxygen consumption rate or one can fractionate the delivery of PDT light which allows for the re-oxygenation of the tissue [62,63].

In the last 20 years, research has shown that PDT treatment can cause microvascular collapse [64-66], leading to severe tissue hypoxia and anoxia [[67,68]]. This was an important discovery as the viability of tumor cells is also dependent on the quantity of nutrients supplied to them by the blood vessels and subsequently, the formation and maintenance of blood vessels is dependent on growth factors produced by the tumor or host cell [69,70]. Thus, direct targeting of the tumor vasculature has become quite a promising approach and as been implemented as early as 1989, when Henderson *et al.,* demonstrated that one could induce vascular shutdown and therefore limit the oxygen supply to the tumor by using Photofrin-based PDT in a fibrosarcoma mouse model [71]. Other studies using a range of photosensitizers also showed vascular constriction, thrombus formation and inhibition of tumor growth.

Interestingly, in these studies there was also an apparent increase in expression of two potent angiogenic factors, vascular endothelial growth factor (VEGF) and cyclooxygenase (COX)-2, during PDT [72]. Researchers attributed this upregulation to the ROS formation and subsequent PDT-induced hypoxia. Whilst these results indicate a promising pathway toward tumor

eradication through vascular damage, further studies are needed to truly determine the long-term effects of PDT on tumor vasculature.

The inflammatory process has been shown to be mediated by factors such as cytokines, growth factors, proteinases, peroxidases and other immunoregulators [73]. As such, it was believed that these immunoresponses might play a role in the efficacy of PDT, as the differences in the intensity and nature of the inflammatory reaction between cancerous and normal tissue could contribute to the selectivity of PDT-induced tissue damage. Studies conducted in the late 1980s reported infiltration of lymphocytes, leukocytes and macrophages in PDT-treated tissue. The presence of these molecules indicates the activation of the immune response during PDT treatment [47,74].

Korbelik *et al.* discovered that short-term tumor growth responses to Photofrin PDT were similar in normal Balb/C and immunodeficient mice, whilst long-term effects appeared to be quite different. Their results showed that tumor reoccurrence transpired more frequently in mice which had been previously immunocompromised. Interestingly, this effect could be reversed by bone-marrow transplant from immunocompetent Balb/C donors. These results indicated that inflammation in the tumor micro-environment played a pivotal role in the complete eradication of the tumor and that whilst the direct effects of PDT can destroy the majority of the tumor, the immune response is necessary to eliminate any surviving cells [75].

Conversely, numerous reports by Gomer *et al.* have found that a course of PDT can cause an upregulation in a number of pro-inflammatory molecular markers within the tumor microenvironment, and that this upregulation can give rise to tumor regrowth (Figure 1.8)[75]. This undesirable regrowth will have an obvious impact on the efficacy of the treatment and therefore a considerable amount of work is still needed to be completed to help understand the exact immunological response during and after a course of PDT and whether it is facilitating tumor eradication or regrowth.

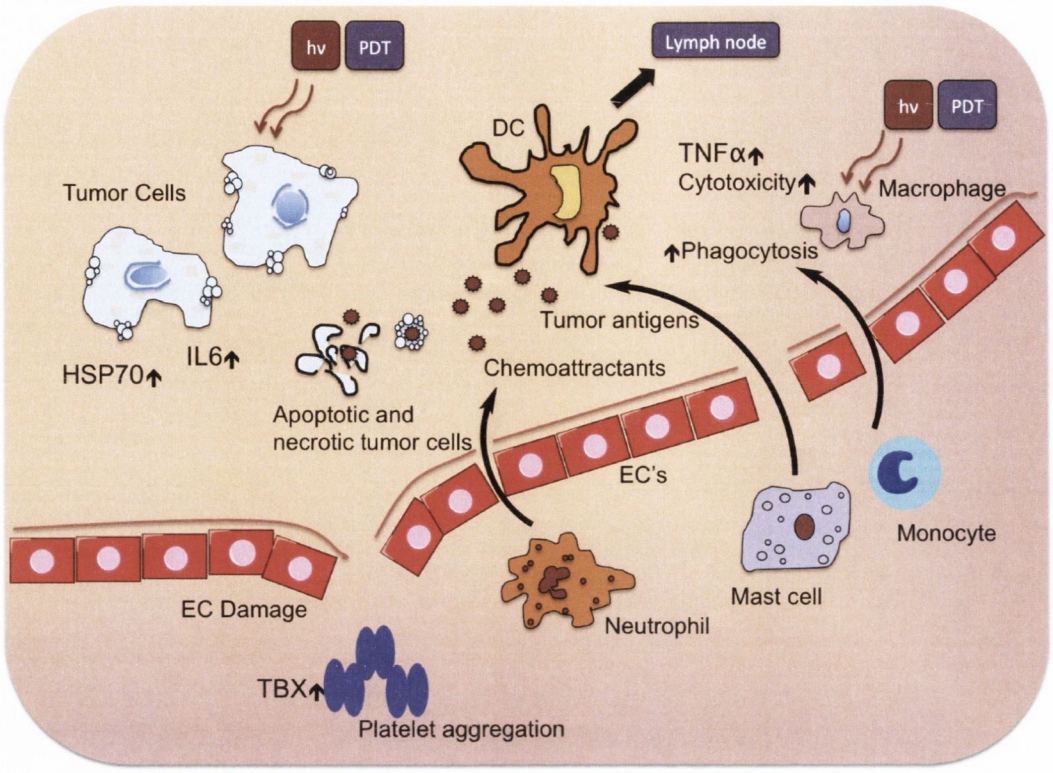

Figure 1.8. PDT-induced inflammation, DC = dendritic cell, EC = endothelial cell (Modified from [76])

Whilst these three mechanisms act through distinct pathways, they can hold influence over each other and the relative importance of each for the overall efficacy of the treatment is still not fully understood. However, it is evident that the combination of all three mechanisms is essential for long-term tumor control.

1.2.3.5 Mechanisms of Cell Death in PDT

The exact mechanism of cell death that these aforementioned pathways induce is far from fully understood. PDT can induce cell death through a number of different signaling pathways and the mode and extent of cell death achieved is governed by a number of different factors, e.g., subcellular localization and concentration of the PS, intensity of the light and the concentration of oxygen in the afflicted tissue [47],[77,78]. The main modes of cell death for PDT are necrosis and apoptosis. These two distinct pathways of cell death were first supported by research conducted by Kerr *et al.* [79]. The first and most common pathway with respect to PDT is apoptosis. Apoptosis is typically characterized by blebbing of the plasma membrane and cell shrinkage and is a form of programmed cell death. It occurs under 'immunological control', i.e. inflammation is prevented through the scavenging of apoptotic cells/fragments by phagocytes (Figure 1.9). An extensive body of literature has been assembled that examines the pathways induced after PDT in tumor cells *in vitro*, e.g. mitochondrial events [80], signaling pathways [81,82] and mediators of apoptosis [83]. *In vivo* PDT induced apoptosis has also been shown to

occur [84,85], however no studies as of yet have been conducted on the investigation of *in vivo* clearance mechanisms of apoptotic cells in tumors after PDT.

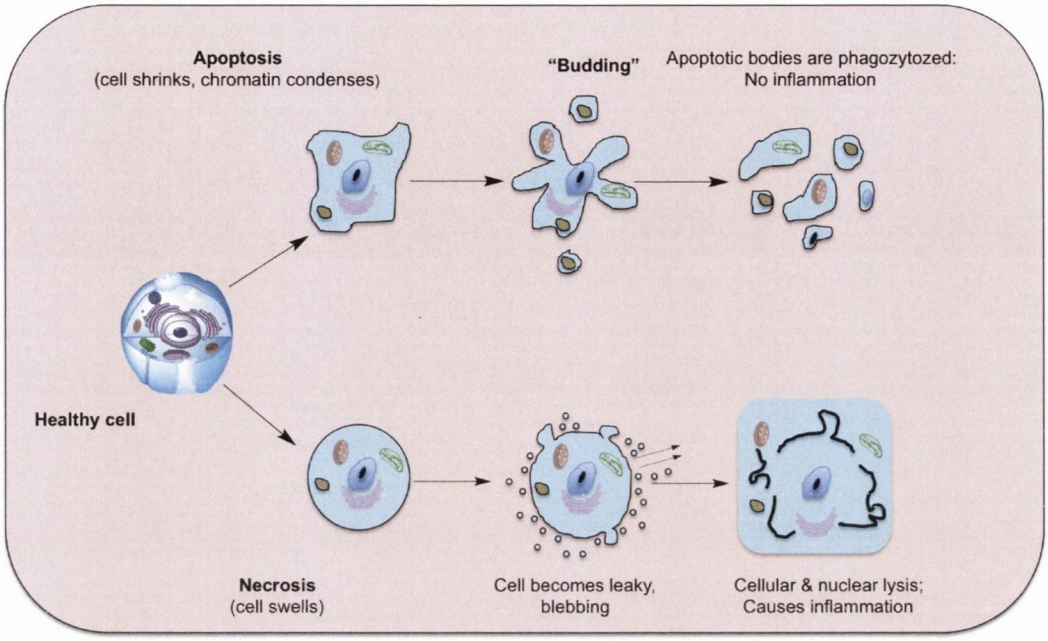

Figure 1.9. Simplified explanation of the apoptotic and necrotic pathways during PDT-induced cell death.

The other form of cell death occurs through a process called necrosis. This process is less ordered than apoptosis as it results from chemical or physical damage to the cell by external stimuli, e.g. PDT. It can be characterized by cytoplasm swelling, destruction of organelles with the eventual release of intracellular contents and inflammation. This cytoplasm swelling causes the eventual spilling of the cytosolic constituents into the extracellular space through the damaged plasma membrane. This sequence of events provokes a robust inflammatory response, and researchers believe that this acute inflammation caused by this PDT-induced necrotic pathway may potentiate immunity by attracting host leukocytes into the tumor and therefore increase antigen presentation.

In more recent times, it has become apparent that these pathways are just a small fraction of the different events that can lead to cell death, with programmed necrosis, mitotic and autophagic cell death to name just a few others [86-88]. Research has demonstrated that there are a number of critical factors when determining the type of cell death, e.g., the localization of the PS, the light dose applied and the cell type. Thus, it has become of critical importance to identify the mechanism of cell death, as from this knowledge one can better understand the biochemical processes at play and better influence them through chemical or physical modification of the treatment parameters.

As such, there has been an increase in interest into the mechanisms of cell death during PDT by researchers in the field. These investigators have studied the frequency of apoptosis and

necrosis, both *in vitro* and *in vivo* and it was discovered that in general, lower dose PDT leads to more apoptosis, whilst higher dose will proportionately lead to more necrosis [89]. A common molecular marker of the apoptotic pathway initiated by a course of PDT treatment is the rapid release of mitochondrial cytochrome *c* into the cytosol with subsequent activation of the apoptosome and procaspase 3. Thus, by measuring the levels of these markers after a course of PDT, researchers where able to differentiate between the two pathways [90].

1.2.3.6 Main Components for PDT

PDT is a three-component treatment modality. These components are:

- Photosensitizer
- Light of an appropriate wavelength
- $^1O_2$

Of these three components, the photosensitizer and light treatment are typically the key parameters in defining the efficacy of a course of PDT treatment. As such, following the very first clinical approval of a photosensitizer for PDT, a race began between researchers to find a second-generation photosensitizer with improved localization and efficiency. Whilst the search is still ongoing to find the ideal photosensitizer, this subsequent research marked the emergence of a number of desirable traits for photosensitizers [91,92].

The principal characteristic of any photodynamic sensitizer is its capacity to preferentially accumulate in malignant tissue and, *via* the production of cytotoxic species, induce a desired biological effect [47]. PDT researchers observed that many of the characteristics of porphyrins translate to desired qualities of a photosensitizer. Porphyrins exhibit a strong absorption in the near infrared region of the electromagnetic spectrum; this absorption allows for deeper tissue penetration by light [93]. They are typically pure compounds with a constant composition; stable shelf life and a high quantum yield of singlet oxygen production. Porphyrins are retained to a greater extent in the diseased tissue over the healthy tissue, however, not to an extent that would eliminate post-operative photosensitivity.

Whilst all of the traits are essential to achieve the effective destruction of tumor cells, some are perceived to be more important than others, in particular the quantum yield of $^1O_2$, and the absorption profile of the photosensitizer. The latter reason is why most of the photosensitizers under clinical evaluation are porphyrin based as they have a natural proclivity to produce singlet oxygen [94]. The other crucial factor is that of photosensitizer absorption and consequently, light penetration. It has become evident that sensitizers with strong absorption bands between 700-800 nm are some of the most efficient because the absorption and scattering of light by tissue increases as the wavelength decreases [95]. Light penetration has been shown to fall off rapidly below 550 nm, however it doubles from 550 to 630 nm (the region where Photofrin is

activated) and doubles again in going to 700 nm. These dramatic increases in penetration culminate in a final 10% rise as the wavelength moves towards 800 nm (Figure 1.10).

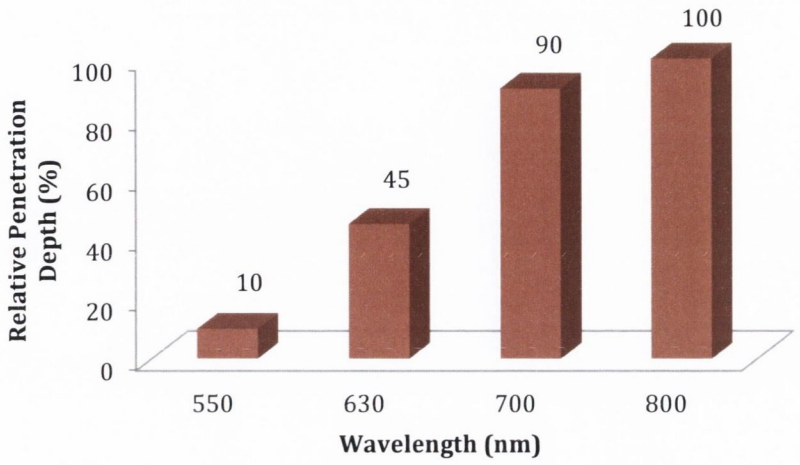

Figure 1.10. Relative diffusion depth of penetration with light at various wavelengths (assuming the depth of tissue penetration at 800 nm is 100%).

It is not, however, overly desirable to have an absorption greater than 800 nm as there is no benefit in terms of deeper tissue penetration and these compounds are not easily obtainable. Also, if the bathochromic shift is as a result of an extension to the π-system of the tetrapyrrole, then the oxidation potential decreases and the sensitizer may become less stable kinetically, and, therefore, more susceptible to photobleaching [96]. Another problem with this long-wavelength absorbing pigment is the possible decrease in efficiency of the energy transfer from the triplet sensitizer to the ground state molecular oxygen. This will occur if the triplet energy of the photosensitizer is below 94 kJ/mol [97].

Molecular oxygen has two low lying singlet excited states, $^1\Delta_g$ and $^1\Sigma_g$, 95 kJ mol^{-1} and 158 kJ mol^{-1} above the triplet state, respectively. Electronic configurations of these states differ only by the structure of the π anti-bonding orbitals. The transition from the $^1\Delta_g$ state to the $^3\Sigma_g$ state is spin forbidden, thus the $^1\Delta_g$ is a relatively long–lived species (Figure 1.11). The second excited state of oxygen, on the other hand, is short–lived due to a spin-allowed transition to the $^1\Delta g$ state. This strengthens the consensus that $^1O_2(^1\Delta_g)$ is the decisive oxidation agent in photodynamic processes [98].

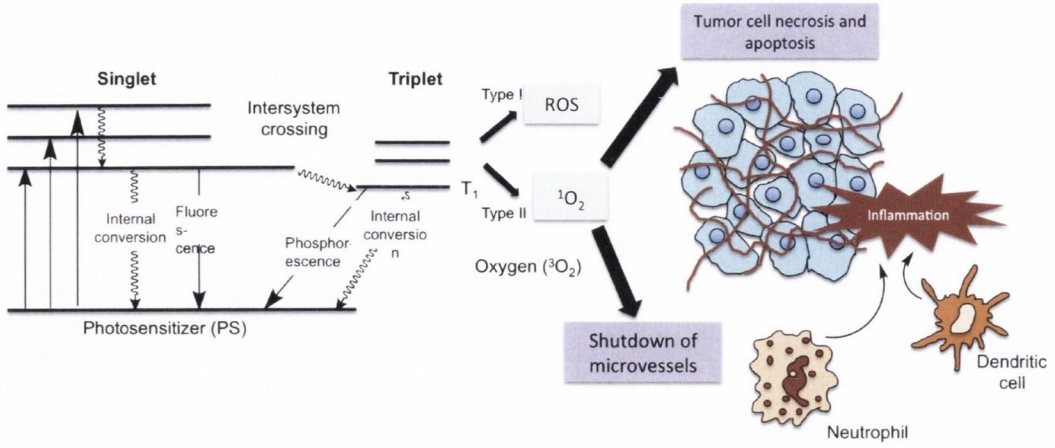

Figure 1.11. The mechanism of action on tumors in PDT, (Modified from [76]).

Whilst excited triplet state molecules can be efficient sensitizers of singlet oxygen in many cases, they are also efficient quenchers of these species once formed [[99]]. Consequently, there can be situations where the sensitizers used to generate singlet oxygen will themselves react to quench it. This could lead to photobleaching and -degradation, where photodegradation refers to the process in which singlet oxygen reacts with a material, resulting in its degeneration, and photobleaching refers specifically to the degradation of dyes by singlet oxygen.

Impetus was given to PDT as a viable treatment in 1993 when regulatory approval was granted in Canada for Photofrin, a commercial preparation of haematoporphyrin derivative (HpD) [100]. Haematoporphyrin is a complex mixture of porphyrin dimers and oligomers connected by ether, ester, and carbon-carbon interporphryin linkages. Photofrin exhibits poor selectivity with only 0.1-3 % of injected PS found in tumor tissue (Figure 1.12). Post-operative photosensitivity in the patient, weak absorption in the red and difficulty to isolate a single highly active component are the major shortcomings associated with this PS [101].

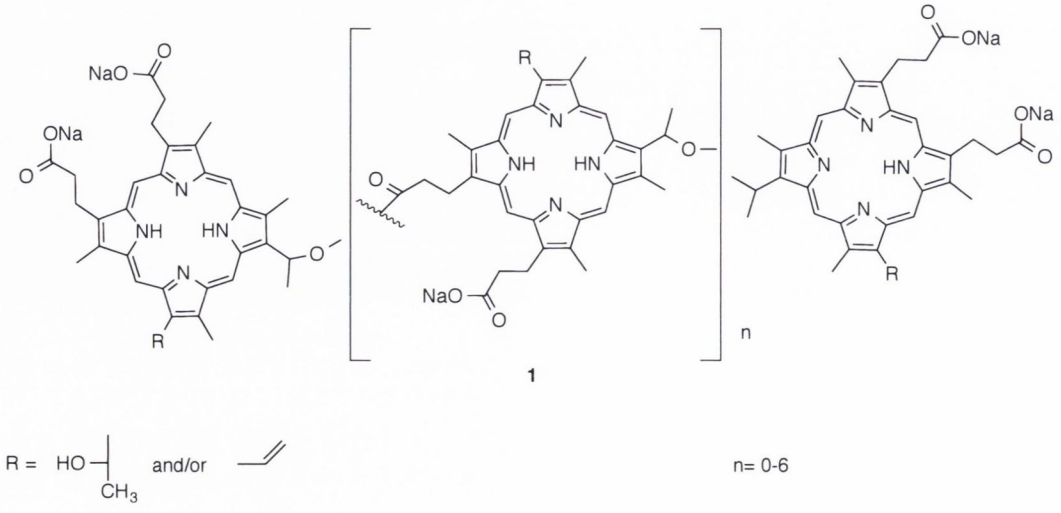

Figure 1.12. Structural representation of the main tetrapyrrolic constituents of Photofrin.

Photofrin was the first photosensitizer approved for patients and it currently holds licenses in the United States, Netherland, Japan and Canada. Whilst, it fits some of the previously outlined criteria for ideal sensitizers, it does suffer from a number of major drawbacks. As mentioned above (*vide supra*), it is not a chemically pure compound as it is a complex mixture of porphyrins with various monomeric and oligomeric forms. Due to this composition, it has proved extremely difficult for researchers to ascertain information on its mode of action and therefore difficult to suggest methodology to improve its efficacy as a photosensitizer in PDT [102].

The main drawback of Photofrin from a clinical perspective was the prolonged induced cutaneous photosensitivity. Thus, the PDT community undertook a large screen of synthetic hematoporphyrin analogues, with several research groups introducing a variety of substituents at diverse positions of the periphery of the macrocycle in the hope of finding a more efficacious photosensitizer.

After the success of Photofrin, a screening process was undertaken by Bonnett *et al.* to discover an effective second-generation photosensitizer [103]. After initial testing was complete, they decided upon the 5,10,15,20-tetrakis(hydroxyphenyl)porphyrins, in particular 5,10,15,20-tetrakis(*m*-hydroxyphenyl)porphyrin (*m*-THPP). This particular porphyrin was selected over the other two as the *ortho* isomer resulted in higher skin sensitivity and the *meta* compound, although comparable in reactivity with the *para,* was deemed better in terms of cost and benefit [104].

From the parent *m*-THPP **2**, the corresponding chlorin **3** [5,10,15,20-tetrakis(*m*-hydroxyphenyl)chlorin, *m*-THPC]; and bacteriochlorin **4** [5,10,15,20-tetrakis(*m*-hydroxyphenyl)bacteriochlorin, *m*-THPBC] were seen as ideal aspirants as photosensitizers (Figure 1.13). Of the three of these compounds, *m*-THPC demonstrated the most favourably qualities of a PDT agent [105,106].

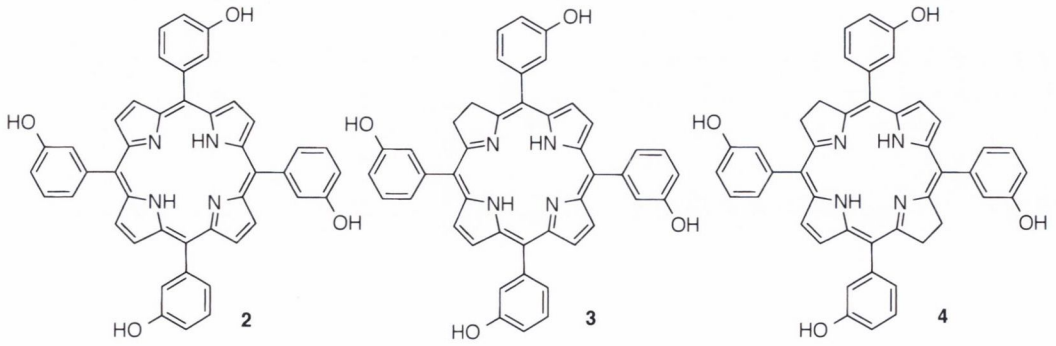

Figure 1.13. Family of 5,10,15,20-tetrakis(hydroxyphenyl)tetrapyrrole-based photosensitizers.

The absorption maximum of the long wavelength absorption band is shifted from 644 nm in **2** to 650 nm in **3** and 735 nm in **4** (Figure 1.14). This bathochromic shift is a highly desirable feature in the chlorin and bacteriochlorin and, along with their high solubility, makes them

excellent candidates as photosensitizers. Unfortunately, photobleaching is a major concern when using *m*-THPBC and results have shown that this occurs too rapidly *in vitro* for it to be used as a clinical PS [99,107]. This leaves *m*-THPC (**3**) as the most viable candidate of the three for use as a PS and it received clinical approval by the EMEA in 2001 under the name Foscan®. Comprehensive uptake, localization and metabolic studies preceded this regulatory approval; however, there are still a number of issues with this second generation photosensitizer that have kept research groups around the world modifying and improving upon the relative success of *m*-THPC in anticipation of discovering the next noteworthy PS [108].

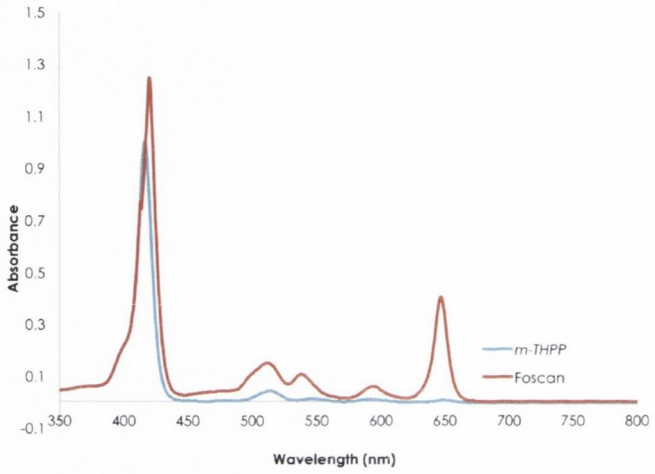

Figure 1.14. UV-vis absorption spectra of *m*-THPP **2** and *m*-THPC **3** in EtOAc.

In the case of Temoporfin, its uptake appears to be pH independent and is up-taken in aggregated form with apparent binding to lipoproteins [109]. The subsequent slow monomerization seems to cause the detected time delay in maximum PDT activity [108]. Researchers undertook a model study to investigate the release and redistribution of Temoporfin from a variety of plasma proteins, with HDL-mediated endocytosis being proposed as the foremost mode of drug transport in cells [110]. However, the uptake of LDL and thereby Temoporfin is a much more efficient pathway and thus, may reflect the real uptake mechanism of the drug.

The specific charge, the hydrophilic or hydrophobic properties, aggregation state and the degree of asymmetry in the molecule are the main parameters that determine the area of localization of the PS. Roughly speaking polar photosensitizers with >2 negative charges are unable to pass through the cell membrane *via* diffusion and therefore must be uptaken through endocytosis. In comparison, more hydrophobic PS with ≤2 negative charges pass through the plasma membrane easily and generally show good uptake. As a result, the various PS exhibit a broad range of intracellular localizations and it is this localization that determines the impact of the PS on the molecular machinery and thus the efficacy of the PDT treatment [111]. Therefore,

a clear understanding of PS localization is necessary when selecting a potential PS for a specific application.

After its initial discovery by Bonnett *et al.* and subsequent clinical trials, *m*-THPC was hoped to become the apogee of clinical PS. This notoriety was ephemeral as reports began to emerge of patient harm due to burns received mid- and post-treatment caused by the sheer reactivity of the PS [112]. [2]

Post-treatment photosensitivity is still a concern with Foscan based PDT as the photosensitizers reactivity requires such a low dosimetry that even ambient light can cause a photoactivated reaction [113]. Despite these drawbacks, Temoporfin is still the photosensitizer *du jour* for modification and manipulation by PDT researchers attempting to synthesize the next 3rd generation PS. Thus, while dosimetry must be considered for all PDT treatments, it is of specific importance with regard to *m*-THPC based PDT due to the high potential for patient burns and skin irritation during the illumination period. As such, a large body of research has been conducted in light sources and dosage during a course of m-THPC PDT [114-116].

Typically, the light used in courses of PDT treatment is that of the visible and near-infrared region of the spectrum. The specific wavelength of light used is prerequisite on the photosensitizer selected. As a therapeutic effect is desired as deep as possible, light of the longest possible wavelength is chosen. Light dosages are heavily dependent on the photosensitizer used and on the optical properties of the affected tissue. For example, second generation PS typically have stronger light absorption and a light dose of 10 J cm^{-2} will suffice in comparison to Photofrin, which generally requires a light dose between 50-500 J cm^{-2} [117].

Whilst any source emitting the appropriate wavelength of light may be used in a course of PDT, lasers are becoming increasingly popular, as they are able to deliver intense light of a high degree of monochromaticity. The advancement of technology in optical fibers has allowed for the employment of fibers endoscopically and enables PDT practitioners to place the light source interstitially into the tumor tissue and therefore treat classes of cancer previously inapplicable to PDT [50,118,119]. Unfortunately, the use of lasers has drawbacks such as their expense and mobility [97,118-120]. These drawbacks have paved the way for the development of the relatively inexpensive and mobile diode lasers [51,100,121,122]. The continuous research and development of new, cheaper and more efficient light-sources in parallel to photosensitizer development is crucial to the expansion of PDT applicability and implementation as a viable treatment option [51].

[2] These reports had a devastating effect on the proposals for regulatory approval to both the FDA and EMEA. This resulting rejection caused the bankruptcy of Scotia Pharmaceuticals Ltd., the industrial owner to the rights of the drug. Subsequent appeals to the EMEA were successful and eventually the drug was brought to the market in late 2001.

1.2.4 Targeted Systems for the Improved Efficacy of PDT Treatments

The therapeutic effect of PDT is primarily limited to the target tissue due to the 'selectivity' of the treatment and the relatively short *in vivo* lifetime of $^1O_2$ [[47,97,119,123]]. As a result, photosensitization can be minimized in unaffected areas of the body. However, one of the major setbacks to the mainstream clinical success of PDT has been post-treatment sensitivity. This problem arises from the previously discussed less than perfect localization of the PS in the target tissue.

Due to this, the photosensitizer can remain in healthy tissue and in the general blood flow. This failure to accumulate in the target tissue and subsequent exposure to the treatment light makes the patient photo-compromised, i.e., they cannot come in contact with UV-light for a number of weeks after administration of the treatment. To combat this phenomenon, researchers have attempted to mimic the use of molecular delivery systems for chemotherapeutics and toxins on photosensitizers. It was postulated that this type of carrier-mediated delivery system would greatly enhance the efficacy of PDT as not only would it vastly improve the accumulation of the photosensitizer in the target tissue but it also gives researchers the opportunity to use PSs with capable photochemical properties that unfortunately lack the adequate localization properties.

These potential carriers broaden the clinical repertoire of photosensitizers and in turn minimize the amount of precision needed in administration of the light dose. Additionally, there is no necessary need for cleavage of the photosensitizer from the carrier system for activation to occur, which lightens the synthetic burden on medicinal chemists when designing such systems.

1.2.4.1 Current Synthetic Methodology

From a synthetic viewpoint, these targeting molecules can be installed onto the porphyrin scaffold through a litany of different methodologies. The functional groups present on the targeting molecule and porphyrin are the limiting factor for which pathway one wishes to take. There are three main avenues available to a porphyrin chemist when designing a synthetic pathway for PDT conjugates, and they are as follows:

- total synthesis [124-126]
- [2+2] or [3+1] condensation reactions [127-129]
- functionalization reactions [130-133]

All have become increasingly viable due to the improvements made in the synthetic methodology of the different approaches. Each synthetic strategy has its strengths and weaknesses, so the onus is on the researcher as to which pathway better suits the resources available to them and the application and porphyrin that they have in mind (Figure 1.14).

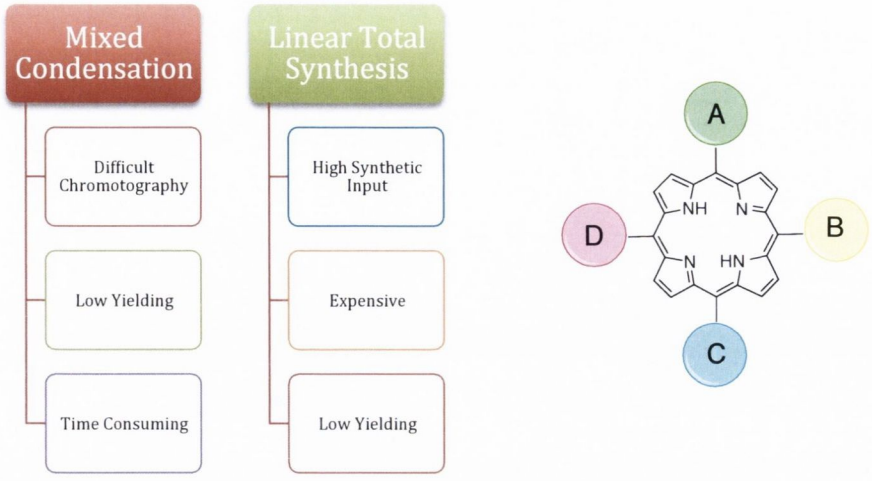

Figure 1.14. Classic synthetic pathways to unsymmetrical tetrasubstituted porphyrins and their weaknesses.

With respect to unsymmetrical porphyrins, the total synthesis route would appear to be the most logical and straightforward pathway. It involves the linear synthesis of the appropriate bilane precursor, followed by subsequent cyclization and oxidation to yield the desired porphyrin species. Theoretically, this methodology could, within reason, yield any porphyrin imaginable; however, it suffers from a lengthy synthesis with a significant number of synthetic steps [126,134,135]. This often time consuming pathway can also suffer from acid-catalyzed scrambling in the final step, which is an ongoing problem that further decreases the overall low yield [136].

The methodology that has seen the most use by porphyrin researchers is the mixed condensation route. This involves the mixed condensation of two or more different aldehydes with pyrrole to yield a reaction mixture containing a number of different porphyrin regioisomers. By controlling the equivalents of aldehydes used, one can achieve some selective formation of your target compound, however, it will typically be a statistical mixture of mono-, di-, tri- and tetrasubstituted porphyrin (Figure 1.15). Archetypally, this lends itself to tedious chromatographic purification and can often fail for selected compounds, such as acid labile groups or sterically hindered residues that can result in porphodimethene formation [137,138]. Progress with regards to this synthetic methodology is continuously improving with significant developments having been made, most notably by Lindsey's group [136].

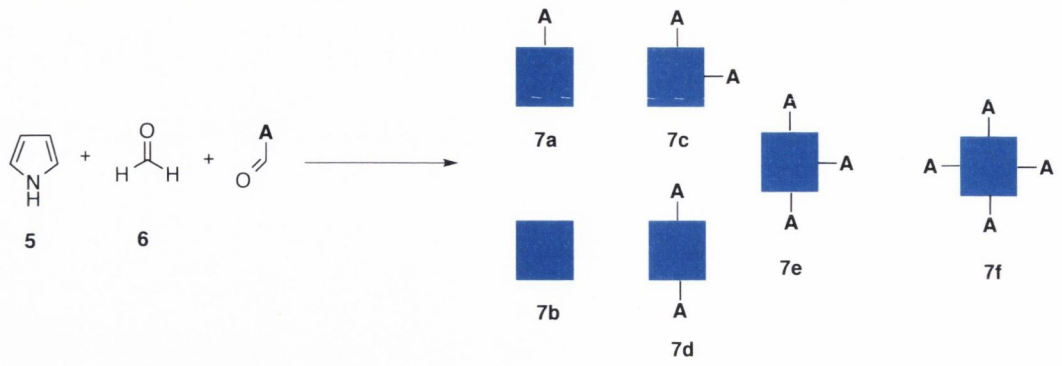

Figure 1.15. Schematic representation of the variety of products produced during a mixed condensation reaction.

The final synthetic approach was developed in house, by the Senge group and involves the controlled functionalization of pre-formed porphyrin scaffolds. The rationale was born from the desire to be able to selectively functionalize porphine (unsubstituted porphyrin) with a range of different substituents at the meso position. This methodology relied on the intrinsic reactivity of this meso position for electrophilic reactions. Whilst this strategy would appear straightforward, difficulties arose with the synthesis and manipulation of porphine, due to solubility issues. This work culminated in the ability of porphyrin researchers to manipulate preformed 5-, 5,10- and 5,15-substituted porphyrins with organolithium reagents and therefore introduce increased meso functionality in a step-wise and predictable manner (Figure 1.16) [129-131,133,139].

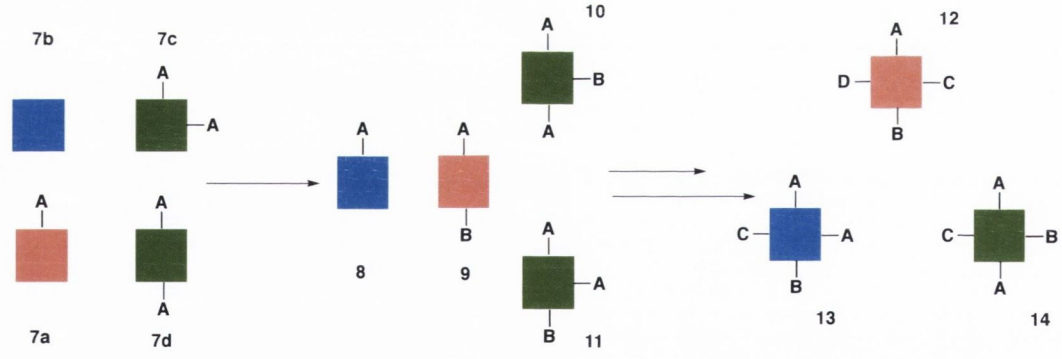

Figure 1.16. Schematic overview of transformations involving Ax-type porphyrins to yield unsymmetrical tetrapyrrole scaffolds.

While there are a number of different viable synthetic pathways to substituted porphyrins (*vida supra*), the eventual selected pathway will depend on a number of different factors, the most influential of which, being the nature of the functional groups present on the targeting motif.

1.2.4.2 Biologically Pertinent Molecules for Improved Targeting of Photosensitizers in PDT

This work will focus on the more established targeting groups, groups that have comprehensively demonstrated potential as biologically targeting agents. Within this section of targeting compounds, there is an extremely large body of literature covering all topics mentioned below and where possible, comprehensive reviews will be cited as excellent entry points into the respective fields (Figure 1.17). The examples discussed below will attempt to focus on the more medicinally relevant instances where *in vitro* and/or *in vivo* data has been obtained.

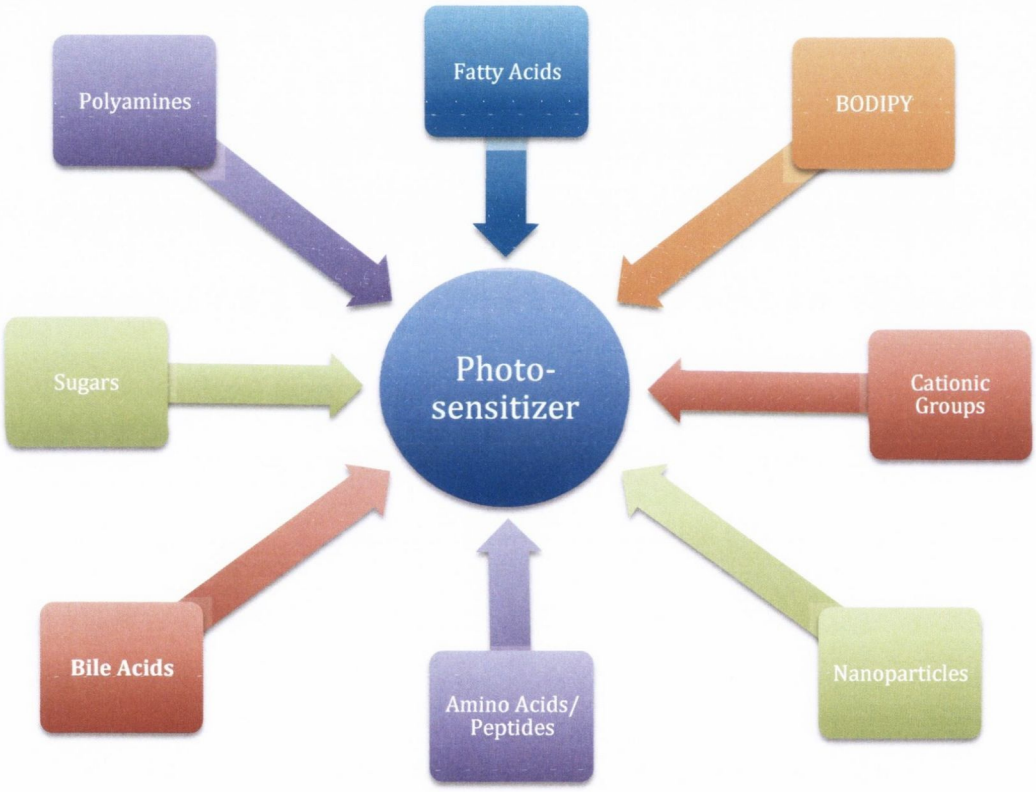

Figure 1.17. Summary chart of the most common biological groups installed onto PS periphery for enhanced PDT efficacy.

Bile acids are steroid acids found predominantly in the bile of mammals and other vertebrates and constituent roughly 80% of the organic profile of bile (Figure 1.18). The main function of bile acids is to facilitate the production of micelles, which promotes digestion and absorption of dietary fat,[140] but they are increasingly being shown to be involved in a number of biological processes throughout the body [141]. Kravlova *et al.* were able to demonstrate this using a library of bile acid-porphyrin conjugates, linked through a tertiary ammonium bond [142]. These conjugates displayed successful *in vitro* cell death in A431NS, HeLaS3, 4T1, and FHC cell lines, along with the ablation of tumors in BALB/c mice that were subcutaneously transplanted with 4T1 mammary carcinoma cells [143]. This *in vivo* and *in vitro* study was the first to demonstrate

the high potential use of these compounds in targeted PDT. This library of conjugates was found through binding studies to have a high potential for recognizing various oligosaccharides under physiological conditions, whilst also having the potential for selective fluorescence detection of cells expressing highly glycosylated markers.

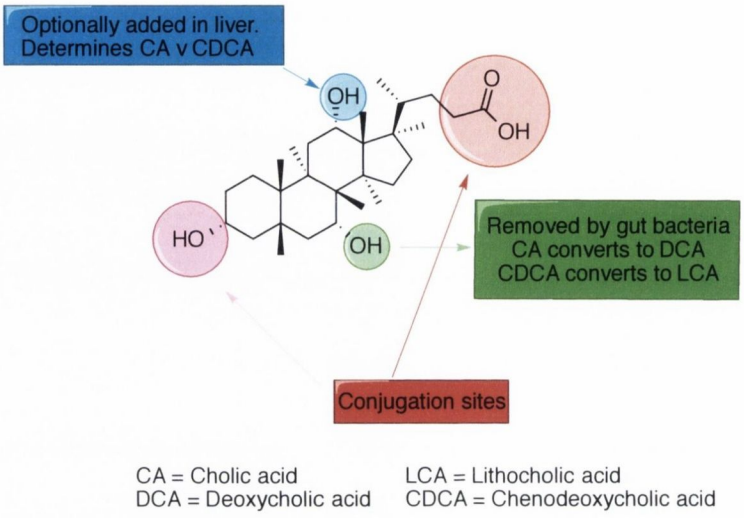

Figure 1.18. Diagram depicting a generic bile acid scaffold with its potential sites of conjugation.

Bile acids (BAs) have also been linked to the development of several different types of cancer including esophagus, liver, colon and pancreas. BAs have been shown to induce oxidative stress and generate reactive oxygen species that can induce DNA damage leading to mutations [144,145]. BAs have also been shown to activate a number of mitogenic and apoptotic signaling pathways. These include the epidermal growth factor receptor and the Raf/Mek/Erk pathway, the activator protein -1 (AP-1) and NF-κB transcription factors, the protein kinase C (PKC) family and endoplasmic reticulum (ER) stress pathways all of which are known to be deregulated during tumourigenesis [146]. Chronic esophageal exposure to bile acids in patients with gastro-esophageal reflux disease is associated with the development of Barrett's metaplasia and associated molecular markers of inflammation which have been shown to support transformation, initiation and progression of tumor development. Another feature of Barrett's is the development of intestinal phenotype including the expression of bile acid transporters such as the apical sodium dependent bile acid transporter (ASBT) along with associated intracellular transporters and a homolog of ilial Ost alpa/beta [147]. The Gilmer group have designed bile acids based on lithocholic acid, deoxycholic acid and chenodeoxycholic acid that are potent inducers of cell death in esophageal cancer cells (SKGT4) [148].

Glycoporphyrins were the first group of targeting conjugates that gained considerable traction as a viable conjugate option. This was due to their innate ability to solubilize tetrapyrrolic PSs that previously could not undergo biological testing due to their insolubility in aqueous media; and due to their potential capability to bind to lectins over-expressed on the surface of cancer cells [149]. Another main reason for this explosion of interest came due to the relative ease of

their synthesis and extensive variety of carbohydrates available for installation onto the porphyrin core. This variability in site of conjugation, nature of linker, porphyrin scaffold and carbohydrate used resulted in the ability of researchers to quickly and efficiently generate large libraries of glycoporphyrin conjugates that showed improved solubilities. As mentioned above, there are a myriad of examples of glycoporphyrins in the literature and for more insight into the field one can read comprehensive reviews by Cavaleiro *et al.* and Moylan *et al.* [150,151].

4,4-Difluoro-4-bora-3a,4a-diaza-s-indacene (BODIPY) is a strong UV-absorbing small molecule that emits a relatively sharp fluorescence peaks with high quantum yields. Extensive research has shown them to be relatively insensitive to the pH and polarity of their environment and subsequently, they are relatively stable to physiological conditions. From the humble beginnings of simple symmetrical derivatives such as the dimethyl-substituted compound arose methodologies for the functionalization of all three distinct positions of the BODIPY scaffold, e.g. nitration [152], sulfonation [153], halogenation [154] and palladium catalyzed functionalization [155], to name but a few (Figure 1.19). Extensive reviews are available that document the various milestones and practical applications of these functionalized BODIPY derivatives [156,157].

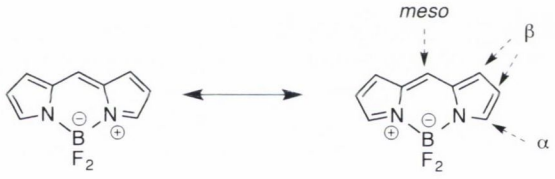

Figure 1.19. BODIPY molecular framework and the three distinct sites of possible functionalization.

Numerous researchers have synthesized porphyrin-BODIPY conjugates previously; however, nearly all of these systems were designed to act as models for photosynthesis [156,157]. These "cassettes" were envisaged to contain a donor and acceptor, where the donor would efficiently collect radiation and then pass it on to the acceptor using through-space energy transfer. This through space energy transfer mechanism is typically used to facilitate an artificial enhancement of the Stokes shift of the receptor molecule.

With respect to PDT, Burgess and O'Shea have completed interesting work on the synthesis of near-IR BODIPY probes [156,158,159]. Researchers have demonstrated these compounds ability to be readily uptaken by cancerous tissue, and a porphyrin-BODIPY conjugate may provide researchers with a possible "seek and destroy" treatment modality. The conjugate may be uptaken into the cell and used as an near-IR probe for fluorescent imaging, with subsequent UV-irradiation facilitating tumor killing through activation of the porphyrin species.

Cationic porphyrins have long captivated the attention of PDT researchers as they contain a number of desirable traits, most of which being their increased water solubility and there is no

sign of this interest depleting [160-162]. Whilst the incidence of positive results has been low in comparison to the high expectations from this class of compound, cationic porphyrins still hold great potential as being the next successful, clinically approved PS. In fact, this family of tetrapyrroles is currently undergoing a renaissance of sorts in the field of anti-microbial PDT, because of their rare ability to destroy Gram-negative bacteria [163-165].

Researchers have been successful in synthesizing a large array of conjugates with quite a variety of different peptides; however, biological results are still not as convincing as the gold standards already in the field. Many of these conjugates do show improved targeting, mainly for the tumor vasculature and it is this potential that merits further investigations into this class of conjugates. Also, with the constant improvement of mainstream peptide synthesis, researchers have been empowered with the ability to attempt more complex and specific peptides to increase the probability of finding a truly selective targeting peptide for PDT [166-169].

Nanoparticles (NP) have undergone an exponential increase in research journals and patent applications across all fields of chemistry and material sciences due to their large range of desirable attributes and relatively straightforward preparation. Not to be left behind or miss out on potential blockbuster photosensitizers, PDT researchers too began investigating the incorporation of nanoparticles into the different PDT treatment modalities [170-172]. These nanoparticle/photosensitizer hybrids offer an attractive route for the administration of photosensitisers (PS), which are, typically, hydrophobic materials and allows for passive and active targeting of cancer tissues and choroidal neovascularization.

Poly unsaturated fatty acids (PUFAs) such as docosahexaenoic acid (DHA), have shown therapeutic promise in the area of anti-cancer research and the treatment of neurodegenerative disorders [173]. Researchers have been able to demonstrate that tumor cells rapidly take up certain PUFAs from the arterial blood. This biologically innate uptake mechanism is presumably for the harnessing of PUFAs as biochemical precursors and energy sources, and therefore makes them an attractive targeting molecule for enhanced PDT efficacy [174].

Antibodies are the final example of an emerging paradigm in the field of bioconjugates for use in PDT. Developments in this field have been greatly enhanced through the development of phage display screening and recombinant DNA technology, making it possible to produce antibody fragments with high antigen affinity [175]. The possibility of site-directed photoactivatable probes having the capacity to generate reactive oxygen species (ROS) while destroying the DNA repair system in malignant cells and tumors was what initially enticed PDT researchers to this strategy. Furthermore, this may denote an effective approach to boost selectivity, penetration and efficacy of current PDT methodologies. A review on the state of the art by Boyle *et al.* acts as an excellent entry point for researchers going into this field as it

details the diverse range of methodologies that are now available for the efficient conjugation of PDT agents to antibodies [[175]].

1.2.4.3 Molecular Targets

The choice of targeting molecule will ultimately depend on the specific cellular machinery or process one wishes to enhance/inhibit. There are a myriad of intracellular targets available for PDT researchers; however, the one that has garnered the most attention is the translocator protein, previously known as the peripheral benzodiazepine receptor.

Since its serendipitous discovery over 30 years ago, the translocator protein (18 kDa)(TSPO) has been demonstrated to play an important role in a multitude of critical biological processes (Figure 1.20). Although implemented as a novel therapeutic and diagnostic tool for a variety of disease states, its most promising role is as a molecular target for anticancer treatments such as photodynamic therapy (PDT). The TSPO is a five transmembrane domain protein that is localized primarily in the outer mitochondrial membrane [176] and is expressed predominantly in steroid-synthesizing tissues and the brain [177]. Although the TSPO is an important regulatory complex in its own right, there is increasing evidence that this protein may represent an attractive target for researchers in the design and development of novel anticancer therapeutics.

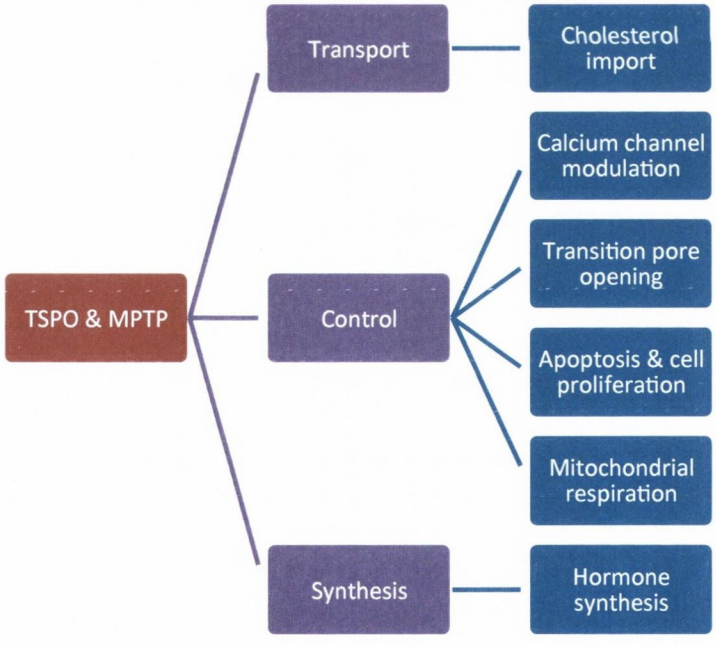

Figure 1.20. Flowchart of the different biological functions of the TSPO.

The focus on porphyrins in connection with the TSPO began with Snyder and co-workers, who in 1987 discovered that porphyrins are endogenous, potent competitive inhibitors of the TSPO [178-180]. In this context it was postulated that the TSPO facilitates the transport of porphyrins into the mitochondria, as the first and final stages of heme biosynthesis take place in the

mitochondria. This hypothesis would then explain the strong affinity of protoporphyrin for the receptor and would create a possible link between a deficiency in this receptor and development of porphyrias [181,182]. This finding of porphyrins as endogenous TSPO ligands opened a new field of studies into porphyrins as therapeutic or diagnostic agents pertaining to TSPO related diseases.

The induction of apoptosis resulting from the opening of the mitochondrial permeability transition pore (MPTP) by ligands such as porphyrins implicates the TSPO in the regulation of apoptotic and necrotic cell death (Figure 1.21) [183]. Ligands of the TSPO also inhibit cell proliferation in cancer cell lines, resulting in an accumulation of cells in the G_1/G_0 phase of the cell cycle. These actions ultimately inhibit the progression of cells to the S and $G_{2/M}$ phase, in which cell proliferation occurs [184]. By targeting the TSPO with endogenous or exogenous porphyrins, one may be able to selectively induce cell death via pro-apoptotic and antiproliferative pathways.

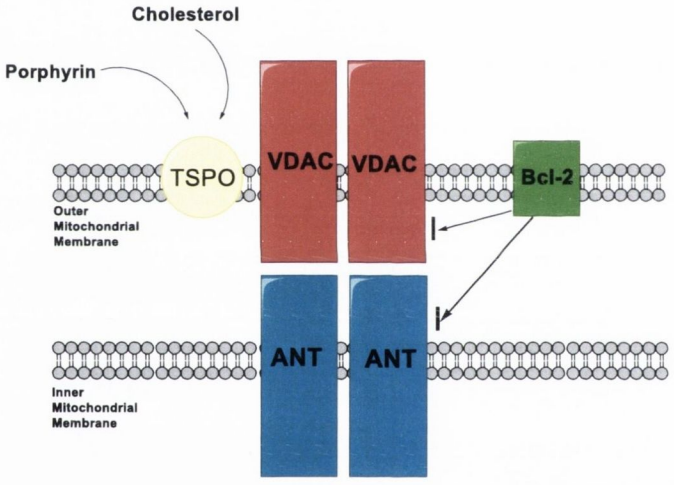

Figure 1.21. Schematic representation of the mitochondrial permeability transition pore and TSPO complex. The translocator protein (TSPO) is labelled yellow and the voltage-dependent anion channel (VDAC) is colored red. The B-cell lymphoma 2 protein (Bcl-2) is shown in green with the adenine nucleotide translocator (ANT) depicted blue.

1.3 Molecular Scaffolds- Triptycene & Light-Harvesting

The other more recent use of the term scaffold in the context of molecular scaffolds for use in the construction of three-dimensional complexes. Whilst nature can infer 3D structural complexity through the tertiary and quaternary structure of proteins, chemists have struggled to mimic mother nature, albeit, not out of lack of trying. Chemists have been limited by the availability of 3-D molecular scaffolds upon which they can functionalize and manipulate compounds to mimic the complex structures found in nature.

One of the key requirements for any potential scaffold system is that the substituents must be arranged in a specific orientation, which is precisely known and invariable under target conditions. Little attention has been paid to saturated hydrocarbon scaffolds, i.e. unconjugated scaffolds, in spite of the many advantages these groups lend in terms of solubility and toxicity. Triptycene and porphyrin or Platonic solids such as cubane are examples of classes of compounds that represent readily accessible molecular scaffolds. Researchers have successfully functionalized their respective peripheries with a litany of different chemical subgroups and have shown examples of these to undergo further reactions to form three-dimensional supramolecular structures [129,185-187].

Whilst the synthesis of porphyrin scaffolds has been discussed in detail previously in relation to medicinal purposes, the same reactions and synthetic strategies can be applied for the construction of porphyrins as 3-D scaffolds. Therefore, it is pertinent to now introduce and discuss triptycene and its merits as a potential scaffold.

Triptycene is the simplest and smallest member of the iptycene family, a group of molecules in which members must contain three or more arene rings connected together by a [2.2.2] bicyclic bridgehead system [188]. This bridgehead system maintains the three arene rings at a constant angle of 120 ° which results in a three dimensional, rigid framework that contains three electron-rich cavities (Figure 1.22).

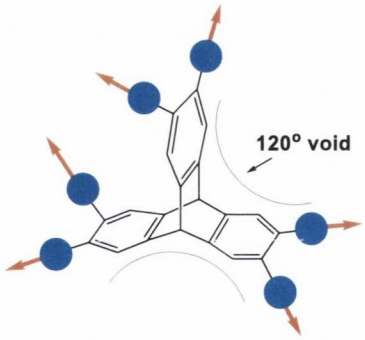

Figure 1.22. "Hexasubstituted" triptycene and the 120 ° voids created by the D_{3H} symmetry of arene "blades" present in the molecule.

1.3.1 Historical Overview of the Development of the Synthesis of Triptycene

It was first synthesized in 1942 by Bartlett *et al.* when they created tribenzobicyclo(2,2,2)octatriene, which they subsequently named triptycene, through a total synthesis styled approach that started with a Diels-Alder reaction of anthracene **15** and benzoquinone **16** (Scheme 1.1) [189]. Unfortunately, this synthetic approach gave quite poor yields and since then, many researchers have made attempts to optimize the synthesis and therefore the yield of triptycene through slight modifications of the pre-existing pathway.

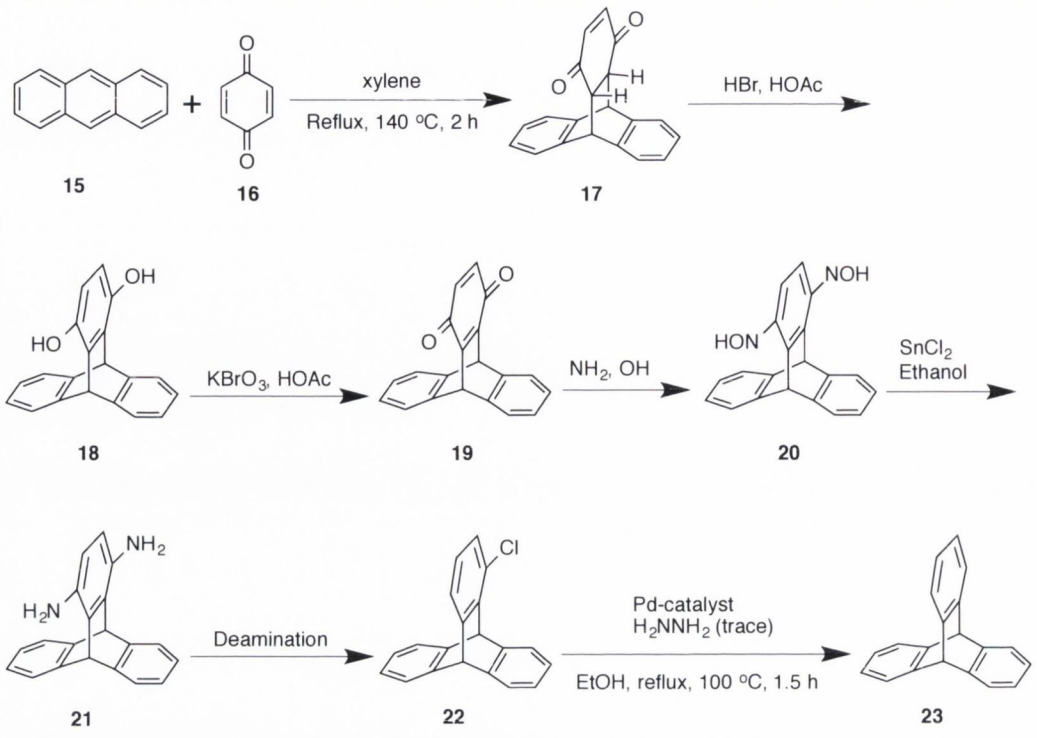

15 16 17 18 19 20 21 22 23

Scheme 1.1. Original synthesis of triptycene by Bartlett *et al.* through a Diels-Alder pathway [189].

Of these numerous attempts, Craig and Wilcox made some of the most salient advances when they produced a simple and direct pathway to triptycene through the reduction of the adduct formed from the reaction between anthracene **15** and *p*-benzoquinone **16**. This was accomplished with $LiAlH_4$ or $NaBH_4$, and subsequent refluxing of the mixture with ethanolic hydrochloric acid before chromatography of the products on acid alumina. While this pathway proved to be considerably shorter than Bartlett's, it still only produced triptycene in an overall yield of 15% [190]. Wittig and Ludwig improved upon this yield almost twice-fold by implementing a reaction between benzyne **25** and anthracene [191]. A modified version of this pathway that uses *o*-bromochlorobenzene **24** with magnesium in a THF solution to give a Grignard reagent, which can then react with anthracene **15** to give the triptycene product, is the most commonly used one today (Scheme 1.2) [192].

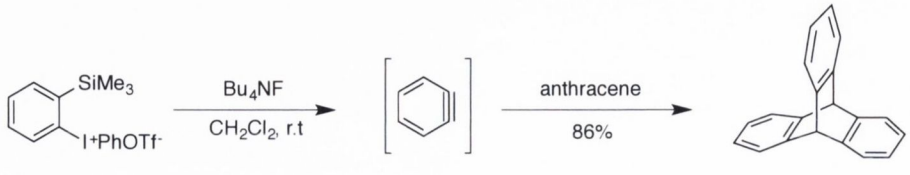

24 25 23

Scheme 1.2. Improved synthesis of triptycene by Craig & Wilcox utilizing a benzyne intermediate [190].

1.3.2 Synthetic Manipulation of the Preformed Triptycene Scaffold

Since its initial synthesis in 1942, there are two quite disparate reaction pathways that allow for the functionalization of triptycene derivatives.

- Total synthesis
- Manipulation of a pre-formed scaffold

A total synthesis approach involves the use of pre-substituted synthetic precursors. These functional groups will be present on the molecule during the triptycene forming Diels-Alder or benzyne reactions. This method is quite practical for the formation of monosubstituted triptycene derivatives with synthetically cumbersome functional groups; however, these precursors are typically rare and/or expensive and therefore, habitually need to be synthesized in house. Also, researchers are limited by which functional groups can survive the relatively harsh conditions of the benzyne pathway.

The other option available to researchers is the manipulation of a pre-formed triptycene scaffold. In terms of cost and number of synthetic steps, this pathway can 'cheat' slightly as triptycene is commercially available at quite an affordable price from Sigma-Aldrich[3]. This readily available triptycene scaffold has successfully demonstrated that it is a versatile molecule that can tolerate a multitude of reaction conditions without subsequent degradation of the framework; and it is now possible to nitrate [193], acylate,[194] halogenate, oxidize, reduce[189] and even perform photochemical reactions[195] on the triptycene scaffold. This ability by researchers to manipulate the core scaffold with a variety of functional groups allowed for triptycene to become a target for a variety of different applications. These applications mainly required the production of symmetrical tri-substituted triptycene derivatives.

Threefold systems such as these started to garner considerable interest, especially in the field of biochemistry as it is now well known that a large number of metallo-protein active sites have a threefold symmetry, e.g. *p*-clusters of nitrogenase [196]. Thus, it was postulated that these trisubstituted triptycenes might allow for the construction of synthetic model complexes for protein studies. Whilst this implementation of triptycene scaffolds is extremely interesting, trisubstituted triptycene scaffolds really came to the fore as building blocks for further functionalization.

In 2006, Zhang and Chen synthesized 2,6,14- and 2,7,14-triiodotriptycene by nitrating triptycene, performing a reduction of the nitrate groups to give the amino functionality, followed by a Sandmeyer reaction to install the iodo-functionality [197]. In 2008, Dahms *et al.* were successful in utilizing this practical synthetic scaffold, i.e. 2,6,14-triiodotriptycene, for the synthesis of triporphyrintriptycene arrays through metal catalyzed cross-coupling reactions [186,198].

---

[3] Triptycene is available from Sigma-Aldrich at 10g for 188.50e

Due to the rigid, three pronged structure of the iodinated starting material, metal catalyzed coupling reactions result in the projection of the newly installed functional groups in a spatially defined manner. This projection increases the internal free volume of the molecule and presents interesting potential applications in the fields of gas storage, light-harvesting mimics or as host-guest complexes in supramolecular chemistry.

1.3.3 Potential Applications of Molecular Scaffolds

1.3.3.1 Artificial Light-Harvesting

There is a growing demand for clean energy due to the limited resources of fossil fuels and ever-increasing global population. From the range of environmentally friendly energy sources, sunlight is the most abundant and one of the cleanest sources of energy and thus has attracted much attention from the research community [199]. Nature has the ability to efficiently harness solar energy *via* the photosynthetic process. The light captured by the antenna systems that are constituted of pigment-protein complexes is transferred to the pigments in the reaction center proteins and the resulting photo-induced electron transfer gives rise to electrochemical potential energy [200]. During photosynthesis extremely long-lived, charge separated states ($t_{1/2}$> 1 s) are formed [201]. This unique feature of the RC has been an important stimulant in the motivation for designing artificial molecular systems aimed at mimicking the structure and/or function of the bacterial photosynthetic RC. The main function of the RC is to generate an energy gradient, using successive electron-transfer (ET) processes to span the cytoplasmic membrane.

It has become of paramount importance to try and comprehend on a molecular level the mechanisms behind some of the key biochemical, enzymatic and photochemical pathways that occur during photosynthesis [202]. X-Ray crystallographic studies of light-harvesting antenna complex LH_2 of *Rhodopseudomonas acidophilia*, has shown that plants and bacteria contain sophisticated self-assembled polypyrrolic architectures. In these natural systems, polypeptides, governed by four levels of structural complexity define the three-dimensional structure of these complexes. These systems are incredibly intricate and therefore present an unfortunate inaccessibility through current synthetic techniques. Consequently, the use of simplified model compounds has become increasingly popular in the last few decades.

Researchers have synthesized both covalently and non-covalently linked antennae systems that can mimic the photosynthetic reaction center. Work by Gust *et al.* produced a molecular hexad that contained five porphyrin antenna moieties and a pH-sensitive dye. The molecule contained a hexaphenyl benzene core with porphyrin sensitizers covalently attached through the meso position. The pH sensitive dye acted as an electronic control unit and was situated at the sixth available position (Figure 1.21). Non-covalently linked or self-assembled antenna systems have received increased interest from the academic community due to their ability to mimic the two

or three-dimensional supramolecular assemblies observed in nature. Antenna model systems constructed by Balaban and coworkers [203,204] Tamiaki [205], Moore and Wasidewski [206] demonstrates the most salient works to date in the field (Figure 1.23).

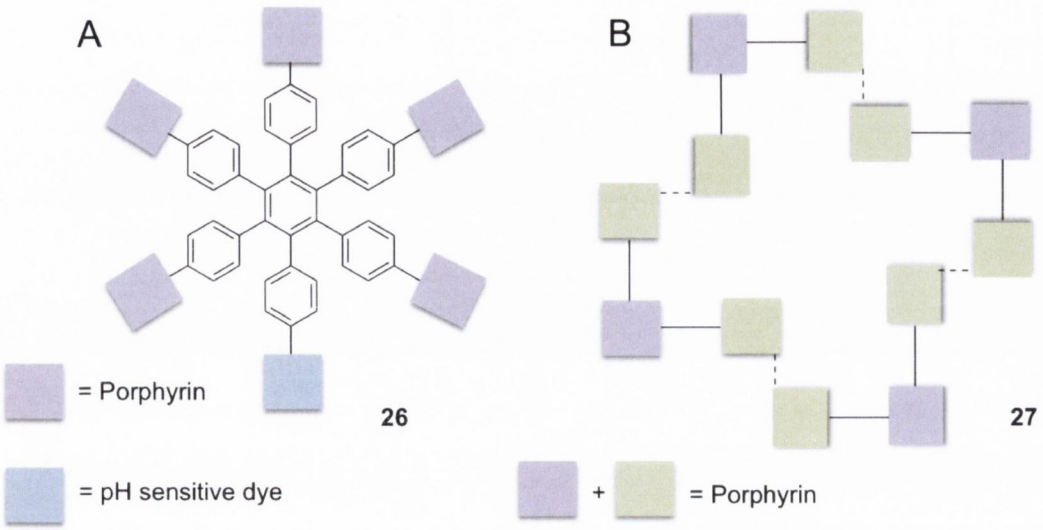

Figure 1.23. Diagrammatic representation of porphyrin based light-harvesting systems. A) A molecular hexad synthesized by Gust *et al.* that incorporates five porphyrin sensitizers and a pH sensitive dye encompassing a hexaphenylbenzene core [207], B) Self-assembled porphyrin tetramer by Osuka *et al.* consisting of meso linked porphyrin trimers [208].

These model systems have encouraged the understanding of the concepts of design and strategies of self-assembly of structures centered on intermolecular interactions. Unfortunately, the majority of these light-harvesting systems suffer from lengthy syntheses and low yields. Whilst porphyrins are considered quintessential building blocks for the construction of artificial molecular assemblies, triptycene provides an excellent scaffold for the formation of light-harvesting antennae mimics as the porphyrin subunits will be projected in a spatially defined manner around the triptycene core. This type of structure is particularly niche in chemistry and could potentially imitate the macrocyclic arrangement of chlorophyll pigments observed in nature.

1.4 Maximizing Scaffold Potential

Due to the capricious nature of research, there is mounting pressure on researchers to become increasingly more inter-disciplinary with respect to their fields of expertise. Thus, whilst two categories of chemical scaffolds have been described with respect to specific applications, the potential for crossover into new and distinct disciplines has become an increasingly attractive but also necessary avenue for researchers to undertake.

1.4.1 The Use of Scaffolds for the Construction of Model Compounds

The use of model compounds by researchers to investigate the underlying mechanistic machinations by biological systems has become increasingly popular, as their syntheses are archetypally more accessible than the innate derivative. Thus, it is essential to not only continue with the creation of new scaffold systems but also investigate the crossover use of scaffolds for a dichotomy of applications, e.g. the implementation of a scaffold traditionally used for medicinal purposes may hold potential for the construction of 3-D compounds for energy or light-harvesting purposes.

1.4.1.1 Cofacial Metalloporphyrins

Metalloenzymes play a critical role in a plethora of biologically important transformations. Objectively the most studied and revered by researchers in the field is the multielectron redox reaction, of which there are many examples, e.g. sulfite reductase [209] nitrate reductase [210] cytochrome c oxidase [211] blue copper oxidases [212] pseudocatalase, [213,214] photosystem II [215] nitrogenase [216] and hydrogenase [[217]]. In most cases, it is believed that the enzymes are thought to have one or more metals at the active site, which makes them an extremely challenging prospect to biochemists and synthetic organic chemists to isolate or recreate.

Recent studies into metalloenzymes has revealed a partial structural and mechanistic description of the active site in these enzymes; however, there is still a great deal to be understood with respect to the mechanisms of substrate transformation. The need for model compounds to mimic this class of enzymes increased with scientists' heightened interest in the four-electron reduction of O_2 to H_2O, the key step in life-sustaining aerobic respiration. The membrane-associated, multi-metalloenzyme, cytochrome *c* oxidase catalyzes this reduction, with the energy derived from this reduction used by a proton pump to establish a membrane potential, which subsequently drives the synthesis of the energy-rich molecule, ATP [218].

The discovery of co-facial porphyrins presented researchers for the first time a synthetically obtainable model compound which they could use to investigate the binding and mechanistic behavior of the reduction of O_2 to H_2O.

The initial goal of preparing the face-to-face porphyrins was to hold two porphyrins rigidly together in a co-planar arrangement, in the hope that the two metal atoms might act in concert to bind and reduce dioxygen (or dinitrogen) in the cavity between the porphyrin rings. The successful synthesis of covalently linked bisporphyrins as model compounds for the study of energy transfer between adjacent chromophores was completed by Schwartz *et al.* [219]. These first bisporphyrin systems were conjugated through the β-pyrrolic position using an amide linkage. This work acted as a precursor to the seminal work by Kagan and Ogoshi who were the first to report the synthesis of cofacial diporphyrins (Figure 1.24), with the first published article appearing almost contemporaneously by Collman *et al.*, Ogoshi *et al.*, Kagan *et al.* [220-222].

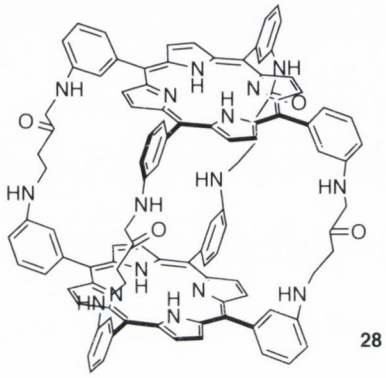

Figure 1.24. A cofacial porphyrin compound designed by Collman and co-workers [223].

These successful syntheses created synthetically obtainable models that allowed researchers to investigate the binding and mechanistic behavior of the reduction of O_2 to H_2O in the hopes of improving the efficiency of power production by fuel cells. This figure that was previously limited by the efficiency of the best catalyst (Pt) for this transformation could now potentially be improved upon.

1.4.1.2 Picket Fence Porphyrins

The reversible binding of oxygen in hemoglobin (Hb) and myoglobin (Mb) has long dominated the interest of researchers, as a fundamental understanding of molecular oxygen's interaction with heme complexes is necessary to develop a basic comprehension of hemoprotein function. In addition to this, research into the utilization of oxygen in the oxidation of small molecules by complexes such as cytochrome P_{450} monooxygenase has come to the fore in recent years. Previously proposed structural models by Griffith [224], Pauling [225] and Weiss [226] included a sideways, triangular structure and an end-on angular bond. The models failed due to unfavorable coordination states or steric demand.

In order to research these interactions and enzymatic functions, researchers needed to look to an easily accessible model compound. In this regard, picket fence porphyrins became very much *in vogue* during the 1970s as they provided researchers for the first time a model system so as to study the interaction of molecular oxygen with hemoproteins.

Myoglobin is a 153 residue peptide and an iron(II)protoporphyrin IX complex [227,228] that is responsible for the storage and transport of oxygen across membranes. The ferrous protoporphyrin IX is held noncovalently in a cleft in the protein largely through apolar interactions. A co-ordinate bond between a proximal imidazole of histidine residues F-8 and the Fe(II) provide the only covalent linkage between protein and porphyrin (Figure 1.25). The Fe(II) deoxy form in Mb is five-coordinate, high spin, with an ionic radius too large to fit within the cavity of the porphyrin [228]. As a result, this iron atom projects out of the mean plane of the four pyrrole nitrogens and subsequently toward the proximal imidazole and away from the oxygen binding site.

Figure 1.25. Previously proposed binding of O_2 to Iron(II) in heme [229].

In order to design an appropriate model compound, researchers needed to create a porphyrin with extreme steric bulk as to create a nonprotic cavity on one side of the porphyrin. This unhindered "face" can then co-ordinate to strong field ligands such as imidazole and truly mimic the oxygen binding seen in hemoproteins. Collman *et al.* were successful in preparing crystalline iron(II) porphyrin-dioxygen complexes [230], which modeled oxymyoglobin, and were able to bind molecular oxygen in solution or in the solid state and have been definitively characterized by Mossbauer through IR spectroscopy [231] and X-Ray crystallographic analysis [232]. As mentioned previously, Collman *et al.* set out to design a picket fence porphyrin to favour five-cordination, whilst simultaneously inhibiting bimolecular reactions, i.e. reactions involving two iron atoms and dioxygen [233].

Conceptually, this model of a picket fence porphyrin stems from work conducted by Ullman and co-workers, when they first demonstrated the ability to resolve the atropiomers of meso-tetra(*o*-hydroxyphenyl)porphyrin [234]. From this development in porphyrin chemistry, Collman *et al.*, were able to synthesize meso-tetra(α,α,α,α)-*o*-aminophenyl)porphyrin in good yield (Figure 1.26). This compound was then used as a scaffold upon which they could functionalize the amino residues with the "fence" moieties. In this particular case, they implemented the use of pivaloyl chloride as a coupling partner in an amide synthesis step.

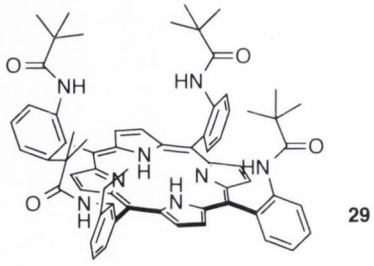

Figure 1.26. An (α,α,α,α)-*o*-aminophenyl)porphyrin derivative synthesized by Collman and co-workers represents the first synthetic example of a picket-fence porphyrin [229].

Metal-organic frameworks

Metal-organic frameworks (MOF) combine the often-disparate disciplines of inorganic and organic chemistry and creates a class of highly crystalline, porous and extensively studied materials. Since the 1990..s, MOFs have emerged as an extremely attractive area of chemistry due to their high degree of variability in both the organic ligand and the inorganic metal component as well as potential applications in gas storage, catalysis, drug storage/delivery and as chemosensors [235-237]. This unparalleled growth can of course be attributed to the wide array of potential applications but also to the relative ease of their chemical synthesis [238,239].

Reactions to synthesize MOFs usually take place in high boiling, polar solvents and the most important parameters of the synthesis are concentrations of the metal salt and organic ligand, temperature and the pH of the solution. The vast selection of organic ligands and metal salts allows for the creation of libraries of topologically diverse and aesthetically pleasing structures, which can be altered for different applications by altering the characteristics of the ligand, i.e., ligand length, bond angles, chirality etc. [240]. All the above factors play a pivotal role in determining the shape of the resultant framework.

The physiognomies of triptycene mentioned previously, fill many of the desired qualities of the organic ligands used in MOFs. Again, it has fixed three-dimensional geometry, which projects covalently attached groups in a spatially defined manner. This trait coupled with its own extremely high internal free volume makes them an extremely attractive class of compounds for research in the field of MOFs.

Objectives:

Molecular scaffolds are an emerging paradigm that offers chemists the use of preformed chemical structures that can be manipulated structurally and synthetically for use in a plethora of applications. The goal of the research discussed herein was to develop new methodologies for the synthesis and manipulation of either new or preformed molecular scaffolds for PDT and light-harvesting technologies. It was hoped to implement techniques and synthetic strategies previously developed in house in the Senge lab, in concert with the development of new pathways for the installation of biologically and photophysically interesting molecules.

To investigate these new pathways and methodologies the project was divided into two disparate sections:

- The use of a preformed photosensitizer scaffold in functionalization reactions as a demonstrative method of simple porphyrin desymmetrization, with subsequent evaluation of synthesized porphyrins in Photodynamic Therapy studies.
- The use of molecular scaffolds for the synthesis of larger, more complex systems, for the construction of complex multi-porphyrin arrays.

By controlling the number of equivalents, one can functionalize the periphery of *m*THPP and *m*THPC, two known photosensitizers in a controlled manner and obtain mono-functionalized porphyrin and chlorin derivatives in high yields and few synthetic steps. This methodology can be used to install practical synthetic handles that allow for the introduction of biologically pertinent groups. As such a library of porphyrin bile acid adducts was synthesized through the copper(I) catalyzed click reaction using a preinstalled propargyl group present on the photosensitizer scaffold. This library of highly soluble PS were readily up taken and accumulated within the cytoplasm of the cell. Unfortunately, they did not exhibit any photocytotoxicity which has been attributed to the presence of the triazole ring.

This methodology was then applied to a library of suitable benzyl coupling partners. A library of monosubstituted mTHPP derivatives could be successfully prepared through a number of simple reactions pathways. By using historic phenolic chemistry, compounds were synthesized through nucleophilic substitution, esterification, and OH activation reactions. This chemistry was updated for porphyrins by using the recently discovered Chan–Lam copper-catalyzed coupling of a heteroatom with a boronic acid. This allowed for the synthesis of some simple, unsymmetrical porphyrin systems.

In an effort in improve post-treatment tumor regrowth due to the upregulation of proinflammatory molecules in the tumor microenvironment, a series of non-steroidal anti-inflammatories were conjugated to the Temoporfin scaffold through a modified Steglich reaction. By monitoring the reaction equivalents and time, it is possible to control the degree of substitution and thus produce mono to tetra-functionalized "iPorphyrins" in reasonable yields and few synthetic steps. All conjugates successfully entered into the cells and whilst no cytotoxicity was observed, due to positive results observed in the $^1O_2$ production assay, we believe that with longer irradiation times, we may be able to improve the cytotoxicity of the conjugates and therefore the efficacy of the treatment.

Finally, to investigate the use of molecular scaffolds as synthetic building blocks for the construction of light-harvesting arrays, triptycene was selected as a readily available rigid scaffold that is susceptible to further functionalization. A library of hexasubstituted triptycene building blocks were synthesized through the use of transition metal catalyzed cross coupling reactions i.e., Suzuki and Sonogashira couplings. All building blocks contained distal functional groups that allow for further functionalization reactions to occur. These highly substituted derivatives may be implemented as synthetic scaffolds in future reactions for applications such as metal-organic frameworks, light-harvesting arrays and drug-delivery vehicle.

A plethora of coupling conditions and pathways were attempted for the synthesis of a hexaporphyrin array. These involved both cross coupling reactions and also more historic esterification and nucleophilic substitution chemistry. Whilst there were some positive spectroscopic results throughout the project, to this date we have not been able to purify and isolate the array and subject it to photophysical measurements.

Chapter 2: *m*-THPP: Always the Bridesmaid, Never the Bride.

2.1 Introduction

Since their discovery by Rothemund in 1935, symmetric meso-aryl-substituted porphyrins have been the workhorses of porphyrin chemistry, as they can be easily prepared in high yielding one-pot reactions on a multigram scale [241-243]. However, most applications such as photodynamic therapy (PDT),[49,244] nonlinear optics (NLO),[245-249] solar energy conversion,[250-252] and photosynthetic reaction center mimics [201,253] call for unsymmetric porphyrin derivatives such as amphiphilic systems for PDT or push-pull systems for energy transfer and optical studies. In the last decades, there have been vast improvements in the synthesis of unsymmetrical porphyrins through either a total synthesis approach,[126,135,243,254] [2+2] or [3+1] condensation reactions, or functionalization reactions. Improvements to the last two approaches are exemplified by Lindsey's large-scale syntheses [126,243,254,255] and Senge's functionalization methodology for ABCD-type porphyrins [131-133] and these synthetic strategies have found wide scale implementation by the porphyrin community.

Drawbacks to these routes are the obvious plethora of steps and synthetic manipulations that are needed to yield the desired bilane as well as the ongoing problem of the acid-catalyzed scrambling that is observed in the final step of the total syntheses [135]. Similarly, the functionalization approach heavily relies on organometallic coupling reactions and the preparation of the required coupling partners are not trivial [129,132,256]. However, within reason, almost any desired meso-substituted porphyrin is now synthetically accessible through these methods. Yet, in practical terms, the most widely used approach is still a mixed pyrrole condensation. This synthetic pathway has drawbacks that include tedious chromatographic steps and low yields, and it cannot deliver the plethora of unsymmetrical porphyrins that are necessary today. Nowadays, the field of porphyrins is driven by application-oriented research with significant contributions from materials scientists and inorganic, physical who lack the synthetic capabilities that are necessary for the more involved syntheses. Thus, there is a pressing need for simple and technically facile syntheses for unsymmetrically substituted porphyrins (Figure 3.1).

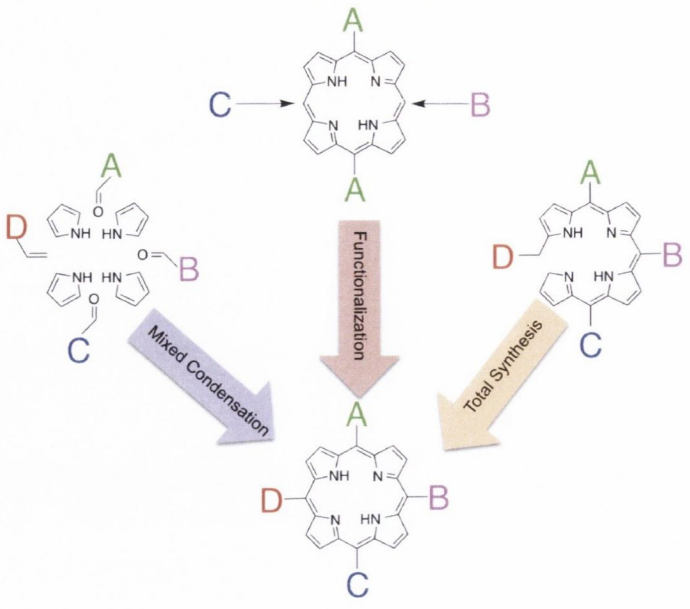

Figure 3.1. Three of the main synthetic pathways available for the construction of unsymmetrical porphyrins.

2.2 Project Concept

The idea of this project emerged from the desire to create a simple and robust methodology for the successful synthesis of monosubstituted *m*-THPP and *m*-THPC scaffolds through nucleophilic substitution reactions. From here, it was theorized that a plethora of different substrates might be installed onto the porphyrin scaffold through this substitution pathway. If this were indeed possible, this would offer porphyrin researchers a photosensitizer scaffold upon which they could install any number of different synthetic handles for future functionalization with an array of different biologically or photophysically pertinent molecules.

2.2.1 Choice of Scaffold

Typically, for investigatory projects such as this, one would wish to employ the use of a model compound. Model compounds are usually cheap and easily synthesized on a large scale and possess many of the desired attributes of the target compound. All of these traits can be used to describe *m*-THPP's relationship to the reduced chlorin derivative *m*-THPC. It can be synthesized on a gram scale, in a two-step synthesis as per the results in the previous chapter, and it is a known photosensitizer for PDT. Unfortunately, in recent times PDT researchers have overlooked this compound due to the history of Temoporfin and its regulatory approval by the EMEA. However, from the promising results in the previous chapter, it is believed that one could use *m*-THPP as a model compound for investigatory reactions of hydroxyphenylporphyrin-based scaffolds in PDT. The promising results could then be applied to the more efficacious *m*-THPC if necessary.

2.2.2.1 Synthesis

m-THPP is a readily available PS produced in high yields through a condensation reaction to create *m*-TMPP (**30**), with subsequent demethylation yielding the desired tetrahydroxyphenylporphyrin (**2**). Boron tribromide, BBr_3 is the reagent of choice for the demethylation of aryl ethers. However, as the target synthesis is on a large scale and the highly toxic BBr_3 must be used in large excess (Scheme 2.6), a number of alternative and more economical synthetic strategies have been developed. These methodologies include microwave condensation reactions to yield *m*-THPP **2** directly or the use of alternate protecting groups such as acetyl groups, which can be cleaved in almost quantitative yield after the condensation step using a simple basic work-up.

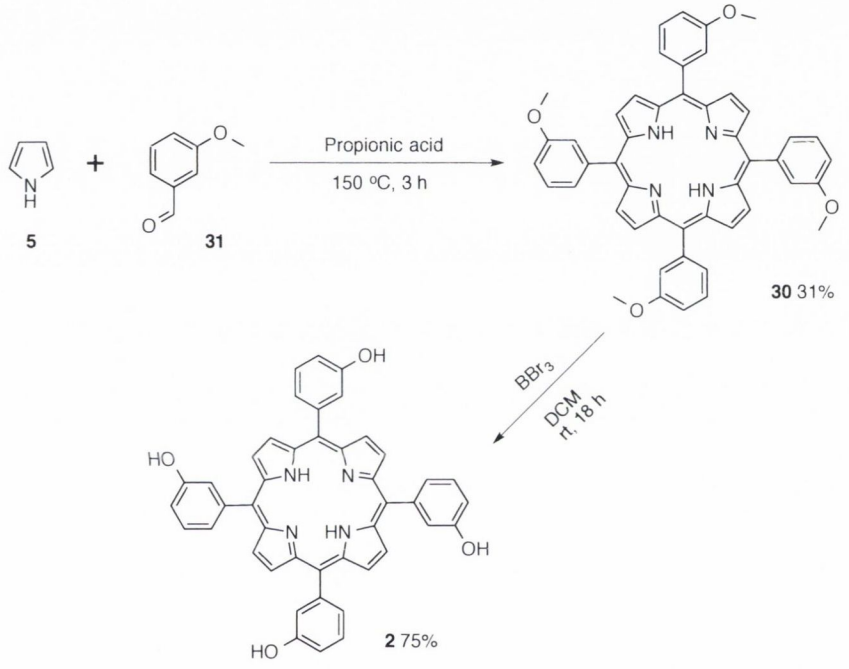

Scheme 2.6. Classical methodology for the synthesis of *m*-THPP [99,307].

The latter was the preferred route of choice for this synthetic pathway as one could quickly synthesize large quantities of the starting aldehyde with very small synthetic input in comparison to other strategies. The protection of the aldehyde followed known literature procedures and the production of the protected aldehyde was completed in high yields and simple purification [308]. From here, this aldehyde **32** was then used in a Rothemund condensation to yield a tetrasubstituted porphyrin **33** in 38% yield. Work-up ensued with the use of 1 M NaOH to liberate the free hydroxyl groups and produce porphyrin **2** in 80% yield (Scheme 2.7).

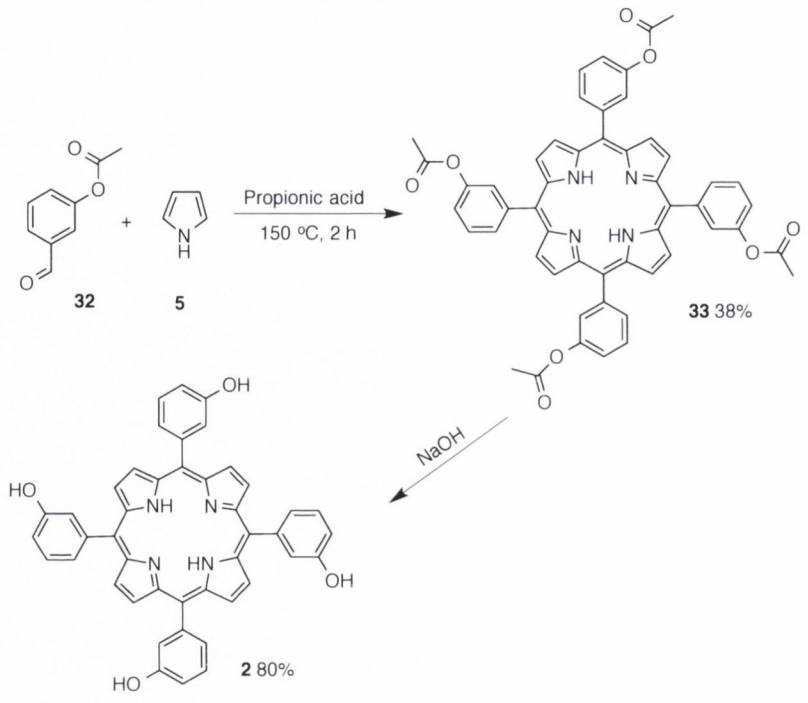

Scheme 2.7. Improved methodology for the synthesis of *m*-THPP [308].

With a large quantity of this PS scaffold now available, trial reactions were undertaken to install the alkyne functionality needed for the subsequent click reaction with the bile acid azide. Propargyl bromide (**34**) is a cheap and readily available reagent that can undergo nucleophilic substitution reactions in the presence of a good nucleophile and aprotic solvent. With respect to this proposed reaction pathway, the inherent difficulty lay with the presence of four equivalent hydroxyl groups being present in the scaffold and whether it was possible to functionalize one position with the propargyl group.

The start point for this investigation was the trialing of a number of different solvents and the use of an excess of propargyl bromide (**34**) to see if one could obtain the tetrasubstituted porphyrin derivative and also to investigate the influence of solvent on the reaction rate. By testing a number of different solvents, as per the table below, it was evident that dimethylformamide (DMF) (Entry 3, Table 2.1) outperformed the other solvents, with ethyl acetate (EtOAc) and tetrahydrofuran (THF) only producing small amounts of lower order functionalized porphyrin, i.e., mono-, di-, etc.. As the reaction was successful in producing the tetrasubstituted porphyrin in near quantitative yield, it suggested that through the careful monitoring of reaction time and equivalents, it would be possible to monofunctionalize the porphyrin scaffold in adequate yields.

Using DMF as the solvent and K_2CO_3 as the base, a number of reactions were run over a variety of reaction times and using a range of equivalents of propargyl bromide, as seen in Table 2.1. Analysis of the results taken from this initial study demonstrated that it was possible to install

one functional group onto the porphyrin periphery in a predictable manner. TLC analysis showed the presence of a predictable substitution pattern, i.e., as the level of substitution increases, so does the R_f in the solvent system used. Therefore, TLC analysis proved instrumental in monitoring the progress of the reaction and the extent of substitution occurring for each potential substituted porphyrin.

Based on TLC analysis and isolated yields after column chromatography, the initial unoptimized conditions which gave the best ratio of monofunctionalized material was 5 equiv. of propargyl bromide for 5 h in the presence of K_2CO_3. This methodology proved successful in the monofunctionalization of **35** in 18% yield (Table 2.1).

Table 2.1. Investigatory reactions into the mono-functionalization of *m*-THPP with propargyl bromide and subsequent metal insertion.

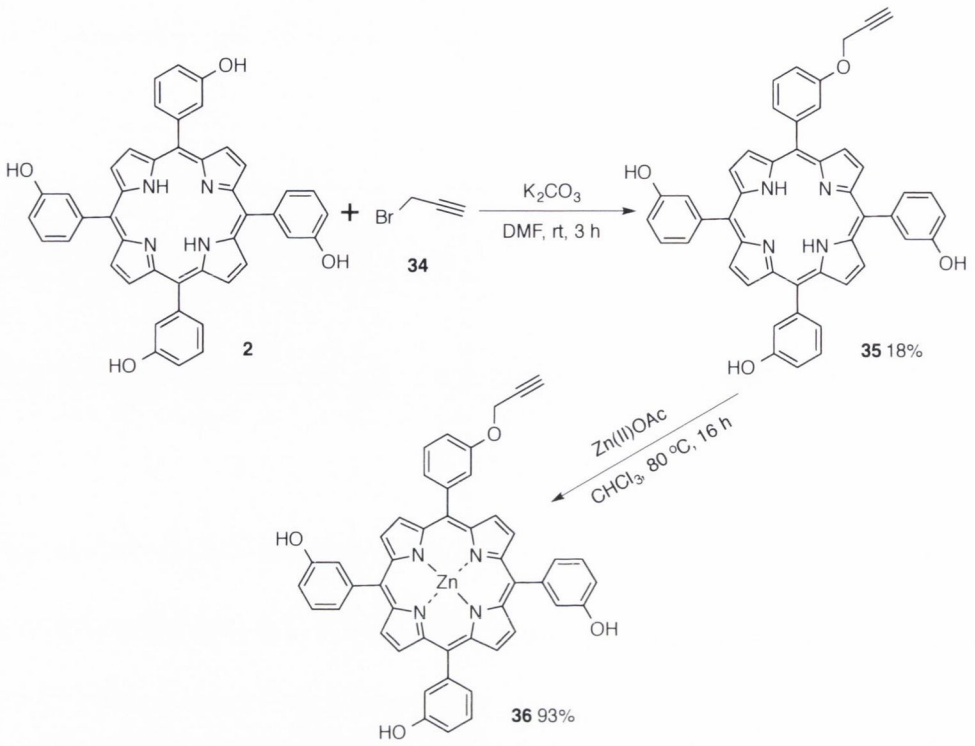

Entry	Base (Eq.)	Time (h)	Solvent	% Yield
1	K_2CO_3 (20)	18	EtOAc	3
2	K_2CO_3 (20)	18	THF	-
3	K_2CO_3 (20)	18	DMF	10
4	K_2CO_3 (20)	18	DCM	-
5	K_2CO_3 (20)	18	Acetonitrile	5
6	K_2CO_3 (10)	5	DMF	8
7	K_2CO_3 (7)	5	DMF	12
8	K_2CO_3 (5)	5	DMF	18

2.2.2 Further Optimization

A series of weak bases were first screened using DMF as a solvent with K_2CO_3 gave the most satisfactory yields. It was anticipated that by using a stronger base, it would be possible to reduce the amount of higher order substituted products in the crude reaction mixture and, therefore, drive the production of monofunctionalized material and ease the purification workload. Examples of this have been reported with regard to alkyl diol compounds, which would normally give a statistical mixture of isomers during attempts to obtain the

monofunctionalized product [257]. The dianionic species that is formed when NaH is used as the base showed a statistical bias towards the functionalization of only one hydroxy group in approximately 90 % yield. A number of bases were screened, with K_2CO_3 and NaH giving the best results for the reaction of **2** and propargyl bromide **34** (Table 3.1). Tests of different solvents indicate that DMF outperformed other candidates when NaH was used, and although it can be difficult to remove in workup, its superior yields far outweighed this drawback. The final factors to be optimized were reaction time and temperature. The reactions employed both optimized bases and propargyl bromide over a number of different time frames, and a reaction time of 2 h at room temperature was deemed most efficient for the monofunctionalization of *m*-THPP. [4]

[4] TLC analysis proved extremely reliable as an analytic tool, as each reaction consistently gave a predictable separation pattern.

Table 3.1. Investigatory reactions for the optimization of the mono-functionalization of *m*-THPP **2** and propargyl bromide **63**.

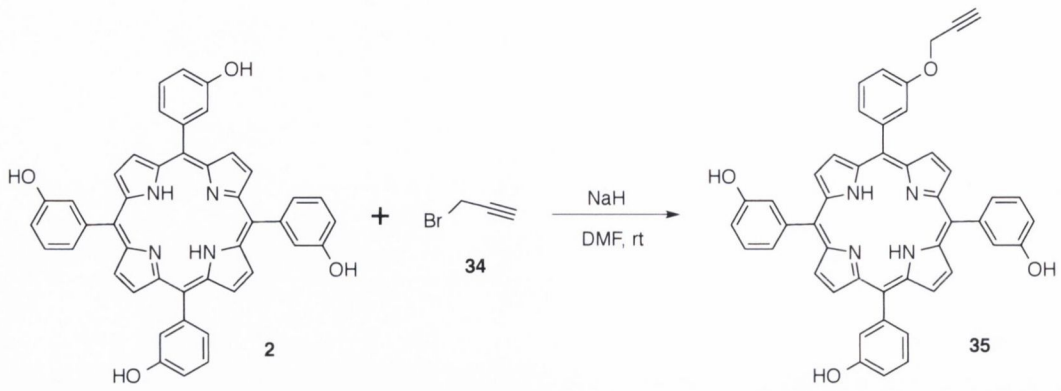

Entry	Base	Equivalents	Solvent	Time (h)	Temp °C	% Yield
1	K_2CO_3	5	DMF	5	r.t	18
2	K_3PO_4	5	DMF	5	r.t	14
3	TEA	5	DMF	5	r.t	15
4	K_2CO_3	5	DCM	5	r.t	-
5	K_2CO_3	5	Dioxane	5	r.t	-
6	K_2CO_3	5	EtOAc	5	r.t	2
7	K_2CO_3	4	DMF	3	r.t	35
8	K_2CO_3	2	DMF	2	r.t	48
9	K_2CO_3	0.5	DMF	2	50	15
10	NaH	1	DMF	2	r.t	45
11	NaOH	1	DMF	3	r.t	23
12	Superbase	1	DMF	2	r.t	15

The optimized conditions for the monofunctionalization of *m*-THPP with propargyl bromide included 1 equiv. of NaH as the base with 2 equiv. of propargyl bromide **34** in DMF at room temperature for 2 h, which resulted in a 45% yield of the product and 30 % of recovered starting material. Although sodium hydride gave a slightly lower yield than K_2CO_3, it was selected as the preferred option, as it produced a paucity of the higher substituted compounds. Higher substituted compounds were available by employing longer reaction times and increasing the equivalents of K_2CO_3 and propargyl bromide. Tetrasubstituted product **37** (Figure 3.2) was synthesized in near quantitative yield, with the di- and trisubstituted species available in yields similar to that of the monofunctionalized derivative. The results indicate that one can maximize the output of mono-, di-, tri-, and tetrasubstituted *m*-THPP by varying the reaction time, equivalents of reagents, and nature of base employed. The di- and trisubstituted derivatives were observed by TLC and confirmed by HRMS analysis, however, their syntheses and isolation have not been optimized within this current project. This demonstrates the

potential for a pathway to obtain complicated unsymmetrical porphyrin scaffolds in high yields, on both small and large scales, with inexpensive and accessible starting materials.

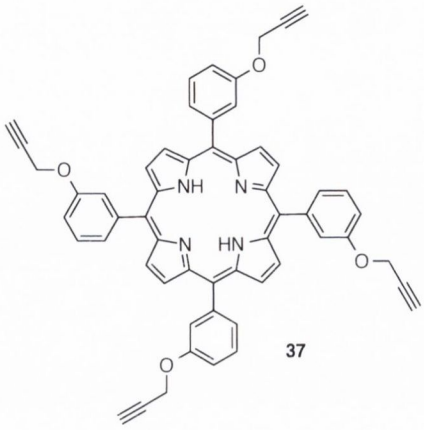

37

Figure 3.2. Tetrafunctionalized *m*-THPP derivative **37.**

2.2.3 Substrate Scope

To expand the scope of this synthetic methodology, a library of reactants were selected that were amenable to nucleophilic substitution chemistry but also contained a chemically distinct distal functional group that was available to use in subsequent functionalization reactions. A clear starting point to investigate the robustness of this method involved the installation of simple aryl or alkyl chains onto the parent *m*-THPP. Test reactions were carried out using 1-iodopropane and benzyl chloride. These reactions successfully afforded monofunctionalized porphyrin products **40a** and **41a**, in 35% and 44% yield, respectively, and again, by altering the reaction time and equivalents, higher order substituted products **40b** and **41b** could be obtained in good yields. The tetrasubstituted products could both be obtained in 95% yields (see Table 3.2).

Table 3.2. Synthesis of mono- and tetrafunctionalized *m*-THPP derivatives **40** and **41**.

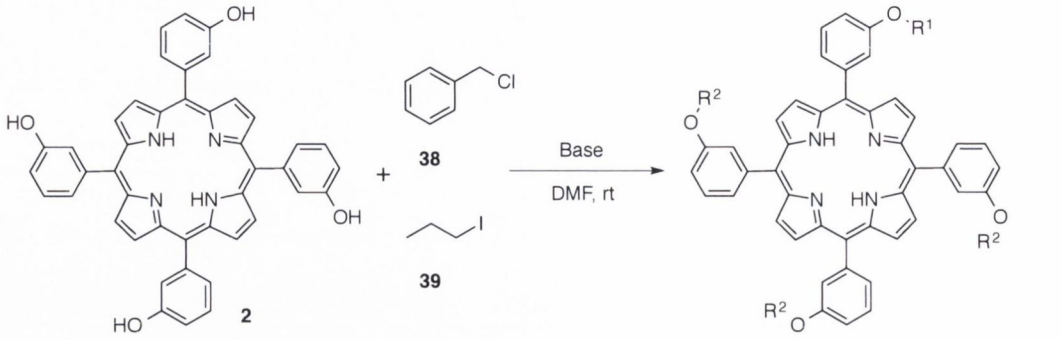

40a: R^1 = benzyl, R^2 = H, 35%
40b: R^1 = R^2 = benzyl, 44%
41a: R^1 = propyl, R^2 = H, 95%
42b: R^1 = R^2 = propyl, 95%

Prod.	Reagent	Base	Eq.	Time (h)	% Yield, mono (a)	Base	Eq.	Time (h)	% Yield, tetra (b)
40	1-iodopropane	NaH	1	2	35	K_2CO_3	10	13	95
41	4-Benzyl chloride	NaH	1	2.5	44	K_2CO_3	10	13	95

Whilst the tetrasubstituted derivatives may be obtained in good yields from a simple condensation reaction, the mono-functionalized compounds **40a** and **41a** would prove cumbersome to synthesize through historical routes due to difficult purification or lengthy stepwise pathways associated with these methodologies. Thus, the ease of introduction of these initial substrates in good yields showed promise for this compound as a scaffold and this synthetic pathway as an access point to more complicated PDT systems in few synthetic steps.

Following on from these simple synthetic systems, the complexity of the reaction products was then increased by installing functional groups that contained synthetically diverse substituents. The presence of these groups could then lend themselves to further functionalization reactions, i.e. the conjugation of biologically pertinent groups, such as in the case of the bile acid project [258]. 4-Bromobenzyl bromide **42** and 4-nitrobenzyl bromide **43** were chosen as suitable reagents to study the effect that peripheral substituents had on the reaction rate and yield. An excess of base and reagent where used to first ascertain whether a substitution reaction would indeed take place. TLC analysis after 18 h showed almost quantitative conversion of the starting material to the tetrasubstituted porphyrin derivatives. Subsequent work-up and simple recrystallization from CH_2Cl_2:Hexane gave the purified compounds in good yields, with NMR and high resolution mass spectrometry (HRMS) confirming the result observed by TLC.

From here, a number of optimization reactions were performed using reduced equivalents and time as to maximize the yield of the monofunctionalized derivatives. Using NaH as the base gave the best ratio of monofunctionalized material **44a** and **45a** to higher order derivatives,

along with a small portion of unreacted starting material, which again could be recovered during the chromatography step. As per Table 3.3, optimization of this pathway delivered the monosubstituted derivatives **44a** and **45a** in 43 and 35% yield, respectively, which indicated that there was a tolerance for different electronic substituents on the aryl ring. The *para*-bromo substituent allows for the possibility of further metal-catalyzed cross-coupling reactions, whilst the *para*-nitro group may undergo a reduction reaction to yield the free amine, which could then be used for amide couplings or again, metal-catalyzed cross-coupling reactions, e.g. Buchwald-Hartwig amination.

Table 3.3. Functionalization of *m*-THPP scaffold with aromatic groups containing distal functional groups capable of further substitution.

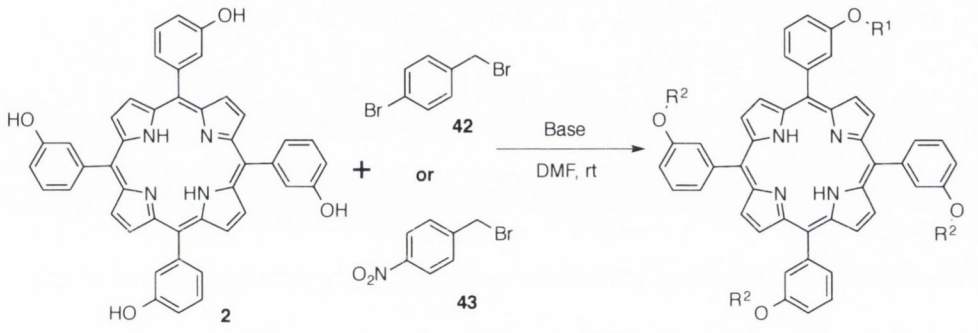

44a: R^1 = 4-bromobenzyl, R^2 = H
44b: R^1 = R^2 = 4-bromobenzyl
45a: R^1 = 4-nitrobenzyl, R^2 = H
45b: R^1 = R^2 = 4-nitrobenzyl

Prod.	Reagent	Base	Eq.	Time (h)	% Yield, mono (a)	Base	Eq.	Time (h)	% Yield, tetra (b)
44	4-bromobenzyl bromide	NaH	1	2	43	K_2CO_3	12	13	96
45	4-nitrobenzyl bromide	NaH	1	3	35	K_2CO_3	10	15	93

After the success of the above substitution reactions, it was necessary to consider other reactions that the free hydroxyl groups could undergo, e.g. controlled esterification of the peripheral OH groups present on the *m*-THPP scaffold **2**. To investigate this, benzoic anhydride **46** and 2-bromobenzoic acid **47** were used under various reaction conditions. Only slight modifications of the previously optimized conditions were needed for the coupling with benzoic anhydride due to the higher reactivity of the anhydride in comparison to the carboxylic acid (Scheme 3.1). Again, through careful monitoring of the reaction using TLC, one can produce the mono- and tetrafunctionalized derivatives **48a** and **48b** in satisfactory yields.

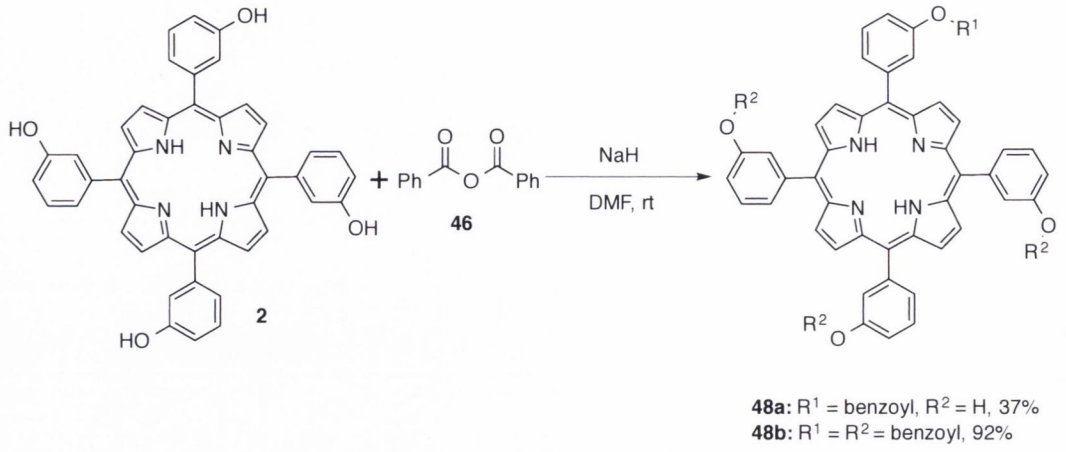

Scheme 3.1. Controlled functionalization of *m*-THPP **2** through esterification reactions with benzoic anhydride **46**.

Initial attempts with 2-bromobenzoic acid and the optimized methodology gave only unreacted starting materials in the reaction mixture (Scheme 3.2). From here, there were two viable routes one could take to achieve a coupling with this species of substrate (Scheme 3.3). The first would be to increase the reactivity of the carboxylic acid derivative through functional group interconversion to either the acid chloride or the acid anhydride derivative, which had worked in the previous example. The second pathway would involve the synthesis of activated ester species, a technique commonly used in peptide synthesis.

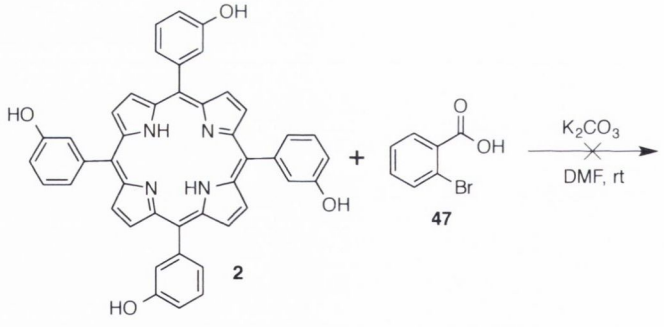

Scheme 3.2. Initial attempts to functionalize **2** with carboxylic acid **47**.

2-Bromobenzoic acid **47** was dissolved in neat thionyl chloride **49** and heated to 80 °C for 3 h. Subsequent distillation to remove excess thionyl choride yielded the desired acid reaction product, with spectroscopic data comparable to the literature values. This more reactive species was then implemented in a number of test reactions with the porphyrin scaffold **2** (Scheme 3.3).

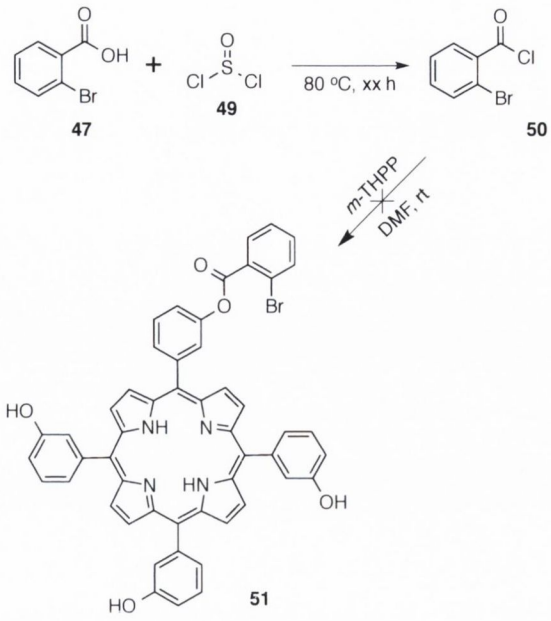

Scheme 3.3. Conversion of 2-bromobenzoic acid **47** to its acid chloride counterpart **50**.

Despite increased equivalents, reaction times and elevated temperatures, all attempts failed to obtain any substituted product, with only unreacted starting materials being recovered. Due to this lack of reactivity toward the acid chloride, it was decided to attempt reactions using the second pathway available, i.e., the synthesis of activated esters.

The Steglich reaction was discovered in 1978 as a method for the esterification of carboxylic acids [259]. It involves the use of dicyclohexylcarbodiimide (DCC) **52** as a coupling reagent and 4-dimethylaminopyridine (DMAP) **53** as a catalyst and can be run in a number of solvent systems. 2-bromobenzoic acid **47** was used with excess DCC and DMAP overnight at room temperature, to again, initially attempt the synthesis of the tetrasubstituted derivative. These conditions proved successful in forming the desired derivative, however, the yields were reduced due to the slow reaction time between the phenol and the activated ester species, with some material lost to a competing side reaction (Scheme 3.4).

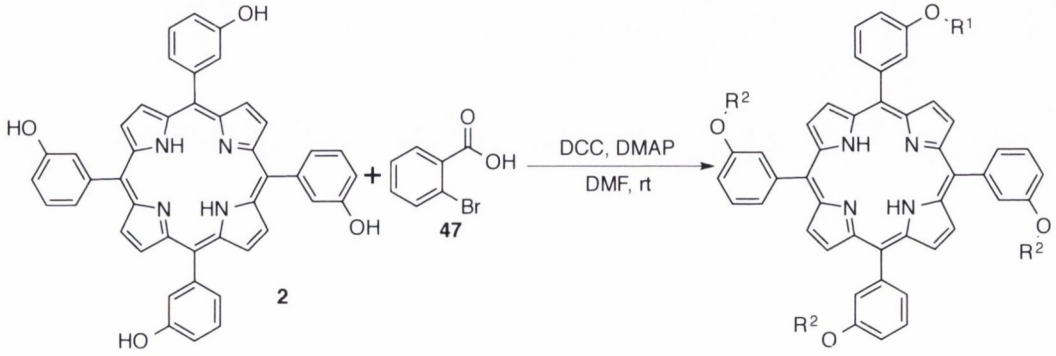

54a: R^1 = 2-bromobenzoyl, R^2 = H, 35 %
54b: R^1 = R^2 = 2-bromobenzoyl, 50 %

Scheme 3.4. Esterification of *m*-THPP using a modified Steglich reaction.

This side-reaction goes through a 1,3-rearrangement of the *O*-acyl intermediate **55** to a *N*-acyl urea, which is unable to further react with the alcohol in the reaction, however, one can suppress this undesirable rearrangement through the addition of surplus DMAP (Figure 3.3).

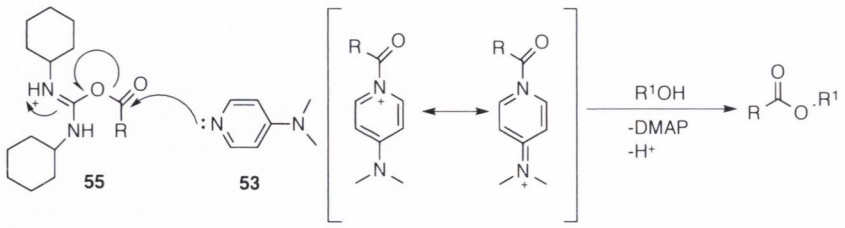

Figure 3.3. Addition of DMAP can suppress the 1,3-rearrangement of the *O*-acyl intermediate observed in the Steglich reaction.

Conditions were optimized for the controlled introduction of this substrate around the porphyrin scaffold yielding the mono- **54a** and tetrafunctionalized derivatives **54b** in good yields of 40% and 59%, respectively (Scheme 3.5). These results suggest the possibility to conjugate a myriad of biologically interesting moieties such as sugars, bile acids, and β-lactams, as the carboxylic acid functional group is present in many biological molecules, to this readily accessible porphyrin scaffold through an esterification reaction to create unsymmetric porphyrin systems of biological interest.

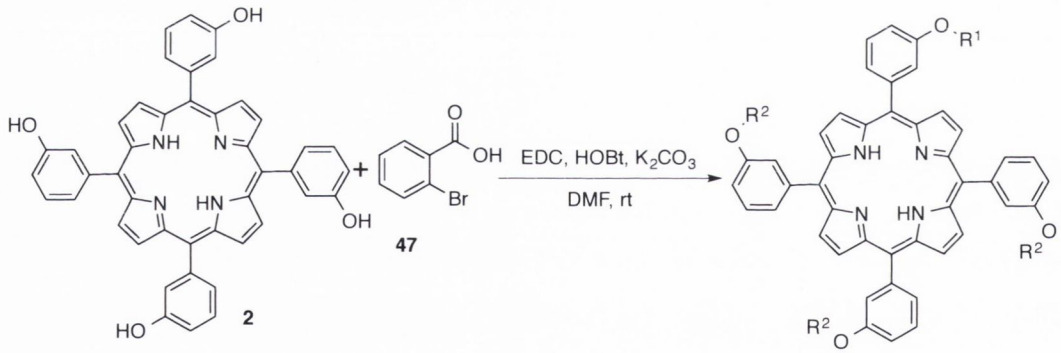

54a: R^1 = 2-bromobenzoyl, R^2 = H, 40%
54b: R^1 = R^2 = 2-bromobenzoyl, 59%

Scheme 3.5. Modified Steglich reaction for the controlled esterification of *m*-THPP **2** with a substituted aromatic carboxylic acid **47**.

It was decided to attempt the synthesis of *m*-THPP derivatives that could themselves become reagents in nucleophilic substitution and esterification reactions. The rationale behind this was that most biological groups contain heteroatoms and as such, will need suitable porphyrin coupling partners. To this end, two apposite coupling partners were again selected to attempt simple, cheap and controlled functionalization reactions with the porphyrin scaffold.

Compounds **56** and **57** were chosen to conduct initial test reactions. If successful, epichlorohydrin, **56** would transform *m*-THPP (**2**) into an electrophile for conjugation reactions with any heteroatom present in an appropriate biological or chemical coupling partner. As the reaction with benzyl chloride had worked, it was believed that a relatively similar primary alkyl halide, such as **56** would not suffer from lack of reactivity. Investigatory reactions begin with excess K_2CO_3 as a base in DMF and excess **56**, again in an attempt to synthesize the tetrasubstituted product, from which optimization work could be carried out to achieve the monofunctionalized scaffold in good yield (Scheme 3.6). These initial reactions proved to be unsuccessful in attaining any substitution product by TLC or NMR, with both starting materials being recovered after work-up. Despite an increase in equivalents and extensive reaction time, no product could be observed in the reaction mixture.

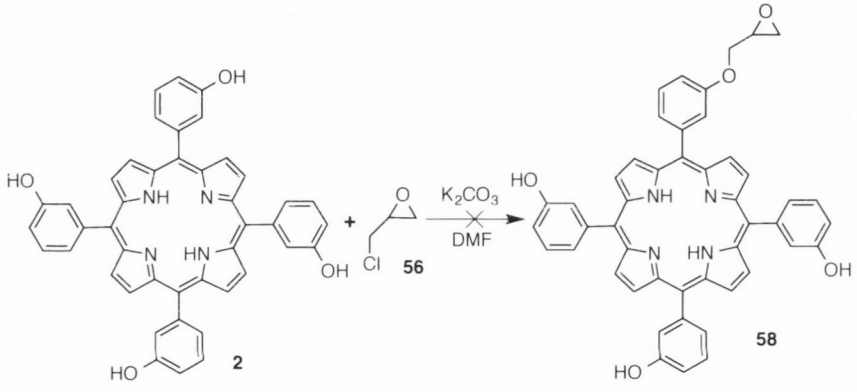

Scheme 3.6. Attempted functionalization of *m*-THPP with epichlorohydrin **56**.

Due to the unreactive nature of **56** for this methodology, limited options were available as the desired epoxide present in the molecule is sensitive to a number of different reactions and as it was hoped to keep the conditions mild as a preventative measure against any possible ring opening reactions that may take place. With respect to halide reactivity in nucleophilic substitution reactions, the general order or reactivity would be as follows: I>Br>OTf>Cl>F. The lower reactivity of the chloride derivative appears to be the only plausible reason for the drop in reactivity of this reaction pathway. To combat this, the reaction temperature was marginally increased from room temperature to 40 °C. This increase in temperature had a dramatic effect on the reaction pathway, with a number of new spots observed by TLC after 2 hours. These compounds appear to be closely related both structurally and chemically and despite multiple attempts, there was no preventing co-elution of a number of the spots. A reasonable explanation for this would be the added temperature allowed for the ring opening of the sterically strained epoxide group, leading to a mixture of ring opened and closed derivatives that have near identical R_f values (Figure 3.4).

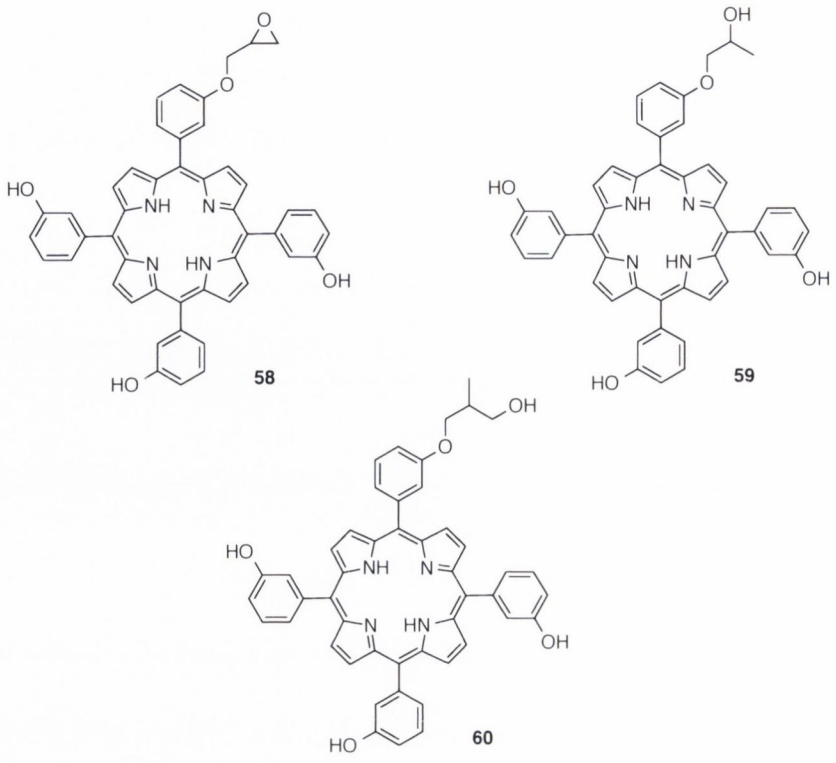

Figure 3.4. Variety of different possible isomers resulting from the functionalization of **2** with epichlorohydrin **56**.

Whilst the bromo-derivative may have improved the reactivity and therefore the potential for success, the potential for a ring-opening reaction and other drawbacks out-weighed the positives of this compound as a substrate for this set of nucleophilic reactions. Also, while this pathway would have provided another degree of accessibility for researchers to install functional groups, there are other options available such as the addition of carboxylic acids. The controlled functionalization of the porphyrin scaffold with a carboxylic group would allow for the conjugation of biologically pertinent molecules in greater yields and fewer steps then the alternative mixed condensation and total synthesis pathways.

A simple short-chained alkyl halide carboxylic acid was selected to begin the test reactions for this possible synthetic pathway. Excess 5-bromovaleric acid **48** was added to a flask containing DMF and K_2CO_3 as the base, in a similar fashion as to before (Scheme 3.7). TLC analysis displayed no indication of a reaction having occurred and even after increased time and equivalents, no reaction was taking place. It was postulated that the carboxylic acid may in fact be interfering with the reaction and a possible method to circumvent this disruption would be to synthesize the corresponding ester derivative. This solution was tested after the conclusion of this project by another member of the group, Dr. Aoife Ryan, for a different project that necessitated long-chain alkyl carboxylic acids linked to a porphyrin [260]. Again, mono- to tetrafunctionalization is possible through the monitoring of reaction time and equivalents (Scheme 3.8).

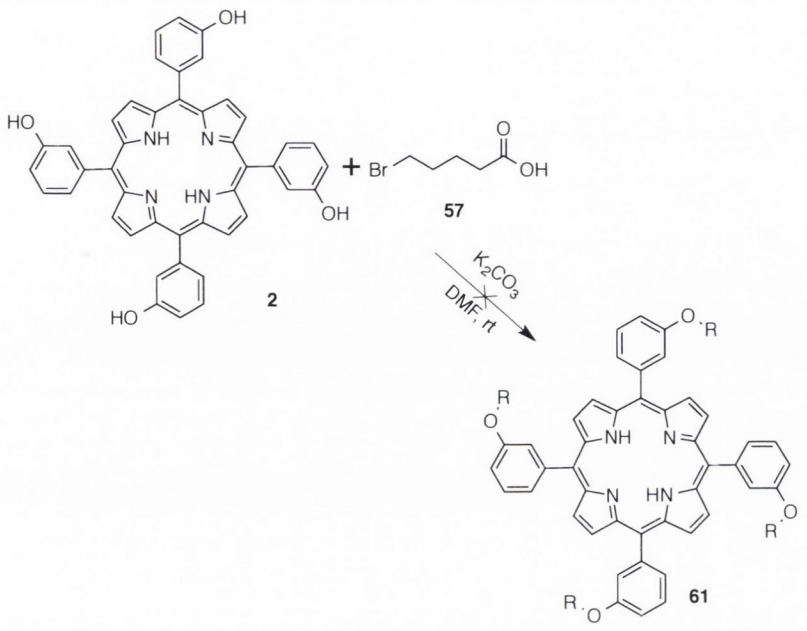

Scheme 3.7. Attempted functionalization of *m*-THPP with an alkyl carboxylic acid **57**.

These final functionalization reactions concluded initial investigations into the robustness of this synthetic pathway for different distal functional groups as well as different functionalization techniques i.e., nucleophilic substitution and esterification reactions. The *m*-THPP scaffold appears to be extremely tolerable of different substrates and functional groups and through careful controlling of the equivalents and reaction time, one can functionalize this porphyrin in a controlled fashion with a litany of different groups in good yields.

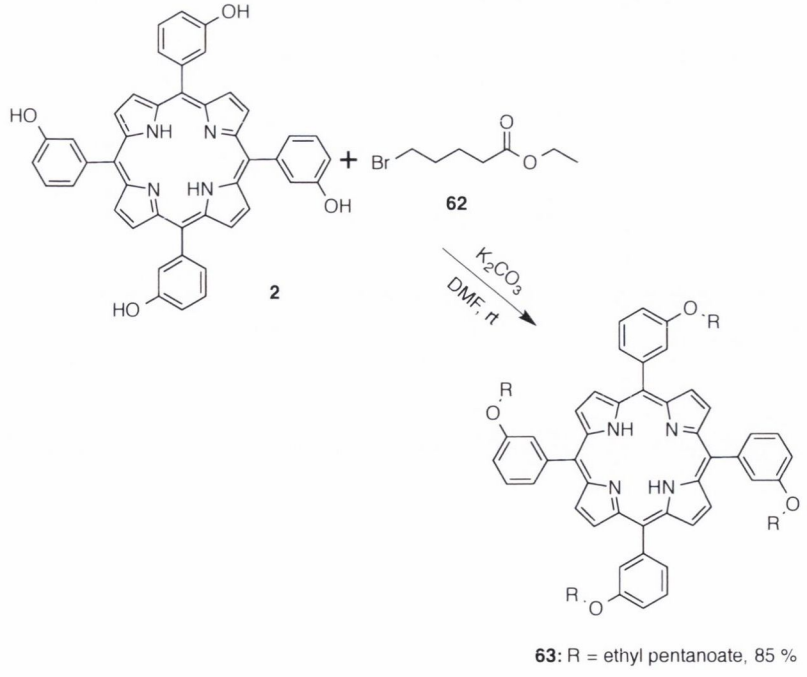

63: R = ethyl pentanoate, 85 %

Scheme 3.8. Successful functionalization through the use of an ethyl ester derivative **62** of **57** [260].

2.2.4 Conversion of *m*-THPP to a Coupling Partner for Suzuki Reactions

It was hoped to expand this new methodology to contemporary chemistry, such as metal-catalyzed cross coupling reactions. Two such approaches were the direct metal-catalyzed coupling of the heteroatom to a substrate or the transformation of an hydroxyl group into a functionality that is susceptible to palladium-catalyzed reactions, such as the Suzuki–Miyaura cross-coupling reaction. Recent and classical publications have shown the capability of triflate and tosylate groups to react in metal-catalyzed cross-coupling reactions under a variety of different conditions and with a number of different catalysts and substrates, with the most widely known of these being the triflate group in Suzuki–Miyaura coupling reactions [261,262]. Previously optimized conditions were implemented to synthesize a range of "activated" *m*-THPP derivatives, which could be selectively functionalized in a controlled manner in a similar fashion to the nucleophilic substitution reactions.

Initial investigations began using the previously optimized conditions. Excess base and substrates **64-65** were used to again investigate if the reaction would occur and from there, an optimization of reaction conditions would give the desired mono-functionalized material **66**. The triflic anhydride **64** outperformed trifluoromethanesulfonyl chloride **65** in the initial investigatory reactions (Scheme 3.9). However, its cost and difficulty of handling far exceeded the greater yield achieved in comparison to trifluoromethanesulfonyl chloride **65**.

Thus, initial reactions began with trifluoromethanesulfonyl chloride **64** and 4-toluenesulfonyl chloride **67** produced the functionalized scaffold, however, conversion to the desired substituted porphyrin using K_2CO_3 was very low.

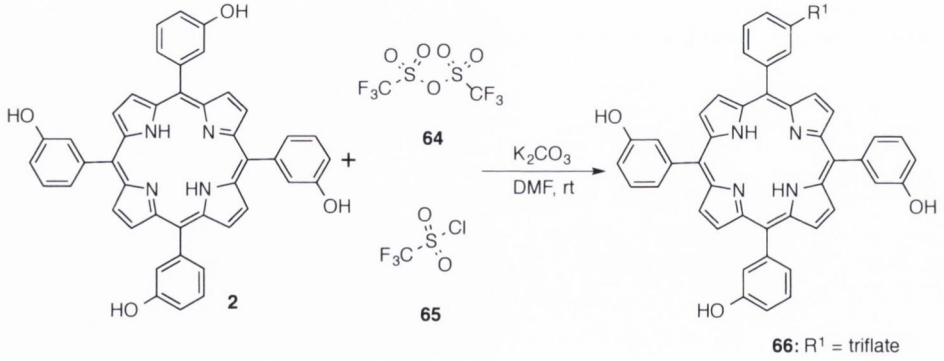

Scheme 3.9. Investigatory reactions into the different reactivities provided by triflic anhydride **64** and trifluoromethanesulfonyl chloride **65**.

Maintaining DMF as the solvent of choice for this reaction, a number of bases were screened, as the strength of the base may be the contributing factor to the lack of reaction taking place. As seen from Scheme 3.10, upon changing the base to pyridine, both trifluoromethanesulfonyl chloride and 4-toluenesulfonyl chloride gave porphyrins **66a** and **68a** in 37 and 35% yield, respectively. Again, by increasing the equivalents of reagent and base, the tetrafunctionalized

derivatives were obtained in excellent yields (for **66b**, 92% yield and for **68b**, 90% yield; see Scheme 3.10).

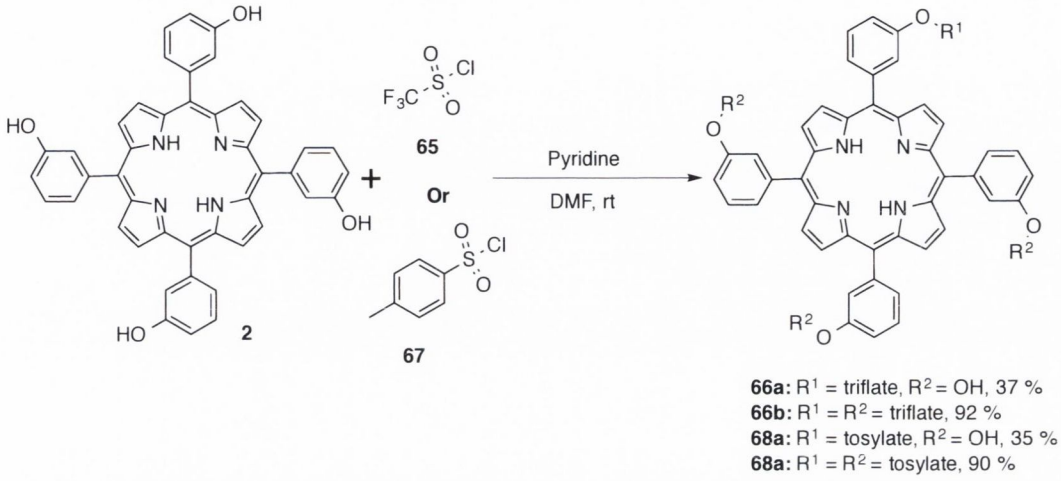

Scheme 3.10. Improved coupling conditions for the controlled installation of both triflate and tosylate groups around the porphyrin periphery.

After the synthesis of activated hydroxyl species for future functionalization reactions through metal-catalyzed cross-coupling reactions, it was decided to investigate the possibility of functionalization through direct coupling reactions involving a phenolic OH and a suitable substrate. By using a metal-catalyzed reaction, it was hoped that one could achieve even greater selectivity for the monosubstituted porphyrin with higher order substitution derivatives presenting as only minor side products.

2.2.5 Metal-catalyzed Couplings

In recent times, a number of reactions have been developed that involve a hydroxyl functional group undergoing a reaction with another specific substrate in the presence of a metal catalyst. Examples include the Buchwald–Hartwig reaction,[263,264] the Ullmann reaction [265] and the Chan–Lam reaction (Figure 3.5) [266]. It was decided to take a number of the aforementioned reactions and conduct trial couplings using each method and after analysis of the reactions, select one to go forward as the example of direct metal-catalyzed coupling with *m*-THPP.

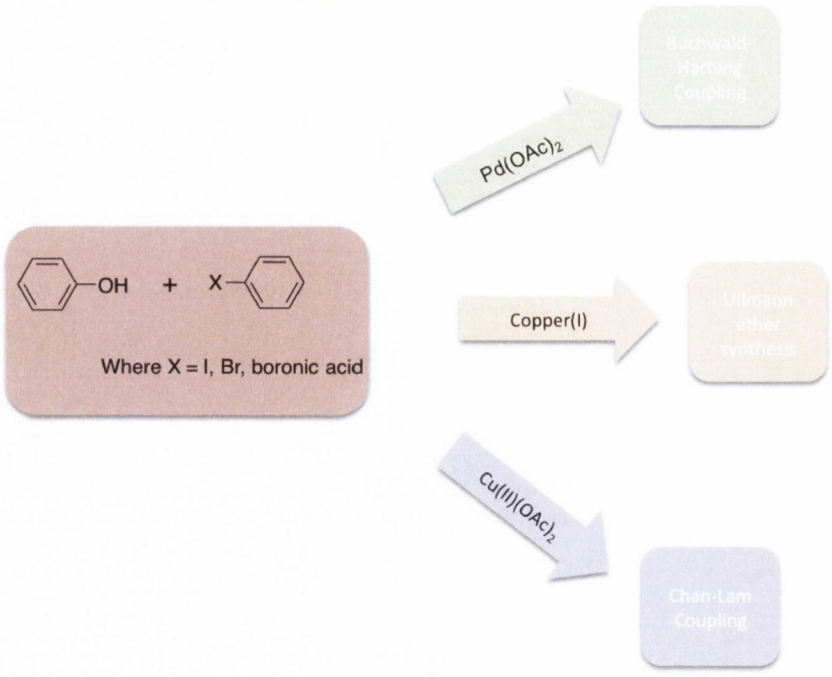

Figure 3.5. A range of different metal catalyzed couplings amenable to heteroatoms.

The Chan–Lam reaction showed the most promise in terms of yield, reaction conditions, and purification. The reaction involves the use of copper(II)acetate, a boronic acid, and a hydroxy or amine functionality. It is a versatile reaction, as it can proceed in a number of different solvents, at room temperature, and in an open reaction vessel. The reaction uses a stoichiometric amount of copper, and, hence, metalloporphyrins were used to avoid copper insertion. First, zinc(II)porphyrin **69** [267,268] was treated with phenylboronic acid (**70**) in dioxane at room temperature. After stirring for 18 h, TLC showed the formation of **71** as the major product (39 % yield) and two faint, closely running spots, which turned out to be the two disubstituted species. After this first example of a Chan–Lam coupling being applied to a porphyrin system, 4-cyanophenylboronic acid **72**, 3-methoxyphenylboronic acid **73**, and 2-iodophenylboronic acid **74** were implemented as examples of systems that are amenable to postfunctionalization reactions. These reactions produced the monofunctionalized species **75**, **76** and **77** were synthesized in 35, 37 and 33% yield, respectively (see Table 3.4). All four boronic acids produced satisfactory yields and correlates with the perceived literature opinion that this reaction is tolerant of a variety of substrates under mild reaction conditions.

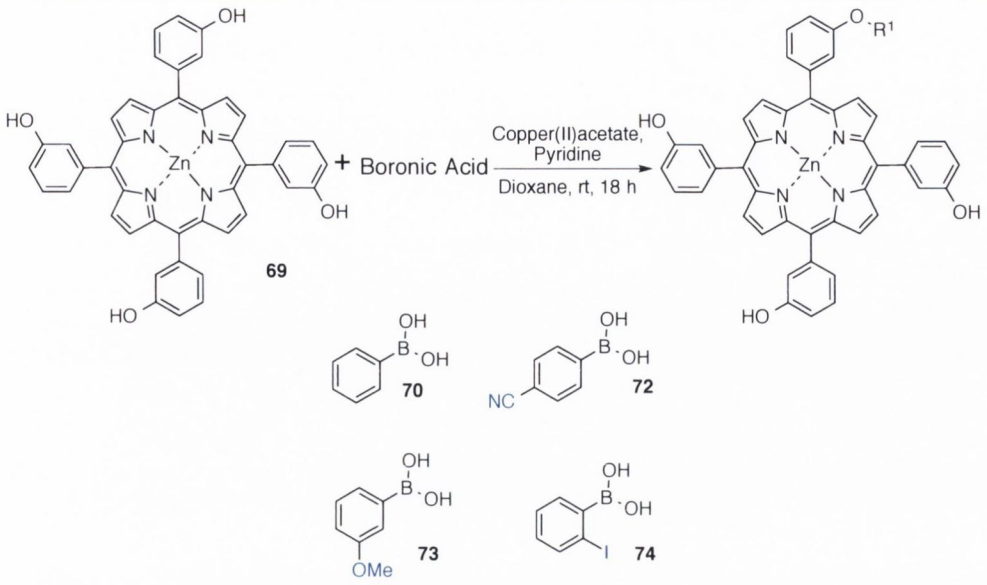

Table 3.4. A library of directly mono-functionalized *m*-THPP derivatives synthesized through Chan-Lam methodology.

Product	Boronic acid	Equiv.	Time (h)	% Yield Mono
71	34	1	13	39
75	36	1	18	35
76	37	2	13	37
77	38	2	24	33

This provides another synthetic pathway to unsymmetrical porphyrin scaffolds by using a simple, readily available, preformed symmetric porphyrin scaffold. Boronic acids are easily installed into compounds through standard synthetic methodology [269], and, therefore, they present the potential for a wide variety of molecules to be conjugated to these porphyrins. Although the reactions above expand the synthetic toolkit for porphyrins, a demonstration of their practical utility in the synthesis of unsymmetrical porphyrins or more complicated systems might be warranted.

2.3 Post-functionalization Reactions

To demonstrate the practical utility of this methodology, attempts were made to synthesize a number of unsymmetrical porphyrin derivatives using the synthetic handles previously installed onto the *m*-THPP scaffold. There were a number of extremely attractive applications that one could attempt to tailor these scaffolds for; however, multi-chromophore arrays for light-harvesting and porphyrin model compounds were selected. Sessler *et al.* were able to synthesize a porphyrin-fullerene pentamer that displayed excellent photophysical results [270]. Nevertheless, this system required multiple-steps, with quite a low overall yield as it relies on a

concurrent four-fold Sonogashira reaction to install the porphyrin antennas around the central porphyrin scaffold (Figure 3.6).

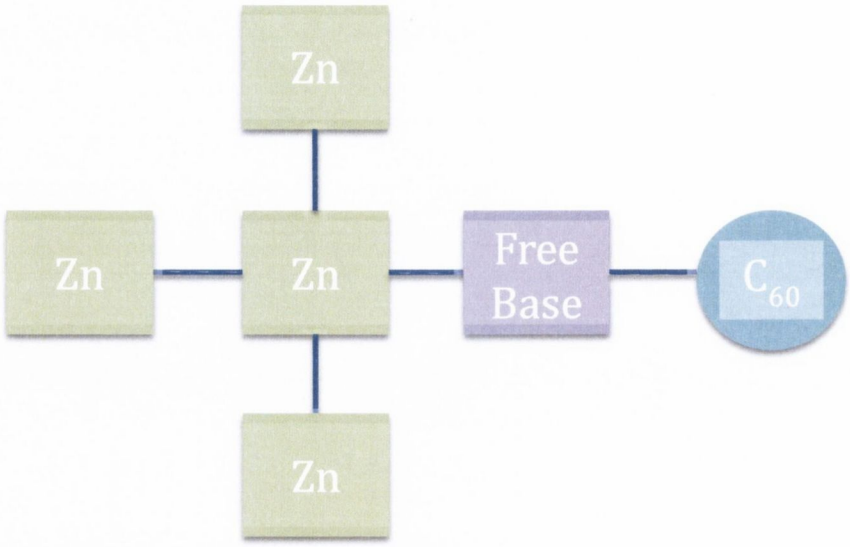

Figure 3.6. Diagrammatic representation of Sessler's porphyrin-C_{60} pentamer.

From a synthetic viewpoint, one can quickly draw parallels between this system and the *m*-THPP scaffold designed above, and as such, it may be possibly to take the *m*-THPP scaffold **2** and functionalize its periphery with the desired porphyrins to make this synthetic antenna complex in good yields and few synthetic steps. To start this synthesis, it was decided to initially mimic the original antenna complex as much as possible. This meant revisiting the infancy of this project, i.e., the tetra alkynyl porphyrin **37** and reacting it with a suitable bromo-porphyrin.

2.3.1 Synthesis of Bromoporphyrins

The porphyrins required were synthesized in an identical fashion to Chapter **2**, as per Scheme 3.11. The trisubstituted porphyrins underwent bromination reactions to yield the A_2BC porphyrins. Brominations of porphyrins can be carried out by numerous methods,[271-273] and involve an electrophilic aromatic substitution (S_EAr) reaction pathway. There are two sites where S_EAr in porphyrins can occur, the meso and β-positions, with preferential substitution at the more reactive meso positions. The most utilised bromination methods involve the use of molecular bromine (Br_2) or *N*-bromosuccinimide (NBS) in chlorinated solvents, the latter of which is preferred for meso-bromination. As such, the 5,10,15-A_2B **78** porphyrin required was brominated using NBS following the standard literature procedure [274] forming brominated porphyrin **79** [275] in 89% yield. Finally, metal insertion following procedures discussed previously produced the desired zinc(II)porphyrin (**119**) in near quantitative yield.

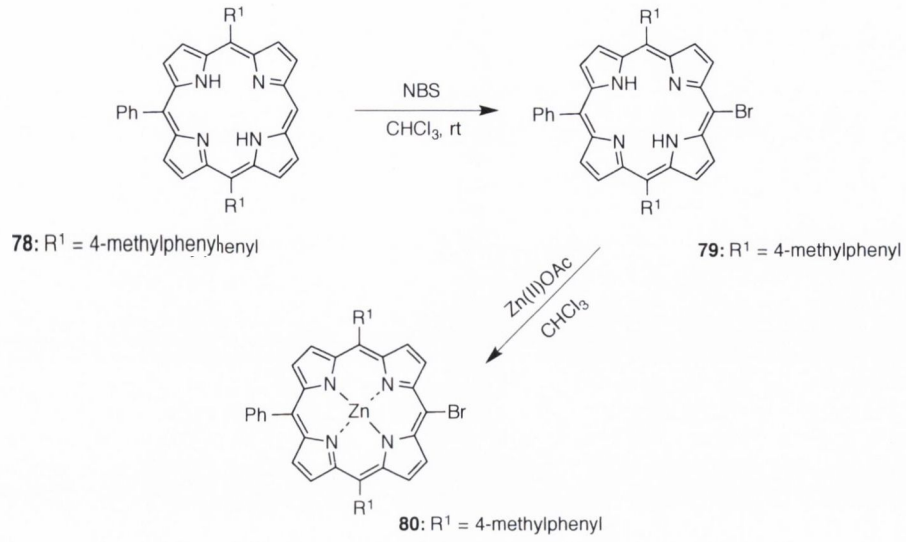

Scheme 3.11. Synthetic pathway for the bromination and subsequent metal insertion of the required A_2BC porphyrin **80**.

With porphyrin **80** in hand, investigatory reactions could begin for the synthesis of this porphyrin pentamer. The first reaction undertook followed the literature standards for Sonogashira reaction conditions, i.e., $PdCl_2(PPh_3)_2$ and CuI in the presence of an amine base. The reaction was quenched after 18 h as per Scheme 3.12 and TLC analysis showed the formation of a number of new spots with the complete consumption of the starting material. After a work-up involving washes with NaCl and $NaHCO_3$ the crude material underwent column chromatography with an eluent system of CH_2Cl_2:*n*-hexane:MeOH (3:1:0.2). Whilst the UV-vis of the reaction mixture showed a bathochromic shift compared to the starting material, the products isolated showed spectra identical to *m*-THPP.

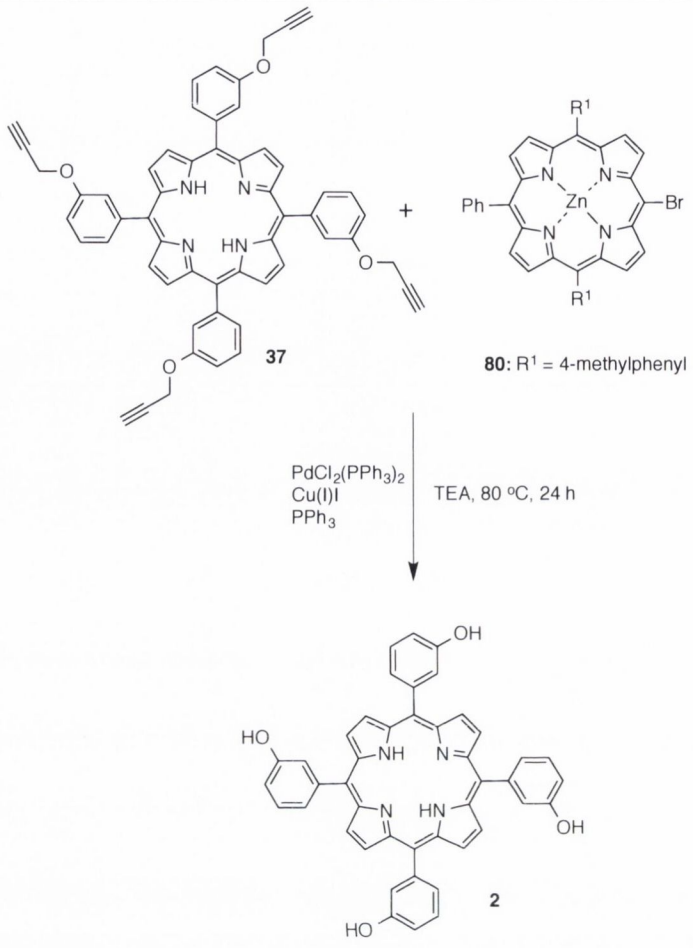

Scheme 3.12. Attempted synthesis of porphyrin pentamer through a Sonogashira coupling.

This reaction was reattempted using a number of different catalyst loadings, amine bases and reaction times in an effort to gain a synthetic insight into what was occurring during the reaction. There was a consistent production of new material as per TLC and NMR, with the complete consumption of the starting material. These new compounds all exhibited a lower R_f, which would be expected from large multi-chromophore arrays such as these. Whilst the alkyne was used with a source of copper(I) implemented previously for the synthesis of triazole adducts, upon consultation of the literature, it appears that *O*-propargyl groups readily cleave in the presence of palladium and this fact has even been exploited in modern synthesis, i.e., using it as a protecting group in natural product synthesis [276]. The new products observed during the TLC analysis were in fact the reversal of the functionalization work, i.e., the systematic cleavage of the propargyl groups to give the tri-, two di- and monosubstituted derivatives of *m*-THPP.

Despite this setback, there were still a number of available options as to how to install the alkyne group needed for this type of reaction pathway. One such method was the use of the modified Huisgen click reaction implemented in Chapter 2, substituting the bile acid azide for an

azidoporphyrin. Triazole systems such as these have been synthesized previously for the construction of light-harvesting reaction centre mimics [277,278]. Another possible synthetic strategy would be to use the Chan-Lam coupling conditions optimized previously with 4-[(trimethylsilyl)ethynyl]phenylboronic acid, and subsequent cleavage of the TMS-protecting group would leave the free alkyne. However, whilst possible, this was adding synthetic complexity to this reaction pathway and as simple post-functionalization examples were desired to demonstrate the utility of this new methodology. Therefore, it was decided to explore the alternative potential applications of these scaffold systems, i.e. the use of porphyrins as model systems. Somewhat arbitrarily, picket fence porphyrins and cofacial bis(porphyrin)s were selected as case materials.

2.4 Case Study 1: Picket-Fence Porphyrins

Picket fence porphyrins are a classic example of the impact of biomimetic model compounds. They became very much *in vogue* for many years after their first reported synthesis by Collman *et al.* in the 1970s as they provided researchers the first synthetic model with which to investigate the binding of O_2 in heme proteins [230,231,279,280]. Large libraries of these picket fence porphyrins were synthesized, but depending on the route selected, their syntheses required a large number of steps, challenging chromatographic purifications, and low yields.

The synthesis for this project began with the use of simple tetrasubstituted porphyrins as examples of picket fence porphyrins. Scaffold **2** was treated with1-iodohexane **81** or 4-*tert*-butylbenzyl **82** bromide under the optimized conditions to give porphyrins **83** and **84** (see Scheme 3.13). These reactions proceeded to give the desired product in quantitative yield; however, systems such as these can also be easily prepared through condensation methods.

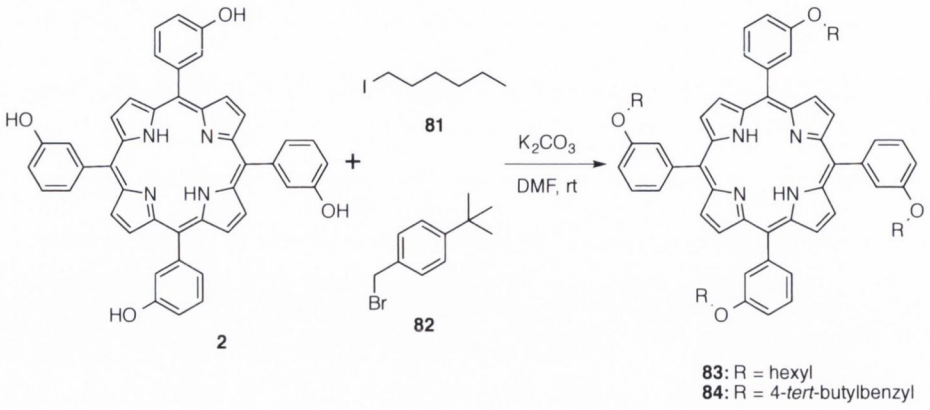

Scheme 3.13. Initial synthetic pathway for the construction of picket-fence porphyrin mimics **83** and **84**.

Tailored picket fence porphyrins may contain an imidazole arm that could bind to the iron metal centre. To mimic this type of unsymmetrical system, more complicated examples related to A_3B-type porphyrins were targeted. By reducing the equivalents and reaction times, trisubstituted species from both 1-iodohexane and 4-*tert*-butylbenzyl bromide were successfully synthesized in yields of 37 and 40% respectively. Once the trisubstituted species **85** and **86** were isolated from the reaction mixture, the final free OH group was subjected to a reaction, with propargyl bromide being selected as it had performed the best in the initial substrate investigations. This reaction proceeded in high yield and produced the stable picket fence porphyrin mimic **87**, that is, an A_3B-type porphyrin with two different "fence types". Thus, by taking **2** as the starting material, a synthetically difficult class of porphyrin was produced in two steps by using simple and cost-effective chemistry in far greater yields than the alternative mixed condensation or total synthesis route. By applying this approach to *o*-THPP,[281] the synthesized compounds could potentially undergo a resolution of the atropisomers to afford the α,α,α,α-derivative, that is, a true picket fence porphyrin.

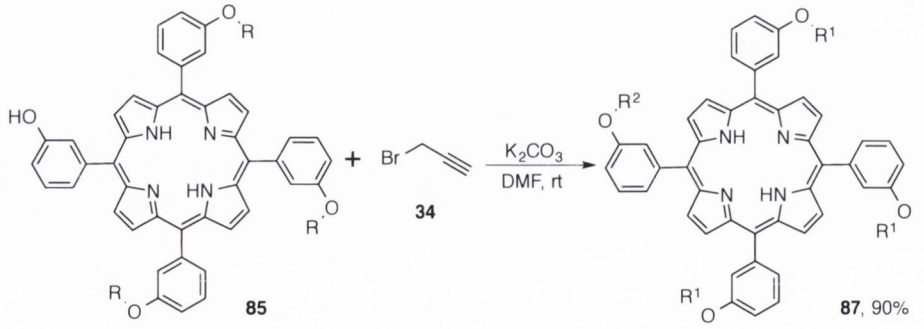

Scheme 3.14. Synthesis of the A_3B picket-fence porphyrin mimic **87**.

2.5 Case Study 2: Co-facial Porphyrins

Another example of a porphyrin system that is frequently used in model studies is porphyrin arrays and, notably, cofacial bis(porphyrin)s. These serve as metalloenzyme [223,282] or special pair mimics in photosynthesis [283,284] and are suitable models for multielectron redox reactions. Again, many of these require lengthy syntheses, can typically contain unstable amide linker groups, and suffer from low yields. It was hoped to extend the previously developed synthetic approach and apply it to the construction of three-dimensional cofacial porphyrin cages [285].

Initial reactions for this synthesis again began with the tetraalkyne scaffold. The co-ordination properties of porphyrins have been extensively studied and researchers have been successful in creating "cofacial" porphyrin systems through the use of bidentate ligands such as 4,4'-bipyridine [201]. One such method for systems like this was the popular field of 'sandwich porphyrins', synthesized through the use of lanthanide metals as the bis-coordinating metal ligand. It was hoped that if one could use a lanthanide ion to co-ordinate the porphyrins into a sandwich-like structure, then the corresponding alkynes would be in the correct orientation to undergo an intramolecular Glaser coupling to yield the caged bisporphyrin (Figure 3.7).

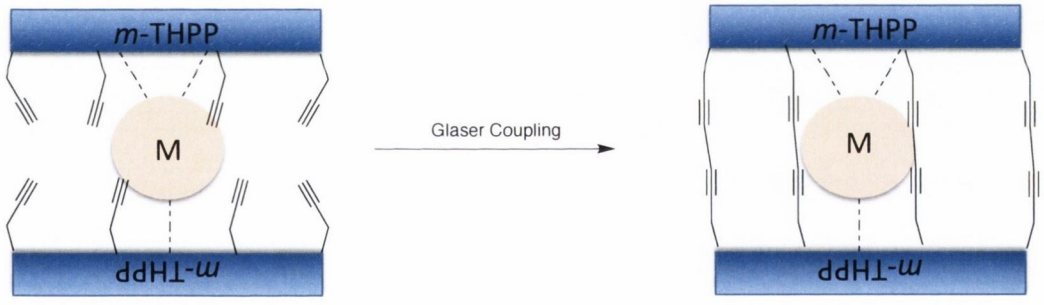

Figure 3.7. Diagrammatic representation of the potential sandwich porphyrin pathway to yield co-facial bis(porphyrin)s.

The synthesis of this class of compounds can suffer from a number of drawbacks, such as extreme sensitivity to aerobic conditions and cumbersome chromatography. Whilst, using a previously synthesized scaffold would have been the ideal route, a literature search gave alternative routes to similar non-porphyrin systems that could be attainable through the newly developed methodology [286]. By using alkyl chains, it was hoped that a degree of flexibility could be imparted into the cage system to enable the molecule to adopt the optimum metal-metal distance that is needed for catalytic activity or substrate binding. The synthesis proceeded again with **2** as the starting material. Treating **2** with an excess amount of 1,4-dibromobutane **88** with K_2CO_3 as the base afforded tetrasubstituted compound **89** in near quantitative yield. The resultant primary alkyl bromide can then undergo another simple nucleophilic substitution reaction with 1 equiv. of [5,10,15,20-tetrakis(3-

hydroxyphenyl)porphyrinato]cobalt(II) [Co(II)*m*-THPP, **90**](Scheme 3.15) to afford cofacial bis(porphyrin) **91** with a free base and cobalt(II) porphyrin unit in a yield of 12% (Scheme 3.16). The use of a cobalt porphyrin to synthesize the cage was to exemplify the ease to make this method applicable for the synthesis of potential four-electron catalysts.

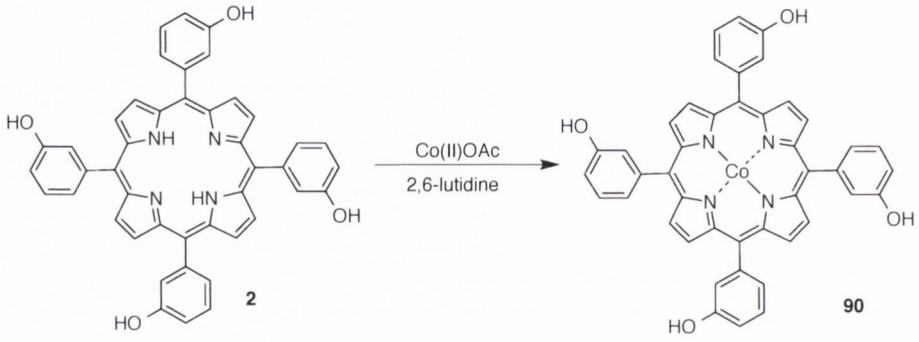

Scheme 3.15. Metal insertion of Cobalt into the *m*-THPP core.

This simple synthesis can be modified to incorporate linkers of different lengths and types, whilst also being amenable to different metal systems, thus, other applications such as the synthesis of artificial photosynthetic reaction centers are possible [201]. The salient strength of this synthetic pathway is the choice of almost any metal center for the porphyrin core along with the option of having mixed metal centers or even co-facial free base versus metalloporphyrins along with a variety of different linkers, all of which are examples of reduced symmetry cage systems. These historically difficult compounds can now be made in two steps by using simple, inexpensive, and reliable chemistry, again from a cheap and accessible preformed scaffold [287].

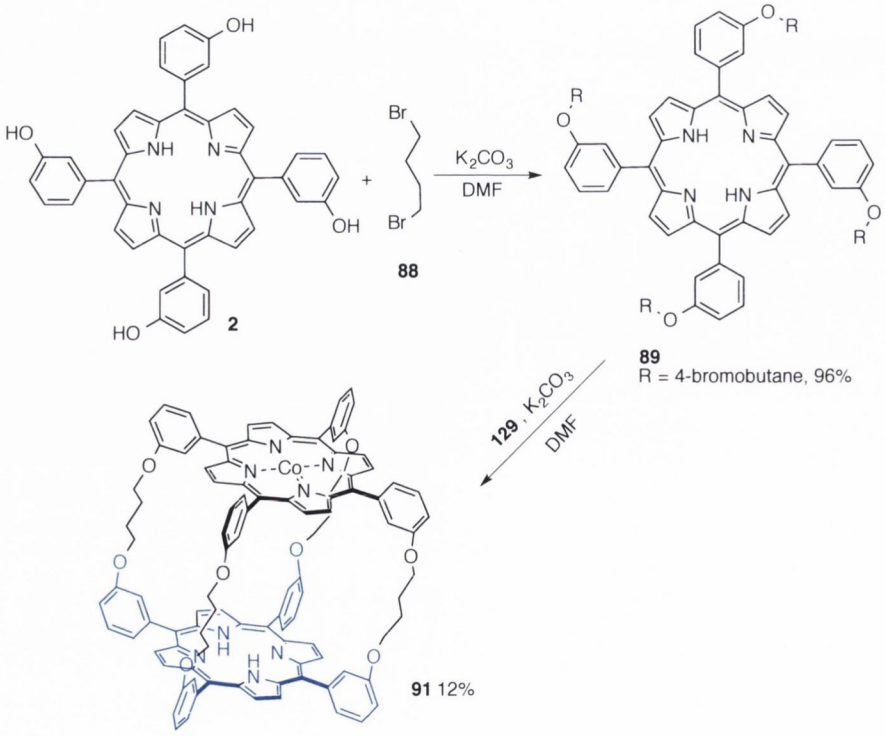

Scheme 3.16. Construction of co-facial porphyrin cages through simple substitution chemistry.

2.6 Conclusions & Future Work

2.6.1 Conclusion

A library of monosubstituted *m*-THPP derivatives were successfully prepared through a number of simple reactions pathways. By using historic phenolic chemistry, compounds were synthesized through nucleophilic substitution, esterification, and OH activation reactions. This chemistry was updated for porphyrins by using the recently discovered Chan–Lam copper-catalyzed coupling of a heteroatom with a boronic acid. This allowed for the synthesis of some simple, unsymmetrical porphyrin systems and demonstrated the ease with which one can quickly generate historically cumbersome compounds such as picket fence and cofacial porphyrins in few synthetic steps. Although this is certainly not a "*conditio sine qua non*" for the optimum preparation of unsymmetrical porphyrins, it presents a rapid, robust, and cost-effective strategy for the synthesis of a variety of soluble, unsymmetrical porphyrins that can be fine-tuned for a plethora of applications by starting from one symmetric parent porphyrin scaffold (Figure 3.8).

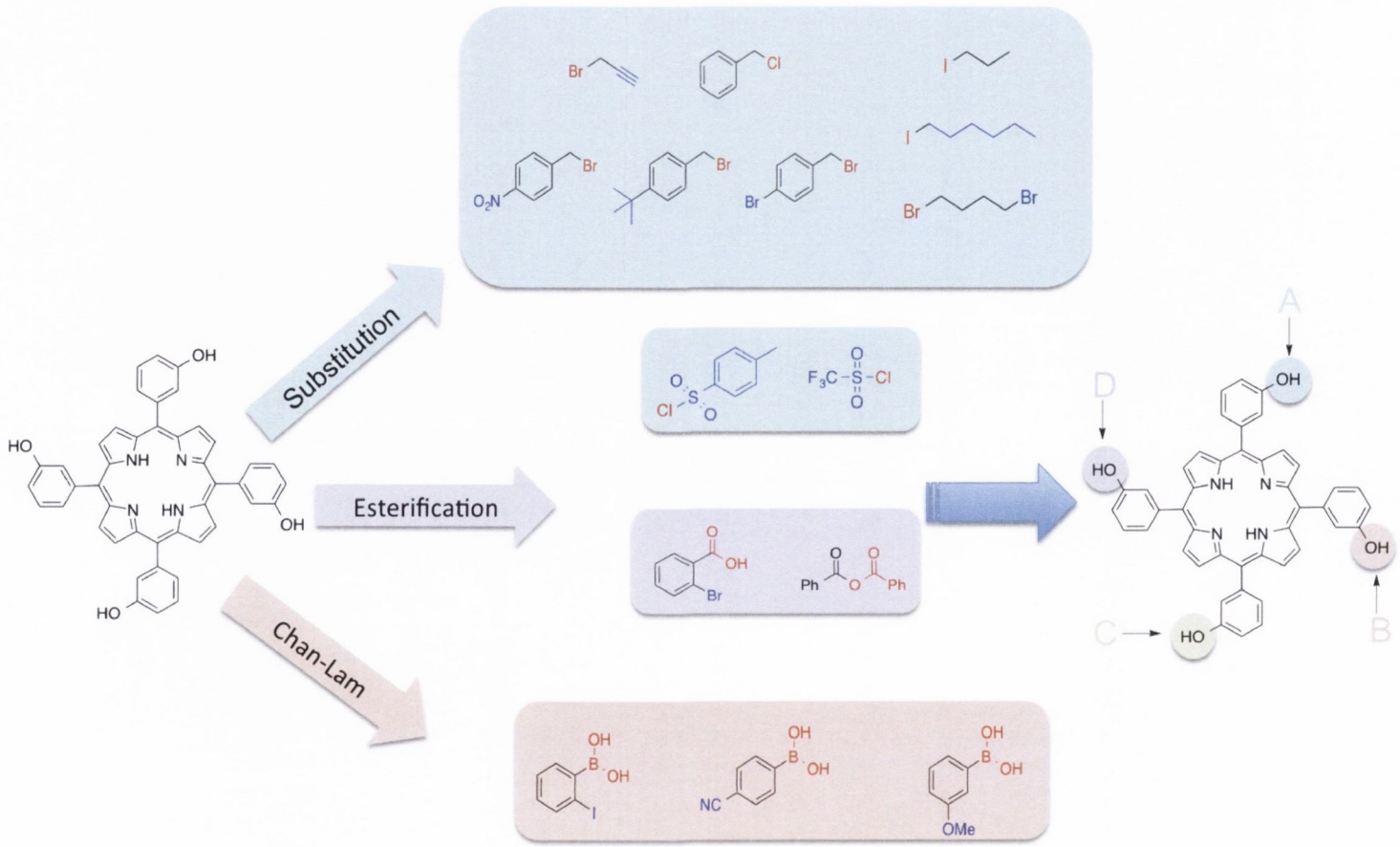

Figure 3.8. A summary of the reactions possible utilizing the one core scaffold, *m*-THPP **2**.

2.6.2 Future Work

The case studies detailed above highlight the synthetic ease of this newly designed methodology for the creation of a library of model compounds and the practical applications one can tailor this porphyrin scaffold for. Initial future work would entail the synthesis of a picket-fence porphyrin using this methodology, i.e., applying the conditions previously optimized to *o*-THPP. Subsequent resolution and isolation of the atropisomers would leave the α,α,α,α-derivative, that is, a true picket fence porphyrin, capable of mimicking the O_2 binding in heme. Secondly, a small library of potential metalloenzyme mimics should be synthesized and evaluated for their ability to catalyze the four-electron reduction of O_2 to H_2O. The strength of this method is the short synthetic input to synthesize these complicated systems and the versatility of metal/free base porphyrins and length and nature of the linker group. As such, the library could be quickly and easily generated to incorporate a variety of different cofacial bis(porphyrin)s as to truly evaluate this class of compounds for their catalytic activity (Figure 3.9).

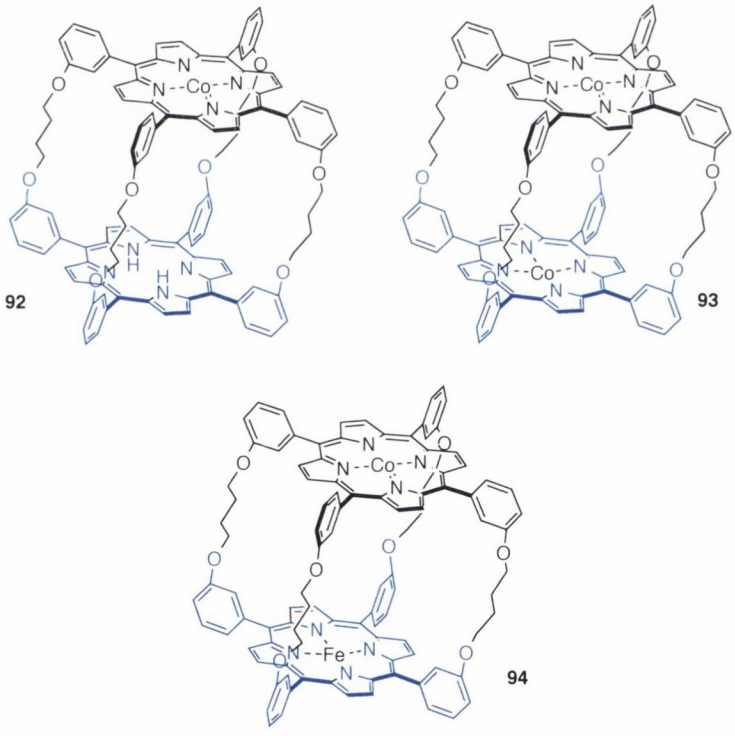

Figure 3.9. A small library of potential catalysts that could be tested for their potential for the 4e reduction of O_2 to H_2O.

Another potential application for these cofacial porphyrins would be in the field of photodynamic therapy (Figure 3.10). As mentioned in a previous chapter, *m*-THPP based porphyrins have a tendency to form aggregates when administered and there is a subsequent delay period before treatment can begin due to the slow monomerization process [108].

However, these caged systems would have to act in a completely alternative fashion with a decreased chance of aggregation occurring. *In vitro* experiments could be undertaken to investigate the uptake, localization and cytotoxic profile of these novel PSs.

Dual-targeting photosensitizers have long been talked about since their conception, however little work has actually been conducted into their practical synthesis. This new methodology would conceptually allow the synthesis of almost any mixed photosensitizer system. For example, glycoporphyrins have received interest from PDT researchers due to their targeting capabilities and solubilizing properties, and one could now install three sugar moieties simultaneously whilst leaving one OH free for functionalization with a bile acid azide, for example, for increased cytotoxicity. Systems like these could potentially not only improve the selectivity of the treatment but also the cytotoxicity (Figure 3.11).

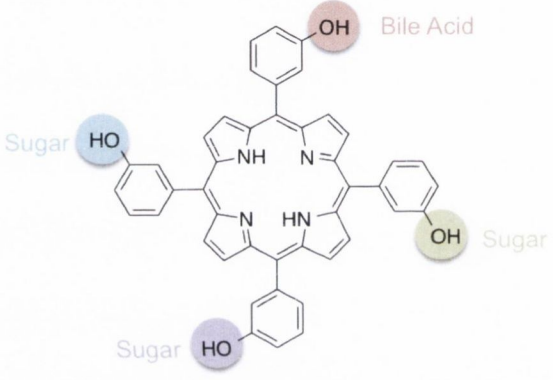

Figure 3.11. A hypothetical dual-targeting PS that can be synthesized through the controlled functionalization of the *m*-THPP scaffold.

Chapter 3: Synthesis and Biological Evaluation of Porphyrin-Bile acid Conjugates

3.1 Introduction

The implementation of biologically targeting systems has potential to advance the field of photodynamic therapy. Whilst there are a myriad of choices available to PDT researchers, one that has shown particular promise in the instances that they have been implemented are bile acids. Bile acids (BAs) such as lithocholic acid (LCA) and deoxycholic acid (DCA) have been shown to induce oxidative stress and generate reactive oxygen species, which can induce DNA damage leading to mutations [148]. BAs have also been shown to activate a number of mitogenic and apoptotic signaling pathways [144,145]. These include the epidermal growth factor receptor and the Raf/Mek/Erk pathway, the activator protein-1 (AP-1) and NF-κB transcription factors, the protein kinase C (PKC) family and endoplasmic reticulum (ER) stress pathways, all of which are known to be deregulated during tumorigenesis [146]. Chronic esophageal exposure to bile acids in patients with gastro-esophageal reflux disease is associated with the development of Barrett's metaplasia and associated molecular markers of inflammation which have been shown to support transformation, initiation and progression of tumor development. Another feature of Barrett's is the development of bile acid transporters such as the apical sodium dependent bile acid transporter (ASBT) along with associated intracellular transporters and a homologue of ilial Ost alpha/beta [147].

Properly positioned, the BAs would be expected to endow the porphyrin with substrate activity towards ASBT which is present in Barrett's esophagus and cancer tissue but not in the normal esophageal squamous epithelium. This approach is expected to increase the selectivity for aberrant cells over the normal type because of this specific distribution of transporter activity. Additionally, the selected BAs, which are activators of cell surface death receptors, could endow the conjugates with additional efficacy in stimulating cell death induction. Previous work carried out by Kralova and co-workers found bile acid porphyrins to show effective cellular uptake and successful ablation of tumors *via* apoptosis and necrosis through PDT [142,143].

3.2 Bile acid Synthesis

The bile acids for this project were supplied to the group through collaboration with Prof. Gilmer's group in the School of Pharmacy and Pharmaceutical Sciences, Trinity College Dublin. Synthetic modifications were made to the bile pigments using known protection and deprotection chemistry to yield compounds 3β-DCA(**100**), 3α-DCA(**101**) and 3β-LCA(**102**) (Scheme 2.1). All reactions were high yielding and capable of gram scale synthesis [148]. The azide group was chosen due to its ease of installation, the opportunity to screen both the 3-α and β functionality and finally to leave the acid fragment of the compound intact as it is theorized to be the group recognized by the transporter that provides cellular uptake. These azides used in conjunction with synthetically available alkyne porphyrins and chlorins make

them the perfect candidate for the robust and high yielding microwave assisted 1,3-dipolar cycloaddition Huisgen [288].

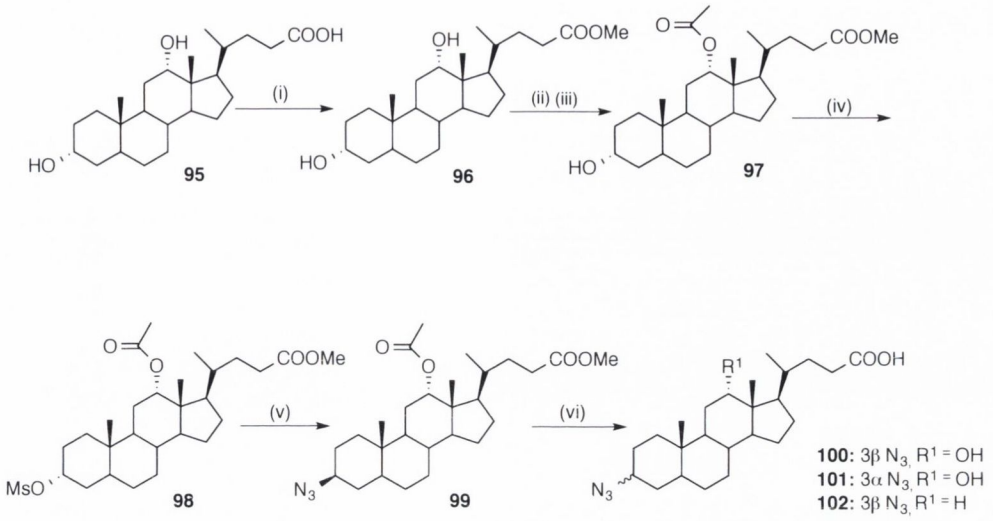

(i): cc. HCl, MeOH, reflux, 1.5 h, 99%; (ii): cat. cc. $HClO_4$, HCOOH, 40 °C to 60 °C, 20 min, 89%; (iii): $NaHCO_3$, MeOH, 0 °C to rt, 7.5 h, 91%; (iv): MsCl, NEt_3, DCM, 0 °C, 1 h, 96%; (v): NaN_3, DMPU, rt (vi): 2M NaOH/MeOH (pH~14), reflux

Scheme 2.1. Exemplary synthesis of a 3-azido bile acid by Gilmer and co-workers for conjugation to a porphyrin scaffold for increased selectivity in PDT [147,148].

3.3 Porphyrin Synthesis

The azide functionality present in the bile acid drew parallels with research previously conducted in Senge's group, i.e., the preparation of glycoporphyrins through microwave-mediated synthesis [289,290]. In that particular case, Senge's group was working with azidoporphyrins and alkynyl sugars that were prepared using known synthetic methodology. For this collaboration, the route chosen for the installation of the alkynyl group was the "organolithium reagent" method, which will be discussed in detail in the next sections (*vide infra*).

3.3.1 Condensation Reactions for Porphyrin Building Blocks

The start of this selected synthetic pathway necessitated the construction of 5,15-disubstituted A_2 type porphyrins through the well-catalogued [2+2] MacDonald condensation [291,292]. This synthetic strategy involves the condensation of dipyrromethane **103** (DPM) with the appropriate aldehyde to yield the desired 5,15-disubstituted porphyrins **108** [293], **109** [294], **110** [295] in yields comparable to those in the literature. The reaction proceeds through an acid-catalyzed condensation *via* a thermodynamically favored porphyrinogen intermediate **104** [293], instead of the competing oligermerization of DPM. This intermediate is consequently oxidized to the desired porphyrin using 2,3-dichloro-5,6-dicyano-1,4-benzoquinone (DDQ) as the oxidant (Scheme 2.2).

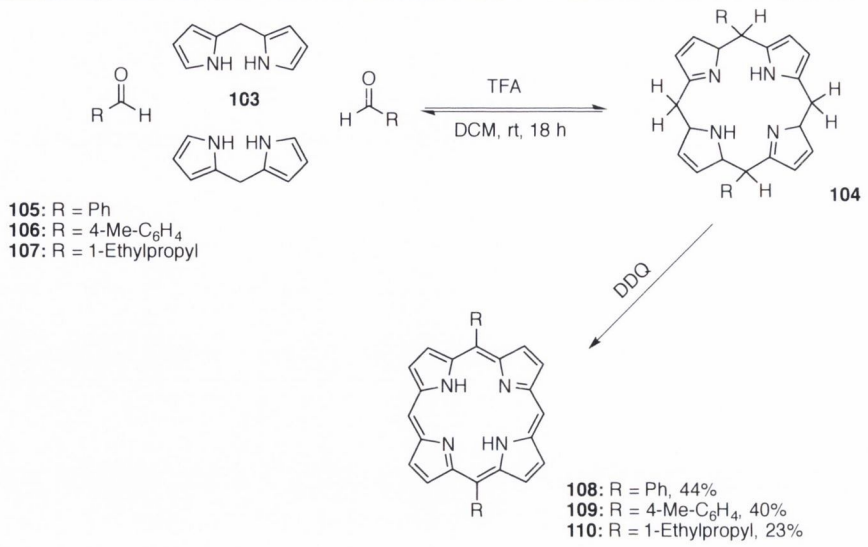

Scheme 2.2. Synthetic pathway towards the construction of 5,15-disubstituted porphyrins.

This synthetic approach has garnered extensive use as it is a mild reaction that is amenable to a large array of functionalities, thus being more advantageous than the harsher Adler-Longo [296] and Rothemund [242] condensation reactions. For the synthesis of **103**, pyrrole was condensed with paraformaldehyde in a one-pot reaction at a temperature of 60 °C for 1 h. An excess of pyrrole was used in this reaction as it acts as both reagent and solvent and the increased temperature is to aid the poor solubility of paraformaldehyde at room temperature. Following a purification procedure optimized by Lindsey *et al.*, **103** was obtained in a 44% yield after Kugelrohr distillation. Whilst this synthesis is quite straightforward in theory, difficulties can arise in practice in determining the end point of the reaction, i.e., maximizing the yield of DPM versus the formation of the higher order oligomers that can occur due to the amount of pyrrole used in the reaction.

The A_2 disubstituted porphyrins **108-110** were synthesized in good yields with simple isolation and purification. Yields were comparable to the literature values and, with two free meso positions; these scaffolds are amenable to further functionalization reactions, such as the installation of alkynyl moieties for future conjugation reactions.

3.3.2 Organolithium Reactions

Senge and co-workers developed a versatile and simple approach to the construction of unsymmetrical porphyrins [132,133,139,297]. By using 5,15-A_2 porphyrins as a starting point, they found that one could introduce meso functionalities in a controlled and predictable manner using, what is now coined "the organolithium approach". Although there are other options available to porphyrin chemists for the synthesis of unsymmetrical porphyrin systems, i.e. mixed condensation reactions or total synthesis, due to the in house expertise with the use

of organolithium reagents for the functionalization of porphyrins, it was decided that this pathway would be the most productive.

Callot *et al.* first observed this organolithium approach with their results involving the butylation of tetraphenylporphyrin (TPP) at the β-position and also meso-butylation of OEP giving stable phlorin products in low yields [298,299]. However, Senge *et al.* were the first to demonstrate the synthetic potential of this methodology by optimizing reaction conditions for the direct installation of phenyl, butyl, hexyl and any other commercially available organolithium reagent or through the *in situ* generation and subsequent reaction of the reagent with the porphyrin of choice [130,133,300]. This methodology proves to be tolerant of a wide range of functionalities and allows for the introduction of synthetically pertinent substituents onto the porphyrin periphery, which can then undergo post-functionalization reactions to yield bio-medical conjugates.

For the purpose of this project, this methodology was used to construct trisubstituted A_3 and A_2B systems from the readily available A_2 precursors **108-110**. A hydroporphyrin intermediate is generated when a 5,15-A_2 porphyrin is reacted with the organolithium reagent (Scheme 2.3), which in the case of free base porphyrins can be dihydroporphyrins or phlorins. The mechanism for this reaction can overall be classed as a nucleophilic substitution reaction that occurs *via* an addition-oxidation mechanism. An anionic species forms at the meso carbon upon reaction of the porphyrin with the organolithium reagent. This anionic species undergoes subsequent hydrolysis to the hydroporphyrin and oxidation through the use of DDQ yields the desired A_3 or A_2B porphyrin [300].

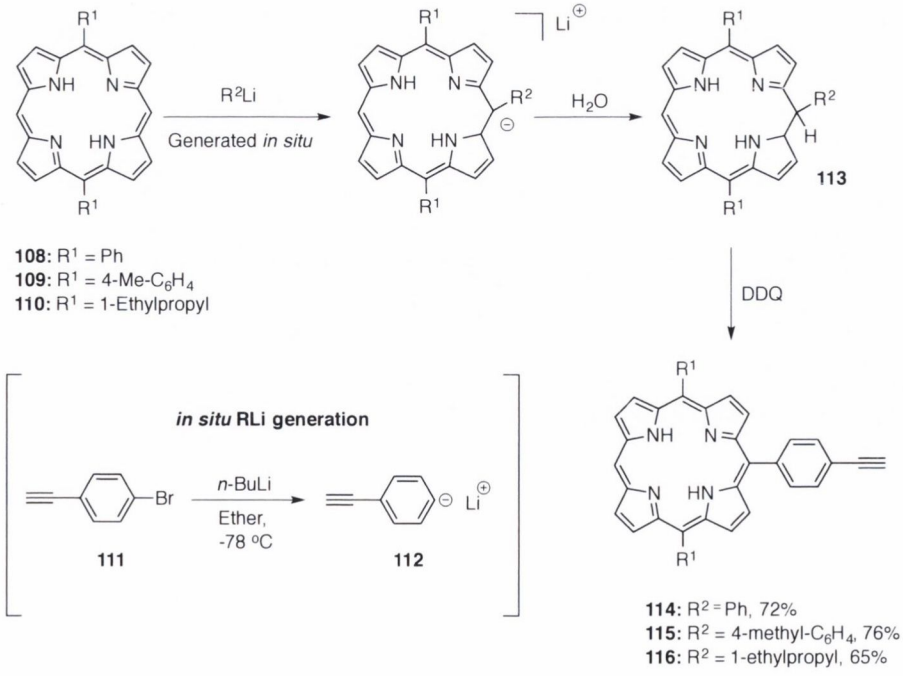

Scheme 2.3. Synthesis of trisubstituted porphyrins **114-116** through the organolithium methodology [301,302].

From a synthetic point of view, this strategy allowed for the introduction of the phenylacetylene functionality to porphyrins **114-116**, whilst leaving an unfunctionalized meso position free for further chemically manipulation if necessary and as a diagnostic peak in the ^{1}H NMR of the synthesized porphyrins. Whilst the introduction of *n*-butyl, *n*-hexyl and phenyl substituents on to the porphyrin macrocycle has now become a trivial exercise, organolithium reagents, which are not commercially available, have to be generated through the *in situ* lithiation of aryl halides with *n*-BuLi *via* a lithium-halogen exchange. The electrophilic porphyrin with the free meso position can then react with this generated organic nucleophile to form the desired trisubstituted porphyrin adduct. In this instance, 4-bromophenylacetylene **111** was reacted at -78 °C in anhydrous diethylether with *n*-BuLi to generate RLi **112**, which was subsequently reacted with porphyrins **108-110** to yield the trisubstituted porphyrins **114-116** in satisfactory yield.

Successful generation can typically be predicted due to a color change of white to pink, followed by the formation of a pink precipitate. Unfortunately, difficulties arose at times during the generation step, due to the complications with the diethylether solvent not being completely anhydrous. Synthetic experience within the group has demonstrated that the solvent is required to be scrupulously anhydrous as minute amounts of water can inhibit the generation of the organolithium species as the water can react with the *n*-BuLi and cause the formation of various different salts instead of reacting with the aryl halide [130,133]. Steps were taken to ensure that the quality of the solvent remained at a satisfactory level as to ensure successful generation of the organolithium reagent. These included the repeated drying of the diethylether over sodium wire and subsequent storage under argon as it was deemed that the anhydrous Sigma-Aldrich derivative was inadequate for successful generation.

3.3.3 Metallation

Following on from the functionalization of the porphyrin periphery with the acetylene synthetic handle, it was necessary to metallate the porphyrin core, i.e., insert a metal into the porphyrin cavity, as a preventative measure against copper insertion in the proceeding reactions. The reactions to insert a metal into the porphyrin core are straightforward and high yielding. The lone-pairs of the inner nitrogen atoms of the porphyrin core can co-ordinate with the metal ion, with subsequent loss of the two inner hydrogen atoms [268,303,304].

For this collaboration, the porphyrin-bile acid conjugates were to be tested for their PDT efficacy *in vitro* using a number of different cell lines. Metal insertion can have quite a pronounced affect on the photophysical properties of a porphyrin as well as their solubility. As such, zinc was selected as the metal center, as it can be easily inserted into the core with short reaction times and is extremely acid labile and therefore can be easily removed if necessary, but

also because research has demonstrated that zinc, due to the heavy-metal effect can impart an additive PDT effect to the porphyrin PS [305]. The methodology implemented was that developed by Buchler *et al.* and involves the addition of zinc(II)acetate dehydrate dissolved in methanol to a solution of the appropriate free-base porphyrin in chloroform and maintained at reflux until complete conversion was observed by TLC. The application of this method produced porphyrins **117-119** in yields ranging from 93-95 % (Scheme 2.4) with short reactions times.

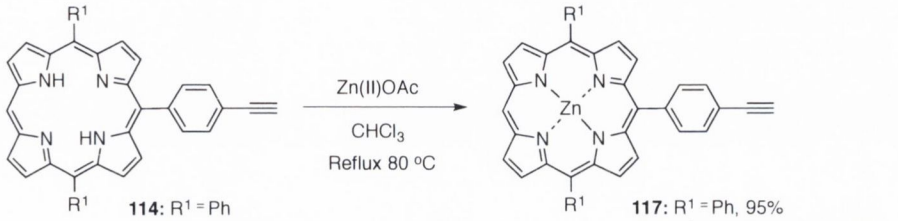

114: R^1 = Ph
115: R^1 = 4-methyl-C_6H_4
116: R^1 = 1-ethylpropyl

117: R^1 = Ph, 95%
118: R^1 = 4-methyl-C_6H_4, 93%
119: R^1 = 1-ethylpropyl, 95%

Scheme 2.4. Zinc insertion on porphyrins **117-119**.

3.3.4 Conjugation Reactions

Previous research in the Senge lab has demonstrated the use of microwave assisted click chemistry for the introduction of targeting moieties onto the porphyrin macrocycle [289,306]. A modified Huisgen cycloaddition reaction [288], which is classified as a 1,3-dipolar cycloaddition between an azide and, in this case, a terminal alkyne to afford a 1,2,3-triazole was implemented for this synthetic approach. They were successful in reacting a number of different *O*-propargyl linked carbohydrates to mono-azido tetraphenyl porphyrin. It was therefore posited whether one could modify the approach to accommodate the use of an azido bile acid and alkynyl porphyrin.

Using the conditions developed previously in the group, a number of microwave reactions were conducted using porphyrins **117-119** with copper(I)chloride as the catalyst and toluene as the solvent. These reactions proved failed to produce the desired product with only starting material being recovered and no trace of conjugation. The catalyst loading was increased in an effort to force the reaction to occur. Again, however, no reaction proceeded with starting material and some decomposition material being recovered. Due to the polar functional groups present on the bile acids, it was envisaged that the bile acid might suffer from low solubility in toluene and this could therefore limit the transition state from occurring and consequently no reaction product being formed. To counteract this potential issue of solubility, it was decided to move to THF as a solvent system (Scheme 2.5). This switch to a more polar solvent proved efficacious in obtaining the production of porphyrin-bile acid conjugates, however the reaction

suffered from low yields and cumbersome purification, again due to conflicting solubility issues from both porphyrin and bile acid.

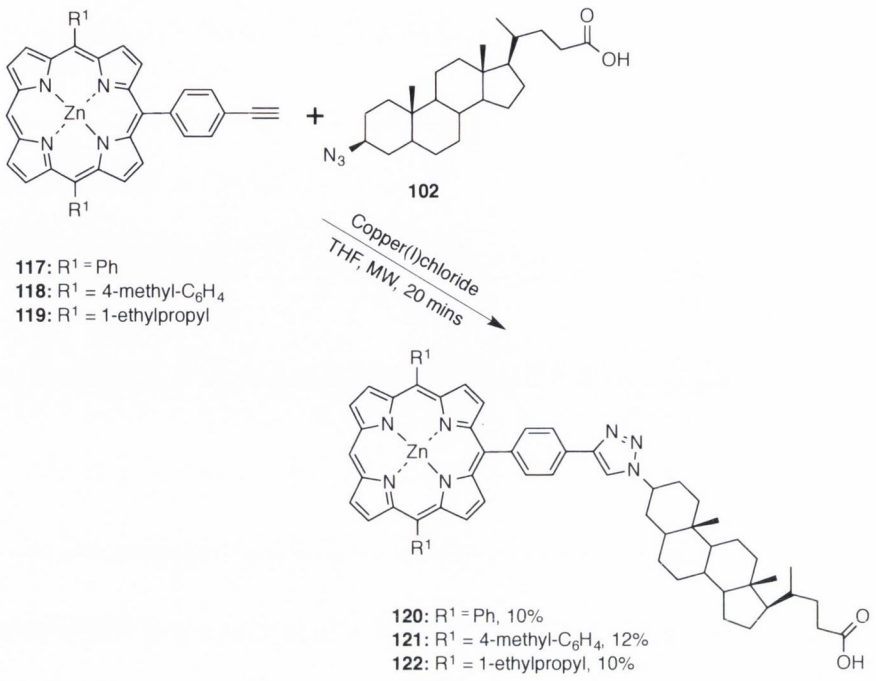

Scheme 2.5. Initial microwave-assisted click reactions using porphyrins **117-119** and bile acid **37**.

3.3.5 Alternative Coupling Partner

Due to the difficulties in obtaining significant amounts of reaction product from the previously discussed synthetic pathway, it was theorized whether an alternative alkynylporphyrin coupling partner would prove more effective. Whilst historically, the *modus operandi* of PDT researchers has been to use the synthetically facile, tetraphenylporphyrin and through known chemistry, synthesize a porphyrin coupling partner; it was decided to investigate whether it would be possible to take a known photosensitizer and introduce the desired alkynyl functional group to the porphyrin periphery. By using a known photosensitizer, the pitfalls of relatively low $^1O_2$ production and poor intracellular localization by 'everyday' porphyrins could be overcome. *m*-THPP is a readily available tetrasubstituted porphyrin and also a known potent photosensitizer [307]. From work conducted in Chapter 2, it is now possible to selectively modify the porphyrin scaffold with a synthetic handle, e.g., an alkyne moiety, through a nucleophilic substitution reaction.

Microwave reactions were carried out as per the scheme below, using the PS scaffold **36** and a range of different bile acids (**100-102**) with copper(I)chloride as the catalyst and a toluene:methanol solvent mixture to accommodate the additional OH groups present on the porphyrin scaffold. Although these reactions were successful in synthesizing the desired products **123-125**, the yields (5-10%) were too low for these conditions to be taken any further. Analysis of the reaction pathway suggested that the hydroxyl groups present may be interfering with the copper(I) catalytic cycle as only small amounts of conversion was occurring, even at elevated temperature. Tetrakis(acetonitrile)copper(I)hexafluorophosphate has been shown to work in 1,3-cycloaddition reactions utilizing similar substrates as the ligands present help stabilize the catalyst and generally improve the yields of the reactions [309].

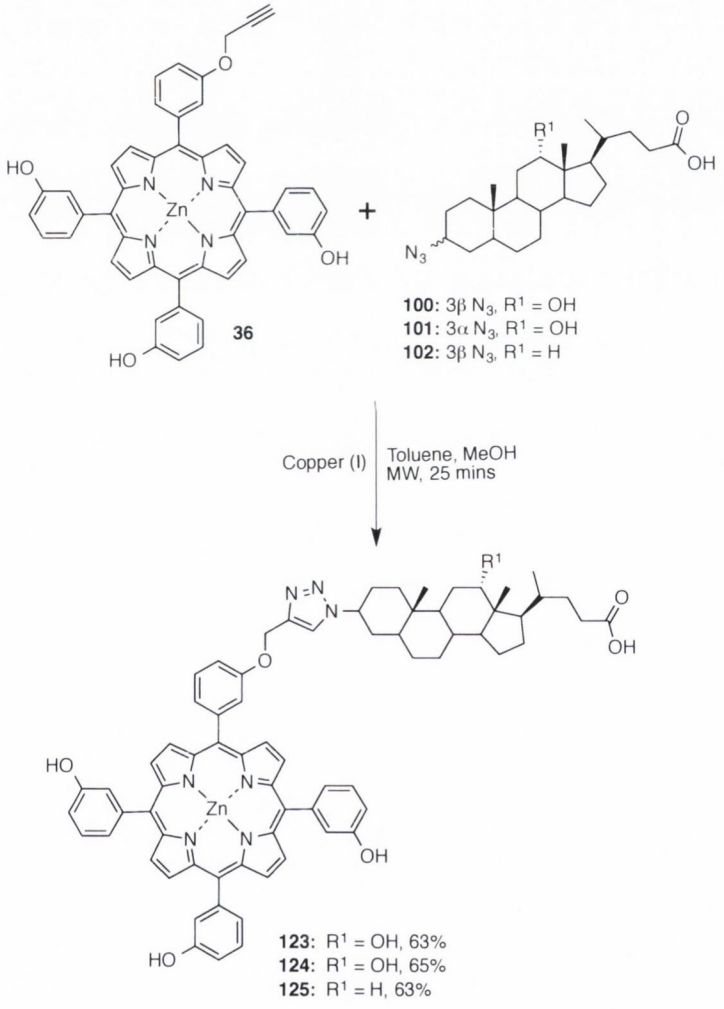

Scheme 2.8. Synthesis of a library of bile acid-porphyrin conjugates through a modified Huisgen cycloaddition with tetrakis(acetonitrile)copper(I)hexafluorophosphate as a catalyst [258].

3.3.5.1 *m*-THPC (Temoporfin) Derivative

A sister compound to *m*-THPP is the photosensitizer *m*-THPC **3**, a reduced porphyrin derivative that differs only by a reduced double bond between carbons 21-22 on the pyrrole D ring. This compound, which was discovered by Bonnett *et al.* has quickly become one of the industry's gold standard [114,115,307]. Thus, a Temoporfin-bile acid conjugate became a synthetic target following the success of the *m*-THPP reactions. Many of the standard chemical reactions, for example, metallation reactions, carried out on porphyrins become cumbersome once translated to their chlorin counterpart. This is due to the sensitivity of the reduced bond and its proclivity to be oxidized back to its porphyrin equivalent. As a result of these limitations, investigations into functionalization reactions of Temoporfin have remained relatively dormant in recent years. A number of attempts were made to metallate Temoporfin **3** using a variety of different metal sources and solvent systems, all under highly anaerobic conditions. Despite best efforts, all reaction mixtures displayed new spots on TLC pertaining to the porphyrin counterpart and no presence of any metallated-chlorin species. This observation was reinforced using UV-vis data, which showed the characteristic peaks pertaining to the *m*-THPP derivative.

Recent research conducted by Nascimento *et al.* into the microwave-assisted synthesis of tetrasubstituted porphyrins revealed the convenient metallation of porphyrins through microwave irradiation [267]. Metal insertion occurs over three 1 min intervals of heating using excess Zn(II)OAc in DMF followed by work-up and recrystallization. This methodology was firstly applied to *m*-THPP **2**, as to test the settings of the conventional microwave oven on a porphyrin previously used by the developers of this synthetic step. This reaction worked in near quantitative yield as per TLC analysis and with standard sodium bicarbonate, brine and water washes ensuing, this reaction appears to be quite a quick and facile step for the metallation of tetrasubstituted porphyrins. With this positive result from the parent **2**, trial reactions began using the reduced *m*-THPC **3** with identical reaction conditions (Scheme 2.9). TLC analysis showed the complete consumption of starting material after the third heating interval and was accompanied by a color change from purple to green. UV-vis analysis displayed the reduction of Q-bands from four to two, the expected result from a metallation reaction and a slight shift in the absorption profile (Figure 2.1). Subsequent NMR spectroscopy confirmed the previous analytical results by showing the disappearance of the inner NH signals between -2 and -3 ppm, again, characteristic of a metallated tetrapyrrole [310]. The final piece of evidence came from HRMS that confirmed the presence of the Zinc(II)chlorin and no trace of the parent porphyrin species.

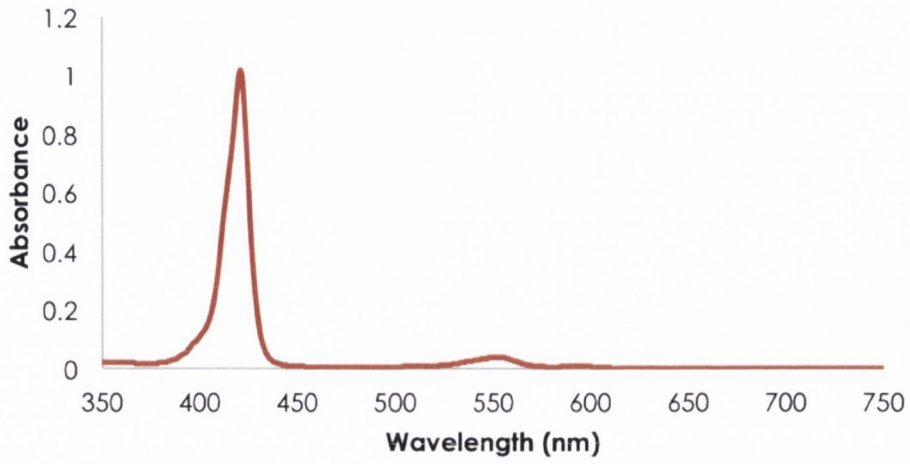

Figure 2.1. UV-vis spectra of a Zn(II)*m*-THPC derivative.

This is the first example of the metallation of *m*-THPC **3** and shows that the brief irradiation provided by the microwave is sufficient to insert the metal, in this case zinc, into the chlorin's core without subsequent oxidation. Not only does this successful reaction help in the synthesis of precursors for this particular project, it also opens a wide array of potential reactions one can now perform on *m*-THPC without the threat of oxidation back to the parent porphyrin.

Following on from this metal insertion reaction; methodologies developed from the porphyrin functionalization were implemented on the chlorin scaffold with similar yields being obtained for the installation of the propargyl group (Scheme 2.9). With this synthetic precursor now available, the m-THPC scaffold was ready for initial reactions with the bile acid azides.

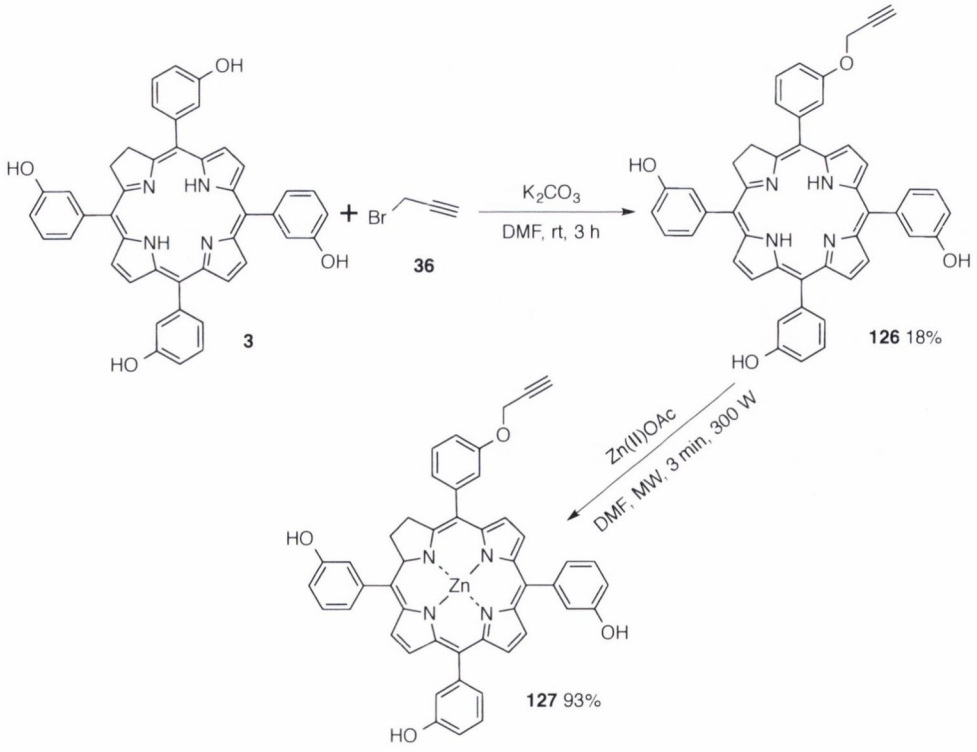

Scheme 2.9. Controlled functionalization and subsequent metallation of *m*-THPC.

The modified Huisgen cycloaddition reaction produced a bile acid-chlorin conjugate **127** in similar yields to its porphyrin counterpart, with work-up and purification following the procedure implemented previously (Scheme 2.10). Whilst the scheme below illustrates a defined reaction product, due to the reduced bond present in the chlorin derivative, there was a statistical mixture of regioisomers present in the purified product. NMR analysis proved extremely cumbersome due to the inherent difficulty of isolating chlorin regioisomers [311]. Thus, the NMR assignment of signals is for the major reaction product, but again without a very involved and lengthy NMR study, it is impossible to definitively assign which regioisomer is the major product.

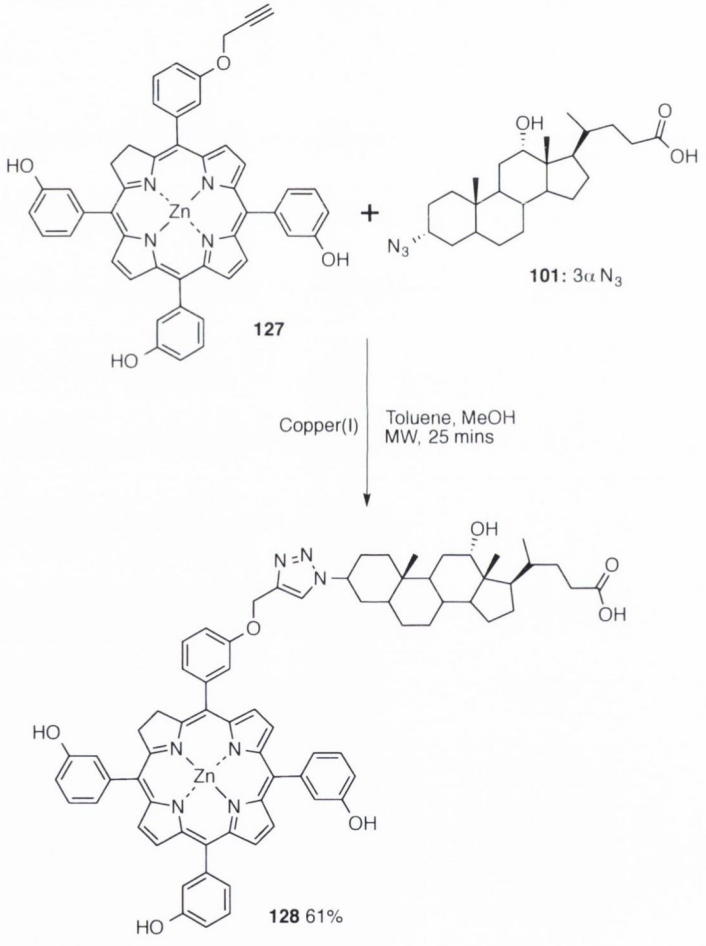

Scheme 2.10. Synthesis of a bile acid-chlorin conjugate through the modified Huisgen cycloaddition.

3.4 Biological Testing

3.4.1 Localization Studies

Compounds **123, 124, 125** and **128** underwent biological screening to assess their localization and cytotoxic properties using esophageal carcinoma OE33, esophagus adenocarcinoma, and well-differentiated SKGT-4 human cell lines by Dr. Natalia Sergeeva and Dr. Edyta Paszko. All

four compounds are taken up into the cell lines and appear to localize in the ER and Golgi apparatus, similar to the accumulation patterns seen with Temoporfin; however, further co-localization studies are needed to definitively confirm this hypothesis (Figure 2.2).

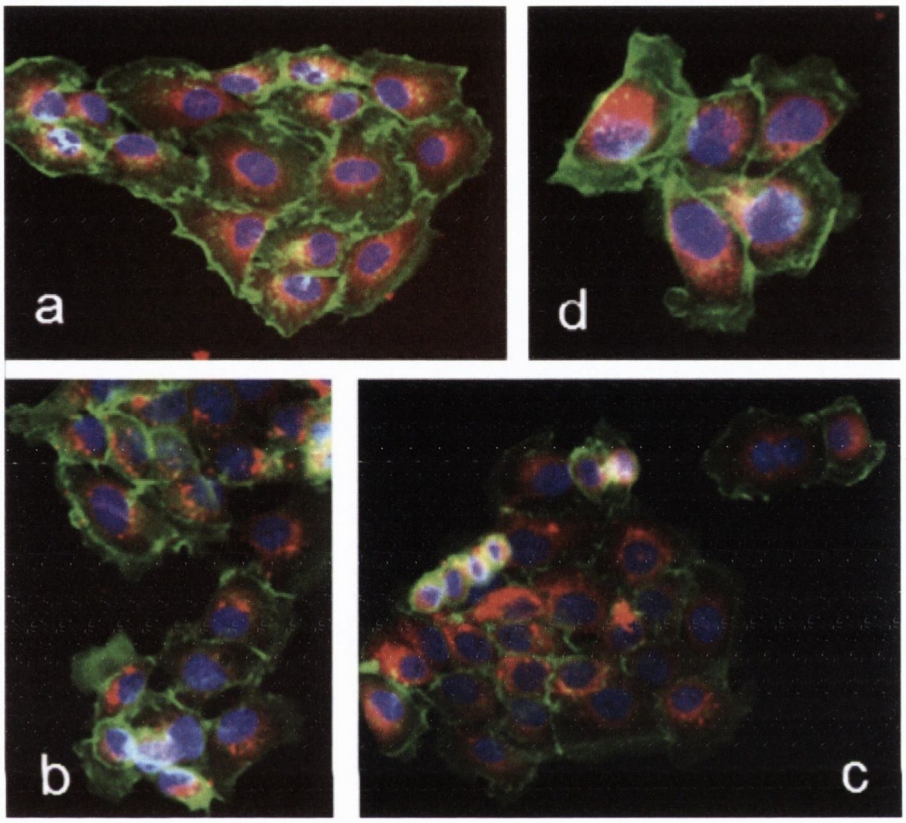

Figure 2.2. OE33 and SKGT-4 cells stained with compounds **123, 124, 125** and **128** (red), nuclear dye—Hoechst 33342 (blue), F-actin dye—Phalloidin 490 (green): (a) **123** 30 μM, SGT-4; (b) **124** OE33 40 μM; (c) **125** OE33 40 μM; (d) **128** OE33 50 μM [258].

3.4.2 Cytotoxicity Evaluation

The standard test of the efficacy of a PS *in vitro* is measured using the colorimetric MTT or MTS assays [312]. Compounds **123, 124, 125** and **128** were analyzed with an MTS assay after 48 h incubation and an illumination period of 2 min [313]. Unfortunately, none of the bile conjugates exhibited any phototoxic effect, which may be due to a number of factors, for example, the triazole ring may be inhibiting the production of $^1O_2$ by the PS, or intracellular quenching may be occurring due to intracellular aggregation of the PS. However, as porphyrins are selectively retained in tumor tissue, the compounds may show promise as imaging agents for phototherapy as they were all readily taken up by the different cell lines and exhibit strong fluorescence, which is ideal for imaging.

3.5 Singlet Oxygen Production

As the compounds failed to produce any cytotoxic effect despite all the compounds successfully entering the cell, it was decided to evaluate the $^1O_2$ production capability of the library of

conjugates. Compounds **123, 124, 125** and **128** were subjected to an assay in order to estimate their $^1O_2$ generation. Their production of $^1O_2$ was determined through the monitoring of the UV-vis spectroscopy of the dye 1,3-diphenylisobenzofuran (DPBF) in solution [314]. DPBF has an absorbance maximum at 410 nm and readily undergoes a ring opening reaction in the presence of $^1O_2$. One can monitor the reduction of this band over time and graph an estimate of $^1O_2$ production.

123, 124, 125 and **128** and *m*-THPC (**2**) as a control, were dissolved in an aerated solution of DPBF in CH_2Cl_2 and irradiated with white light and the intensity of DPBF's absorption band was monitored over time using UV-vis spectroscopy. Even after extended time periods and increased light doses, these compounds failed to produce any level of $^1O_2$, as per Figure 2.3. This result indicates that the triazole ring is inhibiting any potential cytotoxic effect by quenching the production of $^1O_2$. From an organic chemist's standpoint, a triazole ring is an excellent linker as it is a chemically stable group formed from one of the most reliable reactions in chemistry [315]. This has made the triazole ring an extremely popular linker group in medicinal chemistry and can be evidenced by the number of PDT researchers designing porphyrin conjugates containing triazole rings. However, from a photochemists point of view, azides and triazoles are an extremely efficient class of oxygen quenchers and therefore may well be inhibiting the production of $^1O_2$ [316].

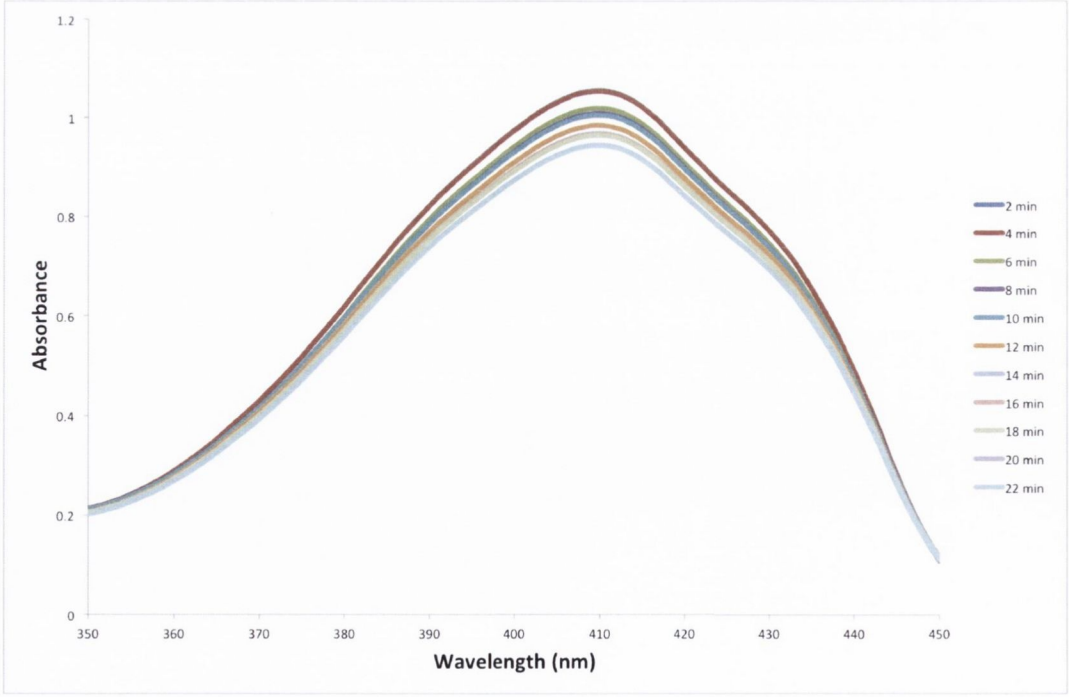

Figure 2.3. Crude assay results for the assessment of compound **66**'s ability to produce $^1O_2$.

3.6 Conclusion & Future Work

3.6.1 Conclusions

A library of porphyrin bile acid adducts were successfully synthesized through the copper(I) catalyzed click reaction. By controlling the number of equivalents, one can control the degree of substitution and obtain monofunctionalized porphyrin and chlorin scaffolds in moderate yields and few synthetic steps. *m*-THPC, as a molecule, has been revealed to tolerate microwave irradiation and S_N2 chemistry with no subsequent oxidation to the parent porphyrin. It is envisaged that this will greatly aid the development of 3rd generation Temoporfin based photosensitizers as new modification reactions that were previously unattainable may now be conducted using microwave irradiation. Thus aiding in the continued search for improved sensitizers. This library of highly soluble PSs **123, 124, 125** and **128** were readily up taken and accumulated within the cytoplasm of the cell. Unfortunately, they did not demonstrate cytotoxicity in any of the cell lines tested and this is due to their inability to produce $^1O_2$.

3.6.2 Future Work

Future work may focus on improving the cytotoxicity of these conjugates through the use of different linkers and bile acids. One such possible linker is an ester bond formed through the carboxylic acid side chain of the bile acid and a phenol group from *m*-THPC (Figure 2.4). Gilmer *et al.* in previous work have shown the enhanced cytotoxic effect of bile acid azides, thus, by conjugating these molecules through the acid fragment, one may not only impart a localization effect from the bile acid but also a therapeutic effect.

Whilst the primary goal of the project was deemed unsuccessful, i.e., the compounds did not produce a photocytotoxic effect, they did however all enter the cell. This result will allow for the investigations into the secondary goal of this collaboration, i.e., is the bile acid imparting selectivity for the ASBT and therefore increasing the incidence of uptake? To answer this question, a number of biological studies must be undertaken to ascertain is the uptake enhanced by the bile acid through active uptake or is the uptake reliant on passive diffusion.

Initial studies should involve uptake and localization studies on the bile acid library and *m*-THPC as a reference. From these experiments, one will be able to ascertain if there is a greater amount of the bile acid conjugate in the cell in comparison to free *m*-THPC. Irrespective of the result from the above, experiments with drugs incubated in the cells at 0 °C will give insight into the mechanism of uptake. If the drugs still enter the cell even at decreased temperatures then it is probable that they are entering due to passive diffusion and not active uptake, i.e., the transporter in not aiding in uptake.

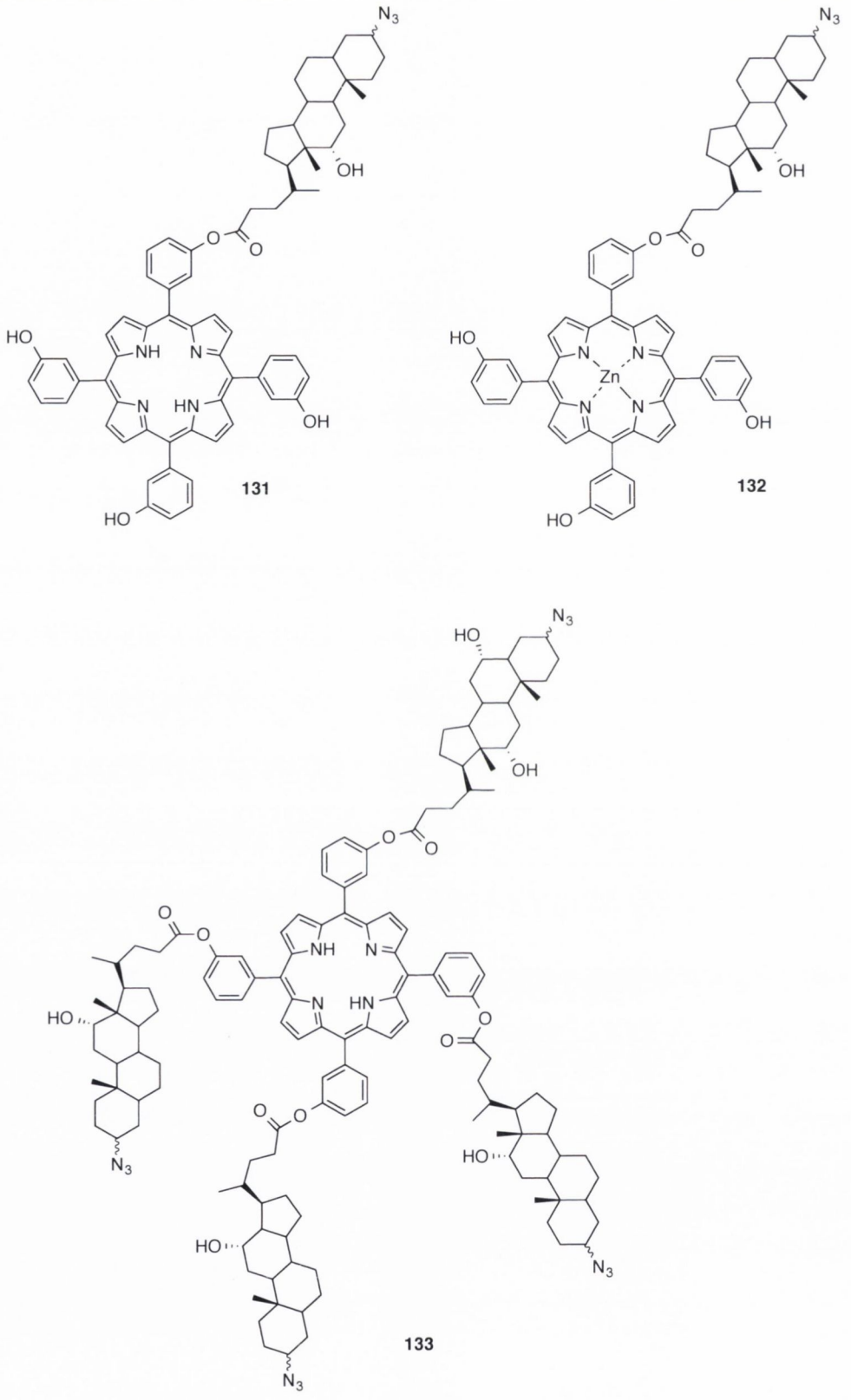

Figure 2.4. A number of potential 2nd generation bile acid-porphyrin conjugates linked through the acid fragment of the bile acid.

Chapter 4: i-Chlorins

4.1 Introduction

PDT as a treatment is continually evolving with constant improvements in photosensitizer efficacy, light source and dosimetry [18,317]. There are a number of new photosensitizers under investigation that have displayed improved clearance rates, targeting properties or photophysical profile [318]. However, as mentioned before, research and advancements in areas such as post-treatment photosensitivity and tumor regrowth still need addressing [319].

Photosensitizer conjugation with biological targeting or therapeutic groups is one possible solution which is current being investigated by researchers. Despite being known for over thirty years, there are no papers detailing any truly synthetic manipulations to the *m*-THPC **3** scaffold, with many involving the addition of silicon-based nano-particles onto the four OH groups [320,321]. The main reason for this has been the perceived difficulty in working with a compound that may re-oxidize to the parent porphyrin derivative during the reaction or the subsequent work-up or purification steps. Also, this compound is believed to be air and light sensitive with any extended amount of exposure to either element resulting in re-oxidation to the parent porphyrin. However, from the work completed in Chapter 2, this supposition of extreme sensitivity to air and light is slowly becoming discredited, as one is now able to complete metal insertions using microwave irradiation. One can also functionalize the chlorin periphery with a simple synthetic handle and allow it to undergo further metal catalyzed cross-coupling reactions. All these steps proceed in good yields with no apparent re-oxidation to the parent porphyrin.

Thus, it is now possible to functionalize the periphery of this potent PS with biologically pertinent groups to reduce post-treatment photosensitivity and tumor regrowth, the latter caused by PDT induced inflammation and hypoxia.

This inflammation can lead to the increased expression of pro-survival and angiogenic molecules such as vascular endothelial growth factor (VEGF), survivin and matrix metalloproteinases (MMPs) [322]. This upregulation of pro-inflammatory molecules within the tumor microenvironment can decrease the efficacy of the treatment due to the occurrence of tumor regrowth [319,323].

Researchers have found that the COX-2 gene is consistently overexpressed after a course of PDT and this result coincides with previous work that demonstrated that PDT stimulated the release of PGE_2 from macrophages and RIF cells grown in culture [324]. This endogenous PG release in mice exhibiting a systemic shock reaction after localized PDT could be attenuated with NSAIDs [325]. Co-administration of celecoxib with PDT improved the long-term tumoricidal activity whilst preserving normal tissue photosensitization [323,326]. Unfortunately, the administration of COX-2 inhibitors can cause a number of side effects, which include cardiovascular or gastrointestinal injuries [327].

A plethora of studies have shown that the tumorcidal actions of coxibs such as celecoxib are independent of COX-2 mediated mechanisms. Studies report that a celecoxib analogue, 2,5-dimethyl celecoxib (DMC), displays cytotoxic properties comparable to celecoxib but without the COX-2 inhibitory activity [328]. Gomer *et al.* were able to demonstrate the efficacy of DMC using a C3H/BA murine mammary carcinoma model. Results showed that DMC increased both the cytotoxicity and apoptosis in BA cells exposed to PDT treatment along with the induced expression of the pro-survival protein survivin [328]. PGE_2 levels remained unchanged despite the enhanced *in vivo* tumorcidal responsiveness to PDT, which means that DMC improved the efficacy of the treatment by causing an increase in apoptosis and tumorcidal activity.

Whilst there is strong evidence for improved efficacy with the co-administration of an anti-inflammatory drug, no research has been conducted on the administration of a photosensitizer-anti-inflammatory agent conjugate [324,328]. It is theorized that a conjugate could undergo biological cleavage to give the PS and anti-inflammatory drug, which would accommodate localized application of the anti-inflammatory agent and therefore an increased therapeutic response.

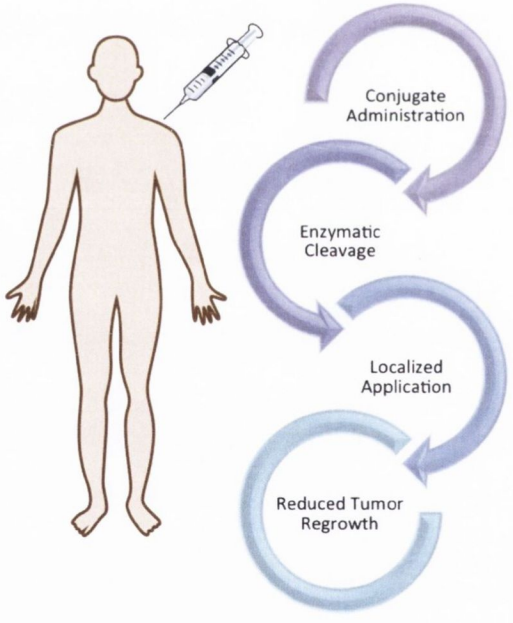

Figure 4.1. Proposed mechanism of action by these porphyrin-anti-inflammatory conjugates.

4.2 Results

As *m*-THPC is perceived as one of the best photosensitizers to this date and on the back of the positive results from Chapter 2, it was considered functional to attempt the synthesis of these anti-inflammatory chlorin conjugate (iChlorins) using this exemplary photosensitizer scaffold. Also, as the carboxylic acid functionality is present in most NSAIDs, and following on from previous work on the functionalization of known PSs, *m*-THPC **3** and *m*-THPP **2**, it was a logical progression to attempt the synthesis of these conjugates through esterification reactions. The ester functionality is a bond that readily undergoes enzymatic cleavage and can be easily installed into molecules. This would allow for the potential *in vitro/in vivo* cleavage to yield both the free porphyrin and NSAID within the tumor microenvironment and therefore produce an increased therapeutic response. There is also a wide array of NSAIDs that are commercially available and therefore provide a large scope for variation for a library of conjugates.

Initial investigatory reactions began by implementing the previously optimized methodology for the esterification of *m*-THPP with simple carboxylic acids (Scheme 4.1). For the initial choice of anti-inflammatory, aspirin provided the best selection with respect to cost and complexity.

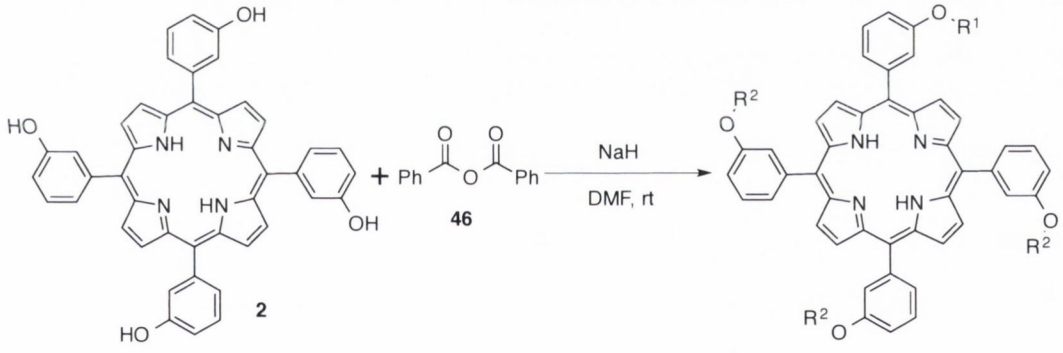

48a: R^1 = benzoyl, R^2 = H, 37%
48b: R^1 = R^2 = benzoyl, 92%

Scheme 4.1. Controlled functionalization of photosensitizer scaffold **3** using benzoic anhydride.

Aspirin **134**, is the most well known anti-inflammatory available on the market. Its mechanism of action relies on the irreversible inhibition of the cyclooxygenase (COX) enzyme, and unlike comparative molecules in its class, it displays greater affect on the COX-1 variant than the COX-2 derivative of the enzyme [329].

Reactions began with the use of K_2CO_3 as a base and DMF as the reaction solvent and an excess of the anti-inflammatory, as to investigate whether the reaction would ensue as expected. The reaction was allowed to proceed for 24 h to ensure an adequate amount of time had been given for conjugation to occur. TLC analysis after the allotted timeframe displayed the characteristic substitution pattern associated with this variety of functionalization products that may be produced. However, NMR and HRMS analysis indicated that the acetylsalicylic acid had undergone deacetylation and subsequent acetylation of the chlorin scaffold (Scheme 4.2).

Whilst the deacetylation had been foreseen has a potential side reaction, the base and mild conditions used prevented the prediction of acetylation of the chlorin.

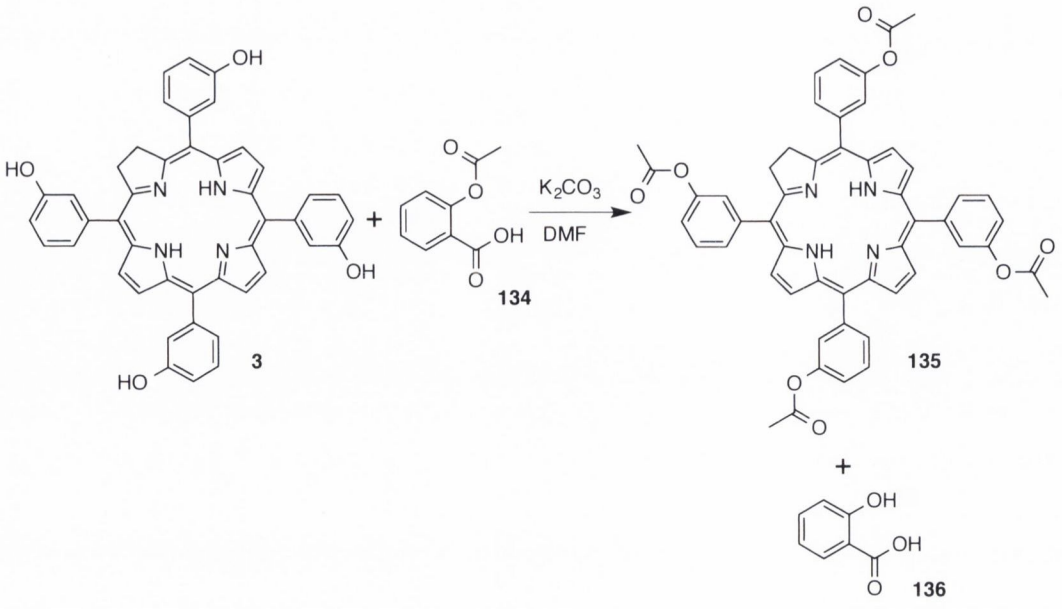

Scheme 4.2. Attempted synthesis of aspirin-chlorin conjugate through previously optimized conditions.

To combat this undesired side reaction, an acid chloride derivative was synthesized through the use of neat thionyl chloride as the chloride source and solvent for the reaction. Excess thionyl chloride **137** which still remained was removed through distillation This provided compound **138** in a yield comparable to the known literature value [330,331]. Reaction of this acid chloride derivative of aspirin **138** with *m*-THPC (**3**) gave a conversion to the desired product however; there were still considerable amounts of the deacetylation/acetylation occurring, even at low reaction equivalents (Scheme 4.3). Whilst another possible route would be to deacetylate the aspirin first, and then conjugate it to the chlorin scaffold; due to the remaining free OH-groups present on the chlorin, selective re-acetylation would be impossible. Due to this, it was decided to attempt the desired esterification reaction with other anti-inflammatory coupling partners.

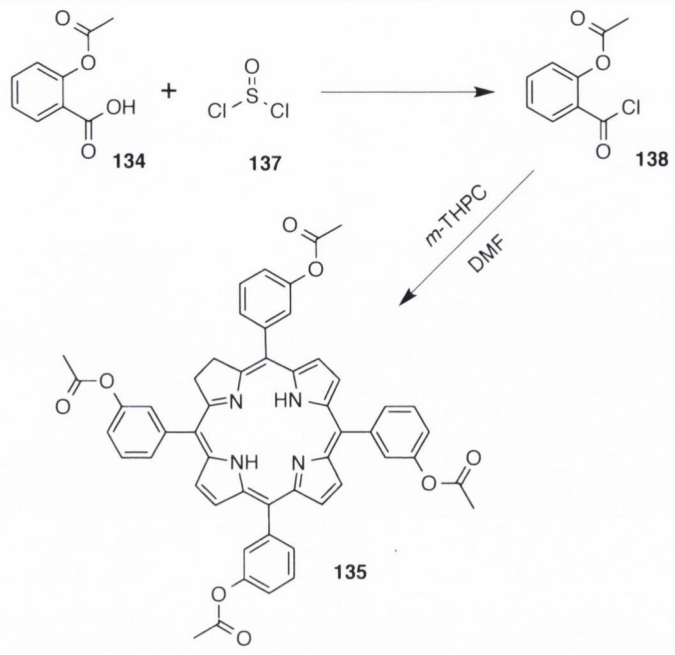

Scheme 4.3. Transformation of aspirin **134** to its acid chloride derivative **138** and subsequent reaction with *m*-THPC **3**.

Fenamic acid **139** serves as a parent structure to a number of different NSAIDs, e.g., tolfenamic acid and flufenamic acid. However, for the initial screen of conditions we wished to optimize our synthetic pathway with a cheap and readily available synthetic precursor, i.e. 5-hydroxyanthranilic acid (**140**). This molecule contains many of the functional groups present in fenamic acid and other NSAIDs and provides an initial increase in complexity from the simple anhydride used in previous work by the group [287]. Also, by avoiding a coxib-based anti-inflammatory, one can circumvent any potential cardiovascular pitfalls associated with that class of compound [327].

The initial screen of conditions began with the use of K_2CO_3 as the base and DMF as the solvent, again to mimic the conditions previously used (Scheme 4.2). These reaction conditions proved unsuccessful in producing any coupling, with unreacted chlorin being the only isolatable material recovered from the reaction mixture. From here, a simple Fischer esterification reaction to yield the chlorin ester product was attempted. A catalytic amount of H_2SO_4 was used with dry CH_2Cl_2 and brought to reflux temperatures overnight. This reaction proved unsuccessful, even at increased temperatures, and it seems that the chlorin macrocycle may be interfering with the electronics of the phenol group by reducing the nucleophilicity of the OH and therefore inhibiting the reaction with the carboxylic acid.

Next, a Steglich reaction using *N,N'*-dicyclohexylcarbodiimide, **52** (DCC) and 4-dimethylaminopyridine (DMAP) **53** as coupling partners was attempted in DMF at room temperature. Initial results from this reaction appeared promising; however, the yield for the

reaction was low and the presence of an insoluble *N*-acylurea (**142**) made purification of the product cumbersome [332].

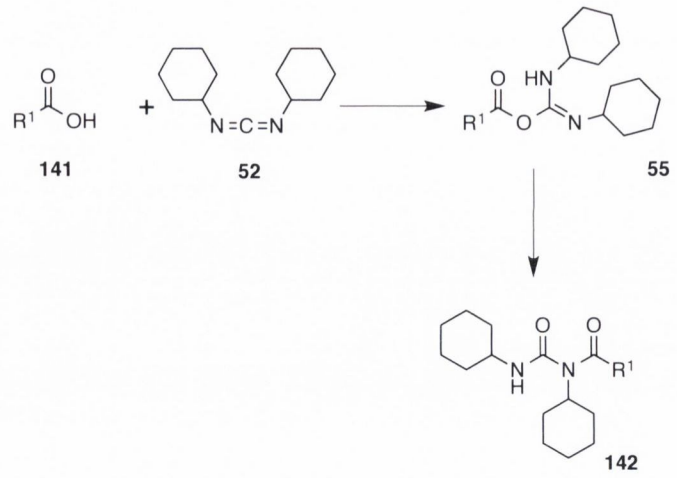

Figure 4.2. Mechanism for the formation of the insoluble *N*-acylurea (**142**) impurity.

A suitable substitute for **90** is 1-ethyl-3-(3-dimethylaminopropyl)carbodiimide hydrochloride, **143** (EDC), a preferred alternate cross coupling agent due to its solubility in water [333,334]. This was used in the presence of a catalyst, DMAP, in DMF and at room temperature with no observable esterification occurring. The reaction was reattempted at elevated temperatures and again, no reaction product was observed by TLC and NMR.

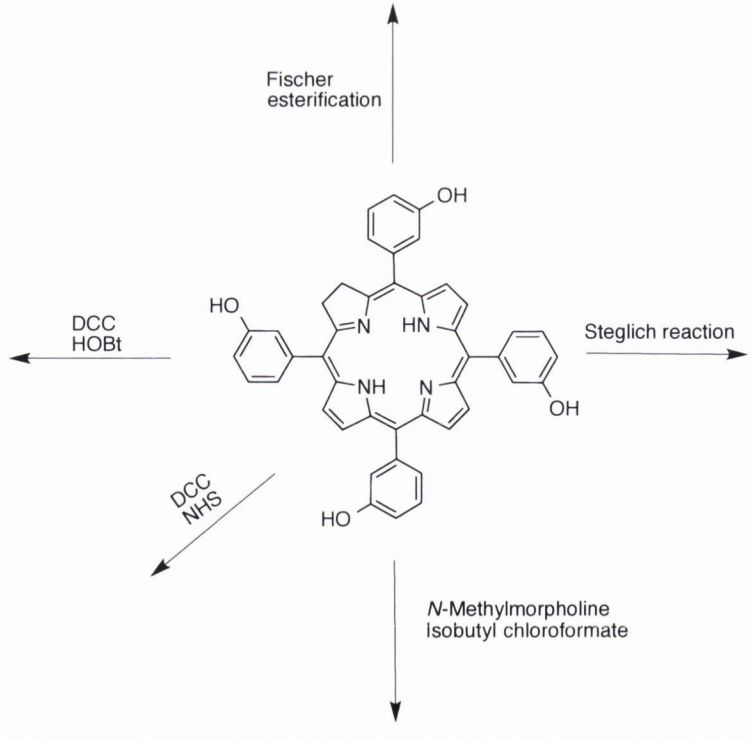

Figure 4.3. A summary of the reaction pathways screened for the attempted synthesis of iPorphyrins.

Hydroxybenzotriazole, **144** (HOBt) may be used in cross-coupling reactions in conjunction with EDC as a carboxy-activating agent [335]. It reacts with the *O*-acylurea formed from the reaction between the carboxylic acid group of the NSAID and the EDC, to form an activated ester **145**, which can be isolated or used *in situ* (Figure 4.4) [332,334]. Generation of this activated ester and subsequent addition of the chlorin photosensitizer allowed for the formation of the ester conjugate. By monitoring the reaction time and equivalents, one is able to maximize the amount of monofunctionalized chlorin in the reaction mixture in comparison to the higher order derivatives. Thin-layer chromatography showed a distinctive degree of substitution, similar to previous work, with the tetrafunctionalized derivative having the highest R_f and the unsubstituted chlorin having the lowest.

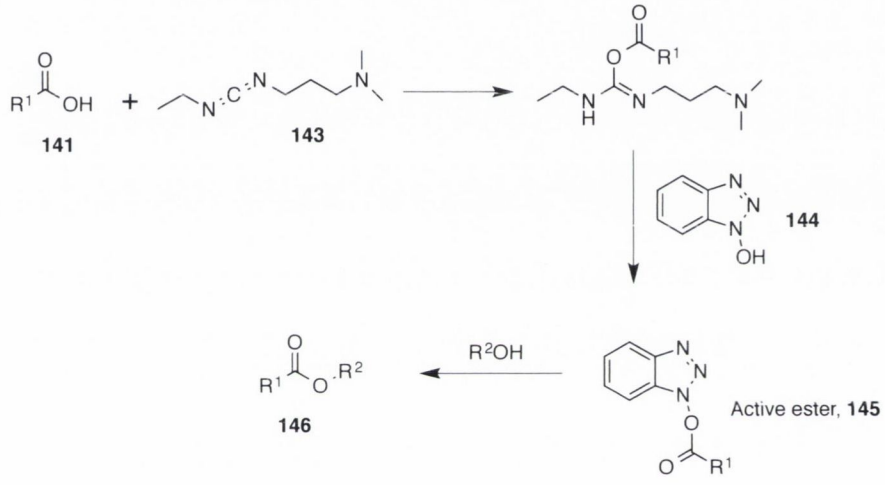

Figure 4.4. Synthesis of *m*-THPC conjugates using modified Steglich reaction conditions.

Following on from the success of these reaction conditions, a plan was devised to investigate the robustness of the synthesis by using a variety of NSAIDs to create a small library of conjugates. Fenamic acid, i.e. 2-(phenylamino)benzoic acid **139** and ibuprofen, (*S*)-2-(4-(2-methylpropyl)phenyl)propanoic acid **147,** were chosen as suitable initial candidates for the screen due to similarities in structure to anthranilic acid and also their prolific record as agents used in the treatment of numerous inflammatory diseases [336,337].

Both NSAIDs readily conjugated to the chlorin scaffold in a controlled and predictable fashion and altering the reaction time and equivalents of reagents used could maximize the degree of functionalization.

The final section of this library of conjugates was completed with the introduction of diclofenac, 2-(2-(2,6-dichlorophenylamino)phenyl)acetic acid **148** and nicotinic acid **149**. Diclofenac was selected because it is an effective anti-inflammatory and analgesic agent, whilst being one of the most patient tolerated NSAIDs on the market [338]. Nicotinic acid, whilst traditionally

clinically implemented for diseases such as cholesterol, research has shown it to have quite promising anti-inflammatory properties in cases of atherosclerosis [339].

Diclofenac was obtained as its sodium salt and for the purpose of this project was acidified back to the carboxylic acid. Again, controlled functionalization was achieved through reaction equivalents and length. Nicotinic acid (**149**) did not readily undergo conjugation with the chlorin photosensitizer under these optimized conditions. After the investigation into a number of different bases and modified procedures, it was found that pyridine and EDC worked to yield the mono- and tetrafunctionalized derivatives in comparable yields to the previous conjugates.

Table 4.1. Modified Steglich reaction with a variety of NSAIDs to afford novel chlorin-NSAID photosensitizers.

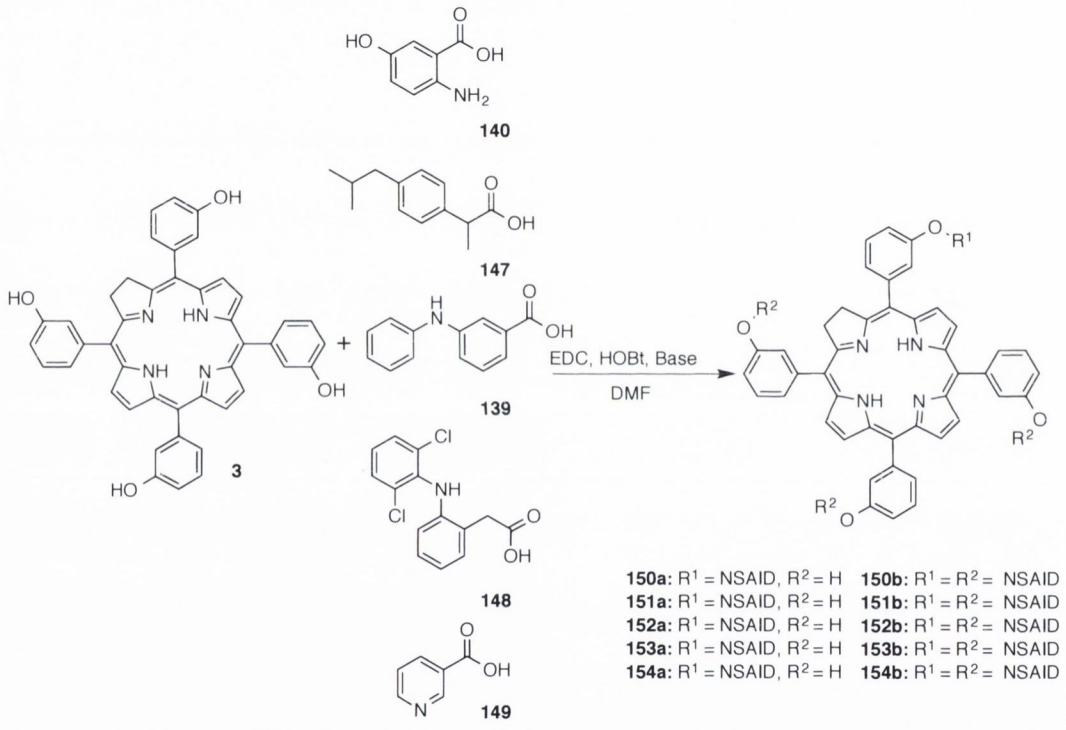

Conjugate	NSAID	Base	% Yield of Mono (a)	% Yield of Tetra (b)
150	5-hydroxyanthranilic acid (140)	K_2CO_3	36	61
151	Ibuprofen (147)	K_2CO_3	35	65
152	Fenamic Acid (139)	K_2CO_3	45	83
153	Diclofenac (148)	K_2CO_3	37	60
154	Nicotinic Acid (149)	Pyridine	43	70

4.3 "Complex" Anti-inflammatories

The synthesized library of "iChlorins" above was deemed adequate for the purpose of demonstrating the conjugation of anti-inflammatories with carboxylic acid functionalities to the *m*-THPC scaffold. Conjugation reactions were attempted with more "complex" anti-inflammatories to further probe the robustness of the synthetic pathway. Again, a small library of suitable candidates were selected and tested (Figure 4.5).

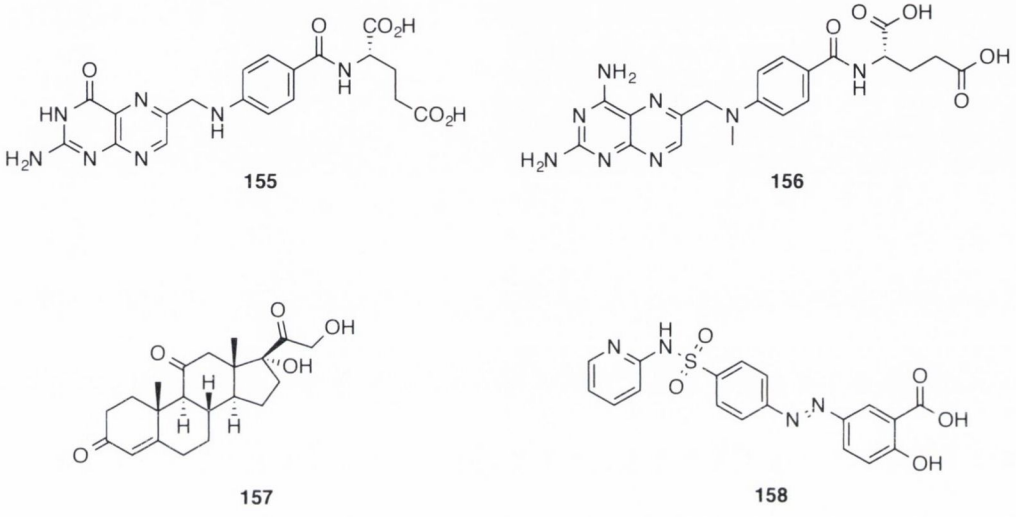

Figure 4.5 A library of "complex" anti-inflammatories for conjugation onto the *m*-THPC scaffold.

Methotrexate (**155**) was first implemented as an anti-cancer drug by competitively inhibiting dihydrofolate reductase (DHFR), an enzyme that participates in the tetrahydrofolate synthesis [340]. Its mechanism of action for auto-immune diseases such as rheumatoid arthritis or Crohn's disease is completely different, with the inhibition of a number of biological processes leading to deactivation of enzyme activity relevant to immune system function.

The synthesis for this section began with the use of folic acid **156** as a model compound for methotrexate as this is extremely expensive and only commercially available in small quantities in comparison to folic acid, which is cheap and commercially available. Also, methotrexate acts as a competitive inhibitor of folic acid, thus they act at the same site.

Difficulties arose with the synthesis due to the conflicting solubilities of folic acid **156** and the chlorin scaffold **3**. Folic acid is soluble in water but its solubility is limited in organic solvents, which is in stark contrast to *m*-THPC. Despite this difficulty, the use of DMF overcame this problem, with enough folic acid in solution for test reactions to begin. The next difficulty associated with this reaction was the presence of two carboxylic acid functionalities within the folic acid framework. It was believed this could be overcome because of the variety in reactivity of these carboxylic acids due to them being primary and secondary derivatives. The terminal

carboxylic acid should be less sterically hindered and therefore react first with the coupling agents to form the activated ester, which in turn can react with the chlorin (Scheme 4.4).

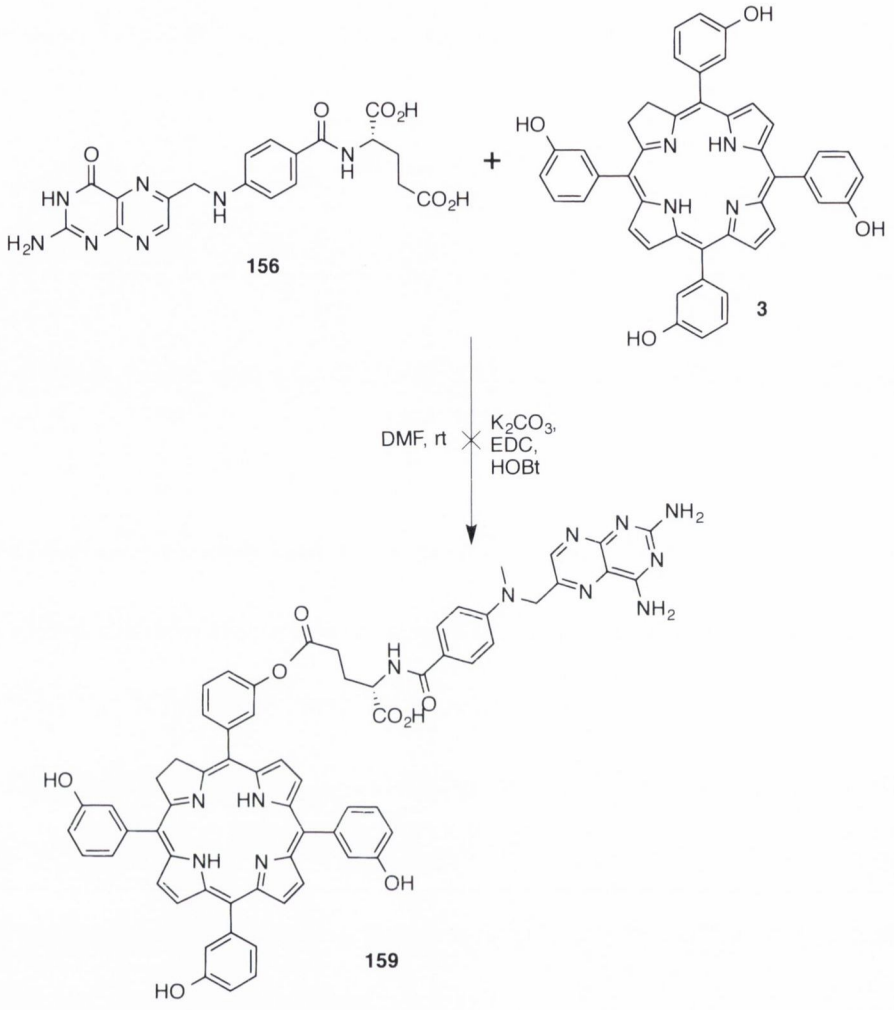

Scheme 4.4. Attempted coupling of folic acid **156**, a cheap model compound of methotrexate **155**, to the *m*-THPC scaffold **3**.

Using excess equivalents of base and coupling agents EDC (**143**) and HOBt (**145**) gave a mixture of reaction products, which suffered from a low R_f in a number of different solvent systems. The use of a centrifuge has become common practice for the isolation of folic acid conjugates, again due to their poor solubility. However, more traditional methods were attempted such as precipitations and filtrations. Whilst unreacted folic acid was obtained from these purifications efforts, no observable conjugates were isolated.

Cortisone **157** and sulfasalazine **158**, again, were chosen as cheap and commercially available anti-inflammatories that have regulatory approval and are well known for their treatment of joint-pain in arthritis sufferers. These two compounds have drastically contrasting molecular frameworks, and as such, had to be conjugated to the chlorin through different methodology. Thus, from herein, their properties and attempted conjugation are discussed separately.

Cortisone **157** is one of the most widely used over-the-counter anti-inflammatory agents on the market today. It has multiple methods of delivery that include orally, intravenously or particularly interesting for PDT researchers, by topical administration of the drug. It is a 21-C corticosteroid produced by the adrenal gland in times of stress. Cortisone works by suppressing the immune system and therefore reduces inflammation and swelling at the therapeutic region [337]. For the purpose of this library, cortisone was the only anti-inflammatory used that was devoid of the carboxylic acid functionality. It does however contain both a primary and secondary alcohol. Again, it was hoped that there would be some variance in reactivity between the two alcohols due to the presence of a more hindered secondary alcohol.

The primary alcohol was to be activated through the use of mesyl chloride **160** to form a reactive mesylate species that would then be susceptible to nucleophilic substitution by a hydroxyl group from the chlorin. Trial investigations began by using excess mesyl chloride **160** to attempt the activation of both alcohols. From there, it was hoped that the steric hindrance surrounding the secondary alcohol would prevent nucleophilic displacement and therefore one would obtain selectivity for the primary alcohol (Scheme 4.5). The steric effects did not prevent a reaction from occurring at this site and as a result, the reaction mixture contained a complex mixture of products with varying degrees of substitution. Standard column chromatography methods were unable to separate this mixture and therefore this synthetic route had to be abandoned.

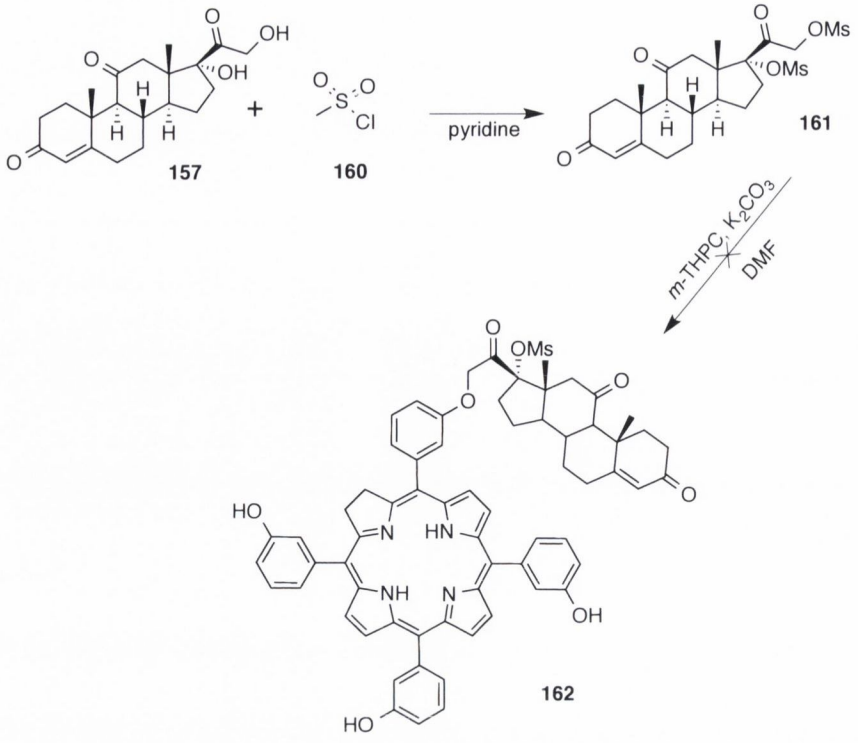

Scheme 4.5. Reaction of cortisone **157** with mesyl chloride **160** and subsequent conjugation with *m*-THPC **3**.

Thus, efforts shifted toward the final complex anti-inflammatory, Sulfasalazine **158**, an azo bond-containing drug developed primarily for the treatment of rheumatoid arthritis. The drug is synthesized through the combination of sulfapyridine and salicylate through the aforementioned azo bond. The theorized breakdown of the molecule can be observed in Figure 4.6. The dissolution of the azo bond leaves a hydroxyanthranilic acid derivative, an anti-inflammatory implemented above. Reactions began using the methodology described above and an excess of reagents in comparison to the chlorin. No observable chlorin reaction product was isolated from the reaction mixture; however, a new spot with a low R_f on TLC suggested the possible formation of a sulfasalazine dimer formed from the hydroxyl group present on its salicylate ring. Another possible side reaction was the decomposition of the azo bond to yield anthranilic acid derivative and the sulfa-pyridyl compound. Again, this was a side reaction which was known could occur and the lack of any desired conjugation may be explained by the steric bulk of the chlorin.

These reactions brought to an end this small-side project involving complex anti-inflammatories and although, initially unsuccessful, there is much scope for future work with these compounds to yield biologically interesting iChlorins.

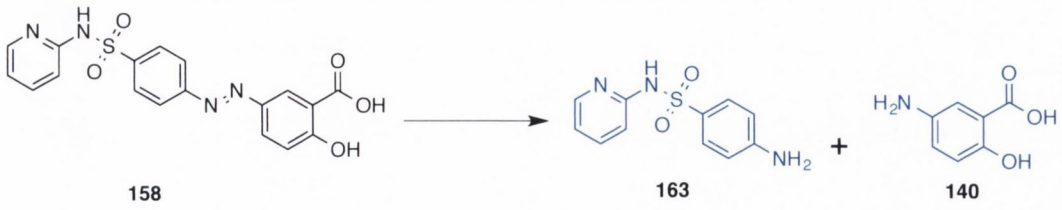

158 163 140

Figure 4.6. The theorized major decomposition material from the reaction of Sulfasalazine **158** and *m*-THPC scaffold **3**.

4.4 Photochemical & Biological Evaluation

4.4.1 Singlet Oxygen Studies

For any molecule to be considered a potential clinical PS, they must possess a high quantum yield of $^1O_2$. To evaluate the $^1O_2$ production capability of the library of conjugates, compounds were subjected to a DPBF assay in order to estimate their $^1O_2$ generation. Their production of $^1O_2$ was determined through the monitoring of the UV-vis spectroscopy of the dye 1,3-diphenylisobenzofuran (DPBF) in solution. The results obtained for compounds **151b** and **152a** from this assay were then compared to results obtained with the known $^1O_2$ producer *m*-THPC to give a relative indication of their $^1O_2$ producing potential.

Compounds **151b** and **152a** were dissolved in an aerated solution of DPBF in DMF and irradiated with white light and the intensity of the DPBF's absorption band was monitored over time using UV-vis spectroscopy. Both compounds showed good production of $^1O_2$, as per Figure 4.7, however not to the same extent as *m*-THPC (**3**). This suggests that a longer irradiation time *in vitro* may provide cytotoxic results comparable to those of the control, i.e. *m*-THPC.

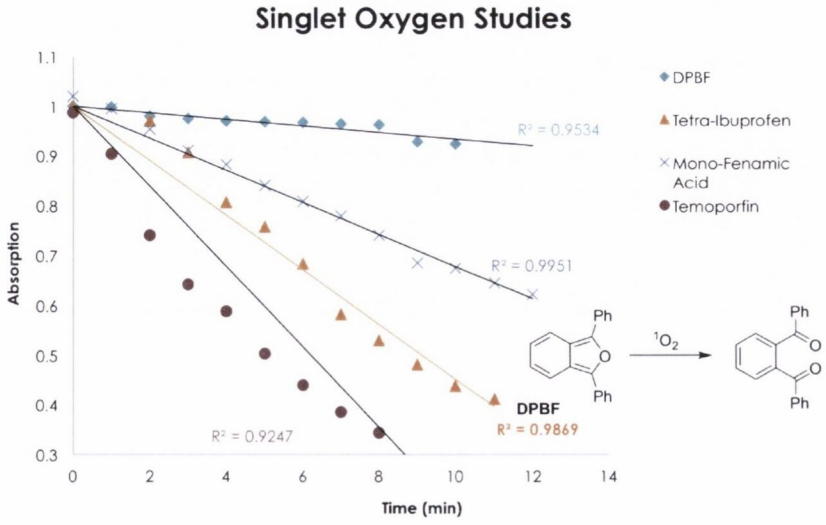

Figure 4.7. Graph displaying the reduction in absorbance of DPBF at 410 nm over time due to the production of $^1O_2$.

4.4.2 Biological Testing

Compounds **150a-154b** underwent biological testing [312] to ascertain their localization and cytotoxic properties using esophageal carcinoma OE33, esophagus adenocarcinoma, and well-differentiated SKGT-4 human cell lines by Dr. Natalia Sergeeva and Dr. Edyta Paszko. All compounds were successfully taken up into the cells and in accordance with previous research conducted with the same PS core, appear to localize in the ER and Golgi apparatus (Figure 4.8). The compounds were then subjected to a colorimetric MTS assay to assess their cytotoxicity. The compounds were tested over a range of concentrations (10-40 μM) with an illumination period of 2 min [313]. None of the conjugates exhibited any phototoxic effect, which may be due to the relatively short illumination period. As per the graph in Figure 4.7, *m*-THPC has a considerably large yield of $^1O_2$ after 2 min of illumination, where as the conjugates tested only begin to become comparably to *m*-THPC after an illumination period of 12 min. This suggests that a longer irradiation period may yield positive cytotoxicity results for these conjugates. Whilst longer irradiation times are not ideal from a clinical standpoint due to potential patient discomfort caused from burns, any reduction in post-treatment photosensitivity would offset this complication.

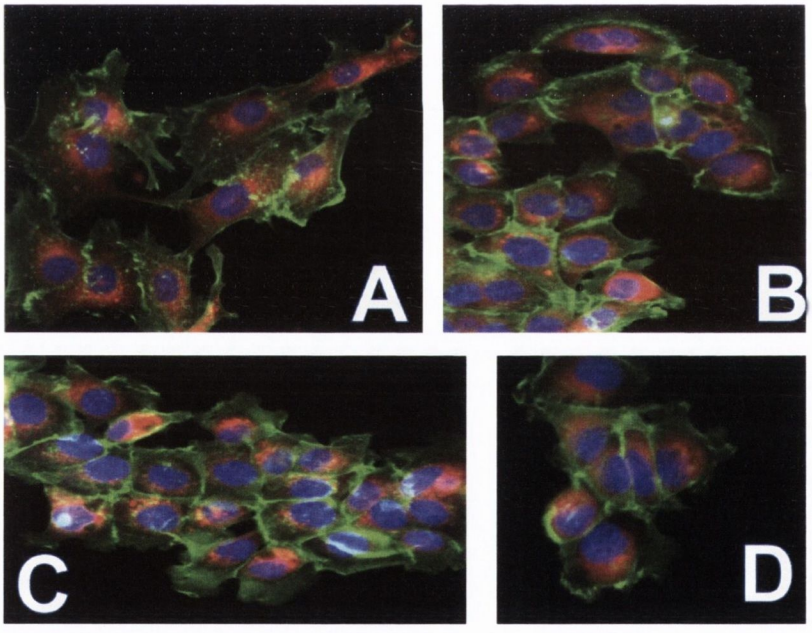

Figure 4.8. OE33 and SKGT-4 cells stained with compounds **150a, 151b, 152a** and **154b** (red), nuclear dye Hoechst 33342 (blue), F-actin dye Phalloidin 490 (green): (a) **150a** 30 μM, SKGT-4; (b) **151b** OE33 40 μM; (c) **152a** SKGT 40 μM; (d) **154b** OE33 40 μM [341].

4.5 Conclusions & Future Work

4.5.1 Conclusions

A small library of chlorin-conjugated NSAIDs has been successfully synthesized through the controlled functionalization of the chlorin core using a modified Steglich reaction. This

methodology proved to be simple, robust and produced mono- and tetrafunctionalized conjugates in reasonable yields and few synthetic steps. All conjugates successfully entered into esophageal carcinoma OE33, esophagus adenocarcinoma, and well-differentiated SKGT-4 human cell lines and whilst no cytotoxicity was observed, due to results obtained in the $^1O_2$ production assay, it is believed that longer irradiation times may be able to improve the cytotoxicity of the conjugates and therefore the efficacy of the treatment.

The co-administration of coxibs and NSAIDs has been shown to improve the overall efficiency of PDT and with this new conjugate approach, it is hoped to further progress the reduction of post-PDT inflammation and tumor regrowth [319].

4.5.2 Future Work

Work from this project from a synthetic standpoint will move towards the production of mixed treatment modality systems. These systems will take advantage of the robust methodology developed in Chapters **2** and **3** to synthesize systems with multiple biologically pertinent groups, i.e., a sugar or bile acid for targeting and anti-inflammatories for improved tumor ablation and reduced occurrence of tumor regrowth.

Compounds **150a-154b** synthesized previously and the library of mixed conjugated systems must be evaluated for their cytotoxicity over a range of illumination periods, as the crude DPBF assay demonstrates their $^1O_2$ producing capabilities. This fact, coupled with their successful transportation into the cell's molecular machinery suggests a system that could demonstrate positive results.

Despite the negative results for the synthesis of complex iChlorins, it is a section of this project that could achieve great success by introducing slight synthetic modifications to the complex starting materials. These alterations will limit the possibility of the aforementioned side reactions from occurring and with the use of some more specialized purification techniques, e.g., a centrifuge, it may be possible to isolate these folic acid conjugates.

This library of conjugates could also undergo *in vivo* experiments in mice in conjunction with researchers in the biochemists. Ideally, these potential collaborators would administer one of the conjugates intravenously and through the use of Western-blot analysis, observe reduced levels of the pro-inflammatory molecules associated with this tumor regrowth (Figure 4.9).

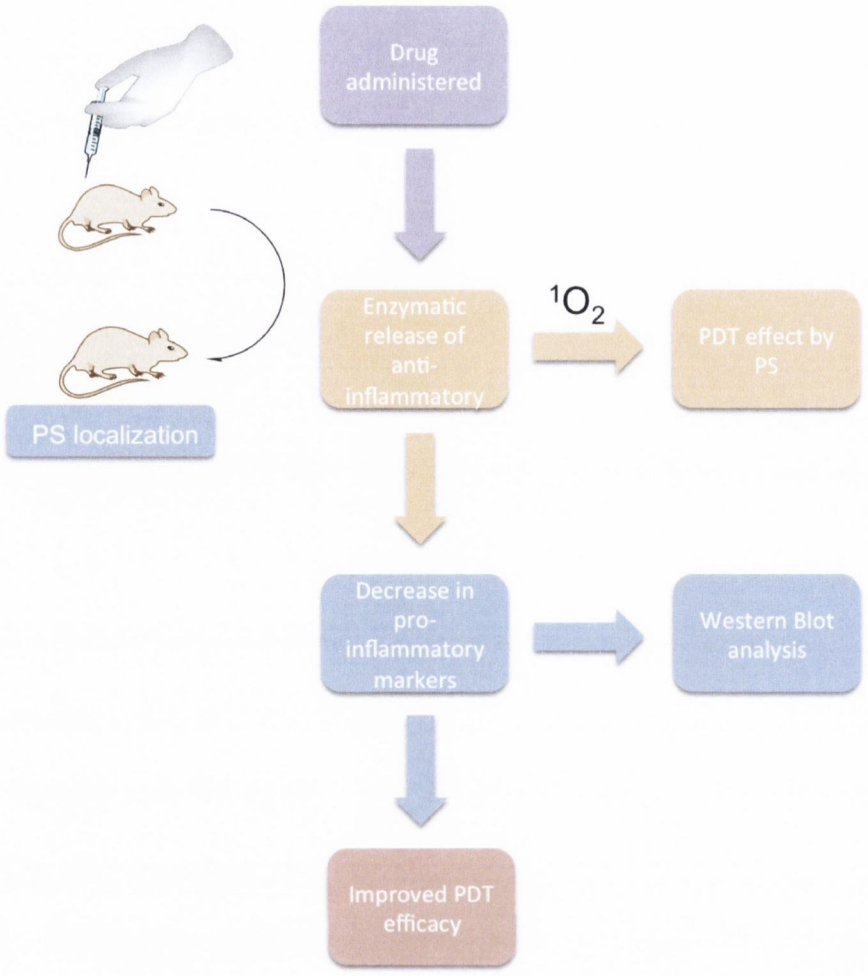

Figure 4.9. Potential *in vitro* study for the investigation of the efficacy of anti-inflammatory conjugates in an appropriate mouse model.

With respect to the complex anti-inflammatory section, there are standard methods available to selectively protect the primary alcohol, then protect the secondary alcohol with a orthogonal protecting group and subsequent selective deprotection of the primary alcohol, to leave a viable coupling partner for reactions discussed previously (Figure 4.10). This synthetic pathway would leave a suitable activated anti-inflammatory, for this investigatory type project.

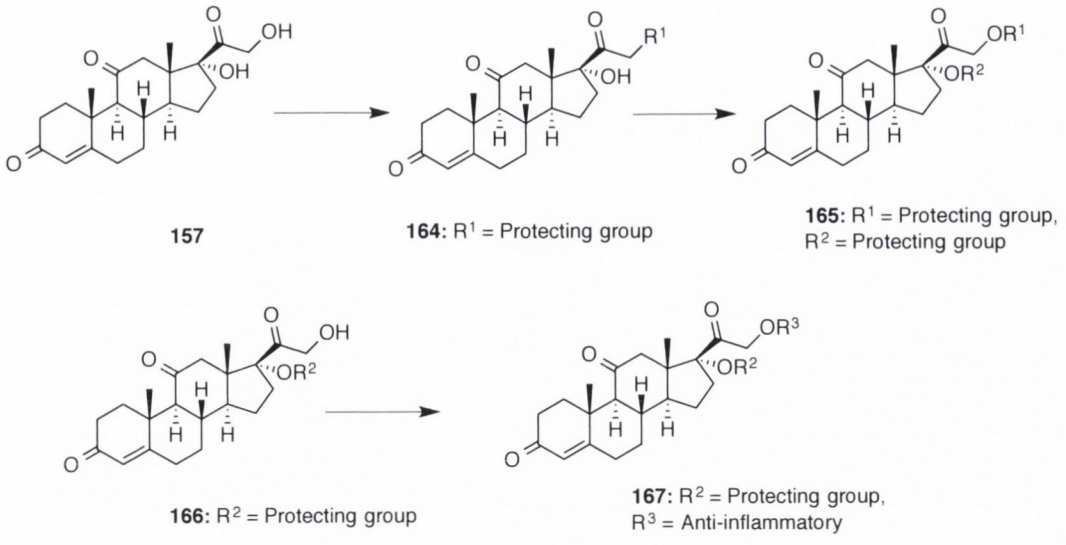

Figure 4.10. Potential synthetic pathway for the construction of a selective cortisone synthon.

Chapter 5:

Triptycene as a Rigid Molecular Scaffold

5.1 Introduction

Rigid molecular frameworks are required as molecular scaffolds for a variety of applications. Examples are molecular machines or the design and synthesis of porphyrin arrays for electronic devices and as light-harvesting antenna systems [342]. In this area, porphyrin assemblies with highly conjugated π-systems with rigid, well-defined geometries are of interest [343]. In nature, the antenna chlorophylls in photosynthetic bacteria are arranged as macrorings in a spatially defined manner to absorb and transfer solar energy efficiently [277,344].

Triptycene belongs to a unique family of homoconjugated aromatic compounds consisting of three separate arene units fused together through a bicyclic [2.2.2] octane framework [345]. This rigid three-dimensional framework makes this class of compound suitable for applications such as host-guest complexes, molecular inclusion compounds and co-ordination compounds with unusual geometries. The 120° orientation provided by the triptycene scaffold **23** makes it a useful linker for multichromophore assemblies and an important component of molecular motors [189].

Despite their rigidity, symmetry and ability to project groups in a spatially defined manner, the use of triptycene derivatives as scaffolding material is limited [346]. This may be due to the limited success of triptycene in organometallic C-C coupling methods, owing to the previous absence of suitable halogenated triptycene partners. Previous work in the Senge group has shown the successful preparation of triporphyrin triptycene scaffolds, starting from triiodo triptycene [186,198].

Work on this project centered on triiodotriptycene as an excellent synthon for metal-catalyzed cross coupling reactions. This scaffold could be synthesized using classical triptycene chemistry, i.e., nitration **168-169**, followed by amination **170** and a subsequent Sandmeyer reaction to install the iodo-functionality **171** (Scheme 5.1). Using both boryl- and alkynyl-porphyrins, Dahms *et al.* were successful in functionalizing the triptycene periphery with three porphyrin sub-units [186]. These reactions occurred using known literature procedures in good yields. These trimers were subsequently tested for their host-guest properties using the bidentate ligand, 4,4'-bipyridine (bipy) [198].

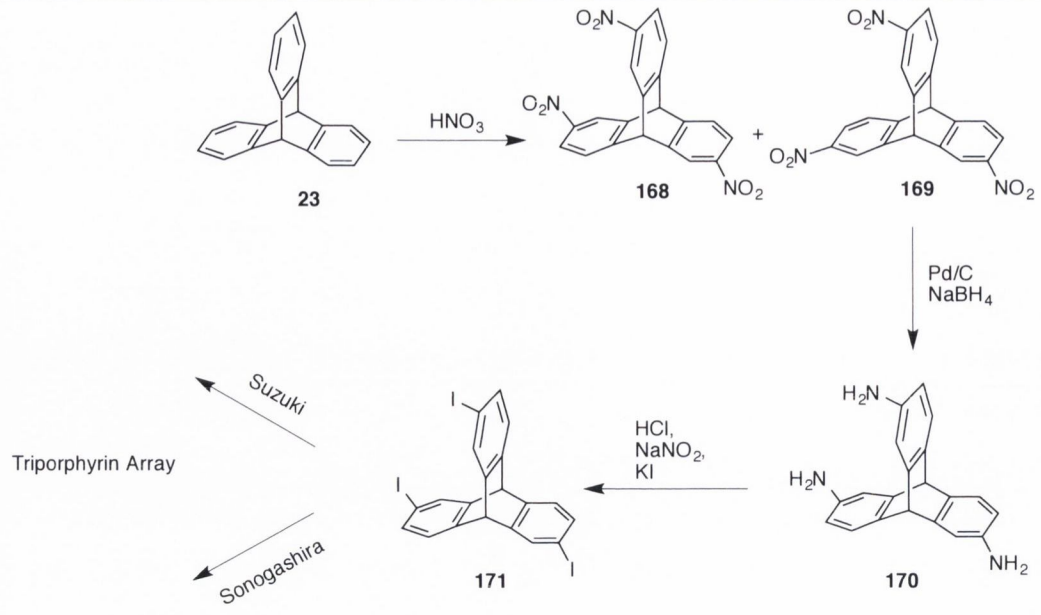

Scheme 5.1. Synthesis of triporphyrintriptycene arrays through both Suzuki and Sonogashira reaction conditions [197,198].

5.2 Hexafunctionalization coupling partner

Hilton *et al.* recently reported the synthesis of hexabromotriptycene **172** [187]. It was conceived that this scaffold would act as an excellent coupling partner in Suzuki cross-coupling reactions and help update work previously established within the Senge group, i.e., the synthesis of triptycene-porphyrin trimers, to include hexasubstituted triptycene derivatives (Figure 5.1).

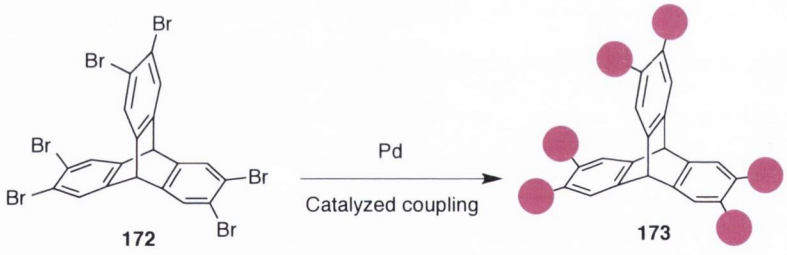

Figure 5.1. Potential synthetic pathway to yield hexafunctionalized-triptycene scaffolds.

5.2.1 Hexafunctionalization through alkyl Suzuki reaction

Attempts began for the generation of a library of hexafunctionalized triptycene systems through the use of a range of palladium-catalyzed cross coupling reactions. Initial work conducted by Dr. Yasser M. Shaker on the hexafunctionalization of triptycene through an unoptimized Suzuki methodology formed the basis for the initial investigatory reactions. By using alkyl boronic acids and dichloro[1,1'-bis(diphenylphosphino)ferrocene]palladium(II), [Pd(dppf)Cl_2], he was successful in the six-fold introduction of alkyl moieties around the triptycene scaffold in moderate yields (Scheme 5.2) [347].

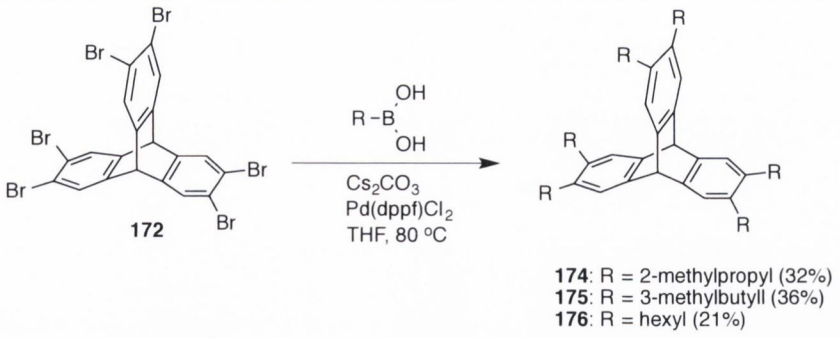

Scheme 5.2. Synthesis of a small library of alkyltriptycene derivatives through an unoptimized Suzuki reaction methodology.

5.3 Results

5.3.1 Suzuki Couplings

Investigatory reactions for the six-fold functionalization of triptycene began with the use of the Suzuki cross-coupling reaction as it is an extremely robust and relatively cheap transition metal catalyzed reaction. It was hoped to create a library of hexasubstituted triptycene derivatives that contained additional chemical functionalities that would allow for further functionalization, i.e., macrocyclization, cyclocondensations, or even metal chelating ligands [185,348,349].

This project was conducted in conjunction with another member of the research group, Ms. Claire Moylan. Work was bifurcated with the initial goal being set at a library of five to ten examples of six-fold Suzuki reactions with the triptycene scaffold. Thus, a screen of boronic acids/esters was conducted in order to investigate the viability and robustness of this synthetic pathway. Starting with routine Suzuki reaction conditions, i.e., $Pd(PPh_3)_4$ and K_3PO_4 as the base, attempts were made on the six-fold introduction of substituted aryl moieties around the triptycene periphery (Table 5.1).

4-Formylphenylboronic acid was the first boronic acid selected for this investigation. The formyl group should be mildly electron withdrawing and provides a synthetic scaffold for future functionalization reactions such as the installation of porphyrins through dipyrromethane formation or, the next-step further, BODIPY dyes. This reaction proceeded without complication; with minor adjustments to the reaction equivalents used eventually giving the hexasubstituted product **177** in 64% yield (Table 5.1). Purification of the product initially proved cumbersome due to the minor products, i.e., the lower substituted products and excess boronic acid used. One can slowly increase the polarity of the mobile phase, removing the boronic acid and lower order derivatives. Finally, a switch to a CH_2Cl_2:MeOH (98:2) gives the desired hexasubstituted scaffold.

Following on from this, both 4-cyanophenylboronic acid and 3-cyanophenylboronic acid were trialed as to investigate if small changes in electronics would interfere with yields. Again, with

near identical conditions to the formylboronic acid, these compounds proved to be model coupling partners for the bromotriptycene scaffold **172** with their optimized yields being 63% and 61%, respectively for compounds **178** and **179** (Table 5.1). The cyanofunctionality provides an entry point into a number of different synthetic handles and again, feeds into the ethos that the installation of distal functional groups provides rigid molecular scaffolds that have the ability to be tailored to a range of applications.

Difficulties within the group with the direct Suzuki coupling of a benzoic acid derivative have occurred previously and therefore the methylester derivative was implemented [260]. Using identical conditions to the reactions mentioned above, this group was installed onto the triptycene scaffold. Standard work-up procedures gave the crude product as a yellow solid **180a**. Deprotection of the ester functionality ensued with an excess of KOH used to ensure complete cleavage had occurred. After some initial test reactions, 400 equiv. were necessary to achieve complete deprotection. Isolation of this product was fortuitously straightforward as the material is practically insoluble in CH_2Cl_2. Thus, after neutralization of the remaining KOH with 0.1 M HCl extraction into EtOAc and subsequent removal of solvent *in vacuo*, the crude product was taken into CH_2Cl_2 where the product would form a precipitate that could then be filtered to give the pure product **180b** in a 60% yield.

The field of metal-organic frameworks has seen an almost exponential increase in publications in recent years [237,239,350,351]. Research in this field typical involves the binding of carboxylic acids to metal ions to form these rigid frameworks that often display extremely interesting characteristics such as high porosity [352]. Due to the rigidity of the triptycene scaffold, the binding of metal ions through terminal carboxylic acid functionalities would provide materials of an interesting 3-D structure with many possible applications (Figure 5.2).

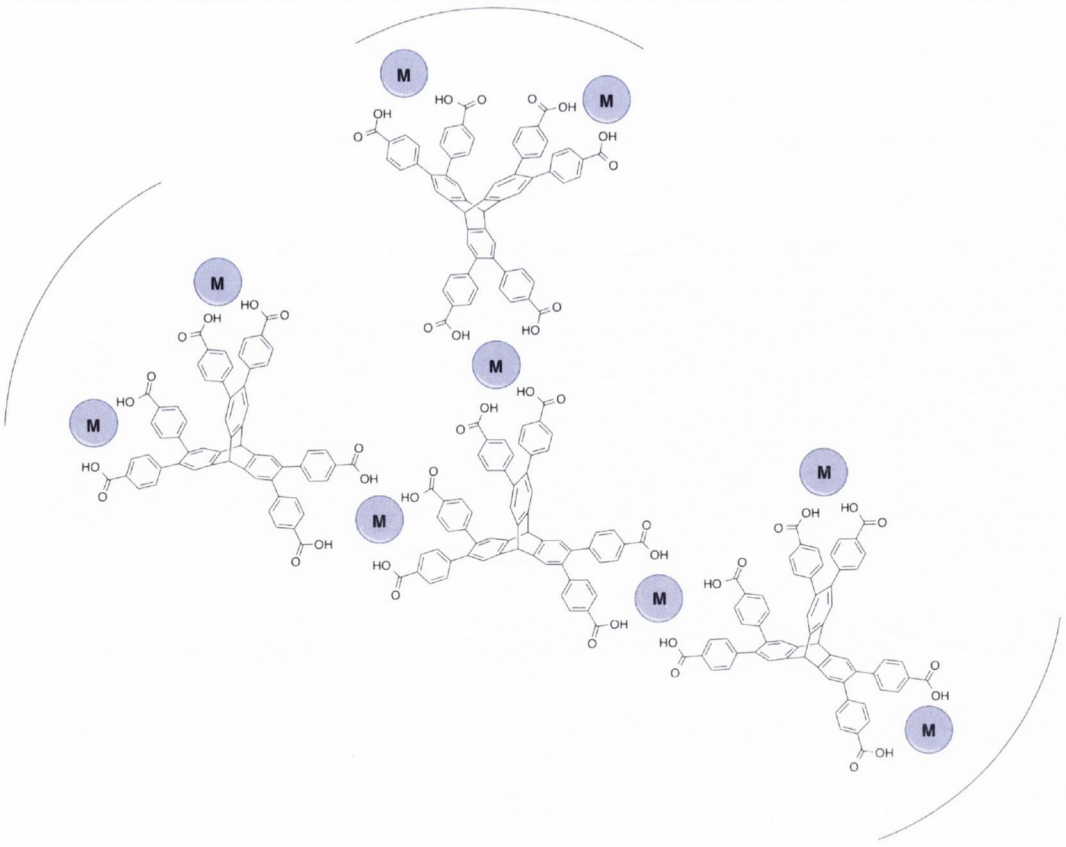

<*Figure 5.2*. An illustrative example of potential molecular frameworks made possible by the synthesis of the hexaphenylcarboxylic acid-substituted triptycene.>

Analysis of this material **180b** proved exceedingly difficult due to its adverse solubility in $CDCl_3$ and other common NMR solvents. The breakthrough came from the use of a 1-2 percent addition of deuterated pyridine, which brought the product into solution and allowed for the successful obtainment of ^{1}H and ^{13}C NMR spectra, as seen below (Figure 5.3).

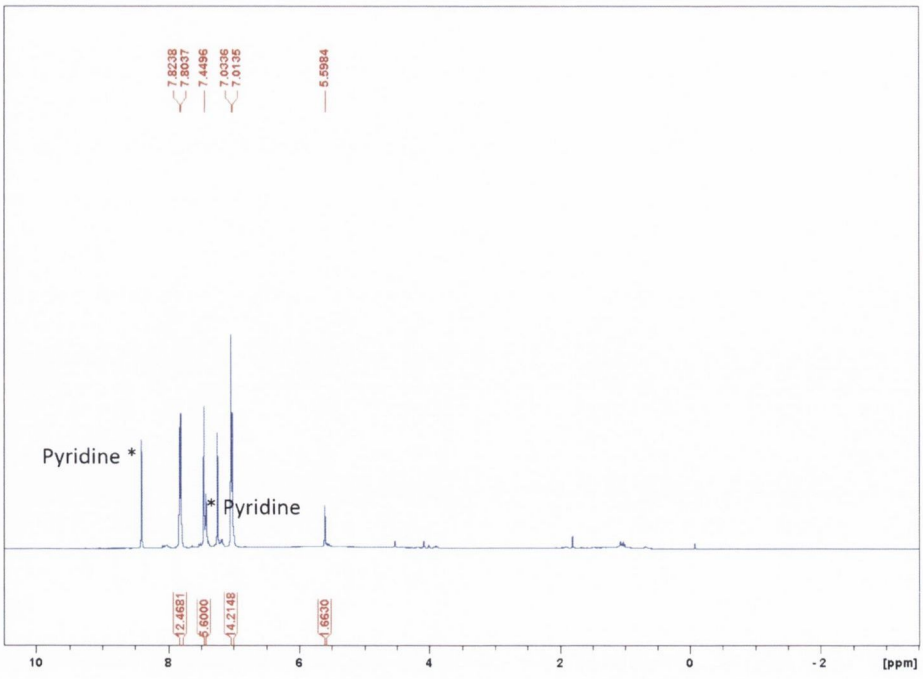

Figure 5.3. NMR spectra of the hexasubstituted scaffold **180b**.

The final boronic coupling partner for this portion of the initial investigation was the bis(pinacolato)ester. The product of this reaction would be the hexaboronic ester triptycene scaffold **184**, which is envisaged to be a pivotal synthetic scaffold for researchers in this field. As aryl halides are more abundant then their corresponding boron counterparts, it would greatly increase the scope of this synthetic pathway. Minor alterations eventually gave the desired scaffold in a yield of 36 %. These included an increase in the boronic ester and the use of solvent for the reaction was changed to 1,2-dichloroethane, a known literature solvent for borylation reactions [353,354].

This synthetic pathway proved itself to be extremely robust in producing hexafunctionalized triptycene scaffolds **177-184** in good yields whilst allowing for the presence of distal functional groups that can be implemented in further reactions. The groups present in the screen can be implemented in a wide assortment of chemical transformations and applications.

Table 5.1. Suzuki cross-coupling reaction with an array of aryl boronic acids/esters with hexabromotriptycene[5].

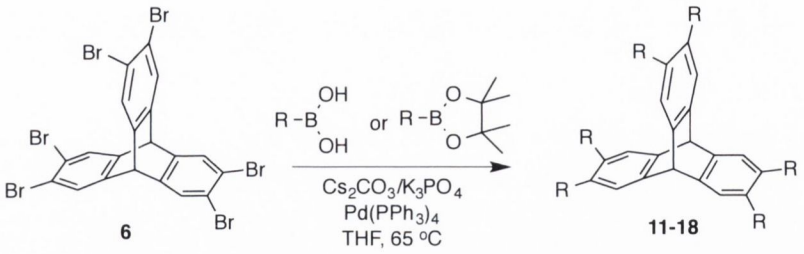

177: R = 4-formylphenyl, 64%
178: R = 4-cyanophenyl, 63%
179: R = 3-cyanophenyl, 61%
180b: R = 4-methoxycarbonylphenyl, 60%
181: R = 3-methoxyphenyl, 45%
182: R = 4-(dimethylamino)phenyl, 72%
183: R = 4-ethynylphenyl, 63%
184: R = boronic acid pinacol ester, 36%

Appendage (R)	Boron Equiv.	Pd (eq.)	Solvent/ Temp.	Base	Yields
4-formylphenyl (**177**)	Acid (12 eq.)	0.3 eq.	THF @ 65 °C	K_3PO_4 (12 eq.)	64%
4-cyanophenyl (**178**)	Acid (12 eq.)	0.3 eq.	THF @ 65 °C	K_3PO_4 (15 eq.)	63%
3-cyanophenyl (**179**)	Acid (18 eq.)	0.3 eq.	THF @ 65 °C	K_3PO_4 (12 eq.)	61%
4-methoxycarbonylphenyl (**180B**)	Acid (15 eq.)	0.3 eq.	THF @ 65 °C	Cs_2CO_3 (20 eq.)	60%
3-methoxyphenyl (**181**)	Ester (12 eq.)	0.3 eq.	THF @ 65 °C	Cs_2CO_3 (15 eq.)	45%
4-dimethylaminophenyl (**182**)	Ester (30 eq.)	1.2 eq.	THF @ 65 °C	K_3PO_4 (30 eq.)	72%
4-phenylacetylene (**183**	Acid (30 eq.)	1.2 eq.	THF @ 65 °C	K_3PO_4 (30 eq.)	63%
Boronic acid pinacol ester (**184**)	Ester (36eq.)	1.2eq.	THF @ 65 °C	Cs_2CO_3 (30)	36%

5.3.2 Sonogashira Couplings

Following on from this application of Suzuki methodology, interest arose in investigating whether other palladium-catalyzed reactions could yield hexafunctionalized systems in a one-pot coupling. Due to its high synthetic applicability and chemical robustness, the Sonogashira reaction obviously appealed in this regard [355-357]. Whilst often more challenging than Suzuki couplings, Sonogashira couplings enable the introduction of the ethynyl group: a powerful synthon in organic chemistry, exemplified in the reviews by Chinchilla and Najera [358,359]. With specific relation to triptycene, the ethynyl functionality is a highly attractive building block due to its potential for extended conjugation, its simple and rigid linear geometry as well as the potential for further functionalization.

[5] Compounds marked in blue in Table 5.1 were synthesized by Claire Moylan.

Many recent publications have shown the strength of microwave assisted Sonogashira reactions and as a result it was decided to commence the screen using Wang's conditions (Scheme 5.3) [360]. Whilst **186** was obtained in 76%, the archetypal goal of this project was to achieve the hexa-ethynyltriptycene derivative through more conventional and fundamentally more accessible methodology. Furthermore, due to the above success with six-fold Suzuki reactions, it was felt possible to achieve six-fold Sonogashira couplings using mechanical heating methods.

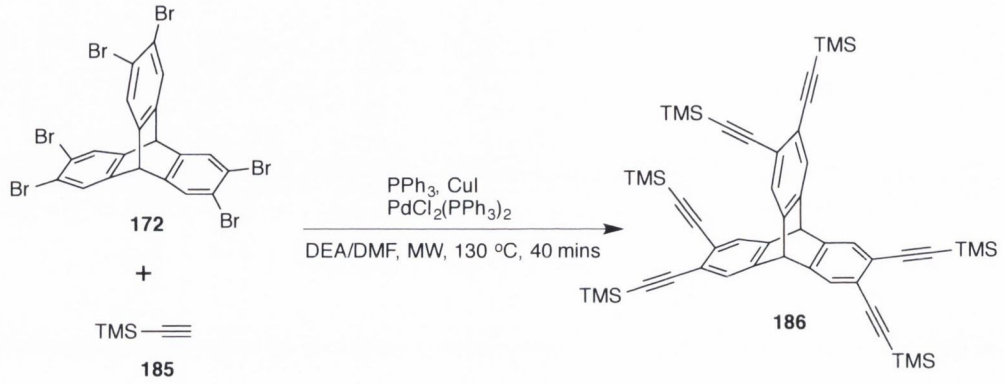

Scheme 5.3. Microwave-assisted synthesis of the TMS-protected alkynyltriptycene derivative **186**.

Initial efforts to couple **172** with TMS-acetylene **185** began by using similar conditions as the microwave reaction, i.e., $PdCl_2(PPh_3)_2$ as the catalyst (Entry 2, Table 5.2). These conditions however, resulted in no formation of the desired product with only unreacted starting material being recovered. A screen of a number of amine-based bases in THF was completed and the first positive result for the potential six-fold reaction came in the presence of a TEA/THF mixture at a temperature to maintain a reflux (Entry 5, Table 5.4).

Table 5.2. Initial attempts at applying similar conditions to the previously successful microwave-assisted synthesis of **186**.

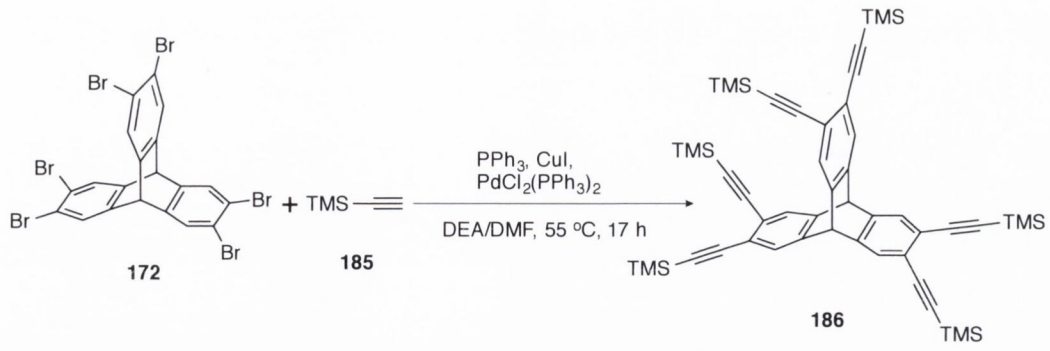

Entry	Substrate	Pd Cat. (eq.)	CuI (eq.)	PPh_3 (eq.)	DEA/DMF (mL)	Time (h)/ Temp (°C)	Observations
1	TMS acetylene (24 eq.)	0.05	0.11	---	1.6/5	17/55	Starting material
2	TMS acetylene (24 eq.)	0.05	0.11	1.2	1.6/5	17/55	Lower order products

The reaction mixture contained many undesired lower order derivatives, which made purification cumbersome. In an attempt to improve the yield and ease the purification workload, the catalyst loading was increased to 10% per position, however, ultimately to no improved success. A number of different catalyst systems were tested using this optimized base/solvent system (entry 1-4, Table 5.3). Again the reaction produced no product with only starting material being recovered from the reaction mixture.

Table 5.3. Investigation into a variety of catalyst/ligand systems for the synthesis of **186**.

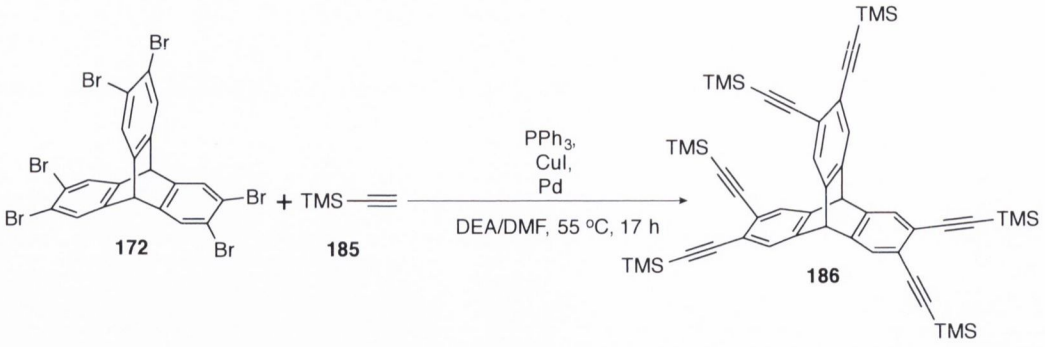

Entry	Catalyst	Pd Cat. (eq.)	CuI (eq.)	PPh_3 (eq.)	DEA/DMF (mL)	Time (h)/ Temp (°C)	Observations
1	$PdCl_2(PPh_3)_2$	0.1	0.11	---	1.6/5	17/55	Starting material
2	$PdCl_2(PPh_3)_2$	0.1	0.11	0.2	1.6/5	17/55	Lower order products
3	Pd2(dba)3/$PtBu_3$	0.05	0.11	0.2	1.6/5	18/55	SM+ trace lower order products
4	Pd2(dba)3/Cy_3	0.05	0.11	0.2	1.6/5	18/55	SM+ lower order, no hexa

Previous literature reports demonstrate the success of 'neat' base solvent systems and this proved to be the pivotal optimization made to the methodology [356,358]. Using 'neat' TEA as the solvent drastically improved the yield of the hexafunctionalized derivative whilst also decreasing the quantity of lower order reaction products. Thus, the reaction would appear to be heavily base dependent and this merits further investigation in the future to determine the rationale behind this.

Table 5.4. A library of different amine-based bases were trialed for their efficacy in the Sonogashira reaction between **172** and **185**.

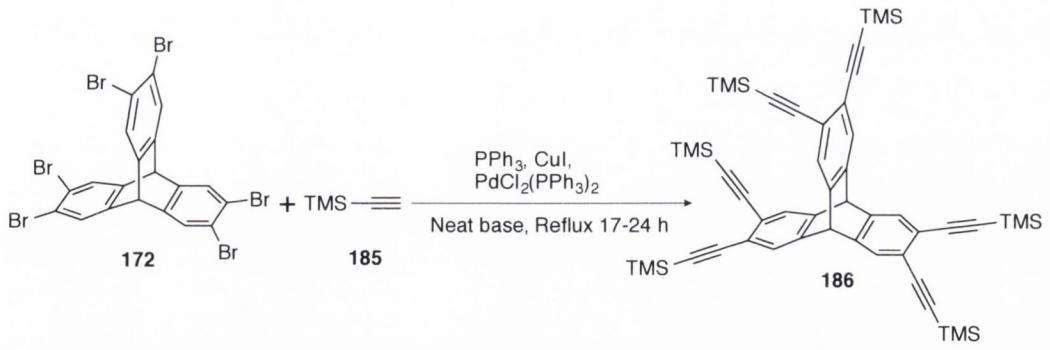

Entry	Substrate (eq.)	Pd Cat. (eq.)	CuI (eq.)	PPh_3 (eq.)	Base (mL)	Time (h)/ Temp (°C)	Observations
1	TMS acetylene (24)	0.1	0.11	1.2	DEA (5)	17/55	Lower order products
2	TMS acetylene (24)	0.05	0.19	0.44	DEA (5)	24/45	Lower order products
3	TMS acetylene (24)	0.05	0.19	0.44	Pyridine (5)	24/100	Lower order products
4	TMS acetylene (24)	0.1 (tetrakis)	0.01	1.2	Piperidine (5)	18/100	SM+trace products
5	TMS acetylene (24)	0.1	0.01	1.2	TEA (5)	18/90	Post deprotection gave 4',5'alkyne

The concluding step of the optimization process was a small screen of reaction times and temperatures in a final attempt to significantly push the reaction to completion. This screen of conditions led to the resulting optimized conditions, which provided compound **186** in 67 %, yield as per *entry* 3 in Table 5.5. Whilst the yield is slightly reduced in comparison to the microwave conditions, it is applicable to a greater synthetic audience and demonstrates the completion of a six-fold palladium catalyzed, one-pot, high yielding reaction through conventional methodology. Subsequent deprotection of the trimethylsilyl group present in **186** was achieved with tetra-*n*-butylammonium fluoride (TBAF) in CH_2Cl_2 at 25 °C for 12 h and gave 2,3,6,7,12,13-hexaethynyl-triptycene **187** in 80% yield, with shorter reaction times only yielding partial deprotection.

Table 5.5. Successful Sonogashira coupling and subsequent deprotection to yield the alkynyltriptycene scaffold **187**.

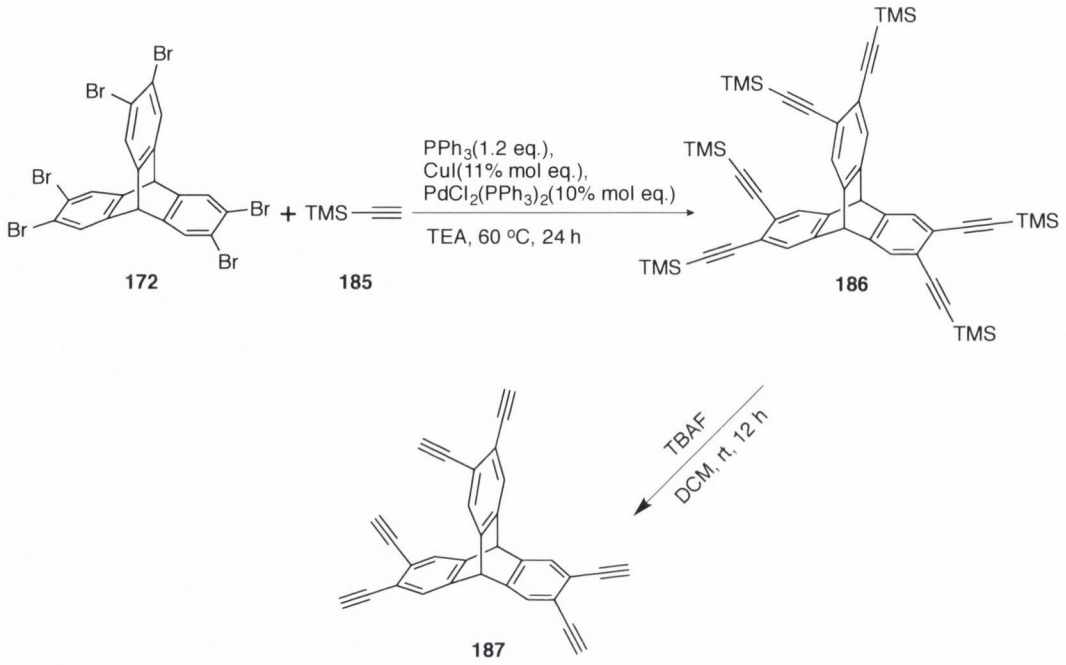

Entry	Substrate (eq.)	Pd Cat. (eq.)	CuI (eq.)	PPh_3 (eq.)	TEA (mL)	Time (h)/Temp (°C)	Observations
1	TMS acetylene (24)	0.1	0.11	1.2	5	17/60	Lower order products
2	TMS acetylene (24)	0.1	0.11	1.2	5	72/60	Higher order/ deprotection
3	TMS acetylene (24)	0.1	0.11	1.2	5	24/60	Hexa-substitution, 67%

It is evident that **187** is a useful synthetic building block. It allows for further functionalization reactions of the triptycene scaffold and will vastly reduce any steric hindrance present in these hexafunctionalization reactions. It is noteworthy that this "extending outwards" of the terminal functional groups also results in significant enlargement of the large internal free volume formed by the concave sides and may allow further studies into shape persistent materials or molecular reactors [344,361].

5.4 Post-functionalization Reactions

Although the above synthetic pathways highlight new methodology for researchers to manipulate the triptycene periphery, it was hoped to showcase a number of both simple and complex post-functionalization reactions that are possible with some of the synthons previously discussed.

Work for this was again bifurcated into:

- Arm extensions and simple functionalizations
- Complex functionalizations

Ms. Claire Moylan conducted the arm extensions and simple post-functionalization reactions. This entailed further Sonogashira and Glaser type couplings to elongate the "reach" of the arms and as a result, increase the internal free volume of the molecule.

5.4.1 Complex post-functionalization

The goal of this project from conceptual beginnings to a successful library of triptycene derivatives was always to synthesize a hexasubstituted triptycene-porphyrin array. The success of these post-functionalization reactions would demonstrate compound **187** versatility as a rigid precursor for transition metal catalyzed coupling reactions. It is hoped that these arrays could closely mimic the light-harvesting complexes of photosynthetic bacteria found in nature.

The starting point for research on this concept was the reaction of **187** with a bromoporphyrin derivative, i.e., **188-189**. By incorporating reaction conditions previously optimized for the extension of the triptycene "arms", it was envisaged that one could obtain the array in good yields and with straightforward purification. Synthetic work began using identical conditions to those used in the synthesis of **187**. These conditions afforded only unreacted starting materials and after a small screen of different catalyst/ligand combinations and a number of different bases/reaction times, standard mechanical heating was deemed inadequate (Table 5.6).

Table 5.6. Attempted bench synthesis of a hexaporphyrintriptycene array through a six-fold Sonogashira coupling.

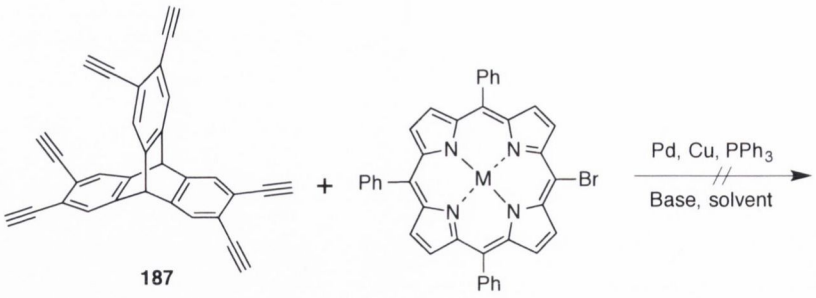

187

188: M = Zn
189: M = Ni

Entry	Porphyrin	Base	Temp °C	Solvent	Catalyst	Comment
1	Zn	TEA	80	-	$PdCl_2$	S. Mat+ debromo
2	Ni	TEA	80	-	$PdCl_2$	S. Mat
3	Zn	TEA	130	DMF	$PdCl_2$	S. Mat +debromo
4	Ni	TEA	130	DMF	$PdCl_2$	S. Mat
5	Zn	DEA	60	-	$PdCl_2$	S. Mat
6	Ni	DEA	60	-	$PdCl_2$	S. Mat
7	Zn	Piperidine	110	-	$Pd(PPh_3)_4$	S. Mat
8	Ni	Piperidine	110	-	$Pd(PPh_3)_4$	S. Mat

From here, it was decided to implement the use of a microwave reactor to assist in the Sonogashira coupling of **187** and **119** (Table 5.7). Initial reactions resulted in the formation of the lower order products, i.e., the mono-, di- and trisubstituted triptycene array and a substantial amount of debrominated porphyrin starting material. This suggested that the catalytic cycle was performing sluggishly and other variants of the Sonogashira reaction had to be attempted in order to obtain the hexaporphyrin array.

Table 5.7. Attempted microwave-assisted synthesis of the hexaporphyrin array using previously optimized Sonogashira conditions.

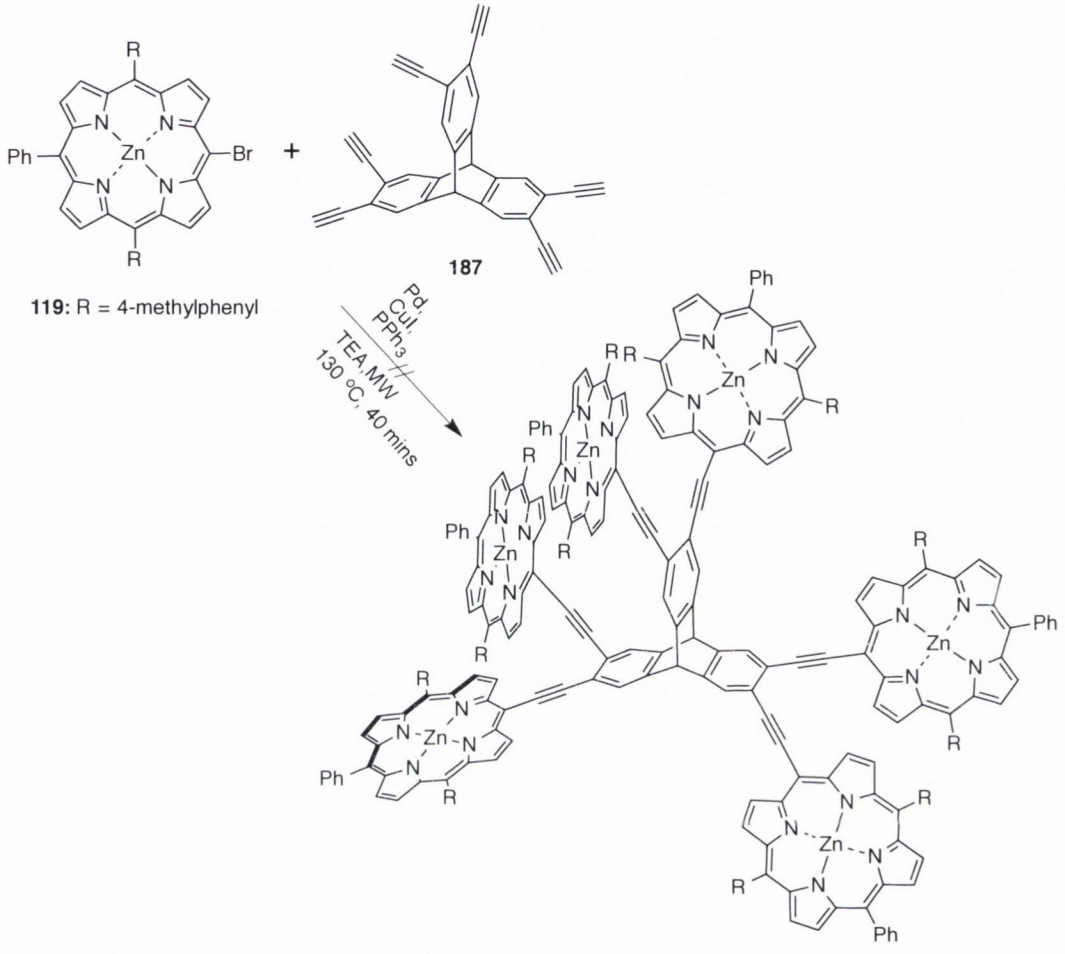

Entry	Porphyrin	Base	Heating	Temp °C	Solvent	Catalyst	Comment
1	Zn	TEA	MW	90	-	$PdCl_2(PPh_3)_2$	S. Mat
2	Zn	TEA	MW	110	-	$PdCl_2(PPh_3)_2$	3 green spots + debromo
3	Zn	TEA	MW	140	DMF	$PdCl_2(PPh_3)_2$	S. Mat
4	Zn	TEA	MW	110	-	$Pd(PPh_3)_4$	1 spot + debromo

5.4.2 Copper-free Sonogashira reaction

The addition of copper(I) salts provided the pivotal improvement in the methodology of alkyne couplings, as the presence of copper greatly accelerates the reaction and even enabled reactions to proceed at room temperature [358,359]. However, the addition of these cocatalysts typically have drawbacks, the most problematic being the occurrence of a Glaser coupling reaction by the *in situ* generated copper acetylide. This coupling proceeds upon exposure of the reaction mixture to air or oxidative agents and it can be problematic when the terminal alkyne is

expensive or difficult to obtain. Significant strides have been made in the development of coupling procedures that work in the absence of copper salts. Generally these methodologies aim to increase the reactivity of the catalytic system and therefore making the presence of the copper obsolete. These typically named 'Copper-free Sonogashira' couplings should perhaps be instead called a Heck and/or Casar coupling[6] (Figure 5.3) [362].

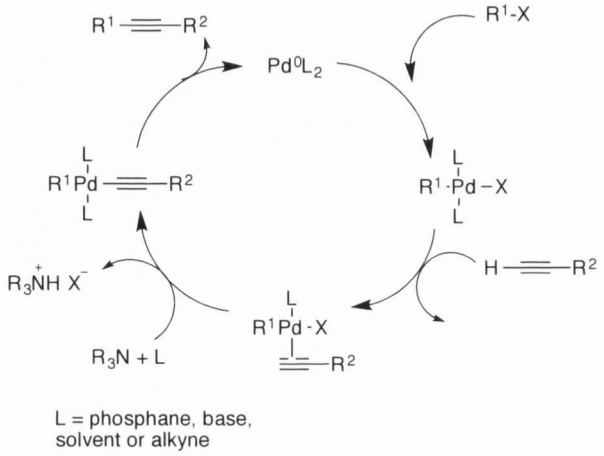

Figure 5.3. Proposed catalytic cycle for the "copper-free" Sonogashira reaction [362].

In an effort to synthesize the array, a number of 'copper-free' Sonogashira reactions were attempted. This class of reaction has been shown previously to work in high yields with porphyrin substrates [363,364]. Habitually, these copper-free reactions rely on either the excess use of amine (often even acting as solvent) or different palladium-ligand systems to increase the reactivity of the reaction. Accordingly, when tris(dibenzylideneacetone)dipalladium(0) [$Pd(dba)_3$] and triphenylaresine ($AsPh_3$) were used as the catalyst/ligand system, an immediate improvement in coupling was evident through HRMS and TLC, i.e., the tetra- and pentafunctionalized derivatives were obtained. Purification through column chromatography was proving problematic and as a result NMR spectra were always of crude material that displayed a complex mixture of reaction products. Despite an increase in catalyst loading and reaction time, no progress was made toward the obtainment of the hexaporphyrin array (Table 5.8). This reaction pathway consistently provided the synthesis of the lower order derivatives.

[6] As all sources of palladium will contain trace amounts of copper, which presumably could still be helping catalyze the reaction.

Table 5.8. Results from the "copper-free" Sonogashira reactions

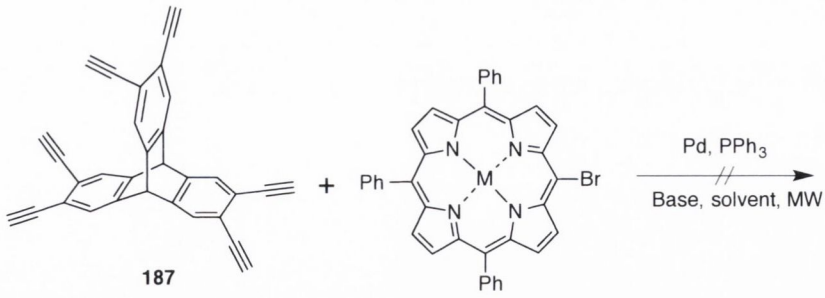

187

188: M = Zn
189: M = Ni

Entry	Porphyrin	Base	Heating	Temp °C	Solvent	Catalyst	Comment
1	**189**	TEA	MW	90	-	$Pd(dba)_3$	3 spots + debromo
2	**188**	TEA	MW	90	-	$Pd(dba)_3$	4 spots + debromo
3	**188**	TEA	MW	140	DMF	$Pd(dba)_3$	S. Mat
4	**188**	TEA	MW	100	-	$Pd(dba)_3$	Tetra and penta derivatives observed by HRMS

A range of different porphyrin coupling partners was synthesized as to investigate whether the porphyrin macrocycle and its substituents were interfering with the reaction pathway (Figure 5.4). Again, these reactions provided a mixture of results with simultaneous reactions occasionally providing completely contrasting results. Most reactions produced the lower order derivatives, proving that the newly employed catalytic system was facilitating the coupling of the porphyrin marcocycle to the triptycene scaffold. However, as per *entry 4* in Table 5.9, the hexaporphyrin array was observed in HRMS studies and the crude material underwent subsequent column chromatography as to isolate the targeted hexasubstituted array. Due to the paucity of material, and the theorized degradation or complexation of the array on the silica column, isolation of the purified compound proved unsuccessful.

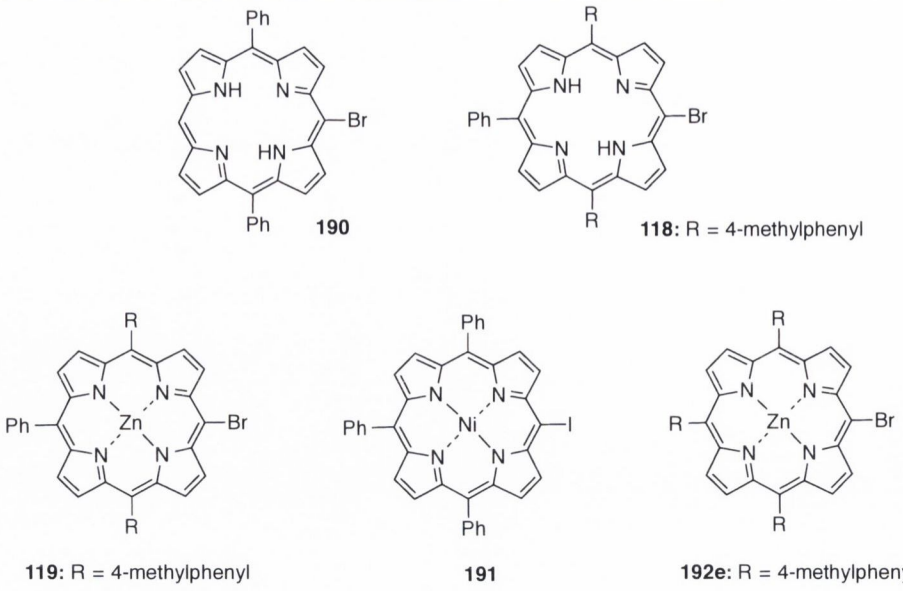

Figure 5.4. A range of different porphyrin coupling partners for use in Sonogashira-style couplings.

Despite an increase of reaction equivalents and catalyst loading, repeats of the reaction did not yield the targeted array. With the investigations into the electronic effects provided by the porphyrin proving unsuccessful in terms of reliable replication, the next logical step was to investigate if steric constraints were preventing the formation of the hexaporphyin scaffold.

Table 5.9. A range of "copper-free" Sonogashira reactions performed on a variety of porphyrins under microwave heating.

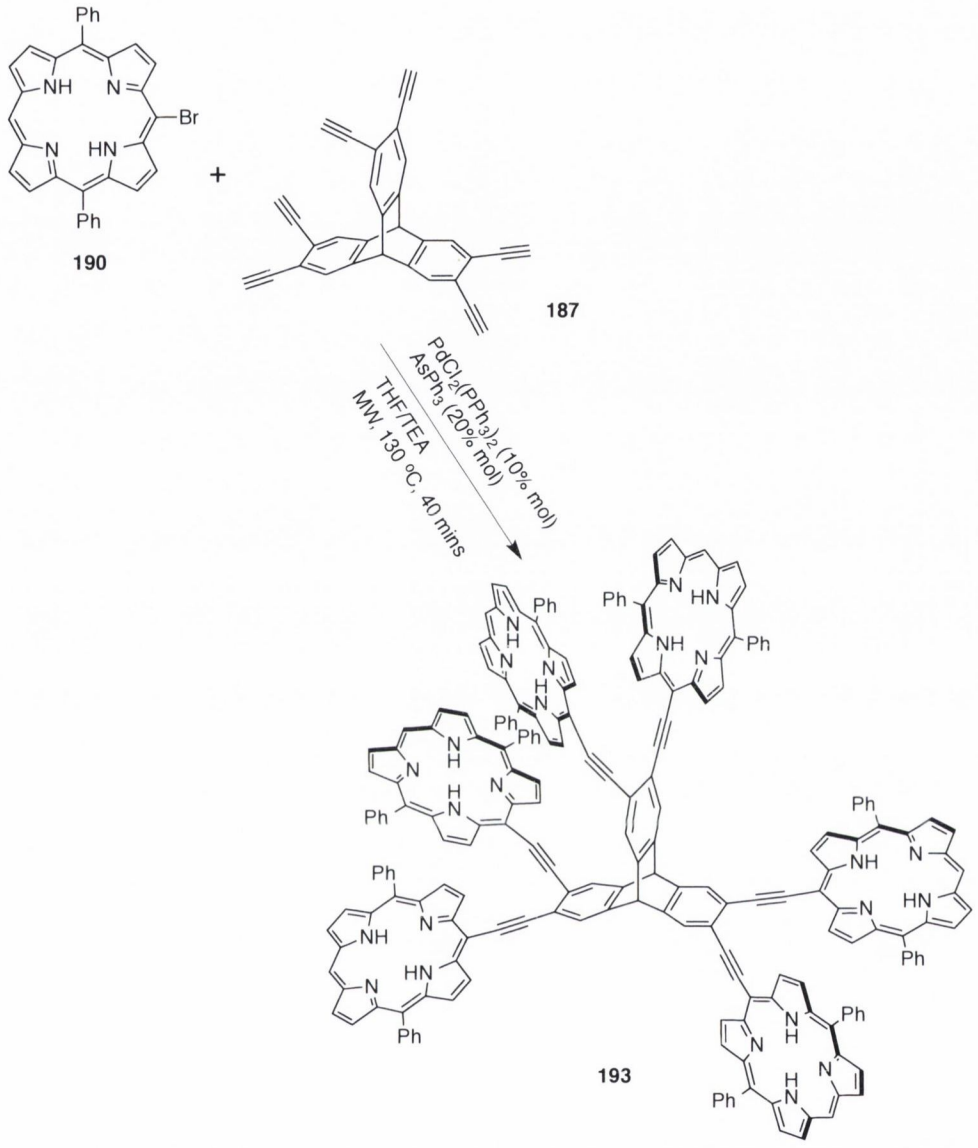

Entry	Porphyrin	Pd Cat. (eq.)	PPh_3 (eq.)	Solvent/TEA (mL)	Time (mins)/ Temp (°C)	Observations
1	**190**	0.05	0.1	0/5	30/90	Lower order products
2	**190**	0.1	0.1	0/3	40/90	S. Material
3	**190**	0.1	0.2	0/5	40/90	Lower order products
4	**190**	0.1	0.2	1:1 THF:TEA	45/130	HRMS hit
5	**118**	0.1	0.2	1:1 THF:TEA	45/130	New spots on TLC, no HRMS hit
6	**192**	0.1	0.2	1:1 THF:TEA	45/130	Lower order products on TLC
7	**119**	0.1	0.2	1:1 THF:TEA	45/130	Debrominated SM, new spots on TLC
8	**191**	0.1	0.2	1:1 THF:TEA	45/130	Faint new spots on TLC

5.4.3 Investigation of Steric Constraints

To investigate the possible effects from steric constraints, a series of alkynyl porphyrins were synthesized through methodology mentioned in Chapter 2. All alkynylporphyrin derivatives were synthesized with a phenyl spacer as to omit any steric strain that may have been occurring with the directly linked conjugates. These porphyrins were also synthesized with different metal centres, again to rule out any possible effects they may be producing (Table 5.10). Porphyrins **50, 53, 54, 194, 195, 196,** were then used in trial reactions with the readily available hexabromotriptycene **172**, and using the copper-free coupling conditions that had produced the promising results mentioned above in Table 5.8. Reactions were run in parallel in order to keep as many of the different parameters constant. This experimental setup could investigate the influence of the metal centre and the relief of any steric strain from using the phenyl spacer unit. The series of meso substituted aryl porphyrins **50, 53, 54, 194, 195, 196** was screened first for their reactivity using the catalyst system of $Pd(dba)_3$ and $AsPh_3$. The reaction for the zinc derivative (Entry 1, Table 5.10) proved moderately successful with HRMS demonstrating the presence of both the tetra- and pentafunctionalized triptycene scaffold. Repeated reactions with increased equivalents and longer irradiation intervals did not lead to the production of the hexasubstituted array, with these results being mirrored by the meso alkyl substituted porphyrin **54** which too could only produce the lower order derivatives.

Table 5.10. A range of alkynylporphyrins implemented in the attempted synthesis of the porphyrin-triptycene scaffold.

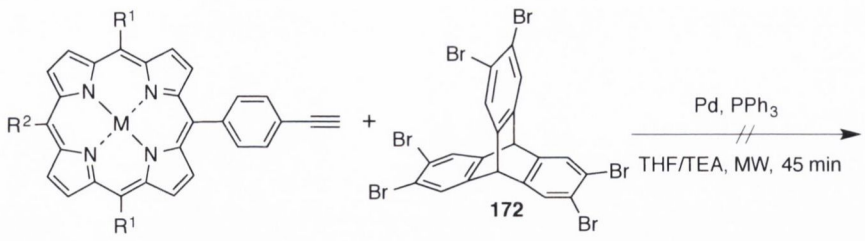

50: R^1 = 4-methylphenyl, R^2 = H, M = 2H
53: R^1 = 4-methylphenyl, R^2 = H, M = Zn
54 : R^1 = 2-ethylpropyl, R^2 = H, M = Zn
194: R^1 = Ph, R^2 = Ph, M = 2H
195: R^1 = 4-methylphenyl, R^2 = Ph, M = 2H
196: R^1 = R^2 = 4-methylphenyl, M = Zn

Entry	Porphyrin	Pd Cat. (eq.)	PPh_3 (eq.)	Solvent/TEA (mL)	Time (mins)/ Temp (°C)	Observations
1	**194**	0.1	0.2	1:1 THF:TEA	45/130	HRMS hit for tetra and penta derivatives
2	**195**	0.1	0.2	1:1 THF:TEA	45/130	Lower order products on TLC & NMR
3	**50**	0.1	0.2	1:1 THF:TEA	45/130	Lower order products on TLC & NMR
4	**196**	0.1	0.2	1:1 THF:TEA	45/130	Faint spots on TLC
5	**53**	0.1	0.2	1:1 THF:TEA	45/130	Faint spots on TLC
6	**54**	0.1	0.2	1:1 THF:TEA	45/130	Lower order products on TLC & NMR

All six reactions produced new spots per TLC; with all containing low R_f values in comparison to the starting porphyrin material. All reactions underwent identical work-up procedures and subsequent purification using a small silica plug and a solvent gradient starting with 6:1, hexane:ethyl acetate, moving progressively to neat ethyl acetate yielded the newly formed spots. These crude material samples were sent for HRMS and NMR analysis. For the majority of this project, MALDI-HRMS has proven difficult to obtain consistent hits with these triptycene systems. NMR analysis of isolated materials displayed the presence of lower order triptycene species, i.e., the triporphyrin array in Entries 2, 3 and 6 of Table 5.10.

Whilst the Sonogashira reaction provided an attractive method for the synthesis of these hexaporphyrin arrays, the results were too unreliable and inconsistent from reaction to reaction to justify it as a viable methodology for now. Accordingly, the project segued to alternative transition metal-catalyzed coupling methods. As the Suzuki reaction had proved to be a robust and reliable method for the six-fold introduction of a variety of functionalities in Section 5.3.2, it was deemed the most attractive alternative to the Sonogashira reaction.

5.4.4 Investigation of Borylated Coupling Partners

Boryl coupling partners are required for the Suzuki reaction, and as such, both triptycene and porphyrin boryl derivatives were synthesized in large amounts for investigatory reactions into the synthesis of the hexaporphyrin array. The hexaboryl triptycene derivative had been synthesized in the initial screen for Suzuki couplings with triptycene (Table 5.1) and was readily accessible for this section of the project. Conversely, borylporphyrin compounds had to be synthesized using known literature procedures first reported by Therien *et al.* who developed their methodology from a procedure to generate aryl boronates developed by Murata and co-workers [354,365]. By taking a previously synthesized bromometalloporphyrin precursor **119** and pinacolborane **197**, a Pd-catalyzed reaction can generate the desired porphyrin borane **198** in 70% yield (Scheme 5.4).

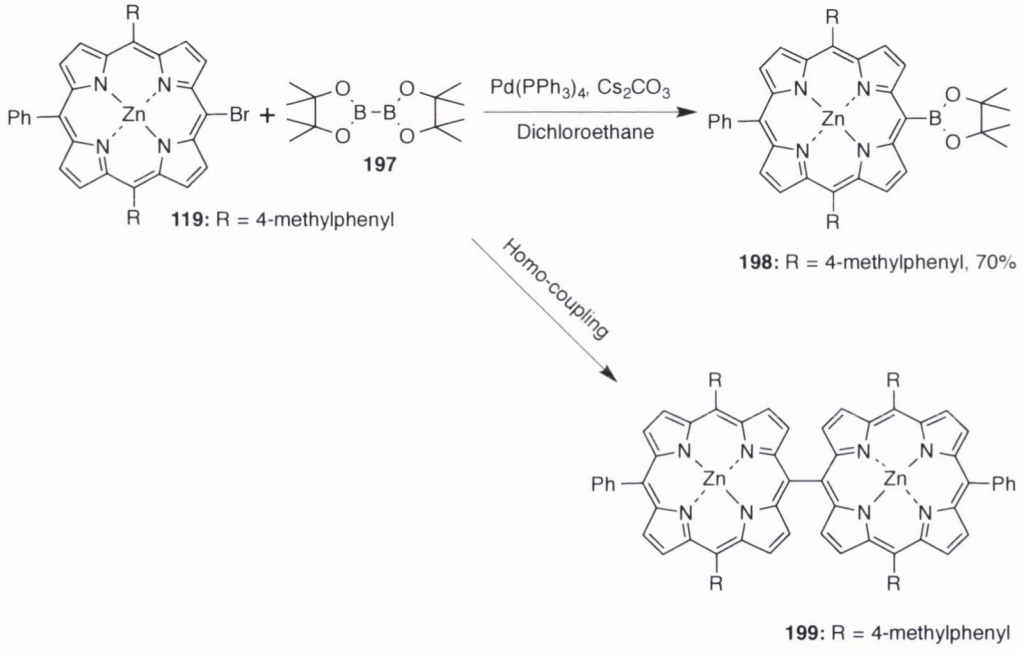

Scheme 5.4. Synthesis of borylated-porphyrin precursors.

Care must be taken with this reaction as the catalyst loading, temperature and reaction time play a crucial part in maximizing the yield of the reaction. Yields can be vastly reduced if more than 0.05 equiv. of palladium catalyst is used, as it can cause the promotion of the competing homo-coupling reaction, i.e. the self-dimerization of the porphyrin **199** through the borylated derivative (Scheme 5.4)[366]. With the proper precaution and appropriate equiv., the reaction proceeds in good yield and with straightforward purification.

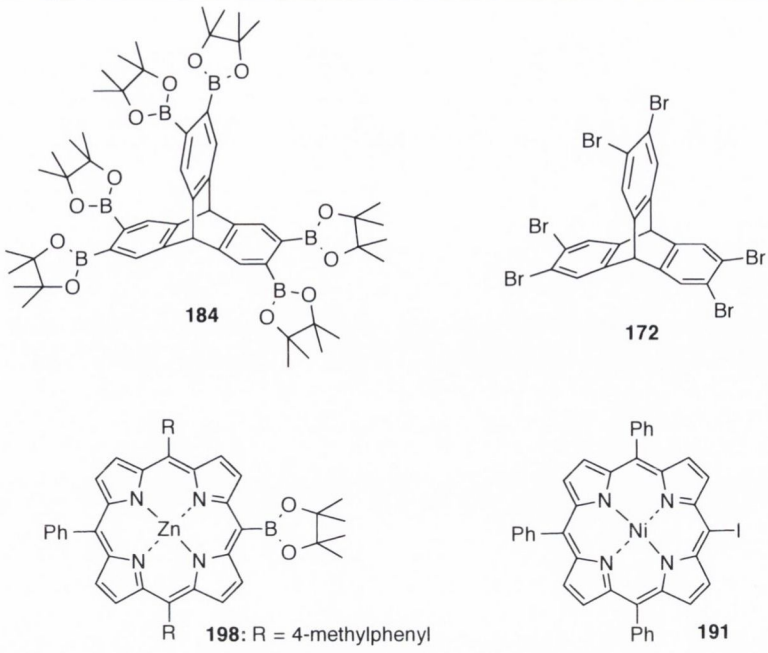

Figure 5.5. A range of boryl and halogenated synthons used in the investigations of the synthesis of hexaporphyrintriptycene arrays.

With this borylporphyrin substrate in hand, a number of different Suzuki reaction conditions could be attempted with hexabromotriptycene for the synthesis of the array. The first two reactions that were attempted used standard Suzuki coupling conditions, e.g., $Pd(PPh_3)_4$ and K_3PO_4 as the palladium source and base, and both mechanical and microwave reactor as the heating source. Using anhydrous toluene for both, the reaction using traditional heating was brought to reflux temperature, i.e., 115 °C and left react for 18 h, where as the reaction in the microwave was allowed react for 40 min at 115 °C (Scheme 5.5). The reaction mixtures were subjected to TLC and identical work-up procedures after the quenching of the reactions.

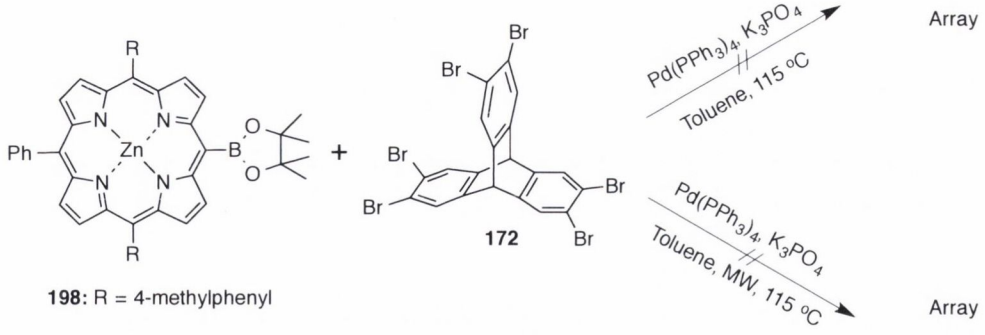

Scheme 5.5. Bench and microwave-assisted Suzuki styled reactions for the synthesis of the porphyrin-triptycene array.

The reaction in the microwave gave mostly homo-coupled porphyrin product, with some debrominated starting material also present in the crude reaction mixture. Conversely, the reaction that was subjected to mechanical heating showed the presence of the lower order derivatives by TLC and HRMS, suggesting that the microwave irradiation promotes the self-

dimerization reaction to a much greater extent than traditional heating. Thus, for future reactions, the traditional heating method was the preferred choice (Table 5.11). These reactions revolved around manipulating the initial conditions as to force the reaction to completion. Despite an increase in catalyst loading, an increase in reaction length and the trialing of different bases and catalytic systems, nothing greater than the trimer was observed by TLC and NMR.

There are a number of possible reasons for this lack of reactivity. The most likely explanation would be that steric congestion around the triptycene scaffold is preventing the coupling of the 4th, 5th and 6th porphyrin equivalent onto the molecule. As a number of reactions gave the trimer reaction product, steric congestion is the most probable explanation. However, it may also be as simple as a lack of equivalents of porphyrin due to the competing debrominating and homo-coupling reactions.

Table 5.11. An array of attempted Suzuki reactions using borylporphyrin **198** and hexabromotriptycene **172**.

Entry	Porphyrin	Catalyst (eq.)	Base	Heating	Temp °C	Solvent	Comment
1	**198**	$Pd(PPh_3)_4$ (0.1)	K_3PO_4	Oil bath	120	Toluene	3 spots + debromo +homocoupled
2	**198**	$Pd(PPh_3)_4$ (0.1)	K_3PO_4	MW	120	Toluene	Homocoupling
3	**198**	$Pd(PPh_3)_4$ (0.1)	Cs_2CO_3	Oil bath	60	THF	S. Mat
4	**198**	$Pd(PPh_3)_4$ (0.2)	K_3PO_4	Oil bath	120	Toluene	Trace lower order derivaitives
5	**198**	$Pd(PPh_3)_4$ (0.2)	K_3PO_4	Oil bath	160	DMF	Homocoupling, faint new spots
6	**198**	$Pd(dppf)Cl_2$ (0.1)	K_3PO_4	Oil bath	120	Toluene	Lower order derivaitives
7	**198**	$Pd(dppf)Cl_2$ (0.2)	Cs_2CO_3	Oil bath	120	Toluene	Debrominated, Trace lower order derivaitives
8	**198**	$Pd(dppf)Cl_2$ (0.2)	K_3PO_4	Oil bath	120	Toluene	Lower order derivaitives

As this reaction pathway was proving unsuccessful, attention switched to the boryltriptycene derivative **184**. It was hoped that this synthetic pathway would prove more efficacious due to the inability of the porphyrin-coupling partner to self-dimerize and therefore the reduction in the potential yield of the reaction. Investigations began with the use of the boryltriptycene **184** with generic halogenated porphyrins, again with standard Suzuki reaction conditions (entry 1-8, Table 5.12). Most of these reactions failed to produce any notable coupling products with only debrominated porphyrin and starting material being recovered from the reaction. Again,

increased equivalents, different bases and longer reaction times had no success in forming the hexasubstituted array, with the trimer being the highest derivative formed.

Table 5.12. An array of trialed Suzuki reactions using boryltriptycene **184** and halogenated porphyrins **188** and **191**.

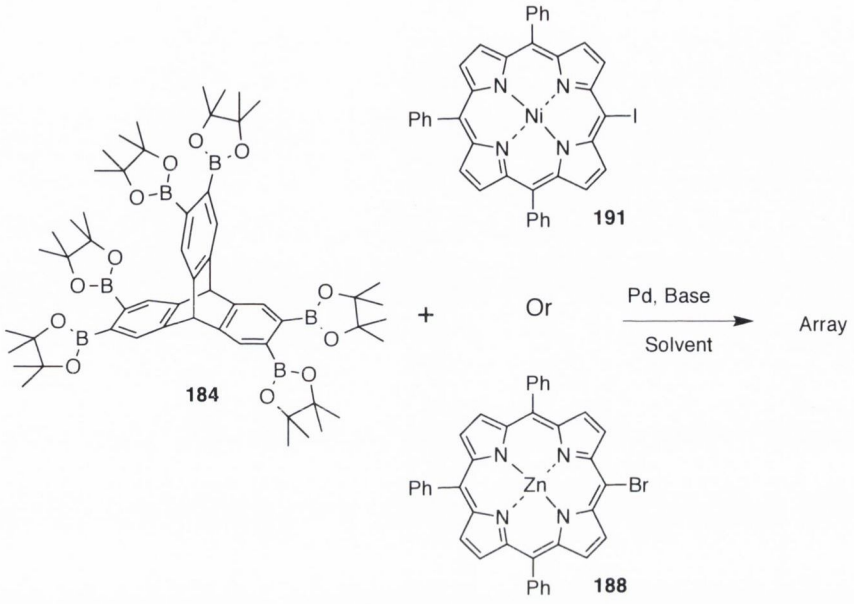

Entry	Porphyrin	Catalyst (eq.)	Base	Temp °C	Solvent	Comment
1	**188**	$Pd(PPh_3)_4$ (0.1)	K_3PO_4	120	Toluene	S. Mat
2	**191**	$Pd(PPh_3)_4$ (0.1)	K_3PO_4	120	Toluene	Trace lower order derivaitives
3	**188**	$Pd(PPh_3)_4$ (0.1)	Cs_2CO_3	60	THF	S. Mat
4	**191**	$Pd(PPh_3)_4$ (0.1)	K_3PO_4	60	THF	Lower order derivaitives
5	**191**	$Pd(PPh_3)_4$ (0.2)	Cs_2CO_3	60	THF	NMR of hexamer
6	**191**	$Pd(dppf)Cl_2$ (0.1)	Cs_2CO_3	60	THF	Trace lower order derivaitives
7	**191**	$Pd(dppf)Cl_2$ (0.2)	Cs_2CO_3	60	THF	Deiodinated, Lower order derivaitives
8	**191**	$Pd(dppf)Cl_2$ (0.2)	K_3PO_4	120	Toluene	Deiodinated, Lower order derivaitives

The perceived breakthrough for this project came with the use of iodoporphyrin **191** with increased equivalents of base and $Pd(PPh_3)_4$ as per Entry 5 in Table 5.12. TLC analysis showed the formation of new spots and subsequent isolation and NMR spectroscopy of the material with the lowest R_f appeared extremely promising as the hexaporphyrin array. The presence of the array could not be confirmed by HRMS and, UV-vis spectroscopy, whilst displaying a bathochromic shift, proved inconclusive. NMR analysis ultimately proved inconclusive as the characteristic signals from the triptycene scaffold were overshadowed by the porphyrin signals. Despite the completion of multiple correlation experiments, no definitive conclusions could be

made on the production of the array. This reaction needs to be repeated with an alkylporphyrin derivative so as the aromatic triptycene signal can be clearly observed in NMR experiments.

5.4.5 Activated Catalyst Systems

A burgeoning field within chemistry is the area of activated catalyst systems for use in known metal catalyzed cross-coupling reactions, e.g., Suzuki, Heck, Negishi [367]. These catalyst aim to not only improve the yields and ease of these reactions, but also to catalyze reactions previously thought cumbersome or impossible using conventional transition metal catalysts. Probably the most successful of these new activated systems would be the seminal work conducted by Mike Organ and co-workers on the preparation of catalysts that they have come to coin as PEPPSI (pyridine-enhanced precatalyst, preparation, stabilization, and initiation) [368]. These complexes are stable to air and moisture and are relatively easy to synthesize and handle. In these species the palladium exists in the +2 oxidation state and thus, must be defined as a "precatalyst" and therefore must be reduced *in situ* to the active Pd(0) form to enable it to enter the cross-coupling catalytic cycle. This is achieved due to the presence of active transmetalating agents such as organo-magnesium, -zinc or-boron reagents [369].

N-heterocyclic carbene ligands with certain flexibility and co-ordination modes can provide several advantages over conventional catalysts for the conversion of sterically demanding substrates [370]. This steric bulk can facilitate the formation of catalytically active species, as well as enhance the reductive elimination step [367,368]. The rationale behind this is that the shape of NHCs differs significantly from that of phosphine ligands as the substituents bound to the carbene's nitrogen atoms point toward the metal center and thus encompass the metal, creating the so called "buried volume". Contrarily, transition-metal phosphine complexes contain phosphine substituents that point away from the metal, forming a cone. This fundamental difference between these two ligands helps the NHC have a unique impact on the metal's coordination sphere and is key to the success of these systems (Figure 5.6).

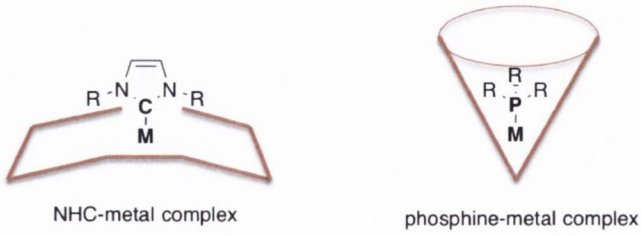

Figure 5.6. Different shape of NHC ligands compared with phosphine ligands.

For these test reactions, PEPPSI-iPr was selected as it has seen the most widespread success throughout the literature and seems to be the most versatile catalyst system from this class of compounds (Figure 5.7) [369]. Whilst it has been widely shown to work with Suzuki couplings, it was decided to test the catalyst with Sonogashira couplings also (Table 5.13).

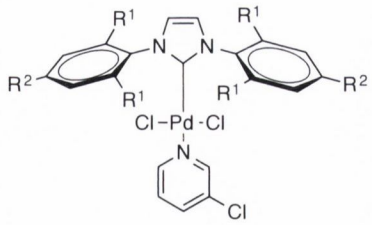

200: R^1 = *i*Pr, R = Me
PEPPSI™.iPr

Figure 5.7. Imidazolydene-Pd-derived precatalysts.

Firstly, the Suzuki pathway was tested using THF as the solvent and traditional heating. This reaction was kept at 65 °C for 24 h and its progression was monitored by TLC at staggered intervals. At no point during the reaction did any production of a porphyrin-triptycene conjugate surface. Attention then shifted to the use of this activated catalyst system with the Sonogashira reaction. Again, a range of reaction conditions were attempted, including the previously optimized conditions, but there was no observable formation of the hexaporphyrin array and only trace amounts of the lower order derivatives in the reaction mixture. Although, enhancements are possible through optimization studies, the price and scarcity of this catalyst outweighed any potential improvements that could be imparted by this activated catalyst system.

Table 5.13. Imidazolydene-Pd-derived precatalysts.

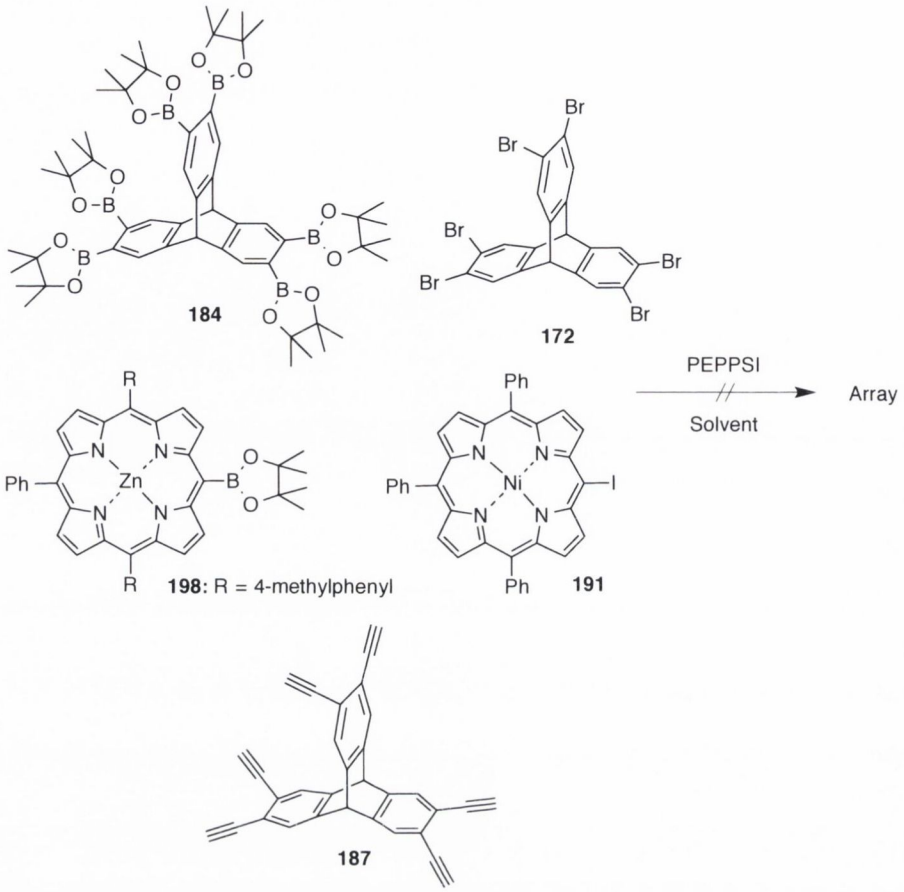

Entry	Porphyrin	Triptycene	Catalyst (eq.)	Temp °C	Solvent	Comment
1	**198**	**172**	(0.05)	65	THF	S. Mat
2	**191**	**184**	(0.05)	65	THF	S.Mat
3	**198**	**172**	(0.1)	65	THF	Trace lower order derivaitives
4	**191**	**184**	(0.1)	65	THF	S.Mat
5	**191**	**187**	(0.1)	90	TEA	Trace lower order derivaitives
6	**191**	**187**	(0.15)	90	TEA	Trace lower order derivaitives
7	**191**	**187**	(0.2)	90	TEA	Deiodinated, Lower order derivaitives

5.4.6 Non-metal catalyzed couplings

As a large number of reactions had been trialed with little reproducible success forthcoming, it was decided to change the synthetic approach for this project. It was hoped to investigate whether one could install six porphyrins onto the scaffold through classic chemical methodology, instead of relying on catalytic systems that, while they are powerful synthetic tools, can be inherently problematic. As such it was decided to attempt new coupling reactions

using other triptycene scaffolds previously synthesized in Section 5.3.1. The carboxylic acid scaffold **180b** immediately came to mind, as the most promising candidate as it could be used in esterification reactions with an amino/hydroxyl porphyrin.

Work on this section of the project began with the synthesis of appropriate porphyrin coupling partners. Two disparate porphyrins **201-202** were selected as to ensure no discrepancies in reactivity due to electronic effects around the porphyrin macrocycle were inhibiting the reaction from occurring. Additionally, a zinc(II) derivative of porphyrin **203** was synthesized again to ensure reaction solubility and potential difficulties during purification could be ruled out. Also, porphyrin **202** could act as an *m*-THPP mimic due to the presence of the *meta*-methoxy functionality. If conjugated to the triptycene scaffold, this array could allow for investigations into the use of triptycene as a drug delivery vehicle for PDT. The porphyrin scaffolds **201-203** were prepared through known literary procedures discussed previously, in comparable yields to their reported syntheses [371-373]. These porphyrins could then be used for conjugation with the carboxylic acid-triptycene scaffold (Figure 5.8).

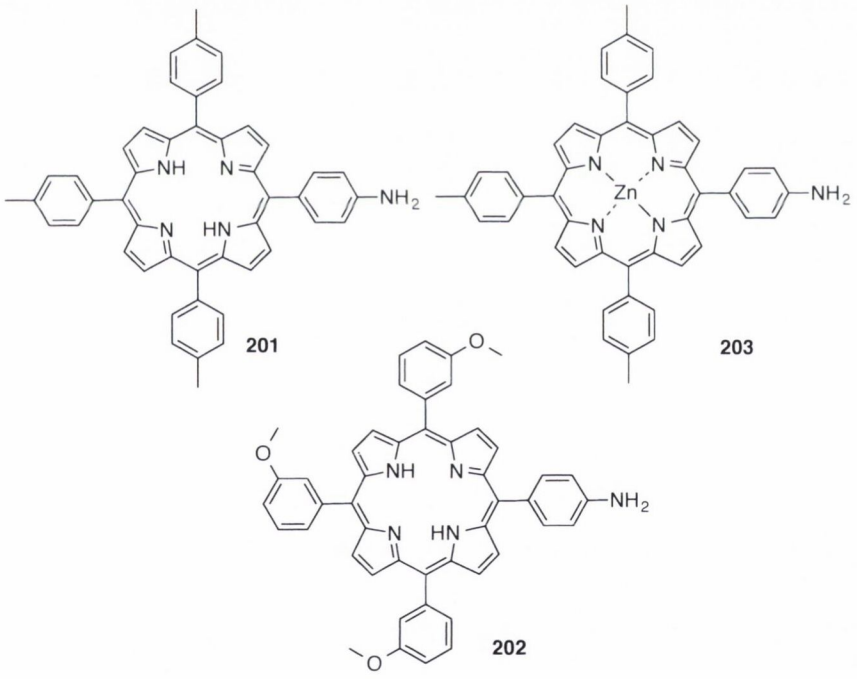

Figure 5.8. A library of porphyrin coupling partners for the conjugation to a preformed triptycene scaffold.

Initial investigatory reactions followed the procedure developed in a previous chapter for the coupling of heteroatom porphyrins and a carboxylic acid functionality. The three porphyrin coupling partners **201-203** underwent a range of reactions with the triptycene scaffold, detailed in Table 5.14 with only the NMR of *Entry 4* showing promise for the successful synthesis of the desired array. Again, HRMS could not provide confirmation of the formation of **204**. Integration and chemical shifts suggest the successful formation; however, similar to previous efforts, the diagnostic signals for the triptycene moiety appear further downfield and are overshadowed by

the porphyrin aromatic signals between 6-8 ppm. Also, the product was synthesized in such low quantities that there was insufficient material to run 2D NMR experiments such as TOCSY and NOE experiments that would unequivocally determine the result of the reaction. Similar to potential positive results discussed previous, further attempts to resynthesize and purify the array in greater amounts proved unsuccessful. Due to project time constraints and eventual lack of porphyrin coupling partner **202**, this pathway could not be investigated further, however, it provides one of the more salient pathways for the potential synthesis of the hexaporphyrintriptycene array and must be investigated further on a larger scale.

Table 5.14. Investigatory reactions for the synthesis of a hexaporphyrintriptycene array through an activated amide-coupling pathway, *Entry 4.*

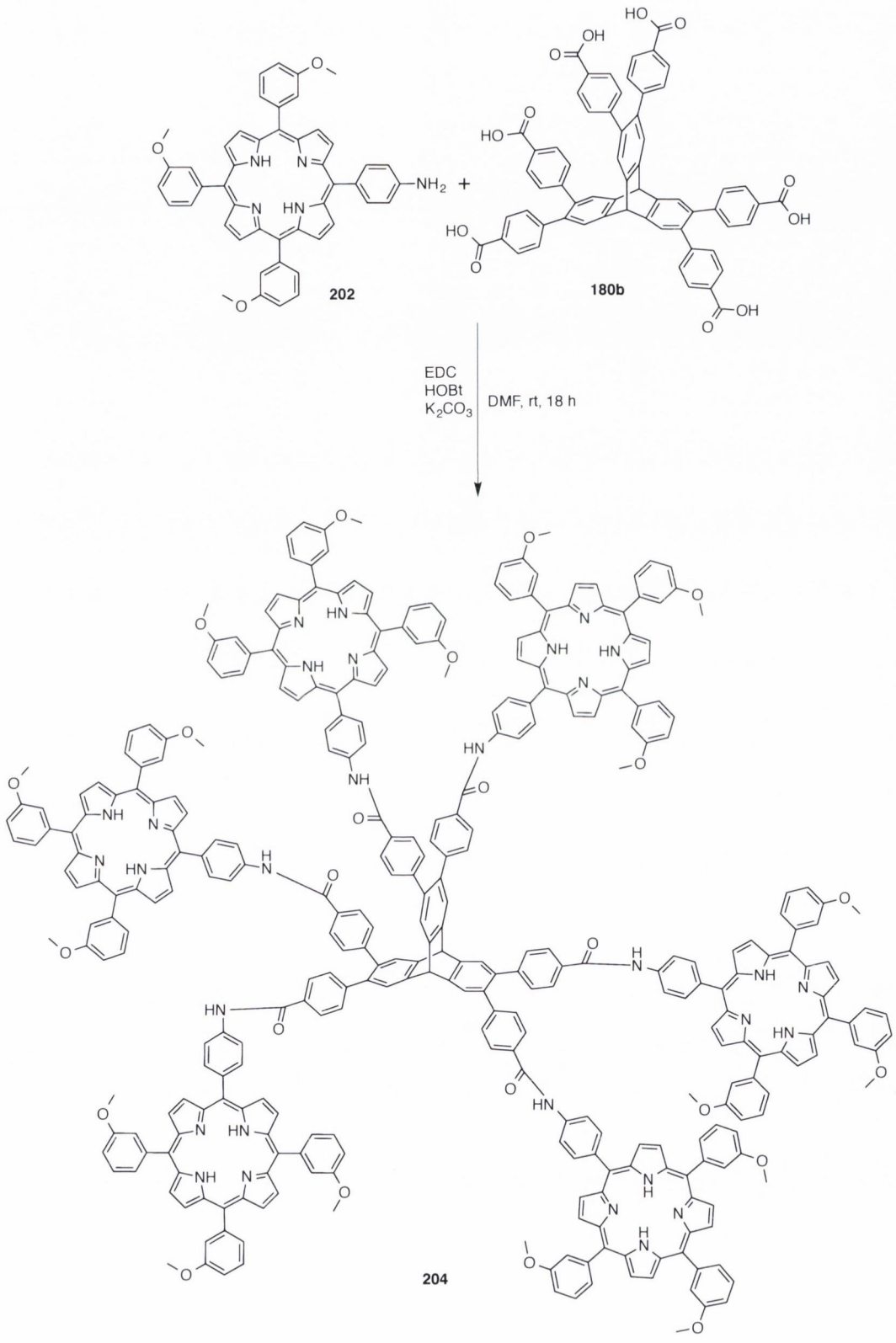

Entry	Porphyrin	Base	Coupling Agents (Eq.)	Temp °C	Solvent	Comment
1	**39**	K_2CO_3	EDC/HOBt (2)	r.t.	DMF	S. Materials
2	**39**	K_2CO_3	EDC/HOBt (5)	r.t.	DMF	Faint spots on TLC
3	**40**	K_2CO_3	EDC/HOBt (2)	r.t.	DMF	Faint spots on TLC
4	**40**	K_2CO_3	EDC/HOBt (5)	r.t.	DMF	Multiple new spots, inconclusive NMR
5	**41**	K_2CO_3	EDC/HOBt (2)	r.t.	DMF	S.Materials
6	**41**	K_2CO_3	EDC/HOBt (5)	r.t.	DMF	Faint spots on TLC
7	**40**	K_2CO_3	EDC/HOBt (5)	65	THF	Faint new spots (lower order)
8	**40**	K_2CO_3	EDC/HOBt (5)	130	DMF	Multiple new spots
9	**40**	K_2CO_3	EDC/HOBt (5)	80	Acetonitrile	Faint new spots (lower order)
10	**40**	DMAP	EDC/HOBt (5)	r.t.	DMF	S. Materials
11	**41**	K_2CO_3	EDC/NHS (5)	r.t.	DMF	S. Materials
12	**40**	DMAP	EDC/HOBt (5)	r.t.	DMF	S. Materials
13	**41**	K_2CO_3	EDC/NHS (5)	r.t.	DMF	S. Materials

With inconclusive results emerging from this section of the project, it was decided to attempt the coupling of less cumbersome chromophores as to exhibit a proof of principle array that could act as the basis for further porphyrin array studies. There were two commercially available chromophores i.e., fluorescein **205** (Scheme 5.6) and luminol **206** (Scheme 5.7) and both molecules have been extensively studied and implemented into planned syntheses due to their fluorescent properties.

Initial reactions with **205** again centered on the conditions previously optimized in Chapter 4. Reactions were attempted with K_2CO_3 as a base and in this instance TLC and NMR indicated the decomposition of the hydrazine bond in **205** with the subsequent formation of a carboxylate species. A mixture of EDC and DMAP as a base/catalyst were implemented in anhydrous CH_2Cl_2 and allowed react with triptycene-carboxylic acid scaffold **180b** at room temperature for 18 h (Scheme 5.6). No reaction occurred according to TLC and NMR analysis with only the starting materials left in the reaction mixture after the allotted time had passed.

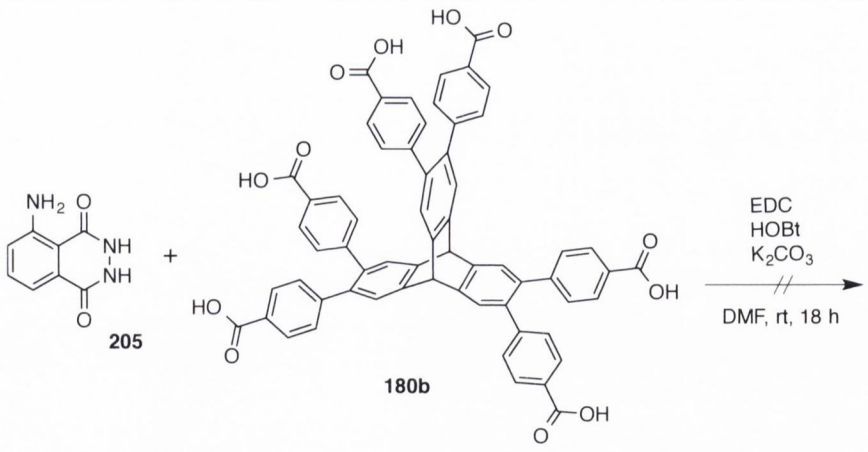

Scheme 5.6. Attempted coupling of luminol **205** with triptycene scaffold **180b**.

Concurrent reactions were undertaken using the other commercially available chromophore i.e., fluorescein, **206**. A number of synthetic manipulations of the fluorescein molecule were required to obtain the desired coupling partner for conjugation reactions (Scheme 5.7).

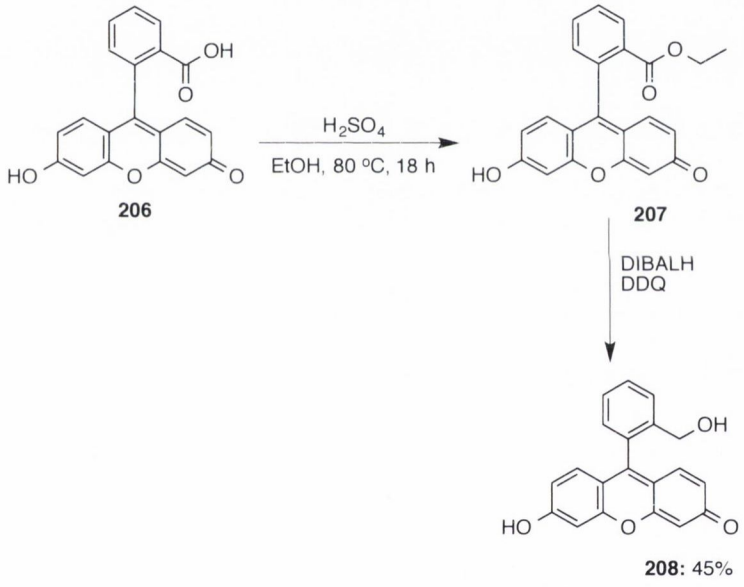

Scheme 5.7. Synthesis of fluorescein precursor.

For solubility purposes fluorescein **206** was initially changed to the ethyl ester derivative **207** before subsequent reduction to the primary alcohol [374]. Care needed to be taken when selecting the reducing agent as powerful reducing agents such as $LiALH_4$ can reduce the quinoid fragment of the molecule. Thus, a more selective reagent was necessary for the reduction of the ethyl ester derivative **207** to the corresponding primary alcohol **208**. Diisobutylaluminium hydride (DIBALH) can be considered an electrophilic reducing agent as it reacts quicker with electron-rich compounds in comparison to electron deficient compounds and therefore it was selected as the initial reducing reagent to be tested. DIBALH was added drop wise over a 10 min period to the reaction flask containing **207** in anhydrous CH_2Cl_2 under an atmosphere of argon and at -78 °C. The resulting solution was allowed to return to room temperature and

subsequently stirred for 2 h. Quenching of the reaction occurred through the addition of a saturated solution of ammonium chloride. DDQ was added to the crude reaction mixture as a preventative measure to re-oxidize any phenol side-products that may have formed.

With synthetic access to compound **208**, conjugation reactions were attempted using EDC, HOBt and K_2CO_3 in anhydrous DMF for 24 h at room temperature (Scheme 5.8). No observable reaction had occurred according to TLC analysis, with crude NMR and HRMS data displaying the presence of both starting materials with some minor conversion of the carboxylic acid to the activated-ester species. This result would indicate that an increase in reaction equivalents is needed to increase the formation of the activated-ester species, which in turn will increase the probability of the synthesis of the multi-chromophore array.

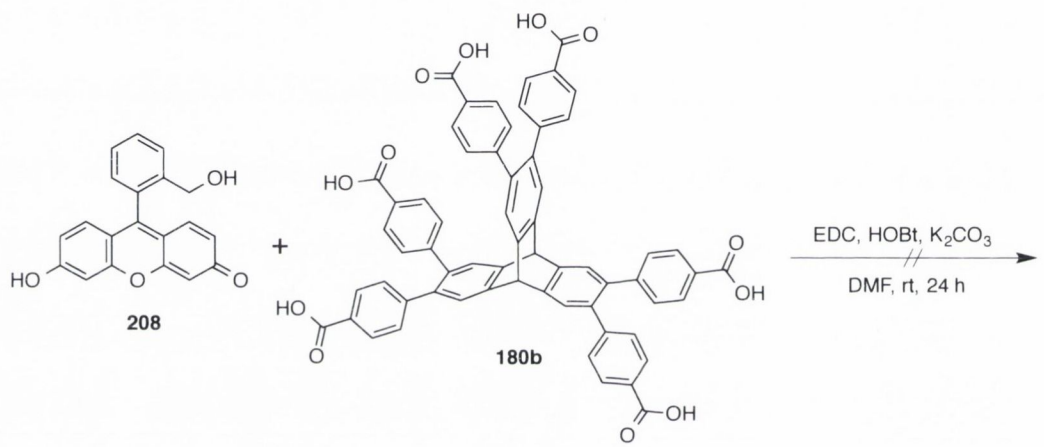

Scheme 5.8. Attempted coupling of fluorescein derivative **208** with triptycene scaffold **180b** through a modified Steglich reaction pathway.

These set of reactions brought to an end investigations into the potential synthesis of multi-chromophore arrays functionalized onto a central triptycene scaffold. Despite the array not being synthesized in this section, both luminol **205** and fluorescein **206** hold promise as less complex, commercially available chromophores that could act as model compounds for the future trialing of coupling partners.

5.5 Triptycene Desymmetrization

Whilst the discovery of the hexabromination of triptycene opened the avenue for the concerted six-fold metal catalyzed cross-coupling reactions mentioned above, similar to porphyrin research thirty years ago, there is a void in the literature pertaining to desymmetrized triptycene systems. There is potential for unsymmetrical scaffold systems in a plethora of applications, e.g.,dual-targeting in PDT, MOFs and light-harvesting arrays.

To initiate this project, investigations began by constructing simple mixed triptycene systems such as those that can be seen in Scheme 5.9. Whilst there are a number of different pathways to yield such systems, 2,6,14 trinitrotriptycene was used due to its ease of synthesis and the variety of functional group interconversions possible with the nitro group. By adding triptycene to concentrated nitric acid and leaving it react for 24 h at 75 °C afforded both the 2,6,14 (**168**) and the 2,7,14 (**169**) isomers in good yield. Subsequent isolation of these isomers provides trisubstituted triptycene with three free positions for further functionalization. From here, investigatory bromination reactions begin using the 2,6,14 derivative (**168**) and varying sources of bromine. The first pathway attempted was with *N*-bromosuccinimide (NBS). The TLC from this reaction after 24 h showed the presence of no new reaction products, with only starting material present (Scheme 5.9). As no reaction had occurred, it was theorized that the triptycene scaffold was not a strong enough nucleophile to react with NBS and form the resulting brominated product.

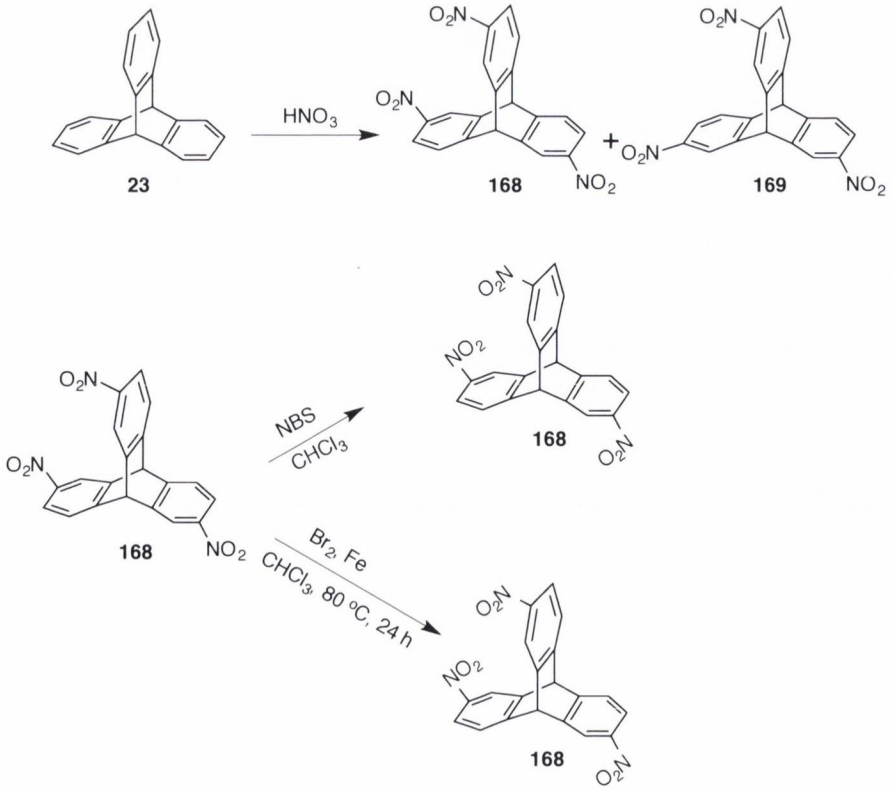

Scheme 5.9. Synthesis of tri-nitrotriptycene **168** and the subsequent attempted bromination of this scaffold.

Tailoring of the nucleophilicty of this triptycene scaffold is impossible, thus, it was decided to implement a stronger source of bromine, i.e., molecular bromine, Br_2 in the presence of iron. The polarized bromine-bromine bond due to iron should create a species electrophilic enough for triptycene to react with. Similar to the conditions used for the hexabromination of triptycene, scaffold **168** was reacted with 3 equiv. of Br_2 and a catalytic quantity of iron shavings in chloroform and brought to reflux temperature for 18 h (Scheme 5.9). Following a work-up involving sodium thiosulfate to quench any toxic bromine species present in the reaction mixture, the crude material was sent for HRMS and NMR testing. Neither method produced the hexasubstituted triptycene derivative; with TLC showing the presence of unreacted starting material. A possible explanation for this was that the NO_2 group was interfering with the electronics of the system, as they are strongly electron withdrawing. This may pull electron density from the triptycene onto the NO_2 therefore making the free triptycene position less susceptible to electrophilic reactions.

In an attempt to circumvent this possible interference, it was decided to synthesize the tri-iodo derivative **171** using the nitro scaffold **168**, as in the pathway described in Scheme 5.10. Subsequent bromination would afford a mixed halogenated compound with potential for mixed coupling reactions due to the difference in reactivity provided by the two opposing halides. Mimicking the conditions attempted previously, the tri-iodo species was placed in a round-bottom flask charged with chloroform. Br_2 and iron shavings were added and the reaction was brought to reflux and allowed react for 24 h (Scheme 5.10). After the allotted time, the reaction was worked-up in identical fashion to previous bromination attempts, with the crude reaction mixture subsequently undergoing NMR and HRMS analysis.

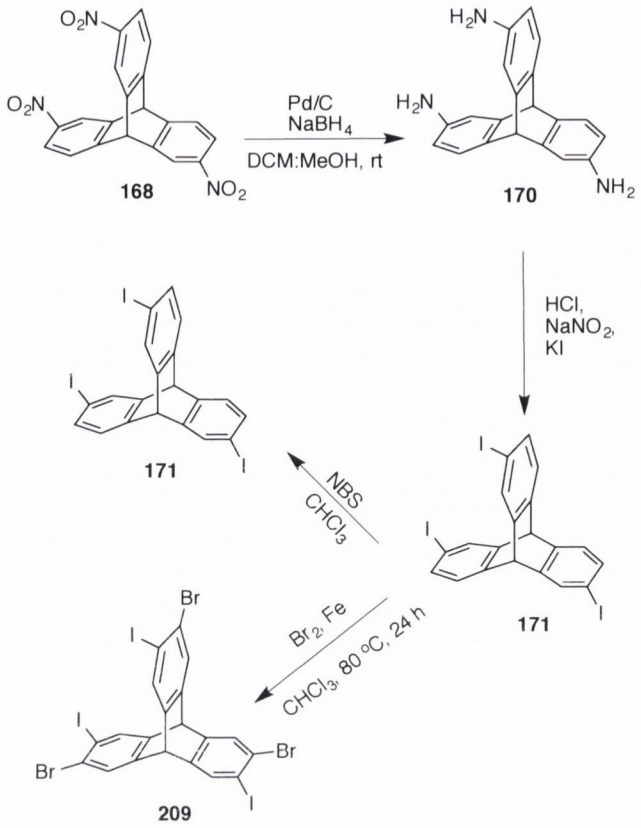

Scheme 5.10. Synthetic pathway for 2,6,14-triiodotriptycene and the attempted bromination.

As seen with most compounds for this project, the HRMS data proved inconclusive, however the NMR spectra showed an alteration to all diagnostic peaks (Figure 5.10). The peak at 7.69, 7.34, 7.09 corresponding to the three free reactive triptycene protons has completely disappeared with the formation of a new peak at 7.61 that integrates for 6H, which could correspond to the unreactive six arene protons typically associated with a hexasubstituted triptycene scaffold. Similarly, the split bridgehead peak associated with the trisubstituted system has been transformed into one broad peak. Although this system has become desymmetrized through the installation of two different halide groups, one would expect a single signal for the bridgehead protons as the difference in through space electronics between a iodo and a bromo group on a arene ring is marginal with respect to NMR spectroscopy.

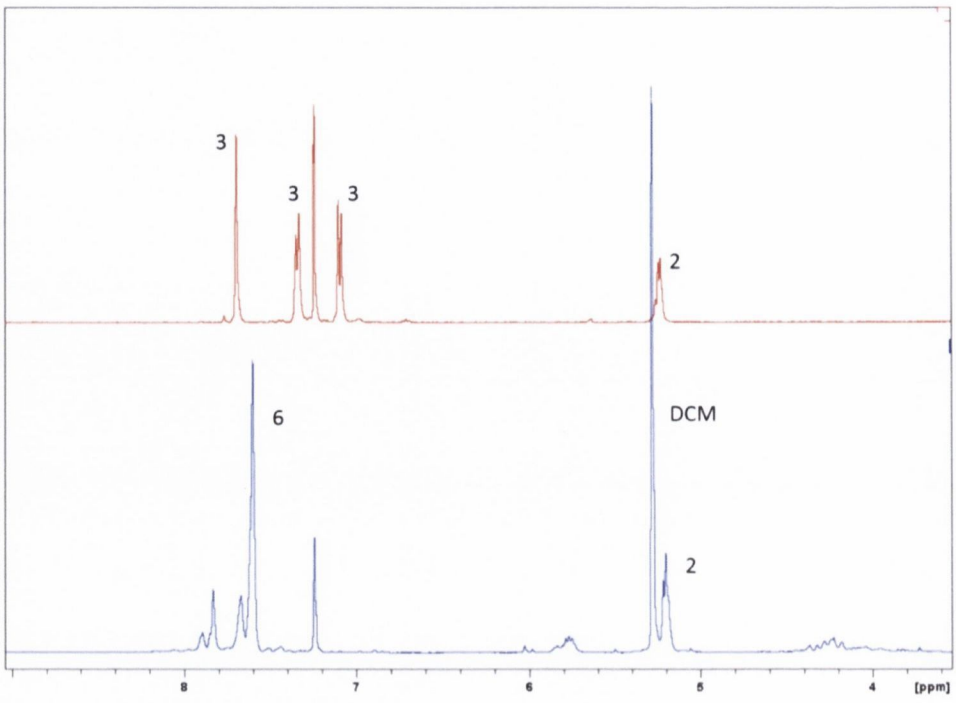

Figure 5.10. ^{1}H NMR spectra for scaffold **46**.

This initial positive result shows great promise for these types of systems and much more work will need to be conducted into the desymmetrization of triptycene, either through similar methodology as described above or through a total synthesis approach.

5.6 Conclusions & Future Work

5.6.1 Conclusions

A library of hexasubstituted triptycene building blocks has successfully been synthesized through the use of transition metal catalyzed cross-coupling reactions i.e., Suzuki and Sonogashira couplings. The success of this method has updated the chemistry of triptycene and brought the synthetic toolkit of this sought after scaffold into the 21st century. With this newly developed methodology, synthetic handles were successfully installed around the triptycene periphery and they allow for further functionalization reactions to occur. Utilizing these triptycene scaffolds, a number of post-functionalization reactions were tested, with varying degrees of success. Although the hexaporphyrin array could not be characterized, fragments of experimental data show that it was formed and larger scale reactions leading on from the optimization work conducted above may prove to be the turning point for this synthetic pathway.

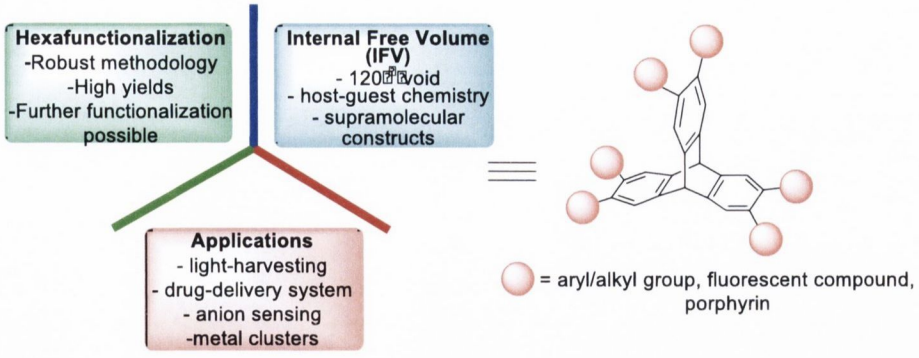

Figure 5.11. A summary of the synthesis and potential applications for the hexasubstituted triptycene scaffolds.

5.6.2 Future Work

Whilst there are many avenues one can take this project, the implementation of the hexacarboxylic acid derivative in the field of metal organic frameworks would appear the most one of the more promising. As mentioned previously, this coupling proceeded with a good overall yield and straightforward workup, devoid of any need for column chromatography. By synthesizing a large quantity of this scaffold, an initial project even a visiting undergraduate student could perform would be to attempt basic frameworks by adding a library of metals to a solution of the triptycene scaffold and then analyzing the crystals one obtains (Figure 5.12). These experiments would serve as an introductory exercise for the group into triptycene MOF's and from here more complex systems could be attempted within a collaboration with a researcher with specific expertise in this field. If successful, these complexes could then be tested for a range of applications, such as gas storage, materials chemistry or drug-delivery.

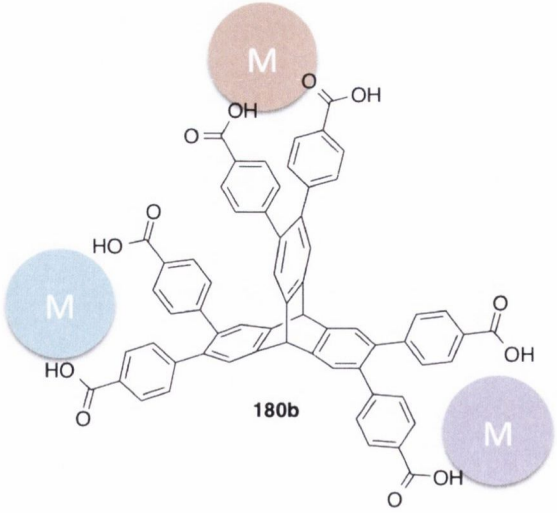

Figure 5.12. Diagrammatic example of the potential MOF's due to the rigid triptycene scaffold.

Another potential avenue to take with these molecular scaffold systems would be, as suggested by the hexaporphyrin array, the implementation of triptycene as a drug carrier system.

Researchers in the field of boron dipyrromethanes (BODIPY) have seen great success with these molecules as not only cytotoxic agents but also as diagnostic tools due to their innate fluorescence. From the synthetic work carried out above, there are a number of different methods one could use to create a hexaBODIPY triptycene conjugate (Figure 5.13). Once synthesized, the triptycene conjugate could act as a delivery vehicle, transporting six BODIPY molecules at a time into the cell. This would have to have an impact on dosage requirements as one would theoretical require a sixth of the dose to achieve the same therapeutic effect as the monomer.

Figure 5.13. A potential BODIPY-triptycene conjugate for use in PDT.

This potential strategy may be applied to a number of different biologically pertinent molecules. For example, the principle of a hexaporphyrin triptycene array for PDT is completely interchangable with the BODIPY premise.

The main focus is to synthesize the hexaporphyrin array and assess its photophysical measurements. The projection of the porphyrin subunits in the spatially defined manner by the triptycene scaffold mimics the macrorings observed in bacteriochlorophyll. To obtain this material in significant quantities, an upscale of reaction conditions is needed. As for the method of conjugation, the best options going forward for this project would be either the use of the hexaethynyl triptycene scaffold or the hexacarboxylic acid scaffold (Figure 5.15). The ethynyl linker would impart its rigidity to the system and truly project the porphyrin subunits out in to space whilst also allowing for complete conjugation between the porphyrin and triptycene species. A critical attribute required if they are to be used as light-harvesting scaffolds. Contrastingly, the amide linkage through the carboxylic acid offers a much more simplistic approach to the synthesis of this array. It will not depend on catalyst loadings or catalytic cycles and therefore should be obtainable over a shorter time frame and would represent less synthetic challenges when scaling up the reaction.

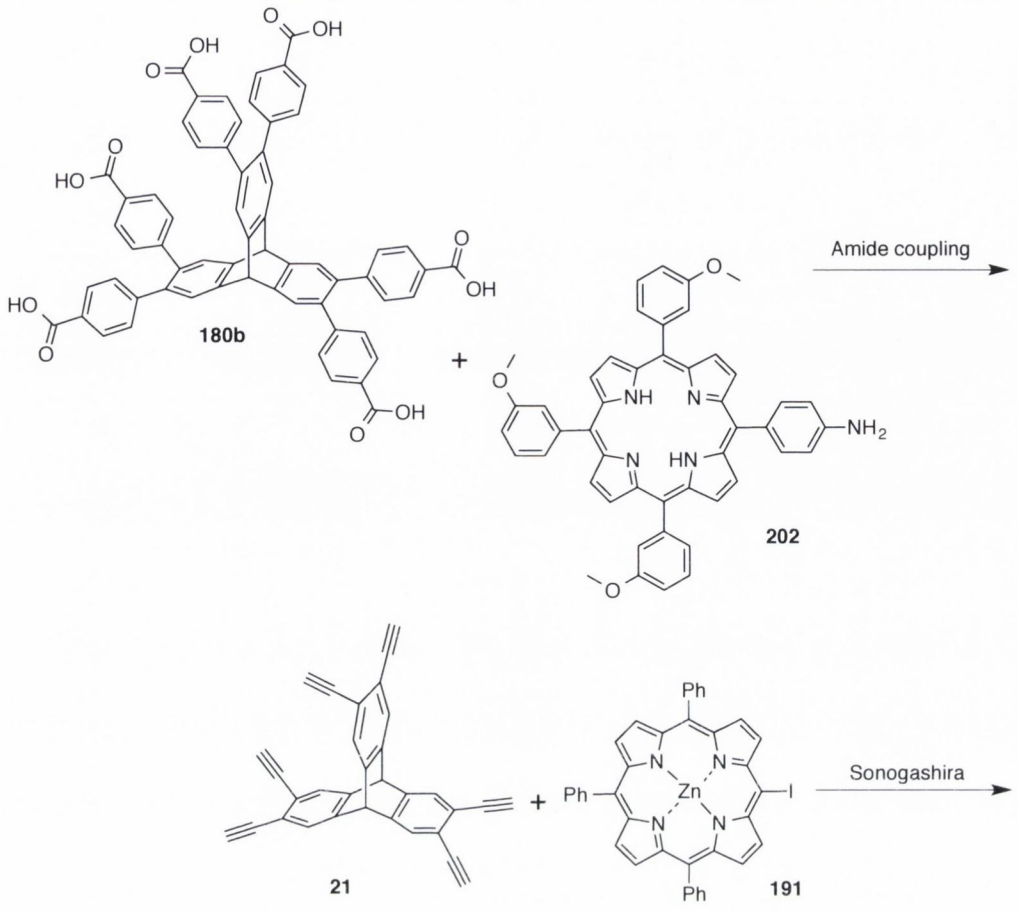

Figure 5.15. Reactions that displayed the most promise and thus merit further investigation.

Each has their own merits for use and are tailored toward different applications i.e., light-harvesting arrays and PDT PSs. Therefore both options should be thoroughly explored and synthesized in sufficient quantities as to enable testing of their properties toward the designated application.

5.7 Triptycene desymmetrization

Work will need to follow on from the initial test reactions into the synthesis of desymmetrized hexasubstituted triptycenes as this has not been attempted before, and also due to the potential of these multi-substituted triptycene scaffolds. The project will be of similar ilk to that of the *m*-THPP desymmetrization venture described in Chapter 3. There are two quite disparate synthetic strategies that one can take in an attempt to synthesize unsymmetric triptycene scaffolds. Method 1: Historically, simple functionalized triptycenes were synthesized by manipulating the anthracenyl scaffold before the Diels-Alder reaction that forms the triptycene scaffold (Figure 5.16). Whilst this method can be effective, it is somewhat limited to more classical chemistry, such as nitration, bromination etc., which can occur in limited positions upon the scaffold. The other synthetic pathway one could use would be the controlled

bromination or iodination of triptycene itself, through the monitoring of reaction time and equivalents.

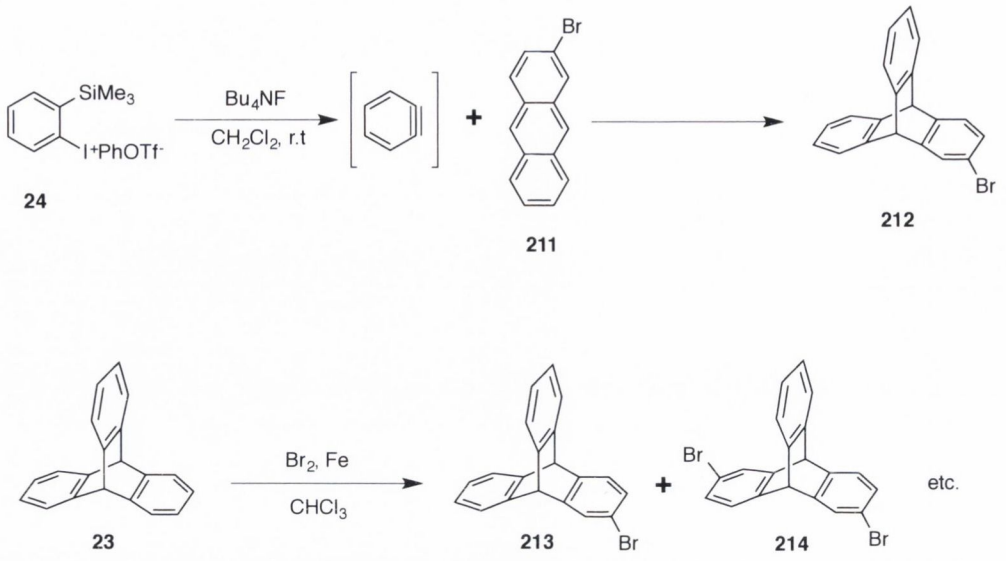

Figure 5.16. Variety of pathways available for the controlled synthesis of unsymmetrical triptycene scaffolds.

As one can observe from this and previous chapters, aryl halides have been widely implemented in organic synthesis to form carbon-carbon and carbon-heteroatom bonds in transition metal-catalyzed processes. Despite the widescale availability of aryl bromides, they are typically less reactive than the corresponding aryl iodides [375]. Unfortunately, the synthetic preparation of functionalized aryl iodides can prove cumbersome [376]. The most common preparative method for the conversion of aryl bromides into aryl iodides, i.e., nickel or copper, suffers from significant limitations. For example, the nickel methodology suffers from incomplete conversion of the aryl halide and is accompanied by substantial biaryl side product formation [377]. Where as the copper methodology is limited by harsh reaction conditions, high temperatures and multiple equivalents of copper(I)iodide [378].

Buchwald *et al.* developed a new method for the conversion of aryl, heteroaryl and vinyl bromides into the corresponding iodides. Their system utilized a catalyst system that comprised of CuI and a 1,2- or 1,3-diamine ligand. The reaction has provided access to a range of electron-rich and electron-deficient aryl iodides and the reaction demonstrates excellent functional group tolerance due to the lack of a strong base in the reaction medium.

As the hexabromotriptycene was proving unsuccessful in the synthesis of the hexaporphyrintriptycene array, the Buchwald methodology could be attempted for the conversion of bromotriptycene into its corresponding iodo-derivative. If the reaction was successful, this hexaiodinated compound could prove to be an effective coupling partner for both Sonogashira and Suzuki based couplings (Figure 5.17).

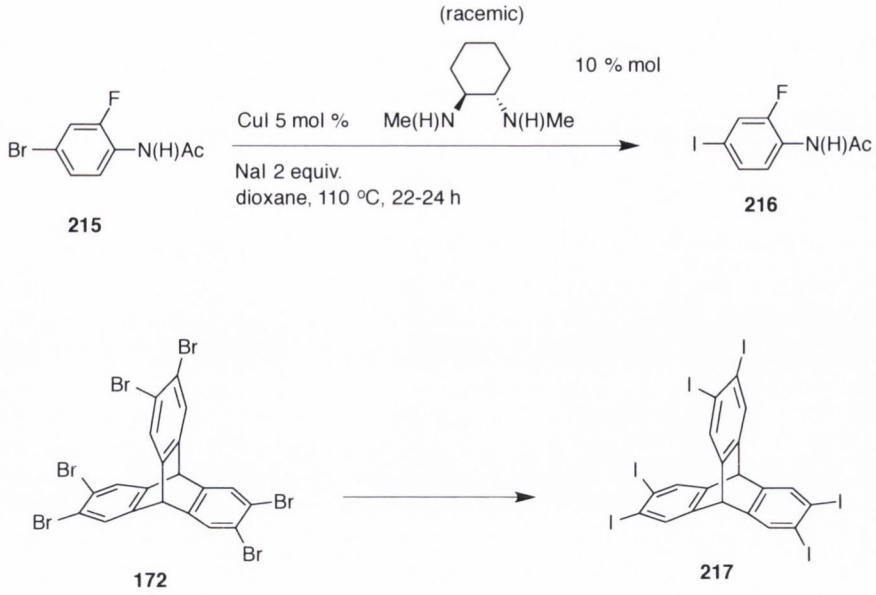

Figure 5.17. Potential pathway for the synthesis of a hexaiodotriptycene derivative.

Chapter 6: Translocator Protein (TSPO, 18kDa), A Review

6.1 Introduction

The translocator protein (18 kDa) is a five transmembrane domain protein that is localized primarily in the outer mitochondrial membrane [176] and is expressed predominantly in steroid-synthesizing tissues and the brain [177]. The TSPO was identified in 1977 whilst researchers were searching for binding sites for benzodiazepines such as diazepam in peripheral tissue [379]. Thus, the receptor was initially named the peripheral-type benzodiazepine receptor. This aimed at distinguishing these 'peripheral type' benzodiazepine receptors from the central benzodiazepine receptor, which is part of the $GABA_A$ receptor complex, typically found in the brain [380]. A number of contentious issues arose with the term 'peripheral-type benzodiazepine receptor' as numerous ligands other than benzodiazepines bind to it. Additionally, this name did not give an accurate representation of the tissue distribution of the molecule as well as the fact that the protein is not in strict terms a receptor itself. To resolve these issues Papadopoulos *et al.* suggested the term translocator protein (18 kDa) (TSPO), as it has since been discovered to be a subunit of the mitochondrial permeability transition pore (MPTP). This pore consists of the TSPO, voltage-dependent anion channel (VDAC) and the mitochondrial inner membrane adenine nucleotide translocator (ANT) (Figure 6.1) [381,382].

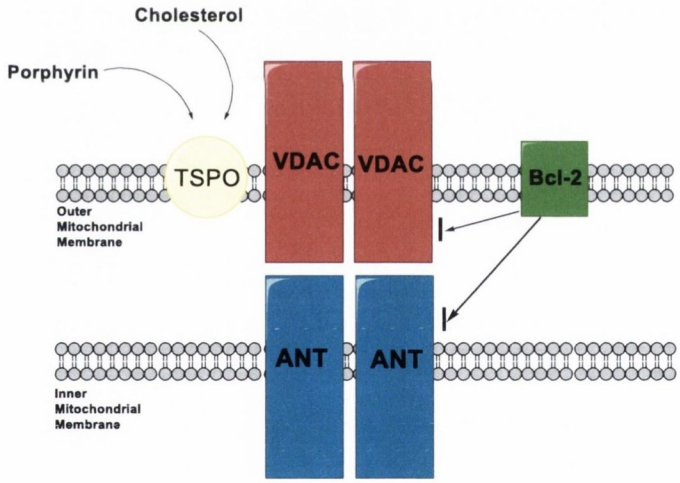

Figure 6.1. Schematic representation of the mitochondrial permeability transition pore and TSPO complex. The translocator protein (TSPO) is labelled yellow and the voltage-dependent anion channel (VDAC) is colored red. The B-cell lymphoma 2 protein (Bcl-2) is shown in green with the adenine nucleotide translocator (ANT) depicted blue.

Although the TSPO is an important regulatory complex in its own right, there is increasing evidence that this protein may represent an attractive target for researchers in the design and development of novel anti-cancer therapeutics. Circumvention of cell death in human cancers is becoming an ever increasing cause of failure in a number of treatment modalities [383,384]. One method to avoid such treatment failure may be the administration of drugs designed to

activate the cell death machinery. This activation can be achieved through the permeabilization of the mitochondrial outer membrane which will result in the convergence of apoptosis-inducing and necrosis-inducing factors to the mitochondria and cause deregulation and permeabilization [385]. Limitless proliferative potential, impaired apoptosis and insensitivity to growth signals are just some of the mitochondrial dysfunctions concomitant with cancer and therefore make mitochondrially-targeted compounds a promising approach as an anti-cancer therapeutic [386,387]. The anti-apoptotic effect of Bcl-2 proteins and myeloid cell leukemia sequence 1 (MCl1) were shown to be blocked by the TSPO [388], which suggests that exploitation of the TSPO may prevent Bcl-2 imposed chemoresistance [389,390].

6.2 Function

The TSPO is a major component of the outer mitochondrial membrane and as a result, mediates various mitochondrial functions, including cholesterol transport and steroid hormone synthesis, porphyrin transport, mitochondrial respiration, mitochondrial permeability transition (MPT) pore opening, apoptosis and cell proliferation
[183,391]. The TSPO has been proposed as a novel predictive indicator of an aggressive phenotype in certain cancers, such as, breast, colon-rectum and prostate [392]. Research has shown glial cells exhibit a similar situation, where TSPO expression levels are characteristic for specific cancer lines [393].

As mentioned previously, the TSPO plays a crucial role in a number of biological functions such as normal cellular homeostasis (Figure 6.2). This pivotal role is demonstrated by a TSPO -/- mutant, which results in an embryonic lethal phenotype in mice [394]. As a member of the mitochondrial permeability transition pore it is responsible for binding and transporting cholesterol into the mitochondria, where it is converted to pregnenolone. The TSPO is also involved in the transport of preproteins into mitochondria. These preproteins are synthesized on cytosolic polysomes and are located within mitochondrial subcompartments. Significant mitochondrial resources and bioenergetic activity are required for cellular proliferation and thus the import of these proteins for mitochondrial biogenesis and metabolism is an important factor in the cell cycle.

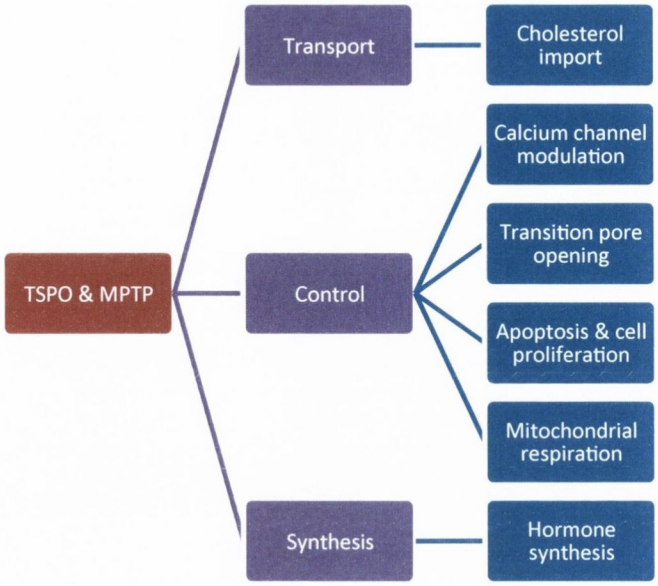

Figure 6.2. Flowchart of the different biological functions of the TSPO.

As a result, the possible use of the TSPO as a target for chemotherapy and as a marker of neoplastic growth has begun to attract considerable attention. The unrestricted growth of tumorgenic tissues is partially due to the altered up-regulation of cellular processes, such as those connected with cholesterol transport and the mitochondria [394].

TSPO ligands induce cell-cycle arrest and, for example, the apoptosis of human colorectal carcinoma cell lines *in vitro* compared with in normal human colon tissues [395]. In addition, a correlation between the progression of prostate, breast and colorectal cancer and the overexpression of TSPO has been shown [396-398]. There may, however, be other contributing factors such as the tissue of origin that may be instrumental in determining the role of the TSPO in cell proliferation [399]. Researchers have discovered that cellular changes such as apoptosis during tumor progression were contributed by the deregulation of TSPO expression or function [400-402]. These observations demonstrate the potential for TSPO as a molecular target and the potential for advancement of future anti-cancer treatment modalities.

The MPTP maintains transmembrane potential through active pore opening and closing during normal homeostatic conditions. Apoptotic factors, such as cytochrome *c* or apoptosis-inducing factor (AIF) may be released from the mitochondria into the cytosol during periods of prolonged opening of the MPTP [183,403]. Cell death may arise from this subsequent release as these apoptotic factors can induce osmotic swelling of the mitochondrial matrix which initiates a necrotic signaling cascade, ultimately ending in cell death [404].

6.3 Structure

Thus far, detailed X-ray crystallographic structural investigations of the TSPO have been hampered by difficulties expressing, purifying and stabilizing this membrane-bound protein.

Other approaches, such as nuclear magnetic resonance and thermodynamic simulations have been employed and resulted in its description as a 18 kDa protein with five transmembrane spanning domains [405]. Recently, single-particle helical reconstruction and electron cryo-microscopy were used to obtain a three dimensional structure of the *Rhodobacter sphaeroides* TSPO at 1 nm resolution [406]. This study details that two TSPO monomers form a tightly associated symmetric dimer in the membrane place, each with five transmembrane a-helices, although the exact functional role of the dimerization is not clear yet.

6.4 Ligands

The two classes of ligands which have been pivotal to the elucidation of the structure and function of the TSPO have been the benzodiazepines and isoquinoline carboxamides (Figure 3). Examples from both classes of compounds show selectivity for the TSPO and display nanomolar affinities [407]. [^{11}C]PK-11195 **221** was the first radiolabelled example of an isoquinoline carboxamide ligand for the TSPO. Although the benzodiazepine [^{11}C]Ro 5-4864 **222** is a competitive binder for TSPO derived from rat kidney, it fails to maintain its affinity across species. Cloning studies have shown a high affinity of **222** for rodent-derived TSPO (K_D = 1-9 nM) but a markedly reduced affinity for human TSPO (K_D = 54 nM) [408].

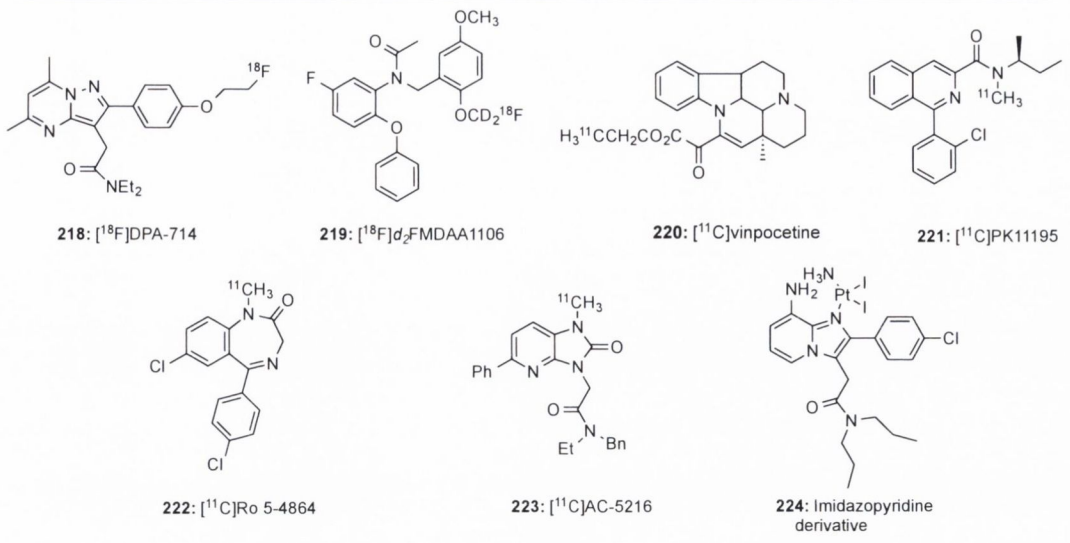

Figure 6.3. Classes of TSPO Radioligands. The phenoxyphenyl acetamides [409-411], *e.g.*, [^{18}F]d_2FMDAA1106 have seen great success as radioligands for TSPO. Other classes of suitable compounds include the pyrazolopyrimidines, *e.g.*, [^{18}F]DPA-714, vinca alkyloids [412] such as [^{11}C]vinpocetine. Aryloxodihydropurines, [413,414] for example [^{11}C]AC-5216 have been used extensively and successfully in animal models. Finally, imidiazopyridine based molecules e.g. **7** have displayed nanomolar affinity for the TSPO [415-417].

However, research has shown that TSPO ligands have no general structure, and porphyrins such as protoporphyrin IX (PP IX, the biosynthetic precursor of heme) **225** have shown to be the only endogenous ligands that bind with nanomolar affinity to TSPO [418]. This high affinity is selective for the TSPO by a factor of 1000 compared to the affinity for central benzodiazepine receptors. In this context it was postulated that the TSPO facilitates the transport of porphyrins into the mitochondria, as the first and final stages of heme biosynthesis take place in the mitochondria. This hypothesis would then explain the strong affinity of protoporphyrin for the receptor and would create a possible link between a deficiency in this receptor and development of porphyrias (*vide infra*).

Despite being extensively studied for over 30 years, the TSPO's role in pathophysiology has still not completely been elucidated. Partly this is the result of the absence of high resolution structures and of difficulties in interpreting imaging and pharmacological data [410]. Growing evidence from recent studies has confirmed that multiple binding sites exist and it is now logical to assume that not all newly discovered ligands for the TSPO will only be competitive binders for the isoquinoline site [419,420].

As a consequence of the marked up-regulation of TSPO in active disease states it has proven an attractive target for *in vivo* imaging of disease progression using functional imaging modalities such as positron emission tomography (PET) [407,421]. Although radiolabelled derivatives of

PK11195 **221** [422] and Ro 5-4864 **222** [42] have been the gold standard of imaging agents for the TSPO (Figure 3), these molecules still suffer from some limitations, such as the poor pharmacokinetic profile of the isoquinolines and poor performance of the benzodiazepines as imaging agents. Thus, a need exists to develop improved TSPO labeling agents for the *in vivo* study of the TSPO [423].

As progression of diseases and diminished survival rates can archetypally be linked with TSPO expression it has been an obvious target for imaging studies. Notably, Manning's group has explored the use of TSPO ligands as imaging agents for colon [424] and breast cancer [425], and glioma [426,427] with agents which potentially could be used as cancer imaging biomarkers. They focused on the pyrazolopyrimidine scaffold, specifically modified at the 5-, 6-, and 7-positions in an attempt to synthesize higher affinity ligands for the TSPO, which in turn may serve as more robust PET agents *in vivo*. They identified 2-(5,7-diethyl-2-(4-(2-fluoroethoxy)phenyl)pyrazolo[1,5-a]-pyrimidin-3-yl)-*N,N*-diethylacetamide to be a selective ligand for the TSPO. It exhibited an excellent 36-fold enhancement in affinity compared to the known pyrazolopyrimidine (DPA-714) [428]. Next they synthesized a ^{18}F radiolabeled analogue, which displayed negligible accumulation in normal brain tissue, but gave first-rate imaging contrast due to strong accumulation in tumor tissue in *in vivo* studies of healthy rats and a preclinical model of glioma. Clearly, there is therapeutic potential for this PS as a novel PET ligand for assessing TSPO expression in tumors [429].

6.5 Photodynamic Therapy

6.5.1 PDT: Principle

Photodynamic therapy (PDT) is a selective treatment, which can be used as an alternative or in addition to classical therapies, *e.g.*, chemotherapy [18,404]. A regime of PDT requires the administration of a tumor localizing photosensitizing agent, typically a tetrapyrrole based molecule, followed by activation of the drug by light of a specific wavelength (Figure 6.4). PDT as a treatment holds many advantages over traditional cancer treatments such as radiation therapy, chemotherapy and surgery as PDT is a relatively non-invasive treatment which has the potential to selectively destroy tumor cells whilst sparing healthy tissue. It can be applied to places deemed non-viable by surgery and has seen success with numerous forms of cancer, including head, neck, throat and breast. It is more controllable and less destructive on the body meaning older patients and others vulnerable to other treatment modalities can be treated with PDT.

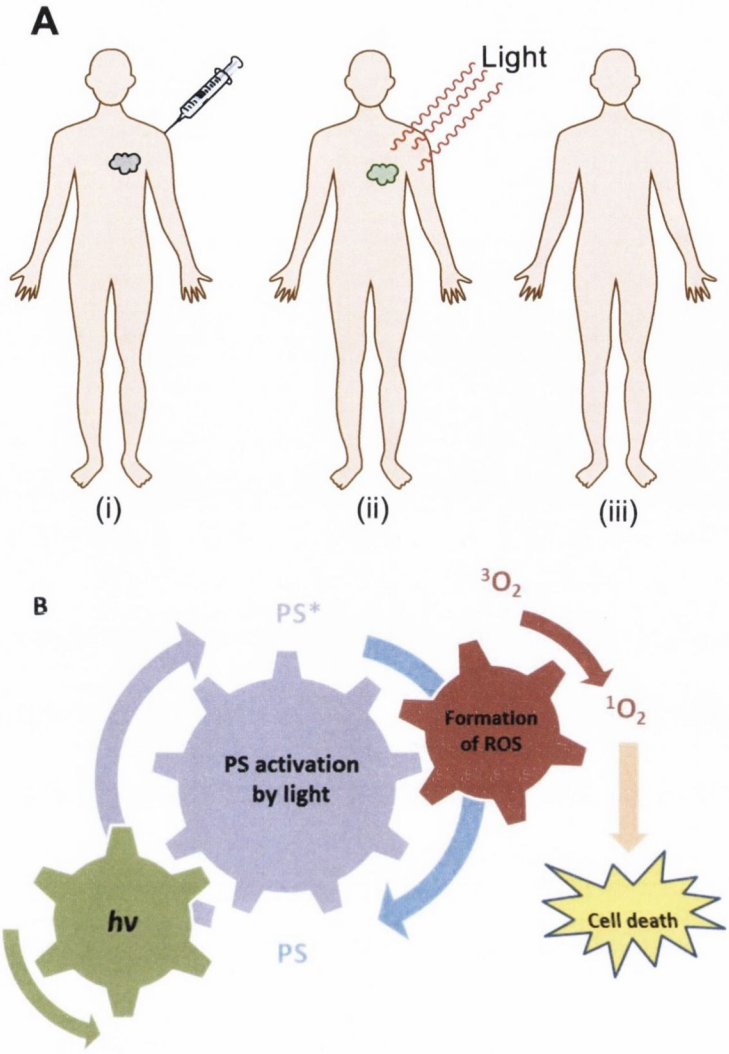

Figure 6.4. Graphical depiction of PDT treatment. (**A**) (i) PS is injected into the body. (ii) The PS is allowed accumulate at the tumor site before irradiation with light. (iii) Selective destruction of tumor. (**B**) Chemically this method is based on the formation of singlet oxygen and other ROS.

Selectivity is achieved partly by the photosensitizer (PS), such as the compounds described below, which have a natural tendency to accumulate in malignant cells/tissue [317], and due to the localized application of the light to the afflicted area. Current developments of efficient delivery platforms focus on bioconjugates [289], liposomal encapsulation [430] or nanoparticle conjugation [431]. These alterations aim to enhance the specificity and selectivity of the photosensitizer which will in turn enhance the cellular uptake of the PS. New molecular targets such as the TSPO may prove pivotal to the improvement of the efficacy and selectivity of new PS's. Verma *et al.* detected that tumor susceptibility to porphyrin-based phototoxicity was directly related to TSPO density in tumors. This data proposes that damage to the mitochondria is the proximal event that leads to observed cell death. Therefore porphyrins may be able to exploit this sequence of events and enter cells and accumulate on porphyrin mitochondrial

transport sites [432-434]. Since the lifetime of the porphyrin triplet state is extremely short and their diffusion in space is limited, the photo-induced reactions primarily affect the cell organelles labelled by the PS.

6.5.2 TSPO as a Porphyrin Target

6.5.2.1 Porphyrins as Endogenous Ligands

But the focus on porphyrins in connection with the TSPO story begins with Snyder and coworkers discovering in 1987 that porphyrins are endogenous, potent competitive inhibitors of the TSPO [178-180]. They found that pure hemin and PP IX **225** competitively inhibit TSPO binding of [^{3}H]PK-11195 and [^{3}H]Ro 5-4864 with K_i values of 41 and 15 nM, respectively. While their binding activity at central-type benzodiazepine receptors saw a 1000-fold lower affinity. Tetra- and octacarboxylic acid porphyrins were to a small degree able to displace isoquinoline and benzodiazepine derivatives from binding to the TSPO and inactive in comparison to their dicarboxylic acid porphyrin counterparts, which displayed nanomolar potencies. This finding of porphyrins as endogenous TSPO ligands opened a new field of studies into porphyrins as therapeutic or diagnostic agents pertaining to TSPO related diseases.

Clearly, if porphyrins can bind to TSPO, this must effect the action of porphyrin-based photosensitizers in PDT. One of the most insightful strategies in PDT involves the administration of d-aminolaevulinic acid (ALA), a biosynthetic precursor of heme, with the aim to boost protoporphyrin IX production in the target cells [435]. Indeed, Furre *et al.* showed that PP IX produced endogenously by hexaaminolaeuvulinate (HAL) localized primarily in the mitochondria of the human cell line Reh [436]. Upon PDT treatment, post irradiation analysis showed that >80% of cells died by apoptosis, as indicated electron microscopy. HAL-PDT turned out to be both light dose and time course dependent.

In the biosynthetic pathway of heme, coproporphyrinogen III traverses the channel from the matrix to the cytosol [437]. It is theorized by Furre *et al.* [436] that HAL-induced endogenous PP IX may also advantageously use this channel for its own transportation into the cytosol. However, the study also showed that exogenous PP IX localizes differently intracellularly than endogenous PP IX and may not target the TSPO sufficiently to produce the same degree of apoptosis. Analysis of competitive binding studies with ligands for ANT suggests that, as a result of its close spatial proximity to the TSPO, the mitochondrial inner membrane adenine nucleotide translocator may be an additional target for HAL-PDT [438]. Their propinquity to HAL-induced endogenous PP IX synthesis at the mitochondrial inner membrane and the possibility that the porphyrin may use ANT for its transportation validates the TSPO as a possible therapeutic target for HAL-based PDT treatment of cancer.

With the exception of ALA and Photofrin® most PS in clinical use or development have chemical substituent pattern quite distinct from PP IX and this raises the question of porphyrin ligand

specifity when targeting the TSPO. Kessel *et al.* conducted a study into the comparative binding of protoporphyrin IX and two structural analogs, PP III **226** and PP XIII **227**, using murine leukemia L1210 cell cultures (Figure 6.6) [439]. The amphiphilicity of porphyrin based PS plays a significant role in the localization and membrane passage [440]. As such, it is important to consider the distribution of polar and hydrophobic substituents around the macrocycle as well as the charge of the side chains present on the molecule [318,441]. Kessel *et al.* suggest that porphyrin accumulation and affinity of the TSPO must be governed by hydrophobic considerations and that a major determinant of PDT efficacy within the PP IX series may be the relative hydrophobicity of the different analogues. All three porphyrins displayed equal hydrophobicity and all three agents induced 30% to 40% cell death *via* apoptosis after light exposure, although only PP IX had a strong affinity for the TSPO. These results suggest that only sensitizers with a configuration similar to protoporphyrin IX may display PDT efficacy as a result of TSPO affinity.

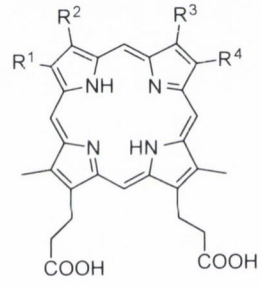

225: R^1 = methyl, R^2 = vinyl, R^3 = methyl, R^4 = vinyl = PP-IX
226: R^1 = methyl, R^2 = vinyl, R^3 = vinyl, R^4 = methyl = PP-III
227: R^1 = vinyl, R^2 = methyl, R^3 = methyl, R^4 = vinyl = PP-XIII

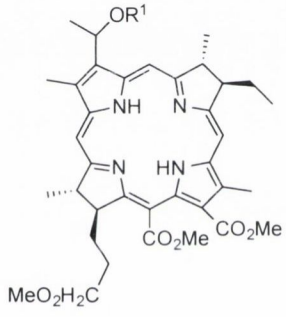

228: R^1 = H,
229: R^1 = CH_3
230: R^1 = $(CH_2)_2CH_3$
231: R^1 = $(CH_2)_6CH_3$
232: R^1 = $(CH_2)_{10}CH_3$

Figure 6.6. Protoporphyrins and rhodochlorin derivatives.

The next question is to what extent can the binding of porphyrins to the TSPO be affected by other factors? Next to hypoxia one other important factor is the intracellular pH. Healthy cells grow in pH 7.4 while cancerous ones, depending on their kind and age, can live in pH 5.5-6.5 [442]. Bombalska and Graczyk observed a decline in binding constants of a series of protoporphyrin and haematoporphyrin derivatives with increasing acidity of the environment [443]. With decreasing pH value porphyrin-type photosensitizers occur in different ionic forms and it is possible that the receptor changes its structural conformation in varying environment conditions. PP IX demonstrated the greatest binding affinity across the pH range, followed by haematoporphyrin (Hp), $Hp(Arg)_2$ and $PP(Arg)_2$ [443]. There is also the possibility that a lower pH value results in porphyrin core protonation [444] with attendant conformational distortion [445] which could impair binding with the receptor [446,447].

This work was followed by studies on the interaction of diamino acid derivatives of protoporphyrin IX (Figure 8), where the vinyl groups have been substituted with amino acids **228-231**. The amino acids were installed to facilitate the entry of the photosensitizer into the cell by binding to amino acid receptors present in the tumor cell membrane. Preliminary studies indicate selectivity of accumulation of the dyes and low cytotoxicity to normal cells [448]. The strongest binding was observed at pH 5.5 for all four amino acid derivatives, which was supported by an observed increase in association constants as compared to pH 7.4. With these results, one can hypothesize that with the progression of cancer, the strength of the binding efficacy will increase as the pH decreases and therefore an increase in photosensitizer concentration is not necessary so as to achieve the required photodynamic effect.

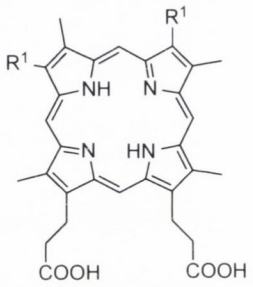

233: R^1 = "Gly"
234: R^1 = "Ala"
235: R^1 = "Ser"
236: R^1 = "Phe"

Figure 6.7. Diamino acid derivatives of protoporphyrin IX

6.5.2.2 Exogenous PDT Drugs

If endogenous porphyrins bind to TSPO or their level and interaction can be modulated through additional protoporphyrin IX availability what effects can be observed upon the exogenous administration of porphyrin-type PDT drugs? Several studies have addressed questions such as this. For example, Pandey's group used a synthetic library of long-wavelength photosensitizers derived from bacteriopurpurinimide and bacteriochlorin p_6 for comparative *in vitro* and *in vivo* PDT studies in RIF tumors [449]. The capacity of the rhodochlorins **232-236** (Figure 6.6) to displace the labeled high-affinity TSPO ligand PK11195 **222** was measured and it was found that photosensitizers **233, 234** and **235** displaced more than 70% of ^{3}H-PK11195 at 10^{-4} M, whilst **236** displaced about 51% of ^{3}H-PK11195. However, no direct correlation between TSPO binding and PDT efficacy was found even though some molecules showed encouraging results in respect to PDT use.

Next, they synthesized a phytochlorin derived from chlorophyll *a* and evaluated its PDT and tumor imaging capacity *in vitro* and *in vivo* [450]. They found methyl 3-(1′-*m*-iodobenzyloxyethyl)-3-devinylpyropheophorbide *a* (HPPH) **237** to be a prospective photosensitizer and imaging agent for photodynamic therapy (Figure 6.8). Five C3H mice

bearing RIF tumors were treated with the non-radiolabelled photosensitizer analogue of **238 (239)** at a drug dose of 1.5 μmol.kg^{-1} and a light dose of 128 J.cm^{-2}, 14 mW.cm^{-2} for 2.5 h (I_{max} = 665 nm) at 24 h post injection. A 100% cure of tumors was achieved, *i.e.* all mice were tumor free within 60 days. The photosensitizer exhibited promising tumor fluorescence and PET imaging abilities and clearly supports the Pandey's concept of this ^{124}I-labeled photosensitizer finding use as a "multimodality agent". In the future, the design and efficacy may be improved upon by incorporating more tumor-avid and/or target specific photosensitizers.

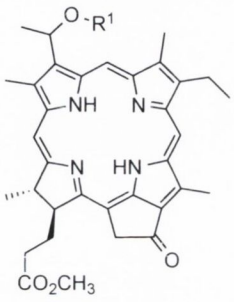

237: R^1 = $(CH_2)_5CH_3$
238: R^1 = 2-benzyliodide
239: R^1 = 2-benzyliodide[^{124}I]

Figure 6.8. Pyropheophorbide derivatives

Another example involved the use of bacteriochlorophyll a derivatives. These relatively unstable bacteriochlorins from *Rhodobacter shaeroides* were converted *in situ* into a series of stable *N*-hexylimide analogues **240-242** and tested *in vitro* and *in vivo* for their efficacy as PDT agents (Figure 6.9) [451]. The bacteriopurpurinimide **240** gave limited *in vivo* PDT efficacy in C3H mice bearing RIF tumors (drug dose 0.2 μmol.kg^{-1}, I_{max} = 780 nm, 135 J.cm^{-2} at 24 h post injection). Two of the more efficacious analogues were **241** and **242** however, despite their improved efficacy, displacement studies suggest that they do not have a significant affinity for the TSPO. Comparative intracellular localization studies with Rhodamine 123 found the less effective photosensitizer to be localized in the lysosomes, whereas the most effective one was localized in the mitochondria indicating the possibility for future improvements.

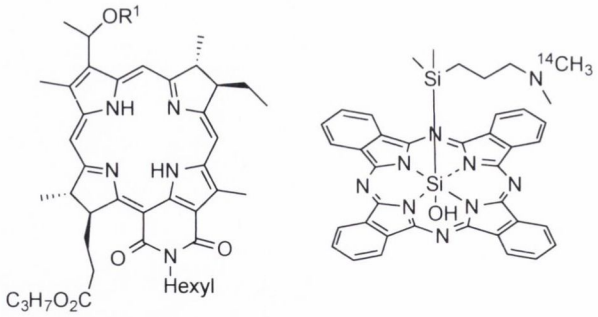

240: $R^1 = CH_3$
241: $R^1 = (CH_2)_6CH_3$
242: $R^1 = (CH_2)_9CH_3$

243: Pc-4

Figure 6.9. Stable bacteriopurpurinimide and phthalocyanine based photosensitizers currently in investigation for use as PDT agents.

Competitive binding studies of a ^{14}C phthalocyanine photosensitizer **243** against ^{3}H-PK11195 (**222**), for binding to rat kidney mitochondria or intact Chinese hamster ovary cells were conducted by Morris *et al.* [452]. Their results suggest the presence of various binding sites for Pc4 (**30**) in mitochondria and cells, other than those attributed to PK11195 binding (Figure 6.9). Chemically this makes sense as phthalocyanines have chemical properties distinct from those of protoporphyrins. Although a low affinity binding site for **243** was identified, it appears that other mitochondrial events, such as photodamage to Bcl-2 are more pertinent to the phototoxicity of Pc4 (**243**) PDT than the binding of the phthalocyanine to the TSPO. This suggests that the observed inhibition of Pc4 (**243**) PDT induced apoptosis by PK11195 likely occurs through a mechanism separate to the TSPO.

6.5.3 Porphyrins for PET and PDT

^{11}C and ^{18}F are the most common PET isotopes used to label drugs [453,454]. Unfortunately, both suffer from relatively short half-lives which limits their use in experiments involving monoclonal antibodies or photosensitizers which take a long time (hours compared to minutes) for accumulation in a tumor. Due to a half-life of 4.2 days, ^{124}I is a more appropriate candidate and this longer half-life makes it compatible for sequential biological imaging using microPET [455-457].

With these facts in mind Pandey and coworkers aimed to develop a TSPO targeting photosensitizer for both imaging (PET) and PDT. As mentioned previously, numerous reports in the literature have shown overexpression of TSPO for both colon and breast cancers [397,400]; hence Balb/c mice bearing Colon-26 (colon adenocarcinoma) and EMT6 (well characterized, undifferentiated mouse breast cancer) tumors were selected. The synthesis of ^{124}I labeled **244** was achieved with high (>95%) radioactive specificity [458].

Use of the radiolabelled derivative of PK11195 (^{124}I-PK11195, **244**) resulted in a significant improvement of the PDT efficacy of the well-known photosensitizer HPPH (**237**), once conjugated. Compounds **245** and **246** possess similar binding affinity to the TSPO, however, **33** exhibited stronger tumor affinity as it possessed a higher standardized uptake value (% ID/g) at every time point (Figure 6.10). Both compounds **245** and **246** are good imaging agents and, interestingly, compound **246** produced significantly less skin phototoxicity than HPPH (**237**) in Scid mice bearing MDA-231 tumors; one of the main drawbacks of contemporary clinical PDT. Optimal tumor imaging for these compounds were obtained at 48, 72 and 96 h post injection, which further rationalizes the necessity to use ^{124}I instead of the shorter lived ^{18}F (Figure 12). These results clearly indicate that a conjugation of PK11195 to photosensitizers increases the PDT efficacy and target specificity compared to the photosensitizer alone.

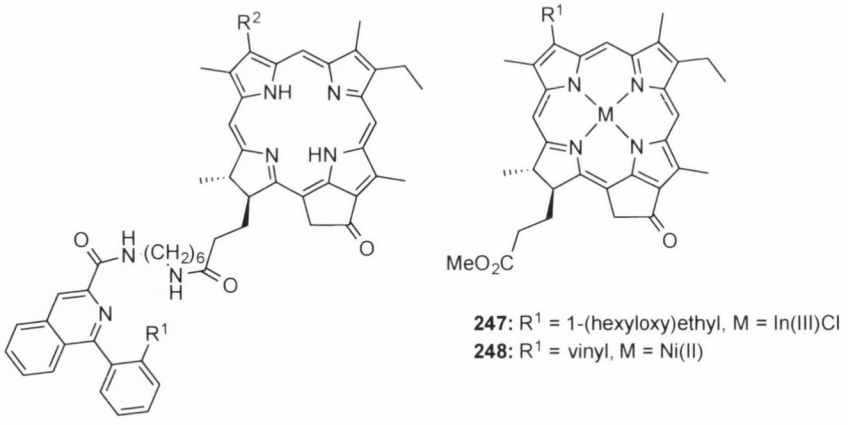

244: R^1 = I, R^2 = 1-(hexyloxy)ethyl
245: R^1 = ^{124}I, R^2 = vinyl
246: R^1 = ^{124}I, R^2 = 1-(hexyloxy)ethyl

247: R^1 = 1-(hexyloxy)ethyl, M = In(III)Cl
248: R^1 = vinyl, M = Ni(II)

Figure 6.10. A Library of phytochlorin derivatives.

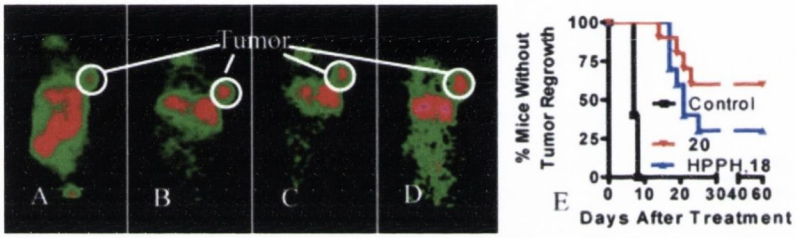

Figure 6.11. Conjugation of the photosensitizer HPPH to a radiolabeled derivative of PK11195. For MDA-231 tumors bearing Scid mice, **244** possesses strong tumor imaging capability. MicroPET emission imaging (coronal view) at 24 h (A), 48h (B),72h (C),and 96 h (D) post-injection of **245** (i.e., ^{124}I-**244**)(dose: 50 μCi(~40 ng)/mouse). (E) Kaplan-Meier plot for the *in vivo* PDT efficacy of compounds HPPH (**237**) and **244** at 0.4μmol/kg dose. Light dose: 135 J/cm^2, 75 mW/cm^2, ten mice for each group. **244** produces significaknt better *in vivo* PDT efficacy than HPPH (**24**) (P<0.0001). "Reprinted (adapted) with permission from [459]. Copyright (2011) American Chemical Society.".

Related studies used pyropheophorbides and their respective metal complexes to ascertain their viability as nonradioactive TSPO binding probes [460]. The TSPO binding and photosensitizing efficacy was influenced substantially by the presence of a core metal and as these compounds display strong fluorescence, they have significant potential to replace radioactive TSPO probes. For example, porphyrin **247**, an indium(III) complex proved to be the most efficacious with respect to photosensitizing efficacy. *In vitro* experiments with mice bearing RIF tumors (light dose 135 J cm^{-2}, 75 mW cm^{-2}, l_{max} = 665 nm) revealed an order of efficacy for the central metal of In(III) > 2H > Zn(II) > Ni(II) (Figure 6.10). This might be related to their singlet oxygen production capabilities. Although the Nickel complex **248** produced no PDT

effect as expected, it did have the strongest binding affinity to TSPO, comparable to that of PK11195. Again *in vitro* efficacy and TSPO binding efficacy showed no direct correlation and no relationship was seen between TSPO binding and *in vitro* PDT efficacy.

As synthetic bacteriochlorins are good prospective PDT agents [318,461] some of them were also investigated in the context of the TSPO [462]. Benzobacteriochlorins derived from *vic*-dihydroxybacteriochlorins have long wavelength absorption in the range of 737 to 805 nm and were used in *in vitro* (RIF tumor cells) and *in vivo* (C3H/HeJ mice bearing RIF tumors) tests (Figure 6.11). The benzobacteriochlorin **244** was found to be the most efficacious and displayed reduced skin phototoxicity compared to Photofrin® at their respective therapeutic doses. Displacement studies were undertaken against ^{3}H-PK11195 (**222**) and indicated that increasing concentrations of mitochondrial located benzobacteriochlorins **249-253** did not result in a higher displacement of ^{3}H-PK11195 (Figure 13). This suggests that, for these benzobacteriochlorins, the TSPO is not the target site.

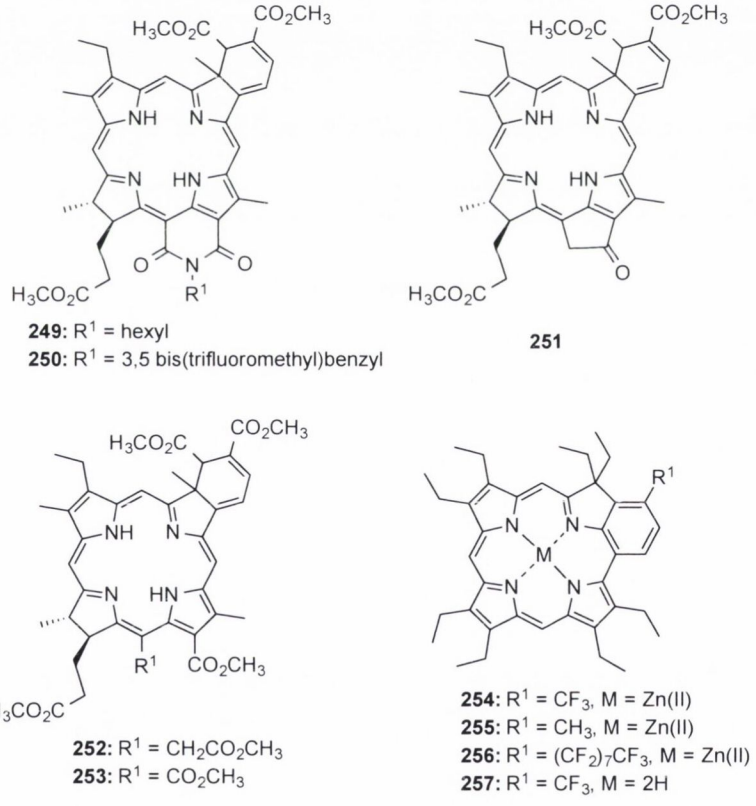

Figure 6.12. A range of tetrapyrrole-based photosensitizers.

Likewise, octaethylporphyrin-derived benzochlorins with varying degrees of lipophilicity were evaluated in an *in vitro* and *in vivo* SAR study (Figure 6.12) [463]. A number of different structural features, such as the length of alkyl or fluoroalkyl groups attached to the exocyclic ring either by a carbon-carbon or ether linkage, were assessed. All of the (benzochlorinato)zinc(II) compounds were found to be effective with analogues **254, 255** and

256 giving the best *in vivo* (C3H/HeJ mice) results, with three out of six mice tumor free after 90 days (1.0 $\mu mol.kg^{-1}$ dose). Of the two compounds **254** and **257** the Zn(II) complex produced 100% cell kill (RIF tumor cells) at 4.0 and 6.0 $J.cm^{-2}$. Comparative intracellular localization and binding studies with Rhodamine-123 and ^{3}H-PK11195 (**222**) indicate that the PSs localize in the mitochondria. However, no specific displacement of ^{3}H-PK11195 (**222**) was observed, *i.e.* no direct correlation exists between binding affinities and photosensitizing efficacy.

■ Modelling and Structural Investigations

Recent studies on the role of the interaction of PP IX and the TSPO in porphyrin-based photodynamic therapy focused on structural and modelling studies. By using *Escherichia coli* Papadopoulos *et al.* were able to express recombinant mouse TSPO in order to investigate the validity of their hypothesis that the interaction of PP IX with the TSPO is involved in the regulation of heme biosynthesis [464]. The *E. coli* protoplasts produced a recombinant gene product that showed specific affinity for PP IX binding.

The interaction of PP IX and TSPO in various cell models [465-467] has been suggested to assist the modus operandi of porphyrin based photosensitization in photodynamic therapy (PDT) of tumors [468]. These experiments found that neither PK 11195 nor Ro5-4864 could increase the PP IX binding or uptake, which was in accordance with previous studies [469]. Protoporphyrin IX could displace a radiolabeled analogue of PK 11195 from the TSPO but not that of Ro 5-4864, which indicated the presence of separate but overlapping binding sites [469,470]. Interpretation of these results suggest that the TSPO protein is solely responsible for PP IX binding and transport [439,464].

Bacterial TspO have been used to develop a functional model of the receptor. A number of TSPO mutants were synthesized by Yeliseev and Kaplan to investigate the significance of a number of amino acid residues on the functional activities of TspO [471]. Many of the amino acid residues involved in TSPO function are highly conserved among *R. capsulatus* CrtK, *R. sphaeroides* TspO and their mammalian analogues. The first putative periplasmic loop of TSPO, located between the first and second membrane spanning domain, contains a clustering of highly conserved amino acid residues. These residues are Leu^{34}, Lys^{36}, Trp^{30}, Trp^{39}, Trp^{44}, Trp^{50}, Trp^{135}, Gln^{80}, and Arg^{96} [472]. This might suggest the direct interaction of the first putative loop with a specific ligand or cofactor, *e.g.*, a tetrapyrrole. This loop contains a number of tryptophan residues, which could support its involvement in tetrapyrrole ligand binding. This is based on the heme binding motif (WWD), which is found in proteins involved in transmembrane heme delivery [473].

This proposed model, where the N-terminus of TSPO is exposed to the cell exterior may contradict the theorized structural model for the mammalian TSPO, which proposes that the N-terminal region of the protein is located on the matrix side of the outer mitochondrial

membrane and that the first putative loop is exposed to the cytoplasm [419,474]. However, it appears permissible to anticipate that the tetrapyrrole binding site on the TSPO be exposed to the periplasmic space due to its part in the biosynthetic pathway for heme. The synthesis of TSPO in the cytoplasm and subsequent importation into the mitochondrial matrix before re-entering the mitochondrial outer membrane supports this new inside-out topology relative to bacterial topology [474]. Previous studies indicated the significance of Lys^{39} (corresponding to Lys^{36} of the TspO sequence) in binding of Ro5-4864, and of Trp^{42} and Trp^{47} (corresponding to Trp^{39} and Trp^{44} of the TspO sequence) in binding of PK11195 and Ro5-4864 [419]. This supports the participation of the conserved amino acids discussed above in binding TSPO ligands in the mammalian TSPO [419]. Parallels between the structural and functional properties of the bacterial TspO and the mammalian homologue are mounting and this study provides further support for the theory [475].

Some information on the binding sites for endogenous ligands of the TSPO dimer model, could be derived from competitive binding studies using PK11195, PP IX and cholesterol. Some level of interaction among all three binding sites of the TSPO appears to be present [476]. These results are representative of a model in which PK11195 and PP IX interacting at somewhat different positions on extra-membrane loop 1 (Figure 6.13). The model suggests that the porphyrin may initially bind at loop 1, en route to transport *via* the dimer interface, as demonstrated in Figure **12**. This proposed binding model matches previous *in vivo* studies in *Rs*TspO [472], which also suggested that loop 1 plays a critical role in the binding and export of porphyrins [471,477,478]. Despite these correlations, it is unlikely that the first putative loop 1 is the only contributor to the binding of PP IX. Using a tryptophan fluorescence quenching assay for TSPO investigations it was observed that the tryptophan fluorescence was quenched evenly and completely by PP IX while no such effect was found with PK11195 and other ligands. Thus, PP IX may interact with a rather large area its binding induces a global conformational change [406].

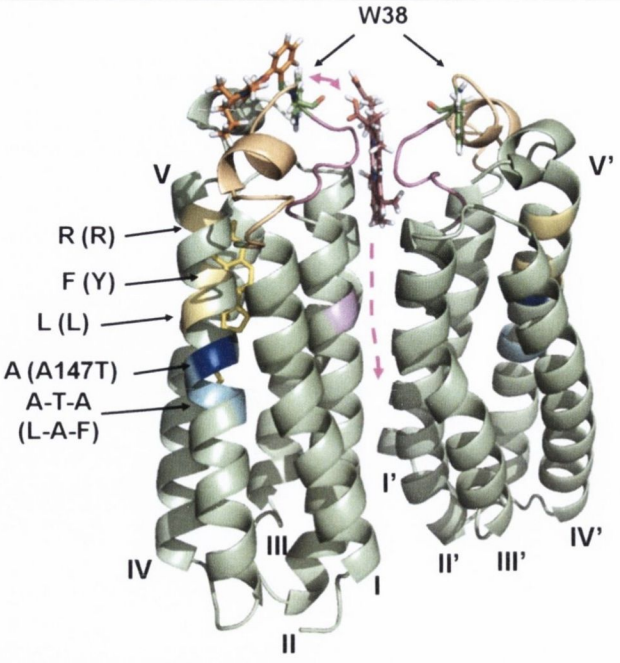

Figure 6.13. Model of PK11195 and PpIX binding in the proposed dimeric *Rs*TSPO state. A suggested model of the binding sites of PP IX, PK11195, and cholesterol on *Rs*TSPO. The ligands have been manually inserted into the model of *Rs*TSPO on one monomer. Roman numerals have been used to illustrate the helices: W38 (green sticks), PK11195 (orange sticks), PP IX (dark purple sticks), and cholesterol (yellow sticks). Proposed PP IX binding sites on loop 1 were colored light purple and PK11195 binding site was colored light orange. The potential role of the dimer in the loading and transport of PP IX has been illustrated by a magenta dotted line indicating the potential route. "Reprinted (adapted) with permission from [477]. Copyright (2013) American Chemical Society."

One suggestion is that protoporphyrin IX may bind to a large area or induce a global conformational change, both of which are conceivable if PP IX is being bound and transported through the dimer interface [476]. This was based on the observed quenching of the tryptophan fluorescence by PP IX but not by PK11195 and other ligands. Decreased porphyrin export activity in phenylalanine mutants of W44 and W50 (single amino acid substitution with elevated levels of accessory pigments), indicates changes in TSPO function [472]. This indicates that aromatic residues on transmembrane helix II play an important role in porphyrin binding and transport. A W38C mutant showed a ~6-fold reduction in affinity of PP IX for *R.s.* TSPO which is the location in loop 1 that initial binding occurs [464]. Although PK11195 was reported to compete with PP IX binding and bind to loop 1 of the TSPO, results from tryptophan quenching experiments indicate that they do not bind in precisely the same location.

All modelling studies suggest that the last two-thirds of loop 1 are highly conserved across all species. The observation that the K_d values of both PK11195 and PP IX were distinctly lower in

the W38C mutant suggests some overlap between PK11195 and PP IX [476]. These independent lines of evidence allowed Miller *et al.* [476] to propose that within the monomer, PK11195 interacts mainly on the first half of loop 1, extending to residue W38 (S41 in human).

6.6 The Situation in Plants

Although unrelated to clinical applications it may be illustrative to take a quick look at the situation in plants. After the initial impetus from studies in mammals the search began for analogous mitochondrial import mechanisms in plants [479] and such a system was first identified by Lindemann *et al* in 2004 [480]. Substantial similarities to the *Rhodobacter* TspO protein and the mammalian TSPO were found in protein sequences from *Arabidopsis thaliana* [480,481]. The recombinant gene product of a TSPO-homologues *Arabidopsis* sequence was cloned and expressed in *E. coli* and displayed high binding affinity for benzodiazepines [480]. A comparative benzodiazpepine-stimulated uptake of PP IX and cholesterol was observed when the protein was applied to *E. coli* protoplasts. This TSPO-like protein appears from these results to be involved in the directing of protoporphyrinogen IX to the mitochondrial site of protoheme formation and steroid import.

The gene sequencing of *Arabidopsis thaliana* identified a single TSPO related gene with a 40 amino acid N-terminal extension compared to the bacterial or mammalian species. This discovery suggest that site of localization may be in the mitochondria or chloroplast [479]. It has also been suggested that the At-TSPO plays a part in the response of *Arabidopsis* to high salt stress as re-localization of the At-TSPO from the ER to chloroplasts through its N-terminal extension occurs under high salt stress.

Further studies on different plant species investigated the central and peripheral-type benzodiazepine receptors in pods and leaves of *Ceratonia Siliqua* [482]. Using [^{3}H]PK 11195 and [^{3}H]RO 15-1788 (8-fluoro-3-carbethoxy-5,6-dihydro-5-methyl-6-oxo-4-imidazo-[1,5-a]-1,4-benzodiazepine) as specific ligands in a radioreceptor binding assay, the authors observed the presence of compounds which could readily displace the radiolabelled ligands from their respective binding sites. TSPO acting compounds were found to be extremely concentrated in young leaves suggesting that these compounds may play a significant role in cell growth and proliferation.

6.7 TSPO and Porphyrias?

The firing patterns of neurons are governed by the electrical properties of neuronal membranes and as such can be influenced by the production of neurosteroids, which can alter these properties. The TSPO seems to play a critical role in the production of these neurosteroids and

therefore may be a contributing factor to the development of some neuropsychiatric disorders. Porphyrias involve deficiencies in the enzymes that typically participate in the production of porphyrins and heme and may give rise to certain aspects of neuropsychiatric disorders, such as schizophrenic-like symptoms [183].

Interestingly, schizophrenia patients who presented with predominantly negative symptoms displayed a significantly reduced binding capacity of TSPO for heme precursors. Furthermore, researchers did not observe any correlation between age, gender, anti-psychotic medication and TSPO density, nor between variations of the TSPO gene and schizophrenia [483]. However, there was a decrease in TSPO density in post-mortem brains of chronic schizophrenia patients [483]. Additionally, Ritsner *et al.* found a connection between decreased TSPO density in blood platelets of schizophrenic patients exhibiting aggressive behavior [181]. The decrease in TSPO density was around 30% in patients and the B_{max} value was inversely correlated with aggressive behavior scores ($r= 0.36$, $p=0.023$).

Porphyrias typically arise due to an accumulation of heme precursors, *i.e.* atypical porphyrins, in tissue due to a deficiency in one or more of the enzymes associated with the heme biosynthetic pathway. Medical conditions associated with porphyrias vary depending on which enzyme in the biosynthetic pathway is deficient. Porphyrias associated with coproporphyrinogen III oxidase and protoporphyrinogen oxidase are the most likely to display neurological symptoms [182]. Interestingly, no research has been conducted into the possible correlation between this decreased TSPO density in aggressive schizophrenic patients and the manifestation of a porphyria. As the TSPO is a transporter for heme precursors into the mitochondria, a 30% decrease in TSPO density may cause an accumulation of porphyrins in the cytosol and therefore potentially a porphyria.

6.8 Future Perspective

Researchers have successfully observed species differences which suggest that *in vitro* results using animal-derived TSPO, may not necessarily translate successfully to human studies. Additionally, new binding sites on the TSPO not related to the family of isoquinoline compounds have been discovered and suggest that the current screening methods prove inadequate in addressing all potential binding sites.

Despite all the major advances in the understanding of the structure and function of the TSPO, it is still unclear precisely how the TSPO acts in the binding of tetrapyrrole substrates [441,484-486]. Several groups have trialed numerous synthetic analogues of the endogenous ligand PP IX but still have no definitive understanding or predictive model of whether a compound will bind to the TSPO. Due to the flexible nature of loop 1, further modeling studies need to be conducted and ligand-protein interactions need to be deciphered to give a more rational

approach to their drug design. Ultimately, this will require a high-resolution structure with bound ligand.

Although PDT efficacy and TSPO binding can still not conclusively be correlated the TSPO still represents an intriguing target for PDT based research for a plethora of cancers, including breast and colon. One possibility may be the use of a larger library of carboxylic acid based porphyrins with varying degrees of hydrophobicity in order to obtain a better understanding of the structural tolerance, if any, of the TSPO for macrocycle variation.

Chapter 7 Future Projects

7.1 Future for PDT?

Trying to predict the next paradigm shift in PDT is a difficult undertaking as most of the rational enhancements made to 2nd generation PS haven't worked, as of yet. Nanoparticles designed for PDT have reached their zenith in terms of research and publications, with concerns still, over their bio-toxicity due to clearance rates. Bio-conjugates has become an ever increasing field with the belief that these biologically pertinent molecules attached to a PS will impart greater selectivity and improve the PS's targeting for the cancer cells. Sugars have received the biggest draw from researchers and, although some mild success has been achieved, none have still managed to pose a threat to replace Photofrin®, Foscan® or any of the other clinically approved PSs. New emerging biological compounds of interest are folic acid, anti-bodies and bile acids. Since the discovery that folate receptors are over-expressed on the surface of numerous cancer cell lines, folic acid conjugates have been a logical route for improved targeting. Studies have shown folic acid conjugates with impressive $^1O_2$ Δ_Φ, whether these results can transfer into *in vitro* experiments, it is yet to be seen. Also issues regarding solubility and ease of purification arise, as specialized equipment is generally needed to purify these conjugates due to the poor solubility of folic acid in organic solvent.

Recent trends in PDT research show that, no matter the biological fragment; choice and location of the linker can be pivotal to the success of the PS. A plethora of groups have received negative results for their potential PSs when conducting *in vitro* experiments, however, all compounds had one common functional group; a triazole ring. Albeit, the triazole ring is a result of the ever popular "click" reaction, the biologically stable heterocycle formed has shown to be quite an efficient scavenger for $^1O_2$. Therefore any compound with this functional group present should suffer from low $^1O_2$ Δ_Φ and therefore display low cytotoxicity in MTT assays or *in vivo* studies in mice.

7.1.1 Anti-microbial PDT

The rapidly increasing emergence of antibiotic resistance among many species of pathogenic bacteria may be bringing to an end a period extending over the past 50 years, termed "the antibiotic era". Whilst PDT has traditionally been used to treat multiple forms of cancer, in recent times researchers have found that PDT can be implemented as quite a potent anti-microbial treatment. It works on the same basis of PDT for cancer i.e. one needs a photosensitizer, light of an appropriate wavelength and O_2. The destruction of the bacteria comes from the cytotoxic species singlet oxygen, not a traditional method for eradication of bacteria and therefore, researchers believe that the development of bacterial resistance to

this treatment will be impossible. It is theorized that due to this lack of resistance, anti-microbial PDT has a number of advantages over current treatment modalities and therefore can be very commercializable for a number of different applications e.g. Periodontal work[487], open wounds/cuts and surfaces in hospital facilities. Another possible advantage of anti-microbial PDT would be that the PS can be targeted to the microbial cell and the light can be targeted to the infected tissue area, thus making PDT double selectivity.

To that end it is hoped to conduct a screen of a large library of novel synthetic porphyrins synthesized in the Senge lab for their anti-microbial activity towards an range of bacteria, in particular, the Gram-positive bacteria *Clostridium difficile* as it is felt that this will possess a greater threat in hospitals, nursing homes or similar facilities in coming times.

From the screen, any lead compounds will be taken forward and a number of derivatives will be synthesized in a systematic approach to find a potent photosensitizer for anti-microbial PDT.

One potential bottleneck for the wider application of PDT for clinical infections is the current lack of effective PS with clinical approval for anti-microbial PDT. Potent PSs for cancer PDT have not yet been subjected to costly clinical trials necessary for drug approval. However PDT for periodontal or surfaces use are not subjected to the same rigorous clinical studies and thus could provide a more lucrative option for PDT researchers.

7.2 Future for Molecular Scaffolds

A somewhat overlooked scaffold by the group up until now is the extremely large field of calix[4]arene based derivatives. Seminal work by David Gutsche into the preparation and synthesis of a large variety of calix[4]arenes gave researchers access to a new class of rigid scaffolds that could be functionalized and implemented in a litany of applications. Research by Atwood, Gale, Sessler have seen these scaffold systems used as molecular sensors, gas-storage materials etc.

A potential interesting application for these structurally defined scaffolds would be their use as tunable pores at the end of synthetic anion channels. By functionalizing the upper rim of the calix[4]arene with four porphyrin moieties through metal catalyzed cross-coupling methodology, one could then start elongating the "channel" through methodology developed in Chapter 3. These synthetic tunnels would have a certain degree of terminal flexibility imparted by the calix moiety. Also depending on the functional groups present on the lower room, one can impart selectivity for different anions and thus make a selective molecular anion channel mimic through this methodology.

Chapter 8:

Experimental

8.1 General considerations and instrumentation:

All commercial chemicals used were of analytical grade, were supplied by Sigma Aldrich, Frontier Scientific, Inc. and Tokyo Chemical Industry (TCI) and used without further purification unless otherwise stated. Anhydrous THF and diethyl ether were obtained *via* distillation over sodium/benzophenone and dichloromethane dried was obtained *via* distillation over P_2O_5. ^1H and ^{13}C NMR spectra were recorded on a Bruker DPX 400 (400 MHz for ^1H NMR; 100.6 MHz for ^{13}C NMR), Agilent MR400 (400.13 MHz for ^1H NMR and 100.61 MHz for ^{13}C NMR) and Bruker AV 600 (600 MHz for ^1H NMR; 150.9 MHz for ^{13}C NMR). CHN analysis was attempted for the triptycene project on an Exeter Analytical CE 440 elemental analyzer fitted with a Varian 55B Spectra AA atomic absorption spectrometer. HRMS experiments were measured on a Waters MALDI Q-Tof Premier in positive and negative mode with DCTB (trans-2[3-4-*tert*-butylphenyl)-2-2-methyl-2-propenylidene]malononitril) as the MALDI matrix. ESI mass spectra were acquired in positive and negative modes as required, using a Micromass time of flight mass spectrometer interfaced to a Dionex UltiMate 3000 LC or a Bruker microTOF-Q III spectrometer interfaced to a Dionex UltiMate 3000 LC. Melting points were acquired on a Stuart SMP-10 melting point apparatus and are reported uncorrected. Thin layer chromatography (TLC) was performed on silica gel 60 (fluorescence indicator F_{254};Merck) pre-coated aluminium sheets. Flash chromatography was carried out using Fluka Silica Gel 60 (230-400 mesh) and aluminium oxide (neutral, activated with 6.5 % H_2O, Brockmann Grade III). Photophysical measurements were performed using EtOAc, THF, and CH_2Cl_2 as solvents with UV-vis absorption measurements performed with a Shimadzu MultiSpec-1501 spectrometer.

8.2 Synthesis of porphyrin monomer precursors

Dipyrromethane **38** was synthesized *via* standard procedures and the spectroscopic data corresponded to that reported in the literature [488].

8.2.1 Synthesis of 5,15-disubstituted porphyrins

General Procedure A:

5,15-Disubstituted porphyrins **40-42** [293,295,489] were synthesized in accordance with the literature using condensation reactions. The procedure was adapted from Lindsey and co-workers [243]. Dry CH_2Cl_2 (1800 mL) was placed in a 2 L, three-necked round-bottomed flask, equipped with magnetic stirrer, and argon inlet. The flask was shielded from ambient light. Dipyrromethane **38** (3.3 g, 22.3 mmol) and the corresponding aldehyde (24 mmol) were added. The solvent was purged with a stream of argon for 30 minutes. Trifluoroacetic acid (0.17 mL, 2.3 mmol) was added dropwise to the reaction vessel *via* a syringe. The reaction was allowed to stir

for 18 hours under argon at room temperature. DDQ (11.1 g, 49 mmol) was added and the reaction was allowed to stir for 30 minutes open to the air. Triethylamine (12 mL) was added to quench the excess acid catalyst and the mixture was allowed to stir for 1 hour. The mixture was passed through a large silica plug, using CH_2Cl_2 as eluent. The porphyrin containing fractions were collected and the solvent was removed *in vacuo* to give a purple residue which was recrystallized from CH_2Cl_2:*n*-hexane.

8.2.2. Synthesis of 5,10,15 trisubstituted porphyrins via organolithium methods

General Procedure B:

A 100 mL Schlenk flask containing *p*-bromophenylethyne (0.91 g, 5.0 mmol) was dried under high vacuum and purged with argon. Dry diethyl ether (10 mL) was added to this solution and it was cooled to -70 °C. *n*-BuLi (4 mL of a 2.5 M solution in *n*-hexane, 10 mmol) was added drop-wise to the flask over a period of 1 h. The reaction mixture was then warmed to -40 °C and anhydrous THF (1 mL) was added drop-wise until a white-pink suspension formed. Porphyrin (200 mg, 0.43-0.55 mmol) in dry THF (80 mL) was added rapidly to the vigorously stirred reaction mixture under argon. The reaction was left to stir for 16 h and was allowed warm to rt forming a brown solution. Saturated NH_4Cl (2 mL) was then added and the reaction was stirred for 1 h, with a subsequent color change to bright green. DDQ was added and the solution turned red and was left to stir for a further 1 h. The crude mixture was then filtered through a silica plug using CH_2Cl_2 as eluent. The solvents were removed *in vacuo* and the crude residue was subjected to column chromatography using CH_2Cl_2 : *n*-hexane (1 : 7, v/v) as eluent.

5,10,15-Trisubstituted porphyrins **49-51** were synthesized *via* methods developed by Senge *et al.* using organolithium reagents and spectroscopic data were in accordance to those reported in the literature [130-133].

8.2.3 Metallated porphyrins

General procedure C – Zinc(II) insertion:

Porphyrins **52-54** [301,302] were metallated with zinc(II) according to standard procedures and the spectroscopic data agreed with that in the literature. Adapting a method by Buchler *et al.* [268], porphyrin (1 equiv.) was dissolved in $CHCl_3$ (25 - 50 mL) and stirred at 60 °C for 10 min. $Zinc(OAc)_2.H_2O$ (5 equiv.) in MeOH (1 mL) was added and the reaction heated under reflux for 30 min. Following reaction completion, the solvents were removed *in vacuo* and the residue was redissolved in CH_2Cl_2. This solution was passed through a plug of silica using CH_2Cl_2 as eluent. The solvents were removed *in vacuo* to give a pink/purple solid which was recrystallized from CH_2Cl_2/MeOH.

8.2.4 Functionalization of *m*-THPP scaffold

General procedure D – Monofunctionalization of *m*-THPP:

m-THPP (1 equiv.) was added to a round-bottomed flask (100 mL) and charged with DMF (10 mL) and K_2CO_3 (5 equiv.). The reaction was left to stir for 30 minutes under argon before the appropriate functionalization reagent (2 equiv.) was added. The progress of the reaction was monitored by TLC analysis and once adequate conversion was observed the reaction was terminated through the addition of CH_2Cl_2 (50 mL). The crude reaction mixture was washed with distilled water (1 × 30 mL), sat. aq. $NaHCO_3$ (1 × 30 mL), brine (1 × 30 mL), and distilled water (2 × 30 mL). The organic phase was dried over anhydrous sodium sulfate, filtered and evaporated under reduced pressure. Crude products were typically purified by column chromatography on silica gel using CH_2Cl_2/*n*-hexane/MeOH (3:1:0.2, v/v/v) with the second last fraction being collected and recrystallized from ethyl acetate/*n*-hexane to give the monofunctionalized product.

5,10,15-Tris(3-hydroxyphenyl)-20-[3-(prop-2-yn-1-yloxy)phenyl]porphyrin 64:

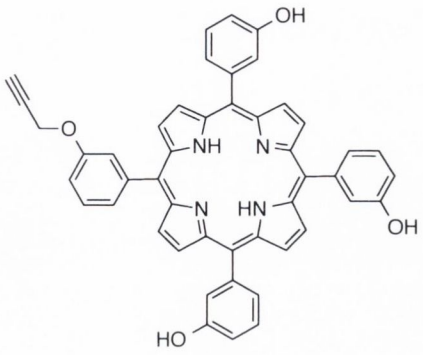

Compound **64** was synthesized *via* general procedure D, using a 50 mL round-bottom flask containing 10 mL of DMF (10 mL), **2** (400 mg, 0.59 mmol), K_2CO_3 (244 mg, 1.8 mmol) and propargyl bromide **63** (214 mg, 1.8 mmol) and was allowed to stir for 2 h. The reaction mixture was diluted with CH_2Cl_2 and washed with water (4 x 100 mL) to remove residual DMF. The solvent was removed *in vacuo* and the product purified by flash chromatography to yield 203 mg of a purple solid **64** (0.28 mmol, 48 %). Analytical data: M.p.: >300 °C; R_f = 0.31 (CH_2Cl_2/*n*-hexane/MeOH =3:1:0.2, v/v/v); ^{1}H NMR (400 MHz, [$(CD_3)_2SO$]): δ_H = -2.74 (br s, 2H, -N*H*), 2.63 (s, 1H, alkyne-*H*), 5.47 (s, 2H, CH_2), 7.51 (m, 4H, -Ar*H*), 7.53 (m, 10H, -Ar*H*), 7.62 (s, 1H, -Ar*H*), 7.68 (s, 1H, -Ar*H*), 8.72 (d, $^3J_{H-H}$ = 4 Hz, 2H, -H_β), 8.76 ppm (d, $^3J_{H-H}$ = 4 Hz, 6H, -H_β); ^{13}C NMR (100 MHz, [$(CD_3)_2SO$]): δ_C = 20.9, 55.9, 60.2, 115.5, 120.4, 122.3, 126.2, 128.3, 129.2, 131.7, 139.8, 141.5, 143.3, 142.9, 156.9, 157.2 ppm; UV/vis (CH_2Cl_2) λ_{max} (log ε): 419 (5.47), 512 (4.03), 546 (3.04), 590 (2.11), 647 nm (1.37); HRMS (MALDI) calcd for $[M]^+$ $C_{47}H_{32}N_4O_4$ 717.2502, found 717.2509.

[5,10,15-Tris(3-hydroxyphenyl)-20-[3-(phenoxy)phenyl]porphyrinato]zinc(II) 65:

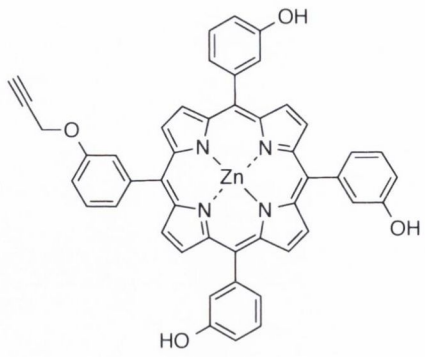

Compound **65** was synthesized according to the following procedure general procedure C: To a 100 mL Erlenmeyer flask DMF (10 mL) was placed **2** (100 mg, 0.14 mmol) and Zinc(OAc)$_2$.H$_2$O (91 mg, 0.4 mmol). The flask was placed in the microwave and the reaction was run in 3 x 1 min intervals at 300 W with allocated time for cooling of the reaction mixture during each interval. The reaction mixture was diluted with CH_2Cl_2 and washed with water (3 x 100 mL) to remove residual DMF. The solvent was removed *in vacuo* and the product purified by recrystallization from EtOAc:*n*-hexane to yield 111 mg of purple crystals of **65** (0.14 mmol, 98 %). Analytical data: M.p: >300 °C; R_f = 0.35 (CH_2Cl_2/*n*-hexane/MeOH =3:1:0.2, v/v/v); ^{1}H NMR (400 MHz, [$(CD_3)_2SO$]): δ_H = 2.63 (s, 1H alkyne-*H*), 5.47 (s, 2H, CH_2), 7.51 (m, 4H, -Ar*H*), 7.53 (m, 10H, -Ar*H*), 7.62 (s, 1H, -Ar*H*), 7.68 (s, 1H, -Ar*H*), 8.72 (d, $^3J_{H-H}$ = 4 Hz, 2H, -H_β), 8.76 ppm (d, $^3J_{H-H}$ = 4.0 Hz, 6H, -H_β); ^{13}C NMR (100 MHz, [$(CD_3)_2SO$]): δ_C = 21.0, 55.9, 60.2, 115.5, 120.4, 122.3, 126.2, 128.3, 129.2, 131.7, 139.8, 141.5, 143.3, 142.9, 156.9, 157.2 ppm; UV/vis (CH_2Cl_2) λ_{max} (lg ε): 421(6.83), 553 (5.40), 593 nm (4.78) HRMS (MALDI) calcd for $[M]^+$ $C_{47}H_{30}N_4O_4Zn$ 778.1578, found 778.1559.

5,10,15-Tris(3-hydroxyphenyl)-20-[3-(prop-2-yn-1-yloxy)phenyl]chlorin 69:

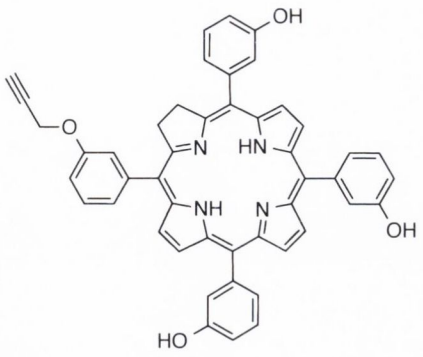

Compound **69** was synthesized using general procedure D: using a 50 mL round bottom flask containing 10 mL of DMF (10 mL), **3** (400 mg, 0.59 mmol), K_2CO_3 (244 mg, 1.8 mmol) and propargyl bromide **63** (214 mg, 1.8 mmol) and was allowed to stir for 2 h. The reaction mixture was taken up into CH_2Cl_2 and washed with water (4 x 100 mL) to remove residual DMF. The solvent was removed *in vacuo* and the crude product was purified by column chromatography on silica gel using CH_2Cl_2/*n*-hexane/MeOH (3:1:0.2, v/v/v) to yield 193 mg of a purple solid **64** (0.29 mmol, 45 %). Analytical data: M.p: >300 °C; R_f = 0.29 (CH_2Cl_2/*n*-hexane/MeOH =3:1:0.2, v/v/v); ^{1}H NMR (400 MHz, [$(CD_3)_2SO$]): δ_H = -2.75 (br s, 2H, -N*H*), 2.63 (s, 1H, alkyne-*H*), 4.13 (s, 4H, -H_β), 5.47 (s, 2H, -CH_2), 7.51 (m, 4H, -Ar*H*), 7.53 (m, 10H, -Ar*H*), 7.62 (s, 1H, -Ar*H*), 7.68 (s, 1H, -Ar*H*), 8.72 (d, $^3J_{H-H}$ = 4 Hz, 2H, -H_β), 8.76 ppm (d, $^3J_{H-H}$ = 4 Hz, 4H, -H_β); ^{13}C NMR (100 MHz, [$(CD_3)_2SO$]): δ_C = 14.1, 20.9, 35.4, 56.0, 60.2, 115.5, 120.4, 122.3, 126.2, 128.3, 129.2, 131.7, 139.8, 141.5, 142.9, 143.3, 156.9, 157.2 ppm; UV/vis (CH_2Cl_2) λ_{max} (lg ε): 418 (5.51), 517 (4.05), 543 (3.04), 599 (2.07), 652 nm (3.08); HRMS (MALDI) calcd for $[M]^+$ $C_{47}H_{34}N_4O_4$ 719.2659, found 719.2658.

[5,10,15-Tris(3-hydroxyphenyl)-20-[3-(phenoxy)phenyl]chlorinato]zinc(II) 70:

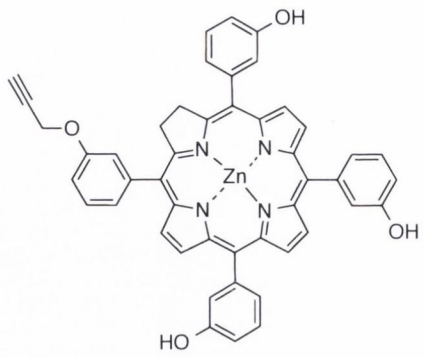

Compound **70** was synthesized using general procedure C: To a 100 mL Erlenmeyer flask containing 10 mL of DMF was placed **3** (100 mg, 0.148 mmol) and Zinc(OAc)$_2$.H$_2$O (91 mg, 0.4 mmol). The flask was placed in the microwave and the reaction was run in 3 x 1 min intervals at 300 W with allocated time for cooling of the reaction mixture during each interval. The reaction mixture was taken up into DCM and washed with water (3 x 100 mL) to remove residual DMF. The solvent was removed *in vacuo* and the product was purified through recrystallization with EtOAc:*n*-hexane to yield 109 mg of purple crystals (0.14 mmol, 97%). Analytical data: M.p: >300 °C; R_f = 0.32 (CH_2Cl_2/*n*-hexane/MeOH =3:1:0.2, v/v/v); ^{1}H NMR (400 MHz, [$(CD_3)_2SO$]): δ_H = 2.63 (1H, s, alkyne-*H*), 4.14 (s, 4H, -H_β), 5.47 (s, 2H, -CH_2), 7.51 (m, 4H, -Ar*H*), 7.53 (m, 10H, -Ar*H*), 7.62 (s, 1H, -Ar*H*), 7.68 (s, 1H, -Ar*H*), 8.72 (d, $^3J_{H\text{-}H}$ = 4 Hz, 2H, -H_β), 8.76 ppm (d, $^3J_{H\text{-}H}$ = 4 Hz, 4H, -H_β); ^{13}C NMR (100 MHz, [$(CD_3)_2SO$]): δ_C = 14.1, 20.9, 56.0, 60.2, 115.5, 120.4, 122.3, 126.2, 128.3, 129.2, 131.7, 139.8, 141.5, 143.3, 142.9, 156.9, 157.2 ppm; UV/vis (CH_2Cl_2) λ_{max} (lg ε): 419 (5.47), 512 (4.03), 546 (3.04), 590 (2.11), 647 nm (1.37); HRMS (MALDI) calcd for $[M]^+$ $C_{47}H_{32}N_4O_4Zn$ 780.1715, found 780.1716.

8.2.5 Modified Huisgen cycloaddiotion to yield bile acid conjugates

Bile Conjugate 66:

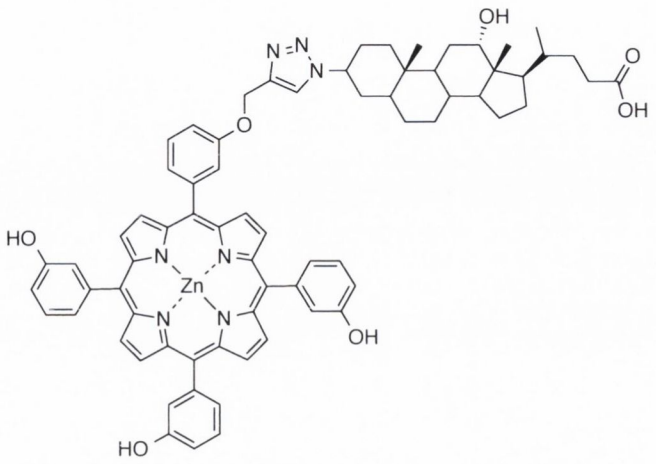

Compound **66** was synthesized using the following procedure: To a 5 mL Pyrex microwave vessel, **65** (14 mg, 0.018 mmol), **35** (16 mg, 0.041 mmol), $Cu(MeCN)_4PF_6$ (20%, 2 mg, 0.0054 mmol) were added to the flask containing toluene (0.6 mL) and MeOH (0.6 mL). The reaction mixture was heated to 125 °C for 25 min under microwave irradiation. The solvents were removed *in vacuo*, and the crude product was purified by column chromatography on silica gel using CH_2Cl_2/*n*-hexane/MeOH (3:1:0.2, v/v/v) Subsequent recrystallization from EtOAc:*n*-hexane yielded 15.4 mg of a purple solid **66** (0.0129 mmol, 63%). Analytical data: M.p: >300 °C; R_f = 0.35 (CH_2Cl_2/*n*-hexane/MeOH =3:1:0.2, v/v/v); ^{1}H NMR (400 MHz, [$(CD_3)_2SO$]): δ_H = 0.88 (m, 9H, -CH_3), 1.79-1.09 (m, 29H, bile acid -*H*), 2.34 (m, 2H, -CH_2), 5.47 (s, 2H, -CH_2), 7.52 (m, 4H, -Ar*H*), 7.53 (m, 10H, -Ar*H*), 7.62 (s, 1H, -Ar*H*), 7.69 (s, 1H, -Ar*H*), 8.29 (s, 1H, triazole-*H*), 8.71 (d, $^3J_{H\text{-}H}$ =4Hz, 2H, -H_β), 8.77 ppm (d, $^3J_{H\text{-}H}$ = 4Hz, 6H, -H_β); ^{13}C NMR (100 MHz, $CDCl_3$): δ_C = 12.9, 17.4, 23.8, 23.9, 24.5, 26.2, 26.6, 27.5, 29.1, 30.1, 30.9, 31.2, 31.3, 32.8, 34.6, 35.4, 35.8, 37.5, 46.5, 46.6, 47.9, 58.7, 71.5, 115.5, 121.3 (triazole), 120.4, 122.3, 126.2, 128.3, 129.2, 131.7, 139.8, 141.5, 142.9, 143.4, 156.9, 157.1, 175.4 ppm (C=O, 24-C); UV/Vis (CH_2Cl_2) λ_{max} (lg ε): 421 (6.83), 553 (5.40), 593 nm (4.78); HRMS (MALDI) calcd. for $[M]^+$ $C_{71}H_{69}N_7O_6Zn$ 1194.4601, found 1194.4624.

Bile conjugate 67:

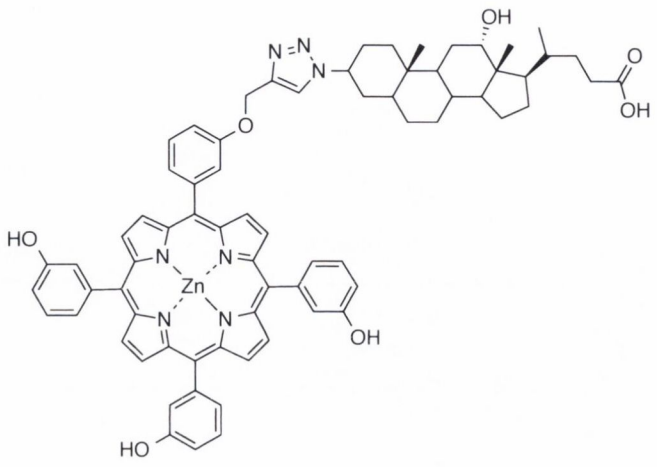

Compound **67** was synthesized using the following procedure: To a 5 mL Pyrex microwave vessel, **65** (14 mg, 0.018 mmol), **37** (16 mg, 0.041 mmol), $Cu(MeCN)_4PF_6$ (20 %, 2 mg, 0.0054 mmol) were added to the flask containing toluene (0.6 mL) and MeOH (0.6 mL). The reaction mixture was heated to 125 °C for 25 min under microwave irradiation. The solvents were removed *in vacuo*, and the crude product was purified by column chromatography on silica gel using CH_2Cl_2/*n*-hexane/MeOH (3:1:0.2, v/v/v). Subsequent recrystallization from EtOAc:*n*-hexane yielded 15.7 mg of a purple solid (0.0131 mmol, 65 %). Analytical data: M.p: >300 °C; R_f = 0.35 (CH_2Cl_2/*n*-hexane/MeOH =3:1:0.2, v/v/v); ^{1}H NMR (400 MHz, $(CD_3)_2SO_2$): δ_H = 0.88 (9H, m, -C*H*$_3$), 1.79-1.09 (m, 29H, bile acid -*H*), 2.34 (m, 2H, -C*H*$_2$), 5.47 (s, 2H, -C*H*$_2$), 7.52 (m, 4H, -Ar*H*), 7.53 (m, 10H, -Ar*H*), 7.62 (s, 1H, -Ar*H*), 7.69 (s, 1H, -Ar*H*), 8.28 (s, 1H, triazole-*H*), 8.71 (d, $^3J_{H\text{-}H}$ =4 Hz, 2H, -H_β), 8.77 ppm (d, $^3J_{H\text{-}H}$ = 4 Hz, 6H, -H_β); ^{13}C NMR (100 MHz, $CDCl_3$): δ_C = 12.9, 17.4, 23.8, 23.9, 24.5, 26.2, 26.6, 27.5, 29.1, 30.1, 30.9, 31.2, 31.3, 32.8, 34.6, 35.4, 35.8, 37.5, 46.5, 46.6, 47.9, 58.7, 71.5, 115.5, 121.0 (triazole), 120.4, 122.3, 126.2, 128.3, 129.2, 131.7, 139.8, 141.5, 143.4, 142.9 156.9, 157.1, 175.4 ppm (C=O, 24-C); UV/Vis (CH_2Cl_2) λ_{max} (lg ε): 421 (6.83), 553 (5.40), 593 nm (4.78); HRMS (MALDI) calcd. for $[M]^+$ $C_{71}H_{69}N_7O_6Zn$ 1197.4706, found 1197.4666.

Bile Conjugate 68:

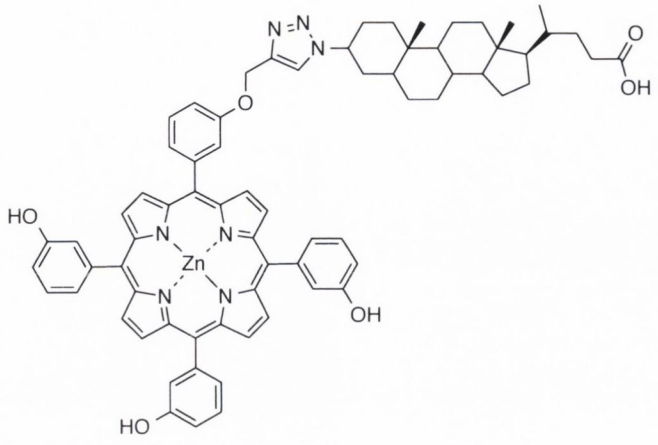

Compound **68** was synthesized using the following procedure: To a 5 mL Pyrex microwave vessel, **65** (14 mg, 0.018 mmol), **38** (15 mg, 0.041 mmol), $Cu(MeCN)_4PF_6$ (20%, 2 mg, 0.0054 mmol) were added to the flask containing toluene (0.6 mL) and MeOH (0.6 mL). The reaction mixture was heated to 125 °C for 25 min under microwave irradiation. The solvents were removed *in vacuo*, and the product was purified by column chromatography on silica gel using (CH_2Cl_2/*n*-hexane/MeOH =3:1:0.2, v/v/v). Subsequent recrystallization from EtOAc:*n*-hexane yielded 13.3 mg of a purple solid (0.011 mmol, 63%). Analytical data: M.p: >300 °C; R_f = 0.32 (CH_2Cl_2/*n*-hexane/MeOH =3:1:0.2, v/v/v); ^{1}H NMR (400 MHz, $(CD_3)_2SO_2$): δ_H = 0.87 (m, 9H -C*H*$_3$), 1.79-1.09 (m, 29H bile acid -*H*), 2.34 (m, 2H, -C*H*$_2$), 5.47 (s, 2H, C*H*$_2$), 7.52 (m, 4H, -Ar*H*), 7.53 (m, 10H, -Ar*H*), 7.62 (s, 1H, -Ar*H*), 7.69 (s, 1H, -Ar*H*), 8.29 (s, 1H, triazole-*H*), 8.71 (d, $^3J_{H\text{-}H}$ = 4 Hz, 2H, -H_β), 8.77 ppm (d, $^3J_{H\text{-}H}$ = 4 Hz, 6H, -H_β); ^{13}C NMR (100 MHz, $CDCl_3$): δ_C = 12.9, 17.4, 23.8, 23.9, 24.5, 26.2, 26.6, 27.5, 29.1, 30.1, 30.9, 31.2, 31.3, 32.8, 34.6, 35.4, 35.8, 37.5, 46.5, 46.6, 47.9, 58.7, 71.5, 112.1, 114.7, 114.9, 119.2, 121.0 (triazole), 121.9, 123.0, 124.9, 127.8, 128.0, 129.2, 131.7, 139.8, 142.4, 143.4, 151.5, 155.8, 156.9, 167.6, 174.3 (C=O, 24-C) ppm; UV/Vis (CH_2Cl_2) λ_{max} (lg ε): 421 (6.80), 5.53 (4.92), 593 nm (4.39); HRMS (MALDI) calcd for $[M]^+$ $C_{71}H_{69}N_7O_7Zn$ 1195.4550, found 1195.4514.

Bile Conjugate 71:

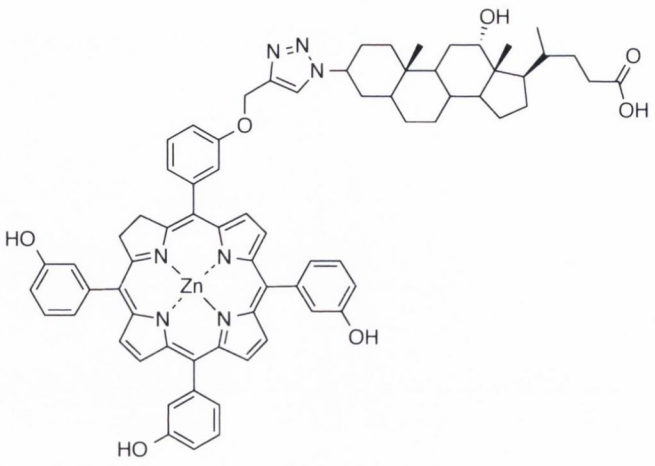

Compound **71** was synthesized in the optimum yield using the following procedure: To a 5 mL Pyrex microwave vessel, **70** (14 mg, 0.018 mmol), **36** (15 mg, 0.041 mmol), $Cu(MeCN)_4PF_6$ (20%, 2 mg, 0.0054 mmol) were added to the flask containing toluene (0.6 mL) and MeOH (0.6 mL). The reaction mixture was heated to 125 °C for 25 min under microwave irradiation. The solvents were removed *in vacuo*, and the crude product was purified by column chromatography on silica gel using CH_2Cl_2/*n*-hexane/MeOH (3:1:0.2, v/v/v) Subsequent recrystallization from EtOAc:*n*-hexane yielded 14.7 mg of a purple solid (0.0123 mmol, 61%). Analytical data: M.p: >300 °C; R_f = 0.34 (CH_2Cl_2/*n*-hexane/MeOH =3:1:0.2, v/v/v) ^{1}H NMR (400 MHz, $(CD_3)_2SO_2$): δ_H = 0.90 (m, 9H, -C*H*$_3$), 1.81-1.09 (m, 29H, bile acid -*H*), 1.81-1.09 (m, 29H, bile acid -*H*), 2.34 (2H, m, -C*H*$_2$), 4.16(s, 4H, -*H*$_\beta$), 5.47 (s, 2H, -C*H*$_2$), 7.52 (m, 4H, -Ar*H*), 7.54 (m, 10H, -Ar*H*), 7.66 (s, 1H, -Ar*H*), 7.79 (s, 1H, -Ar*H*), 8.29 (s, 1H, triazole-*H*), 8.74 (d, $^3J_{H\text{-}H}$ =5Hz, 1H, -*H*$_\beta$), 8.75 (d, $^3J_{H\text{-}H}$ =5.0 Hz, 1H, -*H*$_\beta$), 8.79 (d, $^3J_{H\text{-}H}$ =5.0 Hz, 4H, -*H*$_\beta$) ppm; ^{13}C NMR (100 MHz, $CDCl_3$): δ_C = 12.9, 17.5, 23.7, 23.8, 24.5, 26.3, 26.6, 27.4, 29.2, 30.1, 30.8, 31.2, 31.3, 32.8, 34.6, 35.4, 35.8, 37.5, 46.5, 46.6, 47.9, 58.7, 71.5, 112.1, 114.7, 114.8, 119.2, 121.0 (triazole), 121.9, 122.9, 124.9, 127.8, 128.1, 129.2, 131.7, 139.8, 142.4, 143.4, 151.5, 155.8, 156.9, 167.6, 175.2 (C=O, 24-C) ppm; UV/Vis (CH_2Cl_2) λ_{max} (lg ε): 423 (6.70), 524 (5.33), 609 nm (4.71); HRMS (MALDI) calcd for $[M]^+$ $C_{71}H_{71}N_7O_7Zn$ 1195.4550, found 1195.4514.

8.2.6 Procedures for Biological evaluation of Photosensitizers

Cell cultures and cell proliferation assay (MTS): Cell lines were seeded at a concentration of 8 × 10^4 cells per mL into sterile 96-well plates, and left to attach overnight and treated. To previously prepared 96-well assay plates containing cells in 100 μL of culture medium, the test compounds at different concentrations and appropriate controls were added. After incubation for 24 h the medium was removed and changed for fresh medium, dark controls were left in the dark for a further 24 h. To assess the phototoxicity, the rest of the plates were illuminated for 2 min and incubated for 24 h. Finally, 20 μL of MTS dye solution was added to each well of the dark controls and illuminated plates and these were incubated for 3 h and the absorbance was recorded at 470 nm using a 96-well plate reader. Cell lines were seeded at a concentration of 3 × 10^4 cells per mL into sterile 96-well plates leaving them for 24 h to attach. For imaging experiments, the cell culture medium was removed, replaced with freshly prepared solutions of the porphyrins **66, 67, 68,** and **71** of various concentrations in the medium and incubated at 37 °C under 5 % CO_2 for 24 h. After that the medium was removed and fixed with 4 % PFA in medium and then washed with PBS. Fluorescent images were collected and analyzed by high content screening and imaging technique (IN Cell 1000 instrument, GE Healthcare) [490].

Biological evaluation: Intracellular screening for the compounds **66, 67, 68,** and **71** were carried out in OE33 and SKGT-4 cell lines. Stock solutions of the bile acid porphyrins **66, 67, 68,** and **71** (0.5 mM) were prepared in ethanol. Intracellular experiments were carried out by high-content screening using an IN Cell 1000 apparatus and *in vitro* images were taken at different concentrations 10 μM to 50 μM. Living cells were incubated first with the materials **66, 67, 68,** and **71** for 24 h in the dark and then fixed. Next, fixed adenocarcinoma cells were co-stained using nuclear dye Hoechst 33342 (1 μg/mL) and the bicyclic peptide phalloidin 490 (1:500 in 100 μL) as cytoskeleton stain (F-actin). The images were collected using three independent channels for Hoechst, Phalloidin and the compounds **66, 67, 68,** and **71** with excitation/emission filters of 345 nm/435 nm (blue), 475 nm/535 nm (green) and 620 nm/700 nm (red), respectively.

8.3 m-THPP Functionalization

8.3.1 General methods:

General Procedure E – Microwave assisted synthesis of *m*-THPP **2**:

Propionic acid (3.5 mL) and nitrobenzene (1.5 mL) were added to a Pyrex Erlenmeyer flask (100 mL). Pyrrole (0.74 mL) and 3-hydroxybenzaldehyde (1 mL) were added and the reaction vessel was sealed with hydrophilic cotton wool in order to prevent spillages and, most importantly, to avoid pressure build-ups associated with hazardous explosion risks. The yellowish reaction mixture was placed at the center of the rotating plate in the microwave oven and heated for 5 min (1 min periods intercalated by 3 min intervals with the power off to avoid overheating) at 640 W. The reaction was monitored over time by UV-vis absorption spectroscopy. The cooled crude reaction mixture was washed with MeOH and filtered. The liquid extract was evaporated under reduced pressure and the resulting residue was taken into ethyl acetate. Purification was achieved through flash chromatography packed with silica gel and eluted with ethyl acetate/CH_2Cl_2 = 1:1 (v/v). The red fraction was collected and recrystallized from ethyl acetate/*n*-hexane, yielding **2** in 22 % yield.

General Procedure F – Di-, tri- and tetrafunctionalization of *m*-THPP:

m-THPP (1 equiv.) was added to a round bottomed flask (100 mL) and charged with DMF (10 mL) and K_2CO_3 (5-20 equiv.). The reaction mixture was left to stir for 30 mins under argon before the appropriate functionalization reagent (10-20 equiv.) was added. The reaction mixture was monitored by TLC analysis and once adequate conversion to the desired degree of substitution was observed the reaction was terminated through the addition of CH_2Cl_2 (50 mL). The work-up proceeded as per general procedure D, with the product being recrystallized from ethyl acetate/*n*-hexane.

General Procedure G – Chan-Lam couplings of *m*-THPP:

m-THPP (1 equiv.) was added to a round-bottomed flask (100 mL) and charged with dioxane (10 mL), Cu(II)OAc_2 (2 equiv.), boronic acid (2 equiv.) and pyridine (0.2 mL). The reaction mixture was monitored by TLC and once full conversion to the desired degree of substitution was observed the reaction was terminated through the addition of CH_2Cl_2 (50 mL). The work-up proceeded as per general procedure D, with column chromatography on silica gel using CH_2Cl_2/*n*-hexane/MeOH (3:1:0.2, v/v/v) and recrystallization from ethyl acetate/*n*-hexane.

5,10,15,20-Tetrakis[3-(prop-2-yn-1-yloxy)phenyl]porphyrin 75:

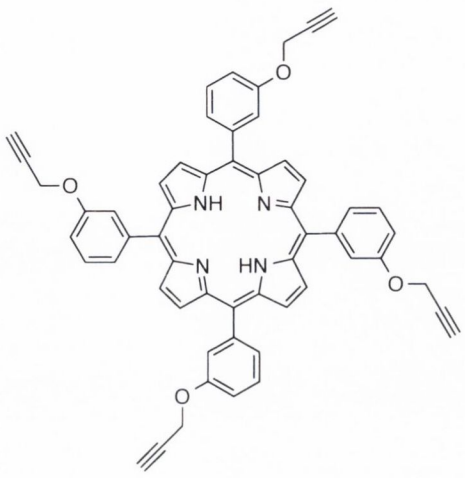

The title compound **75** was synthesized using general procedure F: a 50 mL round bottom flask containing DMF (10 mL), **2** (400 mg, 0.59 mmol), K_2CO_3 (815 mg, 5.9 mmol) and propargyl bromide **63** (0.45 mL, 5.9 mmol) and was allowed stir for 5 h. The reaction mixture was monitored by TLC analysis and once adequate conversion was observed the reaction was terminated through the addition of CH_2Cl_2 (50 mL). The crude reaction mixture was washed with distilled water (1 × 30 mL), sat. aq. $NaHCO_3$ (1 × 30 mL), brine (1 × 30 mL), and distilled water (2 × 30 mL). The organic phase was dried over anhydrous sodium sulfate, filtered and the solvent was evaporated under reduced pressure. The crude product was purified by column chromatography on silica gel using CH_2Cl_2/*n*-hexane/MeOH (3:1:0.2, v/v/v) and recrystallization from ethyl acetate/*n*-hexane yielded 451 mg of purple crystals **75** (0.5 mmol, 92 %). M.p. > 300 °C; R_f = 0.88 (CH_2Cl_2/*n*-hexane/MeOH =3:1:0.2, v/v/v); ^{1}H NM$_R$ (400 MHz, $CDCl_3$): δ_H = -2.82 (s, br, 2H, -N*H*), 2.57 (s, 4H, alkyne-*H*), 4.87 (s, 8H, -C$H_{2)}$, 7.40 (d, $^3J_{H\text{-}H}$ = 7.8 Hz, 4H, -Ar*H*), 7.65 (t, $^3J_{H\text{-}H}$ = 7.8 Hz, 4H, *m*-Ar*H*), 7.8 (m, 8H, -Ar*H*), 8.88 ppm (s, 8H, -H_β); ^{13}C NMR (100 MHz, $CDCl_3$, 25 °C): δ_H = 56.1, 75.9, 78.6, 114.6, 119.6, 119.7, 121.4, 125.6, 127.6, 128.6, 133.8, 143.5, 143.51, 155.9, 157.2 ppm; UV/Vis (EtOAc): λ_{max} (lg ε) = 419 (5.47), 512 (4.03), 546 (3.04), 590 (2.10), 646 nm (1.35); HRMS (MALDI) calcd. for [$C_{56}H_{38}N_4O_4$] [M$^+$] 830.2893, found 830.2896.

5-[(4-Benzyloxy)10,15,20-tris(3-hydroxyphenyl)]porphyrin 78a:

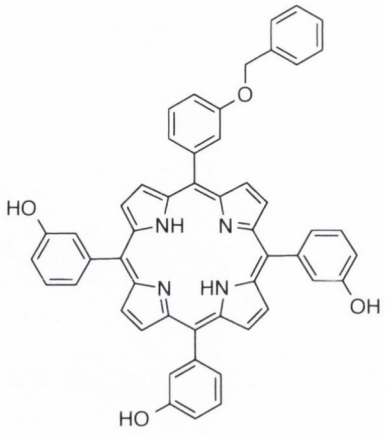

Synthesized *via* general procedure D using **2** (400 mg, 0.59 mmol), NaH (14.2 mg, 0.59 mmol), and benzyl chloride **76** (0.067 mL, 0.59 mmol). The reaction was complete after 2.5 h and the crude product was purified by column chromatography on silica gel using CH_2Cl_2/*n*-hexane/MeOH (3:1:0.2, v/v/v). Recrystallization from ethyl acetate/*n*-hexane yielded 199 mg of purple crystals (0.23 mmol, 44%). M.p. >300 °C; R_f = 0.38 (CH_2Cl_2/*n*-hexane/MeOH = 3:1:0.2, v/v/v); ^{1}H NMR [400 MHz, $(CD_3)_2SO$)]: δ_H = -2.99 (s, 2H, -N*H*), 5.29 (s, 2H, -CH_2), 7.23 (d, $^3J_{H\text{-}H}$ = 7.4 Hz, 3H, -Ar*H*), 7.33 (d, $^3J_{H\text{-}H}$ = 7.4 Hz, 1H, -Ar*H*), 7.39 (t, $^3J_{H\text{-}H}$ = 7.4 Hz, 3H, -Ar*H*), 7.52 (d, $^3J_{H\text{-}H}$ = 7.4 Hz, 3H, -Ar*H*), 7.59 (m, 9H, -Ar*H*), 7.69 (m, 1H, -Ar*H*), 7.87 (s, 1H, -Ar*H*), 8.82 (d, $^3J_{H\text{-}H}$ = 4.8 Hz, 2H, -H_β), 8.82 (d, $^3J_{H\text{-}H}$ = 4.8 Hz, 6H, -H_β), 9.88 (s, 3H, -O*H*); ^{13}C NMR (150 MHz, $CDCl_3$): δ_C = 69.9, 115.5, 119.9, 120.4, 120.4, 122.3, 122.4, 126.2, 128.3, 128.9, 130.9, 137.5, 142.8, 142.9, 156.2, 157.3 ppm; UV/Vis (EtOAc): λ_{max} (lg ε) = 417 (5.41), 514 (4.08), 547 (3.69), 591 (3.59), 648 nm (3.48); HRMS (MALDI) *m/z* calcd for [$C_{51}H_{36}N_4O_4$] [M+]: 768.2737, found 768.2740.

5,10,15,20-Tetrakis[(3-benzyloxy)phenyl]porphyrin 78b:

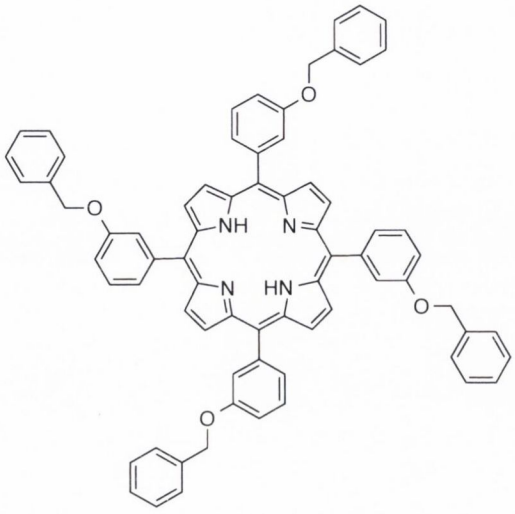

Synthesized *via* general procedure F using **2** (400 mg, 0.59 mmol), K_2CO_3 (815 mg, 5.9 mmol), and 4-benzylchloride **76** (0.68 mL, 5.9 mmol). The reaction was complete after 13 h. Subsequent recrystallization from ethyl acetate/*n*-hexane produced 582 mg of purple crystals (0.56 mmol, 95 %). M.p. >300 °C; R_f = 0.95 (CH_2Cl_2/*n*-hexane/MeOH = 3:1:0.2, v/v/v); ^{1}H NMR (400 MHz, $CDCl_3$): δ_H = -2.60 (s, 2H, -N*H*), 5.32 (s, 8H, -CH_2), 7.41 (m, 4H, Ar-*H*), 7.48 (t, $^3J_{H\text{-}H}$ = 7.1 Hz, 12H, -Ar*H*), 7.59 (d, $^3J_{H\text{-}H}$ = 7.6 Hz, 8H, -Ar*H*), 7.74 (t, $^3J_{H\text{-}H}$ = 7.6 Hz, 4H, -Ar*H*), 7.98 (d, $^3J_{H\text{-}H}$ = 7.6 Hz, 4H, -Ar*H*), 8.03 (s, 4H, -Ar*H*), 9.02 ppm (m, 8H, -H_β); ^{13}C NMR (100 MHz, $CDCl_3$): δ_C = 70.3, 114.6, 119.9, 121.6, 127.6, 127.7, 128.1, 128.6, 128.7, 128.8, 137.0, 143.5, 157.2 ppm; UV/Vis (EtOAc): λ_{max} (lg ε) = 417 (5.02), 515 (3.76), 547 (3.50), 590 (3.15), 647 nm (2.97); HRMS (MALDI) *m/z* calcd for [$C_{72}H_{54}N_4O_4$] [M^+]: 1038.4145, found 1038.4140.

5,10,15-Tris(3-hydroxyphenyl)-20-[(propoxy)phenyl]porphyrin 79a:

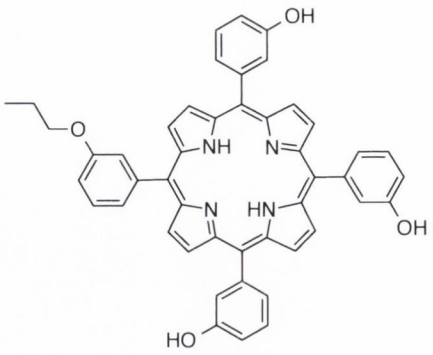

Synthesized *via* general procedure D using **2** (400 mg, 0.59 mmol), NaH (14.2 mg, 0.59 mmol), and 1-iodopropane **77** (0.12 mL, 1.2 mmol). The reaction was complete after 2 h. The crude product was purified by column chromatography on silica gel using CH_2Cl_2/*n*-hexane/MeOH (3:1:0.2, v/v/v) and recrystallization from ethyl acetate/*n*-hexane yielded 149 mg of purple crystals (0.32 mmol, 35%). M.p. >300 °C; R_f = 0.38 (CH_2Cl_2/*n*-hexane/MeOH = 3:1:0.2, v/v/v); ^{1}H NMR (400 MHz, $CDCl_3$): δ_H = -2.88 (s, br, 2H, -N*H*), 0.87 (t, $^3J_{H\text{-}H}$ = 7.3 Hz, 3H, -CH_3), 1.87, (q, $^3J_{H\text{-}H}$ = 7.3 Hz, 2H, -CH_2), 4.08 (t, $^3J_{H\text{-}H}$ = 7.3 Hz, 2H, O-CH_2), 7.17 (t, $^3J_{H\text{-}H}$ = 6.7 Hz, 3H, -Ar*H*), 7.29 (d, $^3J_{H\text{-}H}$ = 6.7 Hz, 1H, -Ar*H*), 7.47 (t, $^3J_{H\text{-}H}$ = 6.7 Hz, 3H, -Ar*H*), 7.61 (m, 7H, -Ar*H*), 7.75 (m, 2H, -Ar*H*), 8.79 (m, 2H, -H_β) 8.85 ppm (m, 6H, -H_β); ^{13}C NMR (100 MHz, [$(CD_3)_2SO$]): δ_H = 31.6, 36.6, 69.7, 114.8, 119.7, 122.0, 127.1, 127.5, 126.2, 127.5, 154.6, 157.4, 162.7 ppm; UV/Vis (EtOAc): λ_{max} (lg ε) = 417 (5.02), 515 (3.76), 547 (3.50), 590 (3.13), 647 nm (2.95); HRMS (MALDI): *m/z* calcd for [$C_{47}H_{36}N_4O_4$] [M^+]: 720.2737, found 720.2734.

5,10,15,20-Tetra[(propoxy)phenyl]porphyrin 79b:

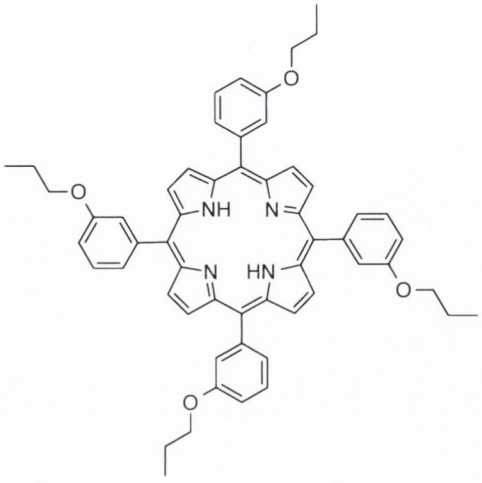

Synthesized *via* general procedure F using **2** (400 mg, 0.59 mmol), K_2CO_3 (815 mg, 5.9 mmol), and 1-iodopropane **77** (0.6 mL, 5.9 mmol). The reaction was complete after 13 h. Recrystallization from ethyl acetate/*n*-hexane produced 484 mg of purple crystals (0.57 mmol, 95%). M.p. >300 °C; R_f = 0.95 (CH_2Cl_2/*n*-hexane/MeOH = 3:1:0.2, v/v/v); ^{1}H NMR (400 MHz, $CDCl_3$): δ_H = -2.77 (s, 2H, -N*H*), 1.10 (t, $^3J_{H-H}$ = 7.4 Hz, 12H, -CH_3), 1.91 (q, $^3J_{H-H}$ = 7.4Hz, 8H, -CH_2), 4.13 (t, $^3J_{H-H}$ = 6.5 Hz, 8H, -OCH_2), 7.35 (m, 4H, -Ar*H*), 7.64 (t, $^3J_{H-H}$ = 7.5 Hz, 4H, *m*-Ar*H*), 7.80 (m, 8H, -Ar*H*), 8.92 ppm (m, 8H, -H_β); ^{13}C NMR (100 MHz, $CDCl_3$): δ_C = 22.7, 29.7, 69.7, 114.2, 119.9, 121.0, 127.4, 127.5, 143.4, 157.5 ppm; UV/Vis (EtOAc): λ_{max} (lg ε) = 418 (5.04), 515 (3.75), 547 (3.53), 590 (3.13), 647 nm (2.99); HRMS (MALDI) *m/z* calcd for [$C_{56}H_{54}N_4O_4$] [M^+]: 846.4145, found 846.4141.

5-[3-(4-Bromobenzyloxy)phenyl]-10,15,20-tris(3-hydroxyphenyl)porphyrin 82a:

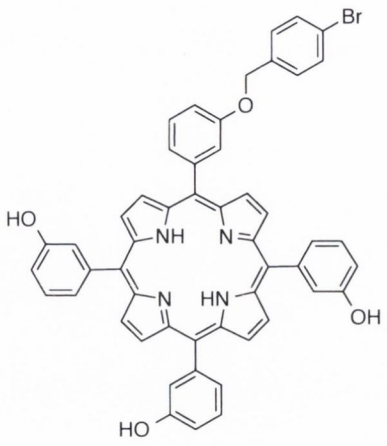

Synthesized *via* general procedure D using **2** (400 mg, 0.59 mmol), NaH (14.2 mg, 0.59 mmol), and *p*-bromobenzyl bromide, **80** (292 mg, 1.2 mmol). The reaction was complete after 2 h with subsequent column chromatography on silica gel using CH_2Cl_2/*n*-hexane/MeOH (3:1:0.2) and recrystallization from ethyl acetate/*n*-hexane yielded 215 mg of purple crystals (0.25 mmol, 43%). M.p. >300 °C; R_f = 0.2 (CH_2Cl_2/*n*-hexane/MeOH = 3:1:0.2, v/v/v); ^{1}H NMR (400 MHz, [$(CD_3)_2SO$]): δ_H = -2.98 (s, 2H, -N*H*), 5.25 (s, 2H, -CH_2), 7.22 (d, $^3J_{H\text{-}H}$ = 7.7 Hz, 3H, -Ar*H*), 7.42 (t, $^3J_{H\text{-}H}$ = 7.7 Hz, 3H, -Ar*H*), 7.57 (m, 12H, -Ar*H*), 7.67 (t, $^3J_{H\text{-}H}$ = 7.7 Hz, 1H, -Ar*H*), 7.76 (m, 1H, -Ar*H*), 7.81 (m, 1H, -Ar*H*), 8.77 (m, 2H, -H_β), 8.88 (m, 6H, -H_β), 9.87 (s, 3H, -O*H*); ^{13}C NMR (100 MHz, [$(CD_3)_2SO$]): δ_C = 69.1, 115.4, 115.5, 119.9, 120.3, 120.4, 121.4, 121.7, 122.3, 126.2, 128.1, 128.3, 128.4, 130.3, 131.9, 136.9, 142.8, 156.2, 156.9 ppm; UV/Vis (EtOAc): λ_{max} (lg ε) = 417 (5.40), 514 (4.07), 547 (3.67), 591 (3.58), 648 nm (3.47); HRMS (MALDI): *m/z* calcd for [$C_{51}H_{35}BrN_4O_4$] [M^+]: 846.1842, found 846.1861.

5,10,15,20-Tetrakis[3-(4-bromobenzyloxy)phenyl]porphyrin 82b:

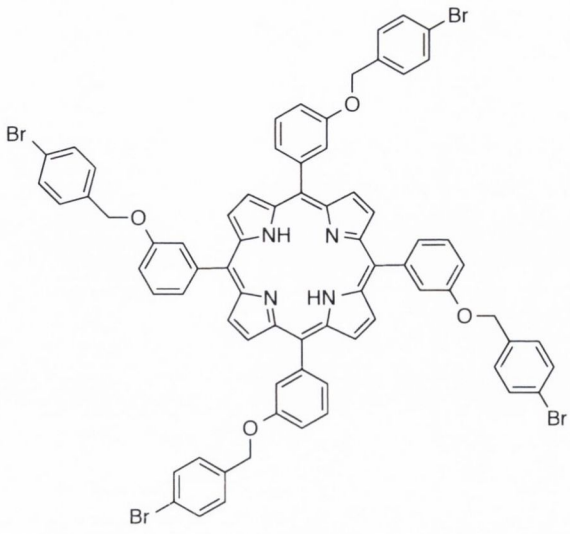

Synthesized *via* general procedure F using **2** (400 mg, 0.59 mmol), K_2CO_3 (815 mg, 5.9 mmol), and *p*-bromobenzyl bromide, **80** (1.75 g, 7.1 mmol). The reaction was completed after 13 h and the product was recrystallized from ethyl acetate/*n*-hexane yielding 765 mg purple crystals (0.56 mmol, 96%). M.p. >300 °C; R_f = 0.91 (CH_2Cl_2/*n*-hexane/MeOH =3:1:0.2, v/v/v); ^{1}H NMR (400 MHz, $CDCl_3$): δ_H = -2.91 (s, 2H, -*N*H), 5.19 (s, 8H, -OCH_2), 7.32 (d, $^3J_{H\text{-}H}$ = 7.8 Hz, 4H, -Ar*H*), 7.45 (d, $^3J_{H\text{-}H}$ = 8.6 Hz, 8H, *o*-ArBr*H*), 7.65 (t, $^3J_{H\text{-}H}$ = 5.5 Hz, 4H, -ArBrH_m), 7.81 (s, 4H, -Ar*H*), 7.86 (d, $^3J_{H\text{-}H}$ = 6.2 Hz, 4H, -Ar*H*), 8.04 (d, $^3J_{H\text{-}H}$ = 8.6 Hz, 8H, -Ar*H*), 8.82 ppm (d, $^3J_{H\text{-}H}$ = 3.8 Hz, 8H, -H_β); ^{13}C NMR (100 MHz, $CDCl_3$): δ_C = 68.7, 114.5, 119.7, 121.5 123.5, 123.6, 123.9, 127.5, 127.9, 128.3, 128.5, 130.7, 143.4, 144.2, 147.4, 156.5 ppm; UV/Vis (EtOAc): λ_{max} (lg ε) = 417 (5.02), 515 (3.76), 547 (3.50), 592 (3.10), 647 nm (3.15); HRMS (MALDI): *m/z* calcd for [$C_{72}H_{50}Br_4N_4O_4$] [M^+]: 1350.0566, found 1350.0520.

5,10,15-Tris(3-hydroxyphenyl)-20-[3-(4-nitrobenzyloxy)phenyl]porphyrin 83a:

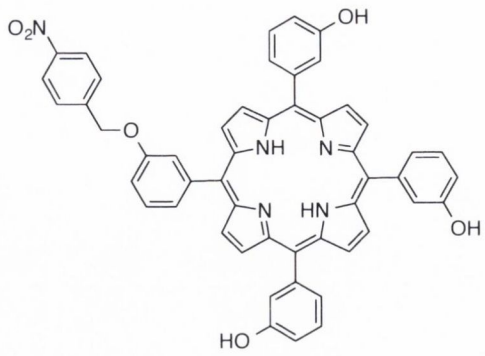

Synthesized *via* General Procedure D using **2** (400 mg, 0.59 mmol), NaH (14.2 mg, 0.59 mmol), and *p*-nitrobenzyl bromide, **81** (254 mg, 1.2 mmol). The reaction was completed after 3 h. Column chromatography on silica gel using CH_2Cl_2/*n*-hexane/MeOH (3:1:0.2) and recrystallization from ethyl acetate/*n*-hexane yielded 187 mg of a purple powder (0.23 mmol, 35 %). M.p. >300 °C; R_f = 0.23 (CH_2Cl_2/*n*-hexane/MeOH =3:1:0.2, v/v/v); ^{1}H NMR (400 MHz, $CDCl_3$): δ_H = -2.99 (s, 2H, -N*H*), 5.44 (s, 2H, -CH_2), 7.20 (d, $^3J_{H-H}$ = 7.5 Hz, 4H, -Ar*H*), 7.48 (m, 1H, -Ar*H*), 7.59 (m, 12H, -Ar*H*), 7.73 (t, $^3J_{H-H}$ = 6.4 Hz, 4H, -Ar*H*), 8.21 (d, $^3J_{H-H}$ = 7.5 Hz, 3H, -Ar*H*), 8.88 (m, 8H, -H_β); ^{13}C NMR (100 MHz, $CDCl_3$): δ_C = 68.7, 115.5, 119.8, 120.4, 120.5, 121.6, 122.3, 124.8, 126.2, 128.3, 128.8, 133.8, 142.8, 146.0, 147.4, 147.5, 156.2 ppm; UV/Vis (EtOAc): λ_{max} (lg ε) = 417 (5.40), 514 (3.87), 547 (2.44), 591 (2.91), 647 nm (3.13); HRMS (MALDI) *m/z* calcd for [$C_{51}H_{35}N_5O_6$] [M^+]: 813.2587: found 813.2609.

5,10,15,20-Tetrakis-[3-(4-nitrobenzyloxy)phenyl]porphyrin 83b:

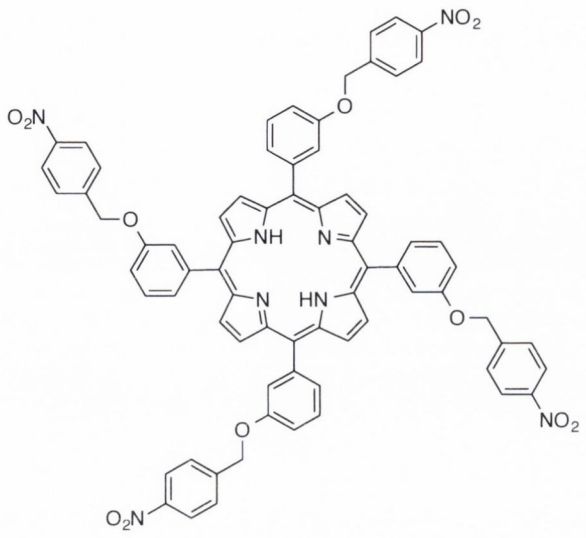

Synthesized *via* general procedure F using **2** (400 mg, 0.59 mmol), K_2CO_3 (815 mg, 5.9 mmol), and 4-nitrobenzylbromide, **81** (1.3 g, 5.9 mmol). The reaction was complete after 15 h and subsequent recrystallization from ethyl acetate/*n*-hexane yielded 446 mg of a purple powder (0.55 mmol, 93 %); M.p. >300 °C; R_f = 0.9 (CH_2Cl_2/*n*-hexane/MeOH = 3:1:0.2, v/v/v); ^{1}H NMR (400 MHz, $CDCl_3$): δ_H = -2.92 (s, 2H, -*N*H), 5.19 (s, 8H, -OC*H*$_2$), 7.32 (d, $^3J_{H\text{-}H}$ = 7.8Hz, 4H, -Ar*H*), 7.47 (m, 8H, -ArH_o), 7.65 (t, $^3J_{H\text{-}H}$ = 5.5Hz, 4H, -ArH_m), 7.81 (d, $^3J_{H\text{-}H}$ = 5.5Hz, 4H, -Ar*H*), 7.86 (d, $^3J_{H\text{-}H}$ = 6.2Hz, 4H, -Ar*H*), 8.04 (m, 8H, -Ar*H*), 8.82 ppm (d, $^3J_{H\text{-}H}$= 3.8 Hz, 8H, -H_β); ^{13}C NMR (100 MHz, $CDCl_3$): δ_c = 68.7, 114.5, 119.7, 121.5 123.5, 123.6, 123.7, 123.9, 127.5, 127.9, 128.3, 128.5, 130.7, 143.4, 144.2, 147.4, 156.5 ppm; UV/Vis (EtOAc): λ_{max} (lg ε) = 417 (5.49), 514 (4.05), 547 (2.61), 591 (3.08), 647 nm (3.39); HRMS (MALDI): *m/z* calcd for [$C_{72}H_{50}N_8O_{12}$] [M$^+$]: 1218.3548, found 1218.3539.

5,10,15,-Tris(3-hydroxyphenyl)-20-(3-phenylbenzoate)porphyrin 86a:

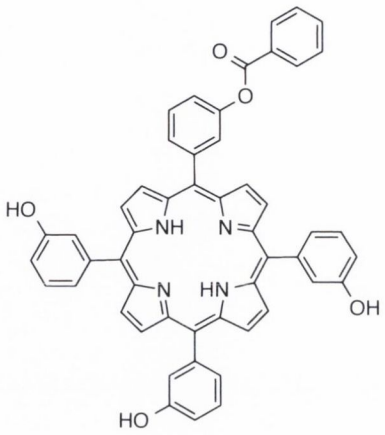

The compound was synthesized using general procedure D: A 50 ml round bottom flask containing DMF (10 mL), **2** (400 mg, 0.59 mmol), NaH (14.2 mg, 0.59 mmol), and benzoic anhydride, **84** (133 mg, 0.59 mmol). The reaction was complete after 1 h. Column chromatography on silica gel using CH_2Cl_2/*n*-hexane/MeOH (3:1:0.2) and recrystallization from ethyl acetate/*n*-hexane yielded 170 mg of a purple solid (0.21 mmol, 37%); M.p. >300 °C; R_f = 0.34 (CH_2Cl_2/*n*-hexane/MeOH = 3:1:0.2, v/v/v); ^{1}H NMR (400 MHz, [$(CD_3)_2SO$]): δ_H = -2.97 (s, 2H, -N*H*), 7.24 (m, 3H, Ar-*H*), 7.59 (m, 11H, Ar-*H*), 7.72 (t, $^3J_{H\text{-}H}$ = 7.4 Hz, 1H, Ar-*H*), 7.77 (d, $^3J_{H\text{-}H}$ = 7.7 Hz, 1H, Ar-*H*), 7.89 (t, $^3J_{H\text{-}H}$ = 8.1 Hz 1H, Ar-*H*), 8.21 (m, 4H, Ar-*H*), 8.89 (m, 8H, H_β), 9.88 (s, br, 3H, -O*H*); ^{13}C NMR (100 MHz, $(CD_3)_2SO$): δ_C = 115.6, 118.9, 120.5, 120.6, 122.3, 125.7, 126.3, 128.3, 128.6, 129.3, 129.4, 130.3, 131.9, 132.1, 142.8, 149.7, 156.2, 165.3 ppm; UV/Vis (EtOAc): λ_{max} (lg ε) = 417 (5.02), 514 (3.76), 547 (3.50), 591 (3.13), 646 nm (2.96); HRMS (MALDI): *m/z* calcd for [$C_{51}H_{34}N_4O_5$] [M^+]: 782.2529, found 782.2531.

5,10,15,20-Tetrakis[3-phenylbenzoate]porphyrin 86b:

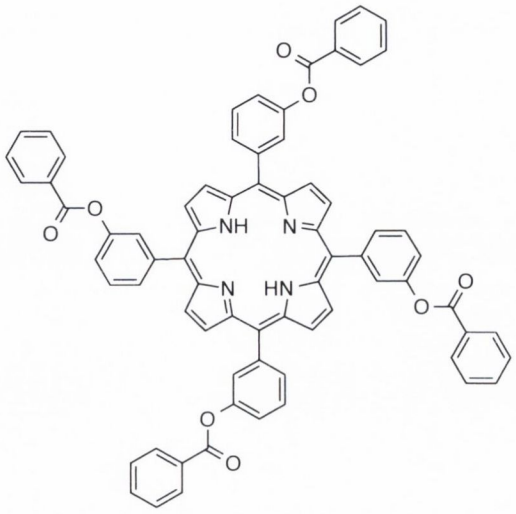

The compound was synthesized using general procedure F: a 50 ml round bottom flask containing 10 mL of DMF, **2** (100 mg, 0.14 mmol), K_2CO_3 (204 mg, 1.4 mmol), and benzoic anhydride (400 mg, 1.77 mmol). The reaction was complete after 7 h and recrystallization from ethyl acetate/*n*-hexane yielded 148 mg of purple crystals (0.13 mmol, 92%); M.p. >300 °C; R_f = 0.9 (CH_2Cl_2/*n*-hexane/MeOH = 3:1:0.2, v/v/v); ^{1}H NMR (400 MHz, $CDCl_3$): δ_H = -2.74 (s, 2H, -N*H*), 7.54 (t, $^3J_{H\text{-}H}$ = 7.4 Hz, 8H, -ArH_m), 7.64 (t, $^3J_{H\text{-}H}$ = 7.1 Hz, 4H, -ArH_m), 7.72 (d, $^3J_{H\text{-}H}$ = 7.8 Hz, 4H, -Ar*H*), 7.86 (t, $^3J_{H\text{-}H}$ = 7.7 Hz, 4H, -Ar*H*), 8.20 (m, 8H, -Ar*H*), 8.34 (d, $^3J_{H\text{-}H}$ = 7.7 Hz, 8H, -Ar*H*), 9.01 ppm (s, 8H, -H_β); ^{13}C NMR (100 MHz, $CDCl_3$): δ_C = 119.1, 121.3, 127.8, 128.1, 128.6, 129.6, 130.3, 132.4, 133.7, 143.5, 149.6, 165.4 ppm; UV/Vis (EtOAc): λ_{max} (lg ε) = 417 (5.02), 515 (3.76), 547 (3.51), 590 (3.15), 646 nm (2.97); HRMS (MALDI): *m/z* calcd for [$C_{72}H_{46}N_4O_8$] [M^+]: 1094.3316, found 1094.3311.

5-[3-(2-Bromobenzoate)phenyl]-10,15,20-tris(3-hydroxyphenyl)porphyrin 92a:

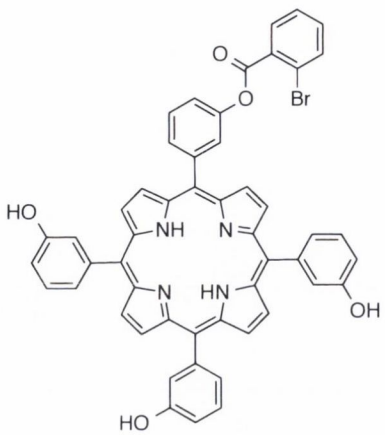

Synthesized *via* a modified version of general procedure D using **2** (400 mg, 0.59 mmol), EDC, **143** (230 mg, 1.7 mmol), *N*-hydroxysuccinimide, **144** (196 mg, 1.7 mmol), K_2CO_3 (235 mg, 1.7 mmol) and 2-bromobenzoic acid **85** (338 mg, 1.7 mmol). The reaction was completed after 3 h. Column chromatography on silica gel using CH_2Cl_2/*n*-hexane/MeOH (3:1:0.2) and recrystallization from ethyl acetate/*n*-hexane yielded 206 mg of a purple solid (0.24 mmol, 40 %); m.p. >300 °C; R_f = 0.32 (CH_2Cl_2/*n*-hexane/MeOH = 3:1:0.2, v/v/v); ^{1}H NMR (400 MHz, $CDCl_3$): δ_H = -2.86 (s, br, 2H, -N*H*), 7.14 (s, 3H, -Ar*H*), 7.39 (t, $^3J_{H-H}$=7.4 Hz, 2H, -Ar*H*), 7.49 (m, 6H, -Ar*H*), 7.70 (t, $^3J_{H-H}$ = 7.4 Hz, 6H, -Ar*H*), 8.07 (d, $^3J_{H-H}$ = 7.4 Hz, 2H, -Ar*H*), 8.52 (s, 1H, -Ar*H*), 8.80 (m, 4H, -H_β), 8.89 ppm (m, 4H, -H_β); ^{13}C NMR (100 MHz, $CDCl_3$): δ_C = 114.8, 119.7, 121.0, 121.8, 123.9, 127.3, 127.7, 131.9, 134.6, 136.3, 143.6, 149.2, 149.3, 153.9 ppm; UV/Vis (EtOAc): λ_{max} (lg ε) = 417 (5.41), 514 (4.08), 547 (3.69), 591 (3.59), 648 nm (3.48); HRMS (MALDI): *m/z* calcd for [$C_{51}H_{35}BrN_4O_4$] [M^+]: 846.1842, found 846.1861.

5,10,15,20-[3-(2-bromophenyl)benzoate]porphyrin 92b:

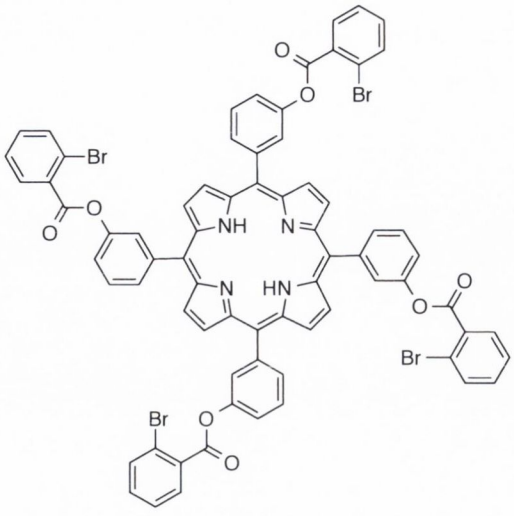

Synthesized *via* a modified version of general procedure F using **2** (100 mg, 0.14 mmol), EDC, **143** (228 mg, 1.4 mmol), *N*-hydroxysuccinimide, **144** (170 mg, 1.4 mmol), K_2CO_3 (203 mg, 1.4 mmol) and 2-bromobenzoic acid **85** (338 mg, 1.7 mmol). The reaction was completed after 6 h, with recrystallization from ethyl acetate/*n*-hexane yielding 83 mg of purple crystals (0.059 mmol, 59%); M.p. >300 °C; R_f = 0.85 (CH_2Cl_2/*n*-hexane/MeOH = 3:1:0.2, v/v/v); ^{1}H NMR (400 MHz, [$(CD_3)_2SO$]): δ_H = -2.95 (s, 2H, -N*H*), 7.51 (s, 8H, -Ar*H*), 7.78 (d, $^3J_{H\text{-}H}$=7.8 Hz, 8H, -Ar*H*), 7.91 (t, $^3J_{H\text{-}H}$ = 7.8 Hz, 5H, -Ar*H*), 8.10 (m, 4H, -Ar*H*), 8.20 (m, 7H, -Ar*H*), 8.94 ppm (s, 8H, -H_β); ^{13}C NMR (100 MHz, $CDCl_3$): δ_C = 119.4, 121.3, 122.0, 128.1, 128.4, 128.7, 131.7, 132.1, 132.7, 134.3, 134.6, 142.9, 149.4, 164.9ppm; UV/Vis (EtOAc): λ_{max} (lg ε) = 417 (5.40), 514 (4.08), 547 (3.68), 591 (3.59), 648 nm (3.49); HRMS (MALDI): *m/z* calcd for [$C_{72}H_{42}Br_4N_4O_8$] [M^+]: 1405.9736, found 1405.9730.

5,10,15-Tris(3-hydroxyphenyl)-20-(3-trifluoromethanesulfonatephenyl)porphyrin 105a:

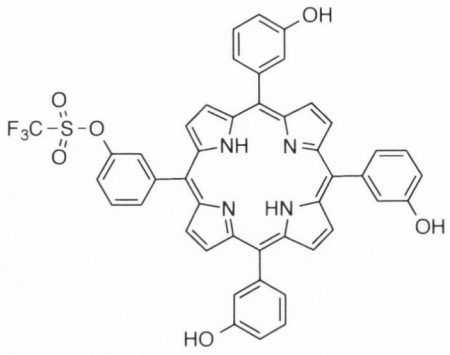

Synthesized *via* a modified general procedure D using **2** (400 mg, 0.59 mmol), pyridine (0.046 mL, 0.59 mmol), and trifluoromethanesulfonyl chloride, **104** (0.12 mL, 1.2 mmol). The reaction was completed after 1 h. Column chromatography on silica gel using CH_2Cl_2/*n*-hexane/MeOH (3:1:0.2, v/v/v) and recrystallization from ethyl acetate/*n*-hexane yielded 177 mg of a purple solid (0.22 mmol, 37%); M.p. >300 °C; R_f = 0.38 (CH_2Cl_2/*n*-hexane/MeOH = 3:1:0.2, v/v/v); ^{1}H NMR (400 MHz, [$(CD_3)_2SO$]): δ_H = -2.99 (s, 2H, -N*H*), 7.22 (m, 4H, -ArH_o), 7.59 (m, 12H, -Ar*H*), 8.86 (s, 8H, -H_β), 9.87 ppm (s, 3H, -O*H*); ^{19}F NMR (150 MHz, $CDCl_3$): δ_F = -39.42 (s) ppm; ^{13}C NMR (100 MHz, [$(CD_3)_2SO$]): δ_C = 115.5, 120.3, 122.3, 126.3, 128.3, 142.8, 156.2 ppm; UV/Vis (EtOAc): λ_{max} (lg ε) = 417 (5.04) ,513 (3.71), 547 (3.32), 591 (3.21), 647 nm (3.03); HRMS (MALDI): *m/z* calcd for [$C_{45}H_{29}F_3N_4O_6S$] [M^+]: 810.1760, found 810.1751.

5,10,15,20-Tetrakis(3-(trifluoromethanesulfonate)phenyl)porphyrin 105b:

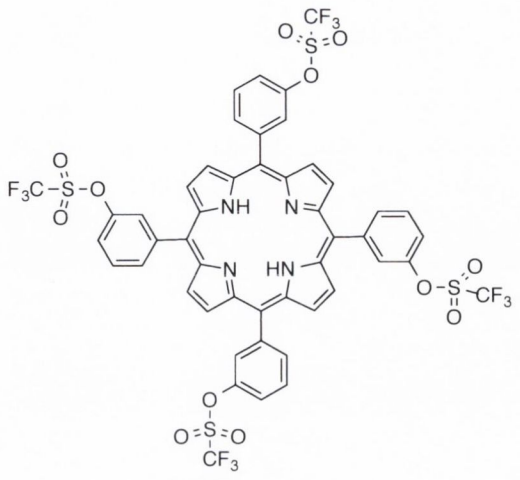

Synthesized *via* a modified general procedure F using **2** (400 mg, 0.59 mmol), pyridine (0.46 mL, 5.9 mmol), and trifluoromethanesulfonyl chloride, **104** (0.63 mL, 5.9 mmol). The reaction was completed after 8 h. Recrystallization from ethyl acetate/*n*-hexane yielded 655 mg of purple crystals (0.54 mmol, 92%); M.p. >300 °C, R_f = 0.95 (CH_2Cl_2/*n*-hexane/MeOH = 3:1:0.2, v/v/v); ^{1}H NMR (400 MHz, $CDCl_3$): δ_H = -2.79 (s, 2H, -N*H*), 7.79 (d, $^3J_{H\text{-}H}$ = 8.0 Hz, 4H, -Ar*H*), 7.90 (t, $^3J_{H\text{-}H}$ = 7.7 Hz, 4H, -Ar*H*), 8.25 (s, 4H, -ArH_o), 8.31 (m, 4H, -Ar*H*), 8.93 ppm (s, 8H, -H_β); ^{19}F NMR (150 MHz, $CDCl_3$): δ_F = -72.55 ppm (CF_3); ^{13}C NMR (150 MHz, $CDCl_3$): δ_C = 114.18, 117.37, 118.19, 120.56, 121.12, 123.75, 127.23, 128.63, 134.42, 134.47, 144.24, 148.35 ppm; UV/Vis (EtOAc): λ_{max} (lg ε) = 415 (5.40), 512 (4.10), 545 (3.63), 589 (3.60), 645 nm (3.24); HRMS (MALDI): *m/z* calcd for [$C_{48}H_{26}F_{12}N_4O_{12}S_4$] [$M^+$]: 1206.0238, found 1206.0226.

5,10,15-Tris(3-hydroxyphenyl)-20-[3-(4-methylbenzenesulfonate)phenyl]porphyrin 107a:

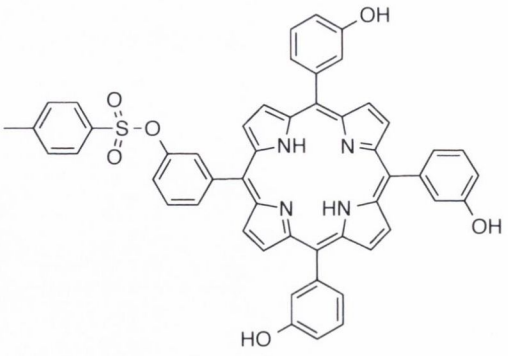

Synthesized *via* a modified general procedure D using **2** (400 mg, 0.59 mmol), pyridine (0.046 mL, 0.599 mmol), and 4-toluenesulfonyl chloride, **106** (448 mg, 2.3 mmol). The reaction was completed after 2 h. Column chromatography on silica gel using CH_2Cl_2/*n*-hexane/MeOH (3:1:0.2, v/v/v), with recrystallization from ethyl acetate/*n*-hexane yielding 171 mg of purple crystals (0.20 mmol, 35%); M.p. >300 °C, R_f = 0.29 (CH_2Cl_2/*n*-hexane/MeOH = 3:1:0.2, v/v/v); ^{1}H NMR (400 MHz, $CDCl_3$): δ_H = -2.92 (s, 2H, -N*H*), 2.2 (s, 3H, -CH_3), 7.51 (m, 2H, -Ar*H*), 7.59 (m, 4H, -Ar*H*), 7.67 (m, 6H, -Ar*H*), 7.76 (m, 4H, -Ar*H*) 7.85 (d, $^3J_{H\text{-}H}$ = 8.0 Hz, 4H, -Ar*H*) 8.06 (d, $^3J_{H\text{-}H}$ = 4.0 Hz, 2H, -H_β) 8.56 (m, $^3J_{H\text{-}H}$ = 4.0 Hz, 2H, -H_β) 8.83 ppm (d, $^3J_{H\text{-}H}$ = 4.0 Hz, 4H, -H_β); ^{13} C NMR (150 MHz, $CDCl_3$): δ_C = 21.5, 115.5, 119.1, 120.4, 120.5, 122.3, 124.3, 125.7, 126.2, 128.2, 128.3, 128.4, 128.6, 129.3, 142.6, 142.8, 150.0, 150.4, 154.7, 156.2 ppm; UV/Vis (EtOAc): λ_{max} (lg ε) = 417 (5.42), 514 (4.10), 547 (3.65), 591 (3.60), 649 nm (3.25); HRMS (MALDI): *m/z* calcd for [$C_{51}H_{36}N_4O_6S$] [M^+]: 832.2356, found 832.2348.

5,10,15,20-Tetrakis[3-(4-methylbenzenesulfonate)phenyl]porphyrin 107b:

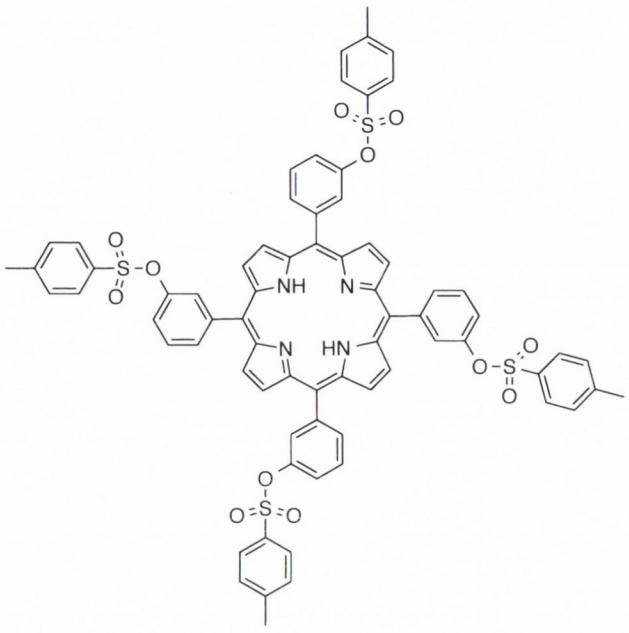

Synthesized *via* a modified general procedure F using **2** (400 mg, 0.59 mmol), pyridine (0.46 mL, 5.9 mmol), and 4-toluenesulfonyl chloride, **106** (1.12 g, 5.9 mmol). The reaction was completed after 4 h and recrystallization from ethyl acetate/*n*-hexane yielded 687 mg of purple crystals (0.53 mmol, 90%); M.p. >300 °C, R_f = 0.91 (CH_2Cl_2/*n*-hexane/MeOH = 3:1:0.2, v/v/v); ^{1}H NMR (400 MHz, $CDCl_3$): δ_H = -3.04 (s, 2H, -N*H*), 2.31 (s, 12H, -CH_3), 7.32 (d, $^3J_{H\text{-}H}$ = 7.9 Hz, 8H, -Ar*H*), 7.56 (m, 4H, -Ar*H*), 7.72 (t, $^3J_{H\text{-}H}$ = 7.9 Hz, 5H, -Ar*H*), 7.79 (m, 3H, Ar-*H*), 7.89 (d, $^3J_{H\text{-}H}$ = 7.9 Hz, 8H, -Ar*H*), 8.06 (m, 4H, -Ar*H*), 8.64 ppm (s, 8H, -H_β); ^{13}C NMR (100 MHz, $CDCl_3$): δ_C = 21.6, 118.5, 122.2, 127.9, 128.2, 128.6, 130.0, 132.4, 133.2, 143.4, 145.6, 148.2 ppm; UV/Vis (EtOAc): λ_{max} (lg ε) = 416 (5.44), 513 (4.11), 546 (3.63), 590 (3.59), 646 nm (3.23); HRMS (MALDI): *m/z* calcd for [$C_{72}H_{54}N_4O_{12}S_4$] [M^+]: 1294.2621, found 1294.2590.

[5,10,15-Tris(3-hydroxyphenyl)-20-[3-(phenoxy)phenyl]porphyrinato]zinc(II) 110:

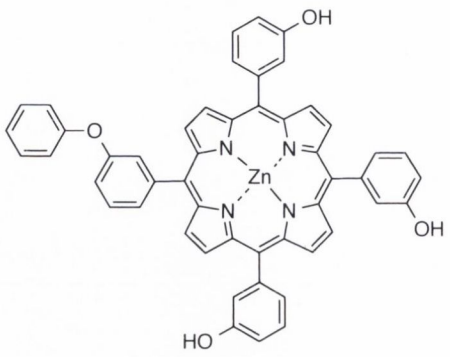

Synthesized *via* general procedure G using **108** (50 mg, 0.067 mmol), $Cu(OAc)_2$ (20 mg, 0.11 mmol), phenylboronic acid, **109** (27 mg, 0.22 mmol) and pyridine (0.2 mL) in dioxane (10 mL). The reaction was completed after 12 h. Column chromatography on silica gel using CH_2Cl_2/*n*-hexane/MeOH (3:1:0.2) and recrystallization from ethyl acetate/*n*-hexane yielding 22 mg of purple crystals (0.026 mmol, 39%); M.p. >300 °C, R_f = 0.31 (CH_2Cl_2/*n*-hexane/MeOH = 3:1:0.2, v/v/v); ^{1}H NMR (400 MHz, [$(CD_3)_2SO$]): δ_H = 7.09 (t, $^3J_{H-H}$ = 7.5 Hz, 1H, -Ar*H*), 7.15 (m, 3H, -Ar*H*), 7.28 (d, $^3J_{H-H}$ = 7.9 Hz, 2H, -Ar*H*), 7.41 (t, $^3J_{H-H}$ = 7.5 Hz, 2H, Ar*H*) 7.45 (m, 1H, -Ar*H*), 7.54 (m, 9H, -Ar*H*), 7.69 (m, 1H, -Ar*H*), 7.76 (t, $^3J_{H-H}$ = 7.8 Hz, 1H, -Ar*H*), 7.91 (d, $^3J_{H-H}$ = 7.4 Hz, 1H, -Ar*H*), 8.79 (d, $^3J_{H-H}$ = 3.5 Hz, 2H, -H_β), 8.80 (d, $^3J_{H-H}$ = 3.5 Hz, 6H, -H_β), 9.75 ppm (s, 3H, -O*H*); ^{13}C NMR (100 MHz, $CDCl_3$): δ_C = 114.3, 115.3, 117.9, 118.8, 120.7, 122.0, 123.2, 127.3, 127.4, 127.5, 127.7, 129.6, 129.7, 129.8, 131.5, 131.6, 131.7, 133.7, 136.6, 145.4 ppm; UV/Vis (EtOAc): λ_{max} (lg ε) = 421 (6.83), 553 (5.40), 593 nm (4.78); HRMS (MALDI): *m/z* calcd for [$C_{50}H_{34}N_4O_4Zn$] [M^+]: 816.1715, found 816.1710.

[5-(3-(3-cyanophenoxy)phenyl)-10,15,20-tris(3-hydroxyphenyl)porphyrinato]zinc(II) 114:

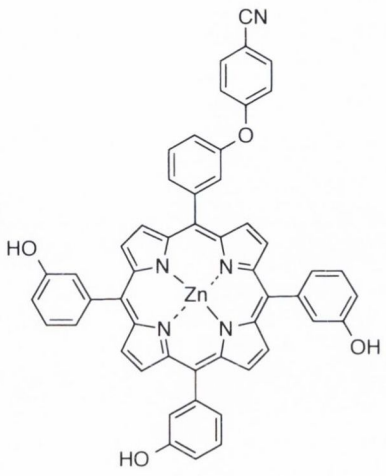

Synthesized *via* general procedure G using **108** (50 mg, 0.067 mmol), $Cu(OAc)_2$ (20 mg, 0.11 mmol), 4-cyanophenylboronic acid, **111** (27 mg, 0.22 mmol) and pyridine (0.2 mL) in dioxane (10 mL). The reaction was completed after 15 h. Column chromatography on silica gel using CH_2Cl_2/*n*-hexane/MeOH (3:1:0.2, v/v/v) and recrystallization from ethyl acetate/*n*-hexane yielding 19.7 mg of purple crystals (0.023 mmol, 35%); M.p. > 300 °C, R_f = 0.31 (CH_2Cl_2/*n*-hexane/MeOH = 3:1:0.2, v/v/v); ^{1}H NMR (400 MHz, [$(CD_3)_2SO$]): δ_H = 7.17 (m, 3H, Ar-*H*), 7.55 (m, 12H, Ar-*H*), 7.64 (m, 2H, Ar-*H*), 7.81 (m, 2H, Ar-*H*), 8.01 (m, 1H, Ar-*H*), 8.80 (s, 4H, H_β) 8.83 (s, 4H, H_β), 9.77 (s, 3H, -O*H*); ^{13}C NMR (100 MHz, $CDCl_3$, 25 °C): δ_C = 112.8, 114.9, 118.9, 120.6, 120.62, 120.65, 120.7, 122.3, 126.2, 127.8, 131.7, 131.9, 144.4, 149.4, 149.5, 149.6, 149.9, 155.9 ppm; UV/Vis (EtOAc): λ_{max} (lg ε) = 421 (6.81), 552 (4.92), 5.94 nm (4.39) ; HRMS (MALDI): *m/z* calcd for [$C_{51}H_{33}N_5O_4Zn$] [M^+]: 841.1668, found 841.1665.

[5,10,15-Tris(3-hydroxyphenyl)-20-[3-(3-methoxyphenyl)phenyl]porphyrinato]zinc(II) 115:

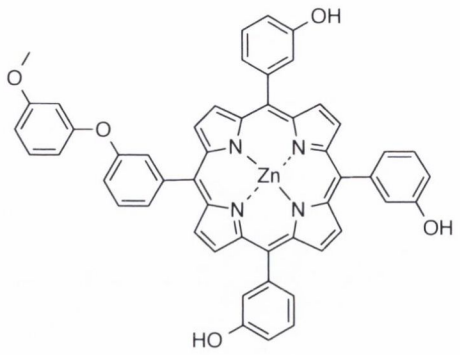

Synthesized *via* general procedure G using **108** (70 mg, 0.095 mmol), $Cu(OAc)_2$ (27 mg, 0.15 mmol), and 3-methoxyphenylboronic acid, **112** (44 mg, 0.29 mmol). The reaction was completed after 2 h. Column chromatography on silica gel using CH_2Cl_2/*n*-hexane/MeOH (3:1:0.2, v/v/v) and recrystallization from ethyl acetate/*n*-hexane yielding 30 mg of purple crystals (0.035 mmol, 37%); M.p. >300 °C, R_f = 0.29 (CH_2Cl_2/*n*-hexane/MeOH = 3:1:0.2, v/v/v); ^{1}H NMR (400 MHz, [$(CD_3)_2SO$]): δ_H = 3.76 (s, 3H, -OC*H*$_3$), 6.70 (d, $^3J_{H\text{-}H}$ = 8.0 Hz, 1H, -Ar*H*), 6.87 (d, $^3J_{H\text{-}H}$ = 8.0 Hz, 2H, -Ar*H*), 7.21 (d, $^3J_{H\text{-}H}$ = 8.01 Hz, 3H, -Ar*H*), 7.34 (t, $^3J_{H\text{-}H}$ = 8.01 Hz, 1H, -Ar*H*), 7.50 (dd, $^3J_{H\text{-}H}$ = 8.0 Hz, 1H, -Ar*H*), 7.58 (m, 9H, -Ar*H*), 7.75 (s, 1H, -Ar*H*), 7.80 (t, $^3J_{H\text{-}H}$ = 8.0 Hz, 1H, -Ar*H*), 7.96 (d, $^3J_{H\text{-}H}$ = 7.12 Hz, 1H, -Ar*H*), 8.84 (d, $^3J_{H\text{-}H}$ = 4.3 Hz, 6H, -H_β), 8.86 (d, $^3J_{H\text{-}H}$ = 4.5 Hz, 2H, -H_β), 9.80 ppm (s, 3H, -O*H*); ^{13}C NMR (100 MHz, $CDCl_3$): δ_C = 55.7, 105.4, 109.8, 111.3, 114.9, 119.4, 120.8, 120.9, 122.3, 126.2, 127.8, 131.0, 131.6, 131.9, 132.1, 144.3, 145.0, 149.4, 149.5, 149.6, 149.7, 155.3, 155.9, 161.2 ppm; UV/Vis (EtOAc): λ_{max} (lg ε) = 421 (6.85), 553 (5.40), 593 nm (4.78); HRMS (MALDI): *m/z* calcd for [$C_{51}H_{36}N_4O_5Zn$] [M^+]: 846.1821, found 846.1819.

[5-(3-(2-iodoophenoxy)phenyl)-10,15,20-tris(3-hydroxyphenyl)porphyrinato]zinc(II) 116:

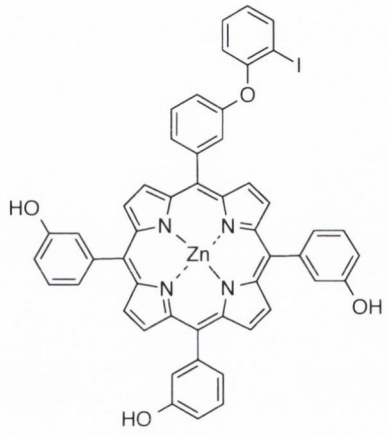

Synthesized *via* general procedure G using **108** (50 mg, 0.067 mmol), $Cu(OAc)_2$ (19.98 mg, 0.11 mmol), 2-iodophenylboronic acid **113** (26.99 mg, 0.22 mmol) and pyridine (0.2 mL) in dioxane (10 mL). The reaction was completed after 15 h. Column chromatography on silica gel using CH_2Cl_2/*n*-hexane/MeOH (3:1:0.2) and subsequent recrystallization from ethyl acetate/*n*-hexane yielded 18.9 mg of shiny purple crystals (0.023 mmol, 34%); M.p. >300 °C, R_f = 0.31 (CH_2Cl_2/*n*-hexane/MeOH = 3:1:0.2, v/v/v); ^{1}H NMR (400 MHz, $(CD_3)_2SO$): δ_H = 7.17 (m, 3H, Ar-*H*), 7.55 (m, 12H, Ar-*H*), 7.64 (m, 2H, Ar-*H*), 7.81 (m, 2H, Ar-*H*), 8.01 (m, 1H, Ar-*H*), 8.80 (s, 4H, H_β) 8.83 (s, 4H, H_β), 9.77 (s, 3H, -O*H*); ^{13}C NMR (100 MHz, $CDCl_3$): δ_C = 112.8, 114.9, 118.9, 120.6, 120.62, 120.65, 120.7, 122.3, 126.2, 127.8, 131.7, 131.9, 144.4, 149.4, 149.5, 149.6, 149.9, 155.9 ppm; UV/Vis (EtOAc): λ_{max} (log ε) = 421 (6.81), 552 (4.92), 5.94 nm (4.39) ; HRMS (MALDI): *m/z* calcd for $[C_{51}H_{33}N_5O_4Zn]$ $[M^+]$: 841.1668, found 841.1665.

5,10,15,20-Tetrakis[3-(hexyloxy)phenyl]porphyrin 122:

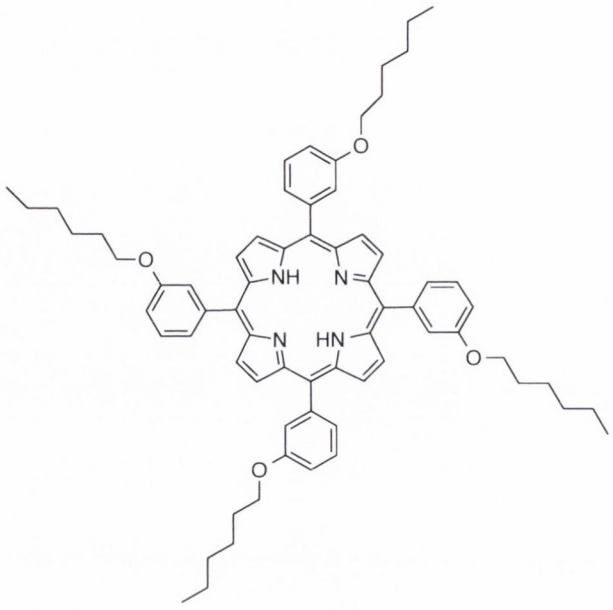

Synthesized *via* general procedure F using **2** (400 mg, 0.59 mmol), K_2CO_3 (815 mg, 5.9 mmol), and 1-iodohexane, **110** (1.4 mL, 5.9 mmol). The reaction was complete after 5 h, subsequent work-up and recrystallization from ethyl acetate/*n*-hexane yielded 569 mg of a purple solid (0.56 mmol, 94%); M.p. >300 °C; R_f = 0.9 (CH_2Cl_2/*n*-hexane/MeOH = 3:1:0.2, v/v/v); ^{1}H NMR (400 MHz, $CDCl_3$): δ_H = -2.81 (s, 2H, -N*H*), 0.88 (m, 28H, alkyl-*H*), 1.55 (m, 8H, alkyl-*H*), 1.87 (q, $^3J_{H\text{-}H}$ = 6.8 Hz, 8H, -CH_2), 4.14 (t, $^3J_{H\text{-}H}$ = 6.7 Hz, 8H, -OCH_2), 7.31(d, $^3J_{H\text{-}H}$ = 8.49 Hz, 3H, -Ar*H*), 7.53 (t, $^3J_{H\text{-}H}$ = 7.9 Hz, 1H, -Ar*H*), 7.61(t, $^3J_{H\text{-}H}$ = 7.9 Hz, 3H, -Ar*H*), 7.70 (d, $^3J_{H\text{-}H}$ = 7.9 Hz, 1H, -Ar*H*), 7.77 (t, $^3J_{H\text{-}H}$ = 8.5 Hz, 6H, -Ar*H*), 8.88 ppm (d, $^3J_{H\text{-}H}$ = 4.6 Hz, 8H, -H_β); ^{13}C NMR (100 MHz, $CDCl_3$): δ_C = 22.6, 25.7, 29.4, 29.7, 31.6, 68.2, 114.2, 119.9, 121.0, 127.4, 127.5, 143.4, 157.5 ppm; UV/Vis (EtOAc): λ_{max} (lg ε) = 417 (5.04), 515 (3.75), 547 (3.50), 589 (3.10), 648 nm (2.97); HRMS (MALDI): *m/z* calcd for [$C_{68}H_{78}N_4O_4$] [M^+]: 1014.6023, found 1014.602.

5,10,15,20-tetrakis[3-(4-*tert*-butylbenzyloxy)phenyl]porphyrin 123:

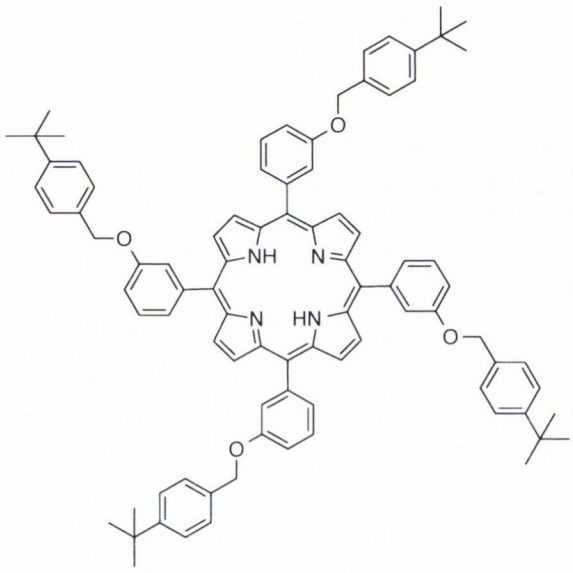

Synthesized *via* general procedure F using **2** (400 mg, 0.59 mmol), K_2CO_3 (815 mg, 6 mmol), and 4-*tert*butylbenzylbromide **121** (1.4 mL, 12 mmol). The reaction was complete after 12 h and recrystallization from ethyl acetate/*n*-hexane yielded 707 mg of purple crystals (0.56 mmol, 96%); M.p. >300 °C; R_f = 0.95 (CH_2Cl_2/*n*-hexane/MeOH = 3:1:0.2, v/v/v); ^{1}H NMR (400 MHz, $CDCl_3$): δ_H = -2.70 (s, 2H, -N*H*), 1.39 (s, 36H, -*t*Bu*H*), 5.28 (s, 8H, -CH_2), 7.49 (m, 20H, -*t*BuAr*H*), 7.70 (t, $^3J_{H\text{-}H}$ = 7.7 Hz, 4H, -ArH_m), 7.89 (d, $^3J_{H\text{-}H}$ = 7.7 Hz, 4H, -Ar*H*), 7.95 (s, 4H, -Ar*H*), 8.94 ppm (s, 8H, -H_β); ^{13}C NMR (100 MHz, $CDCl_3$): δ_C = 27.0, 31.4, 70.2, 114.7, 119.9, 121.4, 125.6, 127.6, 127.7, 127.9, 133.9, 143.5, 151.1, 157.3 ppm; UV/Vis (EtOAc): λ_{max} (lg ε) = 417 (5.02), 515 (3.76), 547 (3.50), 591 (3.16), 645 nm (2.98); HRMS (MALDI): *m/z* calcd for [$C_{88}H_{76}N_4O_4$] [M^+]: 1262.6649, found 1262.6635.

5-(3-Hydroxyphenyl)-10,15,20-tris[3-(4-tert-butylbenzyloxy)phenyl]porphyrin 125:

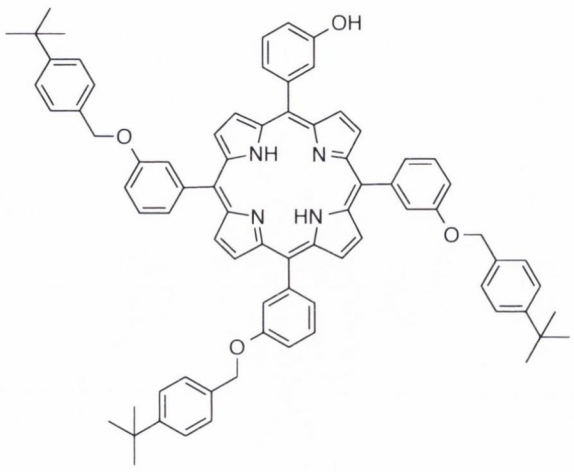

Synthesized *via* general procedure F using **2** (400 mg, 0.59 mmol), K_2CO_3 (800 mg, 6 mmol), and 4-*tert*-butylbenzylbromide (1.4 mL, 6 mmol). The reaction was complete after 7 h. Recrystallization from ethyl acetate/*n*-hexane yielded 382 mg of purple crystals (0.34 mmol, 37%); M.p. >300 °C, R_f = 0.82 (CH_2Cl_2/*n*-hexane/MeOH =3:1:0.2, v/v/v); ^{1}H NMR (400 MHz, $CDCl_3$): δ_H = -2.68 (s, br, 2H, -N*H*), 1.40 (s, 27H, -*t*Bu*H*), 5.27 (s, 6H, -CH_2), 7.48 (q, $^3J_{H\text{-}H}$ = 3.64 Hz, 18H, -*t*BuAr*H*), 7.69 (q, $^3J_{H\text{-}H}$ = 8.0 Hz, 3H, -Ar*H*), 7.78 (d, $^3J_{H\text{-}H}$ = 7.4 Hz, 1H, -Ar*H*), 7.90 (t, $^3J_{H\text{-}H}$ = 7.12 Hz, 3H, -Ar*H*), 7.97 (s, br, 3H, -Ar*H*), 8.90 (d, $^3J_{H\text{-}H}$ = 4.64 Hz, 2H, -H_β), 8.94 ppm (m, Hz, 6H, H_β); ^{13}C NMR (100 MHz, $CDCl_3$): δ_C = 31.4, 34.6, 70.2, 114.7, 114.8, 119.6, 119.9, 120.0, 121.5, 121.8, 125.6, 127.7, 133.9, 133.91, 143.4, 143.5, 143.6, 151.1, 153.8, 157.3 ppm; UV/Vis (EtOAc): λ_{max} (lg ε) = 417 (5.02), 515 (3.75), 548 (3.51), 590 (3.15), 647 nm (2.99); HRMS (MALDI): *m/z* calcd for [$C_{77}H_{72}N_4O_4$] [M^+]: 1116.5554, found 1116.5548.

5-(3-(Prop-2-yn-1-yloxyphenyl)-10,15,20-tris[3-(4-*tert*-butylbenzyloxy)phenyl]porphyrin 126:

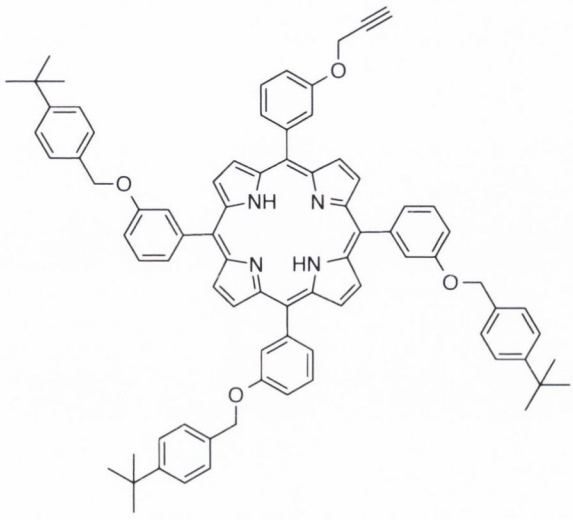

The compound was synthesized using general procedure D: a 50 mL round bottom flask containing 10 mL of DMF, **125** (100 mg, 0.15 mmol), NaH (3.5 mg, 0.15 mmol) and propargyl bromide (0.075 ml, 0.15 mmol) was allowed to stir for 2 h. The reaction was subjected to the work-up described in general procedure D, with recrystallization from ethyl acetate/*n*-hexane yielding 161 mg (0.14 mmol, 95%); M.p. >300 °C; R_f = 0.93 (CH_2Cl_2/*n*-hexane/MeOH =3:1:0.2, v/v/v); ^{1}H NMR (400 MHz, $CDCl_3$): δ_H = -2.80 (s, 2H, -N*H*), 1.33 (s, 27H, -*t*Bu*H*), 2.6 (s, 1H, alkyne-*H*), 4.89 (s, 2H, -CH_2), 5.22 (s, 6H, -CH_2), 7.44 (m, 16H, -*t*BuAr*H*), 7.65 (t, 4H, $^3J_{H\text{-}H}$ = 7.8 Hz, -Ar*H*), 7.81 (d, $^3J_{H\text{-}H}$ = 7.1 Hz, 3H, -Ar*H*), 7.87 (s, 5H, -Ar*H*), 8.86 ppm (m, 8H, -H_β); ^{13}C NMR (100 MHz, $CDCl_3$): δ_C = 23.9, 31.4, 34.6, 56.1, 70.1, 75.8, 114.6, 114.7 119.9, 121.3, 125.6, 127.5, 127.6, 127.9, 133.8, 143.4, 143.5, 151.1, 156.0, 157.2 ppm; UV/Vis (EtOAc): λ_{max} (lg ε) = 417 (5.02), 515 (3.76), 547 (3.50), 590 (3.15), 647 nm (2.99); HRMS (MALDI): *m/z* calcd for [$C_{80}H_{74}N_4O_4$] [M^+]: 1154.5710, found 1154.5716.

5,10,15-Tris[3-(hexyloxy)phenyl]-20-(3-hydroxyphenyl)porphyrin 124:

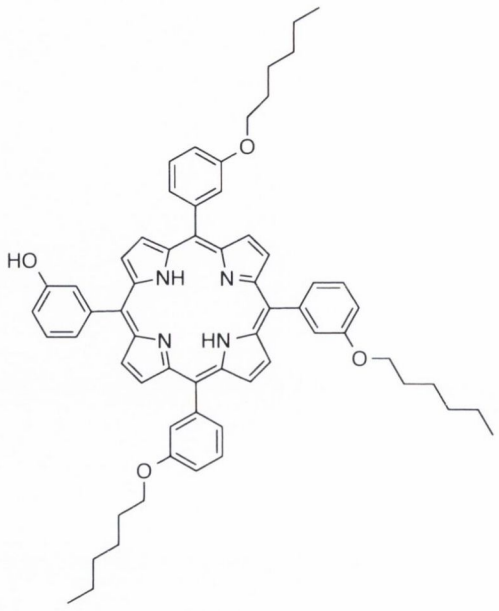

Synthesized *via* general procedure F using **2** (400 mg, 0.59 mmol), K_2CO_3 (815 mg, 5.9 mmol), and 1-iodohexane (1.4 mL, 5.9 mmol). The reaction was complete after 7 h. Recrystallization from ethyl acetate/*n*-hexane yielded 313 mg of a purple solid (0.33 mmol, 40%); M.p. >300 °C, R_f = 0.96 (CH_2Cl_2/*n*-hexane/MeOH = 3:1:0.2, v/v/v); ^{1}H NMR (400 MHz, $CDCl_3$): δ_H = -2.81 (s, 2H, -N*H*), 0.88 (t, 9H, $^3J_{H-H}$ = 6.4 Hz, -CH_3), 1.16 (t, 12H, $^3J_{H-H}$ = 7.3 Hz, -CH_2), 2.81 (q, 12 H $^3J_{H-H}$ = 7.3 Hz, -CH_2), 4.14 (t, 12H, $^3J_{H-H}$ = 6.4 Hz, -OCH_2), 7.31(d, 3H, $^3J_{H-H}$ = 8.5 Hz, -Ar*H*), 7.53 (t, 1H, $^3J_{H-H}$ = 8.5 Hz, -Ar*H*), 7.61 (t, 3H, $^3J_{H-H}$ = 7.9 Hz, -Ar*H*), 7.70 (d, 1H, $^3J_{H-H}$ = 7.9 Hz, Ar-*H*), 7.77 (t, 6H, $^3J_{H-H}$ = 8.5 Hz, -Ar*H*), 8.89 ppm (m, 8H, $^3J_{H-H}$ = 3.9 Hz, -H_β); ^{13}C NMR (100 MHz, $CDCl_3$): δ_C = 14.3, 22.4, 25.6, 29.1, 31.4, 68.1, 114.7, 115.5, 120.0, 120.1, 120.4, 120.41, 121.2, 122.3, 126.2, 127.5, 128.3, 142.8, 142.9, 156.2, 157.5 ppm; UV/Vis (EtOAc): λ_{max} (lg ε) = 417 (5.03), 515 (3.73), 546 (3.50), 591 (3.10), 647 nm (2.98); HRMS (MALDI): *m/z* calcd for [$C_{62}H_{66}N_4O_4$] [M^+]: 930.5084, found 930.5080.

5,10,15,20-Tetrakis[3-(4-bromobutoxy)phenyl]porphyrin 128:

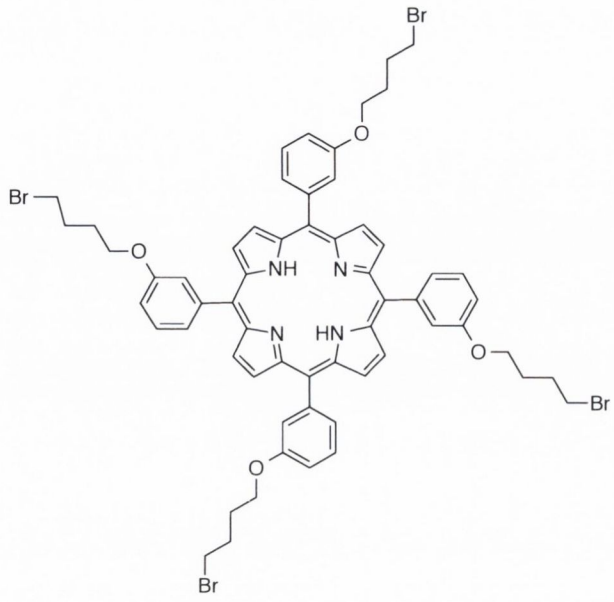

Synthesized *via* general procedure F using **2** (400 mg, 0.59 mmol), K_2CO_3 (815 mg, 6 mmol), and 1,4-dibromobutane, **127** (1.4 mL, 12 mmol). The reaction was complete after 5 h, with recrystallization from ethyl acetate/*n*-hexane yielding 688 mg of purple crystals (0.57 mmol, 96%); M.p. >300 °C; R_f = 0.9 (CH_2Cl_2/*n*-hexane/MeOH = 3:1:0.2, v/v/v); ^{1}H NMR (400 MHz, $CDCl_3$): δ_H = -2.67 (s, 2H, -N*H*), 2.03 (m, 8H, -CH_2), 2.14 (m, 8H, -CH_2), 3.52 (t, 8H, $^3J_{H\text{-}H}$ = 6.2 Hz, -CH_2), 4.19 (t, 8H $^3J_{H\text{-}H}$ = 5.0 Hz, -CH_2), 7.32 (d, 4H $^3J_{H\text{-}H}$ = 6.2 Hz, -Ar*H*), 7.67 (t, 4H $^3J_{H\text{-}H}$ = 5.0 Hz, -Ar*H*), 7.86 (s, 4H, -ArH_o), 7.90 (d, 4H, $^3J_{H\text{-}H}$ = 7.4 Hz, -ArH_p), 8.99 ppm (s, 8H, -H_β); ^{13}C NMR (100 MHz, $CDCl_3$): δ_C = 28.0, 30.9, 32.5, 67.1, 114.1, 119.9, 121.2, 127.6, 127.8 143.5, 157.3 ppm; UV/Vis (EtOAc): λ_{max} (lg ε) = 417 (5.01), 515 (3.77), 547 (3.52), 590 (3.15), 647 nm (2.99); HRMS (MALDI): *m/z* calcd for [$C_{60}H_{58}Br_4N_4O_4$] [M+]: 1214.1192, found 1214.1183.

[5,10,15,20-Tetrakis(3-hydroxyphenyl)porphyrinato]cobalt(II) 129:

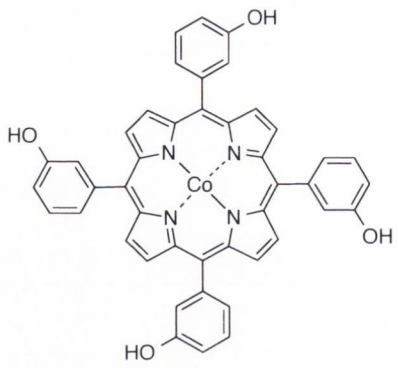

Synthesized according to general procedure C. 100 mg of **2** and $Co(OAc)_2$ (3 equiv.)(78 mg, 0.4 mmol) were added to a 100 mL Erlenmeyer flask containing DMF (10 mL). The flask was placed in a microwave and the reaction was run in 3 × 1 min intervals at 300 W with allocated time for cooling of the reaction mixture during each interval. The reaction mixture was diluted with CH_2Cl_2 and washed with water (3 x 100 mL) to remove residual DMF. The solvent was removed *in vacuo* and the product purified by recrystallization from ethyl acetate/*n*-hexane to yield 106 mg orange/purple solid **129** (0.14 mmol, 98%); M.p. >300 °C; R_f = 0.42 (CH_2Cl_2/*n*-hexane/MeOH = 3:1:0.2, v/v/v); ^{1}H NMR (400 MHz, [$(CD_3)_2SO$]): δ_H = 7.13 (d, $^3J_{H\text{-}H}$ = 7.95 Hz, 4H, -Ar*H*), 7.36 (s, 4H, -ArH_o), 7.40 (d, $^3J_{H\text{-}H}$ = 7.3 Hz 4H, -Ar*H*), 7.49 (t, $^3J_{H\text{-}H}$ = 7.9 Hz, 4H, -ArH_m), 8.75 ppm (s, 8H, -H_β), 9.81 ppm (s, br, 4H, -O*H*); ^{13}C NMR (100 MHz, [$(CD_3)_2SO$]): δ_C = 115.5, 119.3, 121.3, 125.3, 128.5, 129.3, 130.6, 132.2, 132.8, 141.6, 142.3, 156.4 ppm; UV/Vis (EtOAc): λ_{max} (lg ε) = 411 (6.24), 525 nm (5.09); HRMS (MALDI): *m/z* calcd for [$C_{44}H_{28}CoN_4O_4$] [M^+]: 735.1443, found 735.1435.

[5,10,15,20-Tetrakis(3-oxyphenyl)porphyrin]yltetrabutyl[5,10,15,20-tetrakis(3-oxyphenyl)porphyrinato]cobalt(II) 130:

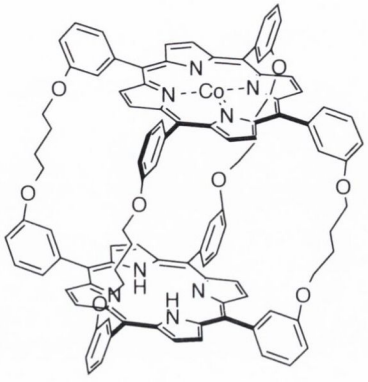

K_2CO_3 (41 mg, 0.3 mmol) was placed in a round bottom flask with DMF (40 mL). The flask was fitted with a dropping funnel containing a solution of Co-*m*-THPP, **129** (22.4 mg, 0.03 mmol) and **128** (40 mg, 0.03 mmol) in DMF (10 mL). The solution was added drop-wise over 24 h and once finished, allowed to stir for a further 12 h. The reaction mixture was diluted with CH_2Cl_2 and washed multiple times with water, brine and sodium bicarbonate. The solution was dried of Mg_2SO_4 and the solvent removed *in vacuo*. The resulting orange/purple solid was subjected to column chromatography, with the first orange band being the desired bisporphyrin. Recrystallization from ethyl acetate/*n*-hexane produced 6.3 mg of reddish orange crystals (0.0038 mmol, 12 %); M.p. >300 °C; R_f = 0.85 (CH_2Cl_2/*n*-hexane/MeOH = 3:1:0.2, v/v/v); ^{1}H NMR (600 MHz, $CDCl_3$): δ_H = -2.77 (s, 2H, -N*H*), 2.06 (m, 8H, -CH_2), 2.16 (m, 8H, -CH_2), 3.55 (m, 8H, -CH_2), 4.22 (t, 8H, -CH_2), 7.34 (d, 8H $^3J_{H\text{-}H}$ = 7.6 Hz, -Ar*H*), 7.66 (t, 8H, $^3J_{H\text{-}H}$ = 7.6 Hz, -Ar*H*), 7.79 (s, 8H, -Ar*H*), 7.84 (d, 8H, $^3J_{H\text{-}H}$ = 7.6 Hz, -Ar*H*), 8.91 ppm (m, 16H, -H_β); ^{13}C NMR (150 MHz, $CDCl_3$): δ_C = 27.9, 29.4, 33.3, 66.9, 113.9, 119.7, 120.9, 127.3, 127.6, 143.3, 157.1 ppm; UV/Vis (EtOAc): λ_{max} (lg ε) = 417 (5.04), 515 (3.75), 547 (3.50), 589 (3.09), 648 nm (2.96); HRMS (MALDI): *m/z* calcd for [$C_{104}H_{84}CoN_8O_8$] [M^+]: 1629.5588, found 1629.5509.

8.4 Anti-inflammatory bioconjugatges

General Procedure H:

Monofunctionalization of *m*-THPC: EDC (2 equiv.), HOBt (2 equiv.), K_2CO_3 (2 equiv.) were added to a 50 mL round bottomed flask and charged with DMF (10 mL). The appropriate anti-inflammatory agent (2-3 equiv.) was added and the reaction was allowed to stir for 60 minutes under argon. *m*-THPC (1 equiv.) was added to the mixture and the reaction was monitored by TLC and once significant conversion to the mono-substituted species was achieved, the reaction was terminated through the addition of CH_2Cl_2 (50 mL). The crude reaction mixture was washed with distilled water (1 × 30 mL), sat. aq. $NaHCO_3$ (1 × 30 mL), brine (1 × 30 mL), and distilled water (2 × 30 mL). The organic phase was dried over anhydrous sodium sulfate, filtered and evaporated under reduced pressure. Column chromatography proceeded on silica gel using CH_2Cl_2/*n*-hexane/MeOH (3:1:0.2, v/v/v) and recrystallization from ethyl acetate/*n*-hexane.

General Procedure I:

Tetrafunctionalization of *m*-THPC: *m*-THPC (1 equiv) was added to a round-bottomed flask (100 mL) and charged with DMF (10 mL) and K_2CO_3 (5-20 equiv). The reaction was left to stir for 60 minutes under argon before the appropriate functionalization reagent (10-20 equiv) was added. The reaction mixture was monitored by TLC and once full conversion to the desired degree of substitution was observed the reaction was terminated through the addition of CH_2Cl_2 (50 mL). The work-up proceeds as per general procedure H.

5,10,15-Tris(3-hydroxyphenyl)-20-[3-phenyl(2-amino-5-hydroxybenzoate]chlorin / 5,15,20-Tris(3-hydroxyphenyl)-10-[3-phenyl(2-amino-5-hydroxybenzoate]chlorin 150a:

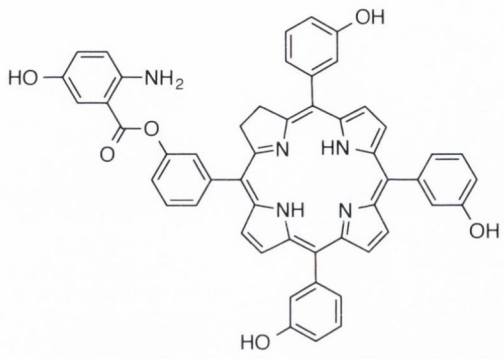

The compound was synthesized using general procedure H: a 50 mL round-bottom flask containing DMF (10 mL), **3** (100 mg, 0.147 mmol), EDC, **143** (46.0 mg, 0.294 mmol), HOBt, **144** (39.7 mg, 0.294 mmol), K_2CO_3 (40.6 mg, 0.294 mmol) and 5-hydroxyanthranilic acid, **140** (44.9 mg, 0.297 mmol) was allowed stir for 4 h. As predicted the NMR spectra indicates a mixture of regioisomers. Column chromatography on silica gel using CH_2Cl_2/*n*-hexane/MeOH (3:1:0.2, v/v/v) yielded 43.1 mg of a purple solid (0.053 mmol, 36%). Analytical data: M.p. >300 °C; R_f = 0.43 [CH_2Cl_2/*n*-hexane/MeOH (3:1:0.2, v/v/v)]; ^{1}H NMR (400 MHz, [$(CD_3)_2SO$]): δ_H = -1.68 (s, 1H, -N*H*), -1.61 (s, 1H, -N*H*), 4.14 (s, 4H, -H_β), 6.84 (m, 2H, -Ar*H*), 7.14 (m, 1H, -Ar*H*), 7.24 (m, 9H, -Ar*H*), 7.47 (m, 7H, -Ar*H*), 8.22 (d, 2H, $^3J_{H\text{-}H}$ = 4.9 Hz, -H_β), 8.3 (s, 2H, -H_β), 8.61 (d, 2H, $^3J_{H\text{-}H}$ = 4.9 Hz, H_β), 9.24 (s, 1H, -O*H*), 9.77 ppm (app d, 3H, -O*H*); ^{13}C NMR (100 MHz, [$(CD_3)_2SO$]: δ_C = 36.1, 115.1, 115.5, 119.7, 120.4, 122.3, 123.5, 123.7, 126.2, 128.3, 129.2, 131.7, 139.8, 141.5, 142.9, 143.3, 156.9, 157.2, 164.2 ppm; UV/Vis (EtOAc): λ_{max} (lg ε) = 420 (6.44), 507 (5.51), 534 (5.31), 589 (5.01), 645 nm (5.94); HRMS (MALDI) calcd for $[M]^+$ $C_{51}H_{37}N_5O_6$ 815.2744, found 815.2731.

5,10,15,20-Tetrakis[3-hydroxyphenyl)-20-[3-phenyl(2-amino-5-hydroxybenzoate]chlorin 150b:

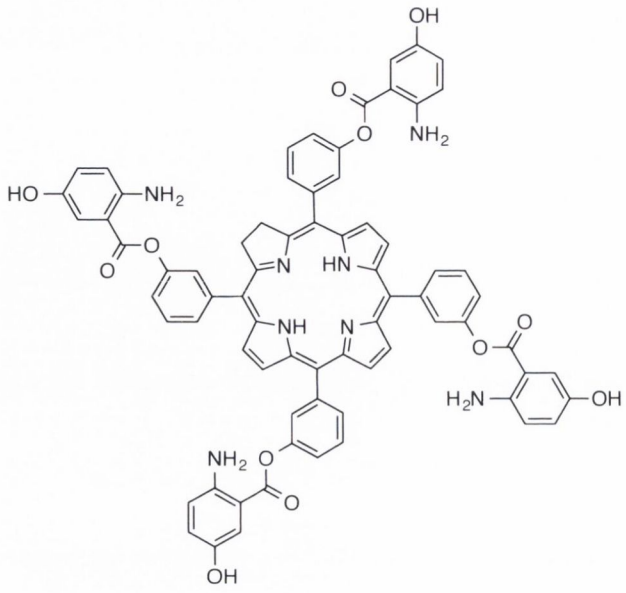

The compound was synthesized using general procedure I: a 50 mL round-bottom flask containing 10 mL of DMF, **3** (100 mg, 0.147 mmol), EDC, **143** (273 mg, 1.76 mmol), HOBt, **144** (238 mg, 1.76 mmol), K_2CO_3 (243 mg, 1.76 mmol) and anthranilic acid, **140** (269 mg, 1.76 mmol) was allowed stir for 20 h. Column chromatography on silica gel using CH_2Cl_2/*n*-hexane/MeOH (3:1:0.2, v/v/v) and recrystallization from ethyl acetate:*n*-hexane yielded 109 mg of purple crystals (0.089 mmol, 61% yield). M.p. > 300 °C; R_f = 0.91 [CH_2Cl_2/*n*-hexane/MeOH (3:1:0.2, v/v/v)]; ^{1}H NMR (400 MHz, $CDCl_3$): δ_H = -1.54 (s, br, 2H, -N*H*), 4.16 (s, 4H, -H_β), 7.05 (m, 4H, -Ar*H*), 7.14 (m, 4H, -Ar*H*), 7.22 (m, 8H, -Ar*H*), 7.29 (m, 8H, -Ar*H*) 7.42 (m, 4H, -Ar*H*), 7.55 (m, 4H, -Ar*H*), 8.59 (d, 4H, $^3J_{H\text{-}H}$ = 4.4 Hz, -H_β), 8.63 ppm (d, 4H, $^3J_{H\text{-}H}$ = 4.38 Hz, -H_β); ^{13}C NMR (100 MHz, $CDCl_3$, 25 °C): δ_C = 35.9, 114.3, 115.0, 115.4, 117.9, 119.6, 120.9, 121.3, 122.8, 123.2, 123.5, 126.3, 128.2, 128.9, 129.1, 139.7, 139.9, 141.7, 142.3, 156.6, 157.1, 168.2 ppm; UV/Vis (EtOAc): λ_{max} (lg ε) = 420 (6.44), 507 (5.51), 534 (5.31), 589 (5.01), 645 nm (5.94); HRMS (MALDI) calcd for $[M]^+$ $C_{72}H_{52}N_8O_{12}$ 1220.3705, found 1220.3693.

5,10,15-Tris(3-hydroxyphenyl)-20-[3-(2-{4-*iso*-butylphenyl}propanoate)phenyl]chlorin / 5,15,20-Tris(3-hydroxyphenyl)-10-[3-(2-{4-*iso*-butylphenyl}propanoate)phenyl]chlorin 151a:

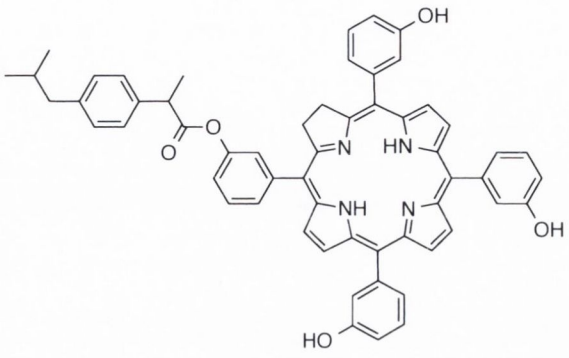

The compound was synthesized using general procedure H: a 50 mL round bottom flask containing DMF (10 mL), **3** (100 mg, 0.147 mmol), EDC, **143** (46.0 mg, 0.294 mmol), HOBt, **144** (39.7 mg, 0.294 mmol), K_2CO_3 (40.6 mg, 0.294 mmol) and ibuprofen, **147** (60.6 mg, 0.297 mmol) was allowed stir for 4 h. Column chromatography on silica gel using CH_2Cl_2/*n*-hexane/MeOH (3:1:0.2) yielded a mixture of monofunctionalized regioisomers in a yield of 45 mg of a purple solid (0.05 mmoles, 35%). Analytical data: M.p. >300 °C; R_f = 0.37 [CH_2Cl_2/*n*-hexane/MeOH (3:1:0.2, v/v/v)]; ^{1}H NMR (400 MHz, [$(CD_3)_2SO$]): δ_H = -1.67 (s, 2H, -N*H*), 1.12 (m, 9H, -CH_3), 2.04 (s, 2 H, -CH_2), 3.00 (m, 2 H, -C*H*), 4.13 (s, 4H, -H_β), 7.07 (m, 2 H, -Ar*H*), 7.13 (m, 2 H, -Ar*H*), 7.28 (m, 6H, -Ar*H*), 7.46 (m, 10H, -Ar*H*), 8.21 (d, 2H, $^3J_{H\text{-}H}$ = 4.9 Hz, -H_β) 8.35 (s, 2H, -H_β), 8.60 (d, 2H, $^3J_{H\text{-}H}$ = 4.9 Hz, -H_β), 9.75 ppm (s, 3H, -O*H*); ^{13}C NMR (100 MHz, [$(CD_3)_2SO_2$)]: δ_C = 8.1, 9.0, 31.1, 35.8, 46.0, 55.3, 112.5, 114.1, 115.1, 115.3, 117.8, 119.7, 121.5, 122.4, 123.4, 123.9, 125.7, 128.3, 128.5, 129.6, 129.9, 132.2, 132.2, 134.6, 140.2, 142.9, 143.8, 151.9, 157.4, 168.0 ppm; UV/Vis (EtOAc): λ_{max} (lg ε) = 420 (6.44), 507 (5.51), 534 (5.31), 589 (5.01), 645 nm (5.94) ; HRMS (MALDI) calcd for [M^+] $C_{57}H_{48}N_4O_5$ 868.3625, found 868.3613.

5,10,15,20-Tetrakis-[3-phenyl(2-{4-*iso*-butylphenyl}propanoate)]chlorin 151b:

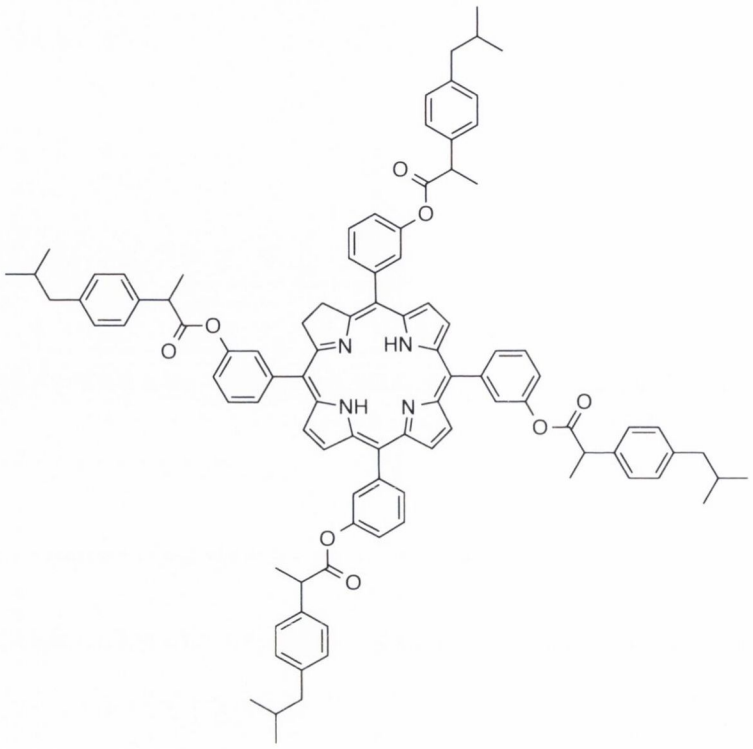

This target compound was synthesized using general procedure I: a 50 mL round bottom flask containing DMF (10 mL), **3** (100 mg, 0.147 mmol), EDC, **143** (273 mg, 1.76 mmol), HOBt, **144** (238 mg, 1.76 mmol), K_2CO_3 (243 mg, 1.76 mmol) and ibuprofen, **147** (363 mg, 1.76 mmol) was allowed stir for 18 h. Subsequent recrystallization yielded 140 mg of purple crystals (0.096 mmol, 65% yield). M.p. >300 °C; R_f = 0.91 [CH_2Cl_2/*n*-hexane/MeOH (3:1:0.2, v/v/v)]; ^{1}H NMR (400 MHz, $CDCl_3$): δ_H = -1.57 (s, 2H, -*N*H), 0.81 (m, 36H, -CH_3), 1.25 (s, 8H, -CH_2), 2.37 (m, 8H, -C*H*), 4.12 (s, 4H, -H_β), 7.07 (m, 8H, -Ar*H*), 7.28 (m, 8H, -Ar*H*), 7.28 (m, 6H, -Ar*H*), 7.46 (m, 10H, -Ar*H*), 8.21 (d, $^3J_{H\text{-}H}$ = 4.9 Hz, 2H, -H_β) 8.35 (s, 2H, -H_β), 8.60 ppm (d, $^3J_{H\text{-}H}$ = 4.9 Hz, 2H, -H_β); ^{13}C NMR (100 MHz, $CDCl_3$): δ_C = 8.1, 9.0, 31.1, 35.8, 46.0, 55.3, 114.6, 114.7, 114.8, 119.3, 119.4, 120.3, 123.3, 123.4, 123.7, 127.6, 129.6, 137.8, 140.4, 144.6 176.2 ppm; UV/Vis (EtOAc): λ_{max} (lg ε) = 419 (6.39), 507 (5.50), 535 (5.29), 590 (4.99), 645 nm (5.93); HRMS (MALDI) calcd for [M^+] $C_{96}H_{96}N_4O_8$ 1432.7228, found 1432.7215.

5,10,15-Tris(3-hydroxyphenyl)-20-[3-phenyl(2-(phenylamino)benzoate]chlorin / 5,15,20-Tris(3-hydroxyphenyl)-10-[3-phenyl(2-(phenylamino)benzoate]chlorin 152a:

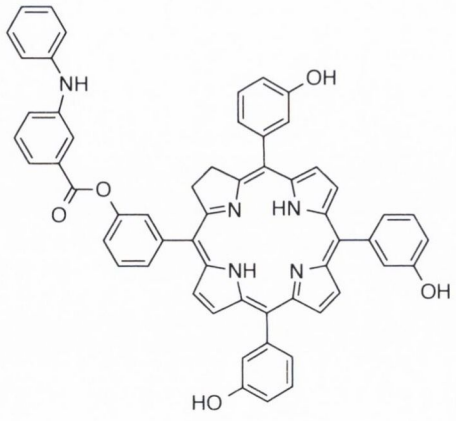

The compound was synthesized using general procedure H: a 50 mL round-bottom flask containing 10 mL of DMF, **3** (100 mg, 0.147 mmol), EDC, **143** (46.0 mg, 0.294 mmol), HOBt, **144** (39.7 mg, 0.294 mmol), K_2CO_3 (40.6 mg, 0.294 mmol) and fenamic acid, **139** (62.6 mg, 0.297 mmol) was allowed stir for 3 h. Column chromatography on silica gel using CH_2Cl_2/*n*-hexane/MeOH (3:1:0.2, v/v/v) produced a mixture of monofunctionalized regioisomers in a yield of 50.6 mg of a purple solid (0.064 mmoles, 45%). Analytical data: M.p. >300 °C; R_f = 0.43 [CH_2Cl_2/*n*-hexane/MeOH (3:1:0.2, v/v/v)]; ^{1}H NMR (400 MHz, [$(CD_3)_2SO$]): δ_H = -1.63 (s, 2H, -N*H*), 4.13 (s, 4H, -H_β), 6.86 (m, 2H, -Ar*H*), 7.06 (m, 3H, -Ar*H*), 7.23 (m, 8H, -Ar*H*), 7.31 (m, 3H, -Ar*H*), 7.46 (m, 8H, -Ar*H*), 7.67 (s, 1H, -Ar*H*), 8.21 (d, $^3J_{H\text{-}H}$ = 4.9 Hz, 2H, -H_β), 8.61 (m, 2H, -H_β), 8.85 (d, $^3J_{H\text{-}H}$ = 4.9 Hz, 2H, -H_β), 9.70 (s, 2H, -N*H*), 9.86 ppm (s, 3H, -O*H*); ^{13}C NMR (100 MHz, [$(CD_3)_2SO$]): δ_C = 36.1, 114.7, 118.3, 119.7, 121.5, 122.2, 122.3, 122.6, 123.9, 125.4, 128.3, 128.5, 129.9, 131.9, 132.0, 132.4, 134.5, 134.6, 142.8, 143.8, 149.5, 152.0, 156.3, 167.5 ppm; UV/Vis (EtOAc): λ_{max} (lg ε) = 420 (6.44), 507 (5.52), 534 (5.30), 589 (5.01), 645 nm (5.93); HRMS (MALDI) calcd for [M^+] $C_{57}H_{41}N_5O_5$ 875.3108, found 875.3117.

5,10,15,20-Tetrakis[3-phenyl(2-(phenylamino)benzoate]chlorin 152b:

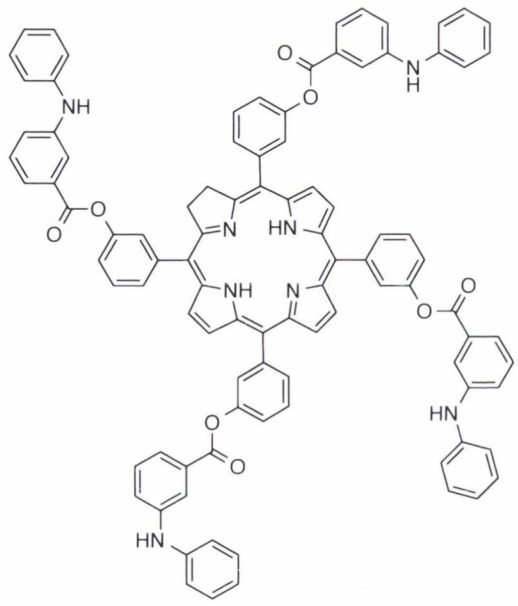

The compound was synthesized using general procedure I: a 50 mL round-bottom flask containing DMF (10 mL), **3** (100 mg, 0.147 mmol), EDC, **143** (273 mg, 1.76 mmol), HOBt, **144** (238 mg, 1.76 mmol), K_2CO_3 (243 mg, 1.76 mmol) and fenamic acid, **139** (257 mg, 1.76 mmol) was allowed stir for 20 h. Recrystallization from ethyl acetate:n-hexane yielded 178 mg of purple crystals (0.122 mmol, 83% yield). M.p. >300 °C; R_f = 0.91 [CH_2Cl_2/*n*-hexane/MeOH (3:1:0.2, v/v/v)] ^{1}H NMR (400 MHz, $CDCl_3$): δ_H = -1.65 (s, br, 2H, -N*H*), 4.17 (s, 4H, -H_β), 7.24 (m, 5H, -Ar*H*), 7.47 (m, 8H, -Ar*H*), 7.62 (m, 8H, -Ar*H*), 7.74 (m, 4H, -Ar*H*) 7.82 (m, 8H, -Ar*H*), 8.04 (m, 4H, -Ar*H*), 8.37 (m, 3H, -Ar*H*), 8.5 (m, 4H, -Ar*H*), 8.64 (m, 4H, -Ar*H*), 8.85 (m, 4H, -Ar*H*), 9.30 (s, 6H, -H_β), 9.70 ppm (s, br, 4H, -N*H*); ^{13}C NMR (100 MHz, $CDCl_3$): δ_C = 36.4, 112.6, 114.6, 114.8, 114.9, 115.5, 118.6, 121.5, 122.2, 122.3, 122.5, 129.1, 129.5, 129.6, 129.7, 129.9, 130.5, 151.9, 156.4, 157.6, 158.5, 167.9 ppm. UV/Vis (EtOAc): λ_{max} (lg ε) = 420 (6.44), 507 (5.51), 534 (5.31), 589 (5.01), 645 nm (5.94); HRMS (MALDI) calcd for [M^+] $C_{96}H_{68}N_8O_8$ 1460.5160, found 1460.5149.

5,10,15-Tris(3-hydroxyphenyl)-20-[3-phenyl(nicotinate]chlorin (11a) / 5,15,20-Tris(3-hydroxyphenyl)-10-[3-phenyl(nicotinate]chlorin 154a:

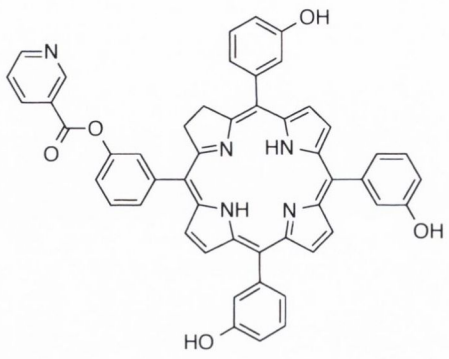

The compound was synthesized using general procedure H: a 50 mL round-bottom flask containing DMF (10 mL), **3** (100 mg, 0.147 mmol), EDC, **143** (46.0 mg, 0.294 mmol), Pyridine (0.3 mL) and nicotinic acid, **149** (36.2 mg, 0.297 mmol) was allowed stir for 2 h. NMR indicates a mixture of regioisomers. Column chromatography on silica gel using CH_2Cl_2/*n*-hexane/MeOH (3:1:0.2) yielded 49.6 mg of a purple solid which consisted of an inseparable mixture of monofunctionalized regioisomers (0.063 mmoles, 43 %). Analytical data: M.p. >300 °C; R_f = 0.43 [CH_2Cl_2/*n*-hexane/MeOH (3:1:0.2)]; ^{1}H NMR (400 MHz, [$(CD_3)_2SO$]): δ_H = -1.67 (s, 2H, -N*H*), 4.13 (s, 4H, -H_β), 7.06 (d, 2H, $^3J_{H-H}$ = 8.3 Hz, -Ar*H*), 7.14 (d, 2H, $^3J_{H-H}$ = 8.3 Hz, -Ar*H*), 7.25 (m, 8H, -Ar*H*), 7.66 (m, 8H, -Ar*H*), 8.21 (d, $^3J_{H-H}$ = 4.8 Hz, -H_β), 8.63 (d, 3H, $^3J_{H-H}$ = 4.8 Hz, -H_β), 9.21 ppm (s, br, 3H, -O*H*); ^{13}C NMR (100 MHz, [$(CD_3)_2SO$)]: δ_C = 36.7, 115.5, 120.4, 122.3, 126.2, 128.3, 129.2, 131.7, 139.8, 141.5, 142.9, 143.3, 156.9, 157.2, 165.4 ppm; UV/Vis (EtOAc): λ_{max} (lg ε) = 420 (6.44), 507 (5.51), 534 (5.31), 589 (5.01), 645 nm (5.94); HRMS (MALDI) calcd for [M^+] $C_{50}H_{35}N_5O_5$ 785.2638, found 785.2615.

5,10,15,20-Tetrakis[3-phenyl(nicotinate]chlorin 154b:

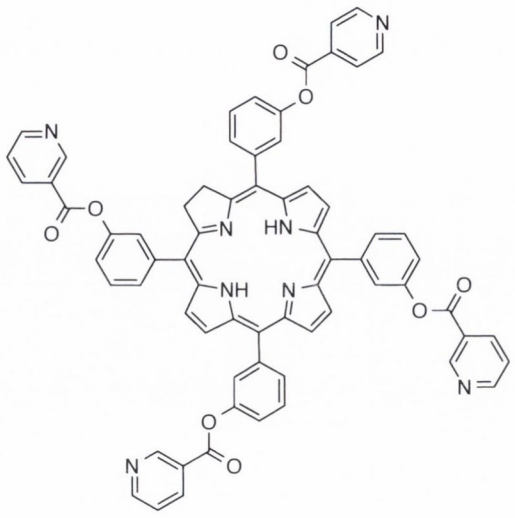

The compound was synthesized using general procedure I: a 50 mL round bottom flask containing DMF (10 mL), **3** (100 mg, 0.147 mmol), EDC, **143** (273 mg, 1.76 mmol), pyridine (1 mL) and nicotinic acid, **149** (216 mg, 1.76 mmol) was allowed stir for 20 h. Recrystalliztion from ethyl acetate:*n*-hexane *y*ielded 113 mg of purple crystals (0.102 mmol, 70% yield). M.p. >300 °C; R_f = 0.91 [CH_2Cl_2/*n*-hexane/MeOH (3:1:0.2, v/v/v)]; ^{1}H NMR (400 MHz, $CDCl_3$,): δ_H = -1.67 (s, br, 2H, -N*H*), 4.17 (s, 4H, -H_β), 7.60 (m, 8H, -Ar$H_{chlorin)}$, 7.83 (m, 8H, -Ar$H_{chlorin)}$, 8.04 (m, 4H, -ArH_{Nico}), 8.49 (m, 4H, -ArH_{Nico}), 8.85 (m, 8H, -Ar$H_{Nico)}$ 9.29 ppm(s, br, 6H, -H_β) ; ^{13}C NMR (100 MHz, $CDCl_3$): δ_C = 114.51, 119.52, 121.27, 127.46, 128.41, 155.85, 171.01 ppm; UV/Vis (EtOAc): λ_{max} (lg ε) = 420 (6.44), 507 (5.50), 535 (5.31), 589 (5.01), 644 nm (5.94); HRMS (MALDI) calcd for [M^+] $C_{68}H_{44}N_8O_8$ 1100.3282, found 1100.3292

8.5 Synthesis of Hexasubstituted Triptycene Derivatives

8.5.1 *General procedure J: Pd-catalyzed six-fold Suzuki coupling of 172 with aryl organoboron reagents:*

A 25 mL Schlenk tube equipped with a stirring bar and rubber septum was flushed for 10 min with argon gas and charged with hexabromotriptycene **172** (0.05 g, 0.07 mmol, 1 equiv.) and K_3PO_4 or Cs_2CO_3 (12-64 equiv.)and dried under high vacuum. The mixture was dissolved in anhydrous THF (5 mL) and was degassed *via* three freeze-pump-thaw cycles and was placed under argon. Boronic acid/ester (12-30 equiv.) and $Pd(Ph_3)_4$ (5-10 % per position) were added and the mixture was heated with stirring at 70 °C under argon atmosphere for 17-24 h. The solvent was removed under reduced pressure and the residue was dissolved in CH_2Cl_2 (10 mL). The crude product was washed sequentially with a saturated solution of sodium bicarbonate (1 x 20 mL) and brine (2 x 20 mL). The organic phase was dried over $MgSO_4$, the solvent was evaporated and the crude product was purified by recrystallization.

2,3,6,7,14,15-Hexakis(4-formylphenyl)triptycene 177:

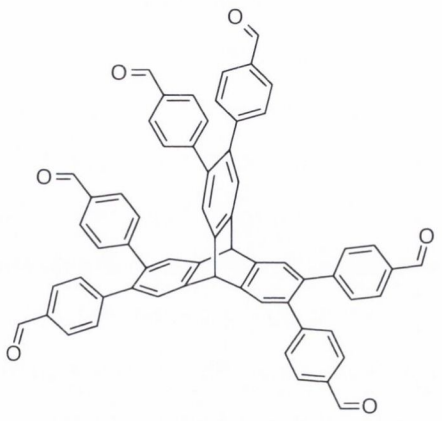

The title compound was prepared *via* general procedure J using Cs_2CO_3 (290 mg, 0.89 mmol), $Pd(PPh_3)_4$ (24 mg, 0.02 mmol,), 4-formylphenyl boronic acid (133 mg, 0.89 mmol). The crude product was purified by column chromatography on silica gel (CH_2Cl_2/methanol, 25:1, v/v) and gave the pure product **177** as the fourth fraction with 39 mg of white crystals (0.04 mmol, 64%). M.p. >300 °C; R_f = 0.55 (CH_2Cl_2/methanol, 20:1, v/v); ^{1}H NMR (400 MHz, $CDCl_3$): δ_H = 5.73 (s, 2H, triptycenyl bridgehead-*H*), 7.12 (d, *J* = 8.0 Hz, 12H, -Ar*H*), 7.49 (d, *J* = 8.0 Hz, 12H, -Ar*H*), 7.55 (s, 6H, -triptycenyl*H*), 9.94 ppm (s, 6H, -CHO); ^{13}C NMR (100 MHz, $CDCl_3$): δ_C = 53.0, 115.4, 125.8, 129.2, 130.1, 131.8, 134.3, 136.7, 144.2, 146.5, 191.3 ppm; HRMS (ES^+) [$C_{62}H_{38}O_6$]: calc. 878.2668, found 878.2683.

2,3,6,7,14,15-Hexakis(4-cyanophenyl)triptycene 178:

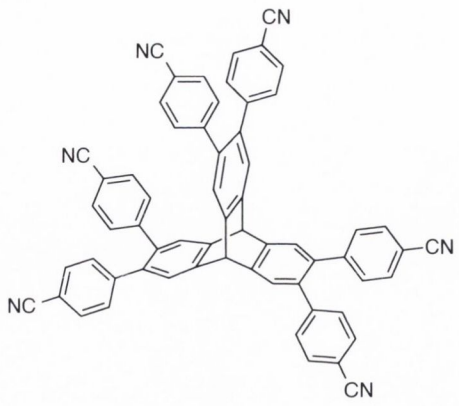

This compound was prepared *via* the general procedure J using Cs_2CO_3 (336 mg, 1.03 mmol), $Pd(PPh_3)_4$ (24 mg, 0.02 mmol), 4-cyanophenyl boronic acid (131 mg, 0.89 mmol). The crude product was purified by column chromatography on silica gel (CH_2Cl_2/*n*-hexane, 1:2, v/v) and gave the pure product as the third fraction as 38 mg of white powder of **178** (0.04 mmol, 63%). M.p. >300 °C; R_f = 0.38 (CH_2Cl_2/*n*-hexane, 1:1, v/v); ^{1}H NMR (400 MHz, $CDCl_3$): δ_H = 5.73 (s, 2H, -triptycenyl bridgehead*H*), 7.12 (d, *J* = 8.0 Hz, 12H, -Ar*H*), 7.49 (d, *J* = 8.0 Hz, 12H, -Ar*H*), 7.55 ppm (s, 6H, -triptycenyl*H*); ^{13}C NMR (100 MHz, $CDCl_3$): δ_C = 52.3, 110.7, 125.8, 129.9, 131.7, 136.1, 144.2, 144.6 ppm; HRMS (ES^+) [$C_{62}H_{32}N_6^+Na$]: calc. 883.2586, found 883.2604.

2,3,6,7,14,15-Hexakis(3-cyanophenyl)triptycene 179:

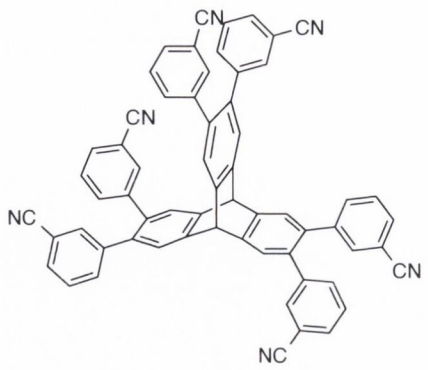

This compound was prepared *via* the general procedure J using Cs_2CO_3 (290 mg, 0.89 mmol), $Pd(PPh_3)_4$ (24 mg, 0.02 mmol),3-cyanophenyl boronic acid (197 mg, 1.3 mmol). The crude product was purified by column chromatography on silica gel (CH_2Cl_2/*n*-hexane, 1:2, v/v) and gave the pure product as the third fraction in 37 mg of white powder of **179** (0.04 mmol, 61 %). M.p. >300 °C; R_f = 0.40 (CH_2Cl_2/*n*-hexane, 1:1, v/v); ^{1}H NMR (400 MHz, $CDCl_3$): δ_H = 5.75 (s, 2H, -triptycenylbridgehead*H*), 7.21 (m, 6H, -Ar*H*), 7.29 (m, 6H, -Ar*H*), 7.39 (s, 6H, -Ar*H*), 7.50 (m, 6H, -Ar*H*), 7.56 ppm (s, 6H, -triptycenyl*H*); ^{13}C NMR (100 MHz, $CDCl_3$): δ_C = 52.4, 112.2, 117.9, 125.9, 128.7, 130.4, 132.6, 133.9, 135.5, 141.2, 144.3 ppm; HRMS (ES^+) [$C_{62}H_{32}N_6^+Na$]: calc. 883.2586, found 883.2585.

2,3,6,7,14,15-Hexakis(4-benzoic acid)triptycene 180b:

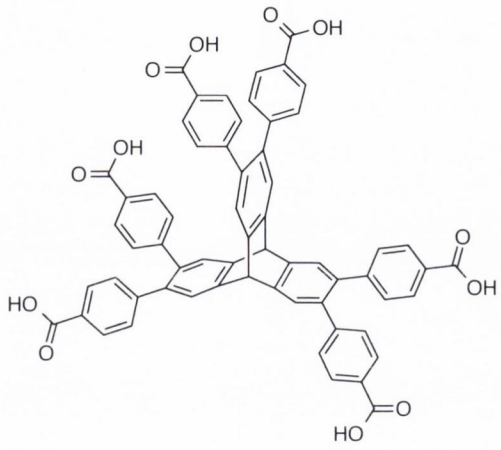

This compound was prepared *via* the general procedure J using Cs_2CO_3 (483 mg, 1.48 mmol, 20 equiv), $Pd(PPh_3)_4$ (24 mg, 0.02 mmol, 0.3 equiv), 4-methoxycarbonylphenylboronic acid (200 mg, 0.82 mmol, 15 equiv). The crude product was taken forward without further purification and isolation with subsequent hydrolysis to the free carboxylic acid. 160 mg (0.15 mmol, 1 equiv) of the crude material and KOH (1.69 g, 0.03 mol) dissolved in a minimal amount of H_2O was added to a flask containing a THF:MeOH (1:1) solvent mixture of 40 mL and brought to reflux for 24 h. After the elapsed time period, a further 100 equiv. of KOH (881 mg, 0.015 mmol) was added and allowed react for a further 18 h to drive the reaction to completion. The reaction mixture was taken into ethyl acetate and washed with 0.1 M HCl solution, then sodium bicarbonate, sodium chloride and water respectively. The solvent was removed *in vacuo* and the product was purified through filtration with DCM as a solvent and yielded 150 mg of a yellow/brown solid **180b** (0.154 mmol, 94%); Mp > 300 °C; R_f = 0.24 (EtOAc/*n*-hexane, 30:90, v/v); ^{1}H NMR (400 MHz, $CDCl_3$): δ_H = 5.59 ppm (s, 2H, -triptycenylbridgehead*H*), 7.02 (d, $J_{H,H}$ = 6.8 Hz, 12H, -Ar*H*), 7.45 (s, 6H, -triptycenyl*H*), 7.82 ppm (d, $J_{H,H}$ = 6.8 Hz, 12H, -Ar*H*); ^{13}C NMR (100 MHz, $CDCl_3$): δ_C = 52.9, 126.0, 129.4, 129.7, 129.9, 137.2, 144.4, 145.1, 168.8 ppm; HRMS (MALDI) calcd for [M^+] $C_{62}H_{38}O_{12}$ 974.2363, found 974.2357.

2,3,6,7,14,15-Hexakis(boronic acid pinacol ester)-triptycene 184:

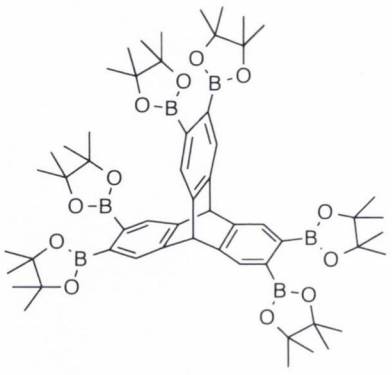

This compound was prepared *via* a modified version of general procedure J, using Cs_2CO_3 (224 mg, 0.687 mmol), $PdCl_2(PPh_3)_2$ (3 mg, 0.0041 mmol), Bis(pinacolato)diboron (837 mg, 3.3 mmol) in DCE (10 mL). The reaction mixture was washed with KCl and then followed the routine procedure with subsequent recrystallization from EtOAc/*n*-hexane afforded 91 mg of white crystals of **184** (0.9 mmol, 36%). M.p. = 129 °C; R_f = 0.23; (EtOAc/ *n*-hexane, 1:5, v/v); ^{1}H NMR (400 MHz, $CDCl_3$): δ_H = 1.33 (s, 72H, CH_3), 5.44 (s, 2H, -triptycenyl bridgehead*H*), 7.63 ppm (s, 6H, aryl -triptycenyl*H*). ^{13}C NMR (150 MHz, $CDCl_3$): δ_C = 24.9, 54.0, 83.6, 128.8, 132.1, 145.7 ppm; HRMS (MALDI) calcd. for [M^+] $C_{56}H_{80}B_6O_{12}$ 1010.6208, found 1010.6243.

8.5.2 Sonogashira Couplings

2,3,6,7,14,15-Hexakis(trimethylsilylethynyl)triptycene 186:

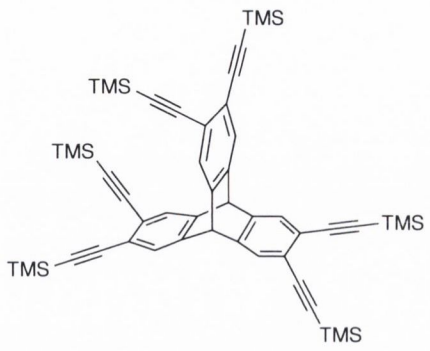

A mixture of hexabromotriptycene **172** (102 mg, 0.14 mmol), CuI (17 mg, 0.09 mmol, 0.65) and PPh_3 (44 mg, 1.68 mmol) were placed in a 50 mL Schlenk flask and dried under high vacuum. The mixture was dissolved in anhydrous triethylamine (5 mL) under an argon atmosphere and was degassed *via* three freeze-pump-thaw cycles. Trimethylsilylacetylene, **185** (0.48 mL, 3.36 mmol, 24 equiv) and $PdCl_2(PPh_3)_2$ (59 mg, 84 μmol,) were added and heated at 80 °C for 24h. The progress of the reaction was monitored by TLC. The solvent was removed under reduced pressure and the reaction mixture was filtered through a small plug of silica eluting with CH_2Cl_2 (50 mL). The crude product mixture was purified by flash chromatography on silica gel (EtOAc/*n*-hexane, 1:99, v/v) to afford 75 mg a brown/orange residue **186** (75 mg, 0.09 mmol, 64%). M.p. >300 °C; R_f = 0.74 (EtOAc/*n*-hexane, 1:99 v/v); ^{1}H NMR (400 MHz, $CDCl_3$): δ = 0.22 (s, 54H, CH_3), 5.19 (s, 2H, bridgehead C*H*), 7.39 ppm (s, 6H, Ar-*H*); ^{13}C NMR (150 MHz, $CDCl_3$): δ_C = 0.9, 52.5, 98.2, 103.1, 123.4, 127.4, 143.2 ppm; UV-vis (CH_2Cl_2): λ_{max} (lg ε) = 279 (3.55), 298 (4.13), 322 nm (3.66); HRMS (MALDI LD$^+$) [$C_{50}H_{62}Si_6$]: calcd. 830.3467; found 830.3483.

2,3,6,7,14,15-Hexaethynyltriptycene 187:

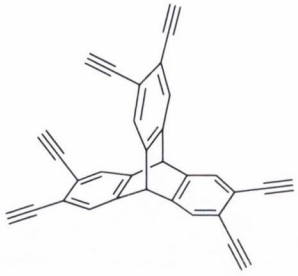

Compound **186** (280 mg, 0.34 mmol) was dissolved in THF (6 mL) and TBAF (1 M in THF, 2.2 mL) was added. The reaction was monitored by TLC using EtOAc/*n*-hexane (1:4, v/v). Upon completion, the solvent was removed *in vacuo* and dissovled in CH_2Cl_2 (20 mL) and dry loaded onto silica gel. The residue was filtered through a plug of silica using EtOAc/*n*-hexane (1:4, v/v). The solvent was removed *in vacuo* and the residue was recrystallized from $CHCl_3$/hexane to gave 107 mg of a off-white solid **187** (0.27 mmol, 80%). R_f = 0.28 (EtOAc/*n*-hexane, 1:4, v/v); M.p. = decomposed at 140 °C; ^{1}H NMR (400 MHz, $CDCl_3$): δ_H = 3.24 (s, 6H, alkyne-*H*), 5.33 (s, 2H, bridgehead, -C*H*), 7.49 ppm (s, 6H, Ar-*H*); ^{13}C NMR (100 MHz, $CDCl_3$): δ_C = 52.4, 81.0, 81.5, 127.9, 123.0, 143.6 ppm; UV-vis (CH_2Cl_2): λ_{max} (lg ε) = 289 (3.78), 300 (3.56), 314 (3.47); HRMS (ES^+) [$C_{32}H_{14}$]: calcd. for 398.1096; found 398.1073.

8.2.3 Brominated precursors

Bromoporphyrins **118** [491], **119** [491], **188** [492], **189** [493], **190** [275], **192** [364]were synthesized *via* methods developed by Boyle and co-workers [275] and NMR data were in accordance to those reported in the literature.

General Prodecure K: Bromination

5,15 porphyrins were dissolved into $CHCl_3$ and NBS (0.8 - 2.1 equiv.) and pyridine (0.1 mL) were added. The reaction progression was monitored by TLC using $CHCl_3$: *n*- hexane (1 : 1, v/v). Once all the starting material was consumed, the solvents were removed *in vacuo* and the mixture was then filtered through a silica gel plug and recrystallised from CH_2Cl_2/MeOH.

5-Bromo-10,20-bis(phenyl)porphyrin 190 [275]**:**

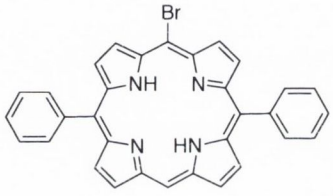

Synthesized from **43,** using 0.75 eq NBS. Column chromatography using *n*-hexane:toluene (3:1, v/v) yielded **190** as a purple powder (60%) and used without further purification. M.p. > 300 °C; ^{1}H NMR ($CDCl_3$): δ_H = -2.80 ppm (br s, 2H, -N*H*), 7.83 (m, 6H, -Ar*H*), 8.27 (m, 4H, -Ar*H*), 9.05 (2H, m, -H_β), 9.07 (m, 2H, -H_β), 9.39 (m, 2H, -H_β), 9.73 (m, 2H, -H_β), 10.29 (s, 1H, -meso*H*) ppm. The NMR data was in agreement with the literature [275].

{5-Iodo-10,15,20-triphenylporphyrinato}nickel(II) 191b [363]:

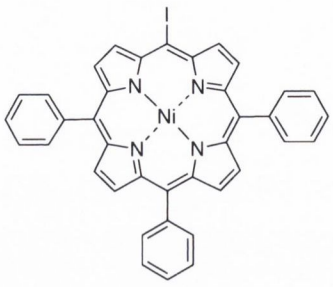

Synthesized from **191a** (200 mg, 0.34 mmol), I_2 (130 mg, 0.52 mmol), and $C_6H_5I(O_2CCF_3)_2$ (160 mg, 0.37 mmol) in $CHCl_3$ (200 mL) to yield 228 mg of **191b** as purple crystals (0.32 mmol, 93%); M.p. = 265 °C. ^{1}H NMR (400 MHz, $CDCl_3$, 25 °C): δ_H = 7.65–7.71 (m, 9H, -Ar*H*), 7.95–7.97 (m, 6H, -Ar*H*), 8.66-8.70 (m, 4H, -H_β), 8.73 (d, $^3J_{H\text{-}H}$ = 5.0 Hz, 2H, -H_β), 9.47 (d, $^3J_{H\text{-}H}$ = 5.0 Hz, 2H, -H_β) ppm.[363]

8.2.4 Borylation

Porphyrin **198** [354] was borylated according to standard procedures and spectroscopic data agreed with those in the literature.

General Procedure L – Borylation of haloporphyrins:

The borylation of haloporphyrins was carried out adapting a procedure by Therien and coworkers [354]. Bromoporphyrin (1 equiv.) and $Pd(PPh_3)_4$ (0.2 equiv.) were charged to a Schlenk flask and dried under high vacuum. 1,2-Dichloroethane (10 mL) and NEt_3 (0.2 mL) were then added and the solution was degassed *via* three freeze-pump-thaw cycles, before the flask was purged with argon. Pinacolborane (15 equiv.) was then added and the flask was sealed and stirred at 90 °C. The reaction was followed by TLC using CH_2Cl_2 : *n*-hexane (2:1, v/v). Once the starting material was consumed, the reaction was quenched with a saturated KCl solution (10 mL), washed with water, and dried over $MgSO_4$. The solvent was removed *in vacuo* and the residue was subjected to column chromatography using CH_2Cl_2 : *n*-hexane (1:1, v/v).

5-(4,4,5,5-Tetramethyl-1,3,2-dioxaborolan-2-yl)-10,15,20-tri(4-methyl-phenyl)porphyrin 198 [361]:

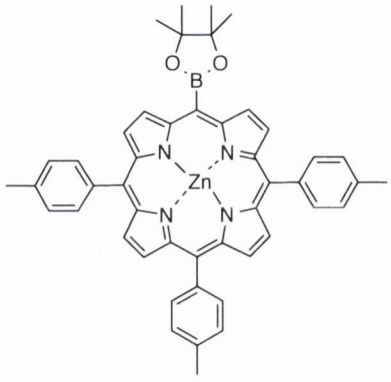

Produced from **83** (63 mg, 0.102 mmol) with $Pd(PPh_3)_4$ (23 mg, 0.020 mmol) and pinacolborane (1.53 mmol, 0.20 mL) following general procedure D. After purification using column chromatography, **128** was obtained as a purple solid (37 mg, 0.056 mmol, 54 %,). M.p. >300 °C; Spectroscopic data agreed with that reported in the literature. ^{1}H NMR (400 MHz; $CDCl_3$): δ_H = 1.82 (s, 9H, -CH_3), 2.69 (s, 3H, -CH_3), 2.71 (s, 6H, -CH_3), 7.53 (d, 2H, $^3J_{H\text{-}H}$ = 7.4 Hz, -ArH), 7.55 (d, 4H, $^3J_{H\text{-}H}$ = 7.6 Hz, -ArH), 8.07 (d, 2H, $^3J_{H\text{-}H}$ = 7.7 Hz, -ArH), 8.08 (d, 4H, $^3J_{H\text{-}H}$ = 7.5 Hz, -ArH), 8.93 (d, 2H, $^3J_{H\text{-}H}$ = 4.6 Hz, H_β), 8.94 (d, 2H, $^3J_{H\text{-}H}$ = 4.6 Hz, H_β), 9.08 (d, 2H, $^3J_{H\text{-}H}$ = 4.6 Hz, H_β), 9.88 ppm (d, 2H, $^3J_{H\text{-}H}$ = 4.6 Hz, H_β). [361]

8.2.5 Synthesis of Aminoporphyrins

Amino Porphyrins 201 [494], 202 [372] and 203 [373] were synthesized according literature procedures and their experimental data agreed with the data in the literature.

5-(Aminophenyl)-10,15,20-tri(4-methylphenyl)porphyrin 201 [378]:

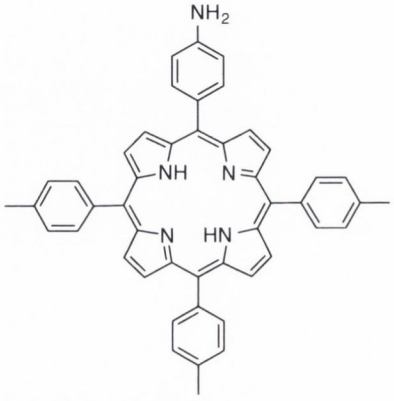

5-(4-acetamidophenyl)-10,15,20-tri(4-methylphenyl)porphyrin (0.71 g, 0.001 mol) was refluxed for 4 h in 50 mL of 1:1(v/v) ethanol/concentrated aqueous HCl. After being cooled to r.t. the solution was added to 50 mL of saturated sodium acetate solution and extracted with 100 mL of $CHCl_3$. The $CHCl_3$ solution was washed twice with 20 mL of H_20 and dried over sodium sulfate. Purple crystals were obtained by reducing the volume to 10 mL and adding 10 mL of methanol; yield 0.61 g (86%). ^{1}H NMR (400 MHz; $CDCl_3$): δ_H = -2.7 (s br, 2H, N*H*), 2.68 (s, -CH_3), 7.01 (m, -Ar*H*), 7.53 (m, -Ar*H*), 7.98, 8.09 (m, -Ar*H*), 8.83 (d, 6H, $^3J_{H\text{-}H}$ = 5.0 Hz, -H_β), 8.87 ppm (d, 2H, $^3J_{H\text{-}H}$ = 5.0 Hz, -H_β). [378]

5-(4-Aminophenyl)-10,15,20-(3-methoxypheny)porphyrin 202 [365]:

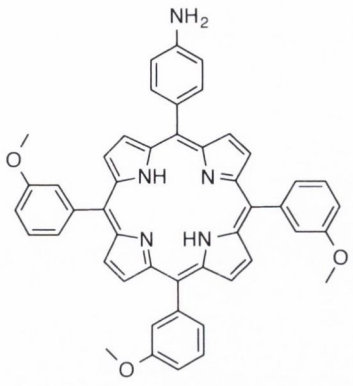

5,10,15-(3-methoxyphenyl)-20-(4-nitrophenyl)porphyrin **218** (100 mg, 0.14 mmol) was dissolved in a mixture of dry dichloromethane (6 mL) and dry methanol (6 mL), 10 % palladium on charcoal (40 mg) was added and the mixture purged with nitrogen. After 5 min sodium borohydride (20 mg) was added and the resultant purple-yellow mixture was stirred under nitrogen for 5 min. CH_2Cl_2 (15 mL) was then added and the mixture was filtered through a short celite 545 (Merck) column and the filtrate was evaporated to dryness. The residue was chromatographed on preparative silica gel plates using dichloromethane as the eluent. The less polar and more abundant band was collected; the resulting residue was recrystallized from dichloromethane/petroleum ether giving porphyrin **202** as purple crystals (43 mg, 45 %). M.p. = 280 °C; ^{1}H NMR (400 MHz, $CDCl_3$) δ_H = -2.78 (s, 2H, -N*H*), 3.93 (br s, 2H, -N*H*), 3.98 (br s, 9H, -OCH_3), 7.00 (d, 2H, $^3J_{H\text{-}H}$ = 9.04 Hz, -Ar*H*), 7.30-7.34 (m, 3H, -Ar*H*), 7.61-7.67 (m, 3H, -Ar*H*), 7.78-7.82 (m, 6H, -Ar*H*), 7.97 (d, 2H, $^3J_{H\text{-}H}$ = 9.04 Hz, 5, -Ar*H*), 8.86-8.93 ppm (d, 8H, $^3J_{H\text{-}H}$ = 5.0 Hz, H_β). [365]

8.2.6 Synthesis of non-porphyrin based chromophores

Ethyl 2-(6-hydroxy-3-oxo-3H-xanthen-9-yl)benzoate 207 [374] :

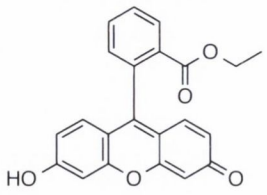

$BF_3{\cdot}OEt_2$ (9.06 mL, 71.5 mmol) was added drop wise to a suspension of fluorescein **206** (3.3g, 8.94 mmol) in EtOH (30 mL) and the reaction mixture was refluxed over night. The mixture was cooled, diluted with EtOAc (100 mL). Water was added and the organic layer extracted with EtOAc (3 x 50 mL). The organic layer was washed with water (2 x 50 mL) and brine (20 mL), dried over sodium sulfate and solvent evaporated to afford 2.9 g of crude ethyl 2-(6-hydroxy-3-oxo-3H-xanthen-9- yl)benzoate (8.88 mmol, 95 %) as a dark red solid which was used without further purification. ^{1}H NMR (400 MHz, [$(CD_3)_2SO$],): δ_H = 0.85 (t, 3H, $^3J_{H\text{-}H}$ = 7.0 Hz), 3.95 (q, 2H, $^3J_{H\text{-}H}$ = 7.0 Hz), 6.54 (m, 3H), 6.78 (d, 2H, $^3J_{H\text{-}H}$ = 9.8 Hz), 7.48 (d, 1H, $^3J_{H\text{-}H}$ = 7.2 Hz), 7.76 (t, 1H, $^3J_{H\text{-}H}$ = 7.5 Hz), 7.85 (t, 1H, $^3J_{H\text{-}H}$ = 7.3 Hz), 8.17 ppm (d, 1H, $^3J_{H\text{-}H}$ = 7.6 Hz).[374]

6-hydroxy-9-(2-(hydroxymethyl)phenyl)-3H-xanthen-3-one 208 [374]:

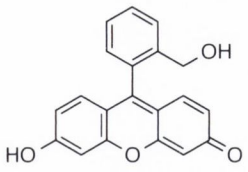

A solution of DIBAL-H (5.48 mL, 5.48 mmol) was added dropwise to a solution of ethyl 2-(6-hydroxy-3-oxo-3H-xanthen-9-yl)benzoate **207** (0.663 g, 1.097 mmol) in DCM (15 mL) at -78 °C under argon. The resulting solution was stirred for 10 min, and then allowed to warm up to rt over 2 h. A saturated solution of ammonium chloride (2 mL) was added and the mixture stirred for 10 min at room temperature. Ether (50 mL) and DDQ (0.274 g, 1.206 mmol) were added and the mixture stirred for another 30 min. The reaction mixture was filtered through a pad of Celite. The solvents were evaporated and the crude mixture purified by silica gel chromatography eluting with EtOAc/Hexane (1:1) to afford 320 mg 6-hydroxy-9-(2-(hydroxymethyl)phenyl)-3H-xanthen-3-one **208** (0.569 mmol, 52% yield) as a yellow oil. ^{1}H NMR (400 MHz, [$(CD_3)_2SO$]): δ_H = 4.63 (s, 2H), 6.54 (m, 3H), 6.78 (d, 2H, $^{3}J_{H\text{-}H}$ = 9.8 Hz), 7.48 (d, 1H, $^{3}J_{H\text{-}H}$ = 7.2 Hz), 7.76 (t, 1H, $^{3}J_{H\text{-}H}$ = 7.5 Hz), 7.85 (t, 1H, $^{3}J_{H\text{-}H}$ = 7.3 Hz) 8.17 ppm (d, 1H, $^{3}J_{H\text{-}H}$ = 7.6 Hz).[374]

Chapter 9 References

(1) Yashchuk, Y.; Tyurin, V.; Beletskaya, I. *Protection of Metals* **2008**, *44*, 569-576.
(2) Austin, B. Y.; Jacob, W.; José, L. M.-F. *Chem. Biol. Drug Des.* **2012**, *80*, 717-724.
(3) Elemans, J. A. A. W.; van, H. R.; Nolte, R. J. M.; Rowan, A. E. *Adv. Mater. (Weinheim, Ger.)* **2006**, *18*, 1251-1266.
(4) Anderson, H. L. *Inorganic chemistry* **1994**, *33*, 972-981.
(5) Anderson, H. L. *Chemical Communications* **1999**, 2323-2330.
(6) Fenwick, O.; Sprafke, J. K.; Binas, J.; Kondratuk, D. V.; Di Stasio, F.; Anderson, H. L.; Cacialli, F. *Nano Letters* **2011**, *11*, 2451-2456.
(7) *Physical Chemistry Chemical Physics* **2014**, *16*, 4386.
(8) *Materials Chemistry and Physics* **2013**.
(9) Koehn, F. E.; Carter, G. T. *Nature Reviews Drug Discovery* **2005**, *4*, 206-220.
(10) Leach, A. R.; Gillet, V. J.; Lewis, R. A.; Taylor, R. *J. Med. Chem* **2010**, *53*, 539-558.
(11) Lyne, P. D. *Drug Discovery Today* **2002**, *7*, 1047-1055.
(12) Kelly, T. R. *Accounts of Chemical Research* **2001**, *34*, 514-522.
(13) Kelly, T. R.; Bowyer, M. C.; Bhaskar, K. V. *Journal of the American Chemical Society* **1994**, *116*, 3657-3658.
(14) Cox, A. M. *Postgraduate medical journal* **1995**, 643-645.
(15) Society, A. C. http://www.cancer.org/research/cancerfactsstatistics/cancerfactsfigures2014/ **2014**.
(16) Sarr, M. G.; Hamilton, S. R.; Marrone, G. C. *Am. J. Surg.* **1985**, *149*, 187-193.
(17) Shaheen, N.; Ransohoff, D. F. *Jama* **2002**, *287*, 1972-1981.
(18) Ethirajan, M.; Chen, Y.; Joshi, P.; Pandey, R. K. *Chemical Society Reviews* **2011**, *40*, 340-362.
(19) Huang, Z. *Technology in cancer research & treatment* **2005**, *4*, 283-293.
(20) Raab, O. *Zeitung Biol.* **1900**, *39*, 524-526.
(21) Lipson, R. L.; Baldes, E. J. *Arch. Dermatol.* **1960**, *82*, 508-516.
(22) Lipson, R. L.; Baldes, E. J.; Olsen, A. M. *J. Natl. Cancer Inst.* **1961**, *26*, 1-11.
(23) Schwartz, S. K.; Abolon, K.; Vermund, H. *Univ. Minn. Med. Bull.* **1955**, *27*, 7-8.
(24) Hasan, T.; Ortel, B.; Moor, A.; Pogue, B. *Holland-Frei Cancer Med* **2003**, *Ch. 40(BC Decker, Inc., Hamilton, Ontario, 2003).*
(25) Diamond, I.; Mcdonagh, A. F.; Wilson, C. B.; Granelli, S. G.; Nielsen, S.; Jaenicke, R. *Lancet* **1972**, *300*, 1175-1177.
(26) Dougherty, T. J.; Grindey, G. B.; Fiel, R.; Weishaupt, K. R.; Boyle, D. G. *J. Natl. Cancer Inst.* **1975**, 115-121.
(27) Kelly, J. F.; Snell, M. E.; Berenbaum, M. C. *Br J. Cancer* **1975**, 237-244.
(28) Kelly, J. F.; Snell, M. E. *J. Urol.* **1976**, *115*, 150-151.
(29) Dougherty, T. J.; Lawrence, G.; Kaufman, J. H.; D., B.; R., W. K.; A., G. *J. Natl. Cancer Inst.* **1979**, *62*, 231-237.
(30) Mang, T. S.; Allison, R.; Hewson, G.; Snyder, W.; Moskowitz, R. *Cancer J. Sci. Am.* **1998**, 378-384.
(31) Dimofte, A.; Zhu, T. C.; Hahn, S. M.; Lustig, R. A. *Lasers Surg. Med.* **2002**, *31*, 305-312.
(32) Ward, B. G.; Forbes, I. J.; Cowled, P. A.; McEvoy, M. M.; Cox, L. W. *Am. J. Obstet. Gynecol.* **1982**, *142*, 356-357.
(33) Hornung, R. *Curr. Drug Targets Immune Endocr. Metabol. Disord.* **2001**, *1*, 165-177.
(34) M.K., F.; Hornung, R.; Schwarz, V. A.; Simeon, R.; Haller, U.; Wyss, P. *Gynecol. Oncol.* **2002**, *80*, 62-66.
(35) Gomer, C. J.; Doiron, D. R.; Jester, J. V.; Szirth, B. C.; Murphree, A. L. *Cancer Res.* **1983**, 721-727.
(36) Favilla, I.; Favilla, M. L.; Gosbell, A. D.; Barry, W. R.; Ellims, P.; Hill, J. S.; Byrne, J. R. *Melanoma Res.* **1995**, *5*, 355-364.
(37) Landau, I. M.; Steen, B.; Seregard, S. *Acta Ophthalmol. Scand.* **2002**, 531-536.
(38) Sandeman, D. R. *Lasers Med. Sci.* **1986**, 163-167.
(39) Popovic, E. A.; Kaye, A. H.; Hill, J. S. *J. Clin. Laser Med. Surg.* **1996**, 251-261.
(40) Biel, M. A. *Laryngoscope* **1998**, *108*, 1259-1268.

(41) Schweitzer, V. G. *Otolaryngol. Head Neck Surg.* **1990**, 225-232.
(42) Barr, H.; Krasner, N.; Boulos, P. B.; Chatlani, P.; Bown, S. G. *Br. J. Surg.* **1990**, *77*, 93-96.
(43) Allison, R. R.; Mang, T. S.; Wilson, B. D.; *Semin. Cutan. Med. Surg.* **1998**, *17*, 153-163.
(44) Taber, S. W.; Fingar, V. H.; Coots, C. T.; Wieman, T. J. *Clin. Cancer Res.* **1998**, *4*, 2741-2746.
(45) Bown, S. G.; Rogowska, A. Z.; Whitelaw, D. E.; Lees, W. R.; Lovat, L. B.; Ripley, P.; Jones, L.; Wyld, P.; Gillams, A.; Hatfield, A. W. R. *Gut* **2002**, *50*, 549-557.
(46) J., D. E. J. G.; Dolmans, D. F.; J., R. K. *Nat. Rev. Cancer* **2003**, *3*, 380-387.
(47) Henderson, B. W.; Dougherty, T. J. *Photochem. Photobiol.* **1992**, *55*, 145-157.
(48) Moan, J.; Berg, K. *Photochem. Photobiol.* **1992**, *55*, 931-948.
(49) Dougherty, T. J.; Gomer, C. J.; Henderson, B. W.; Jori, G.; Kessel, D.; Korbelik, M.; Moan, J.; Peng, Q. *J. Natl. Cancer Inst.* **1998**, *90*, 889-905.
(50) Hsi, R. A.; Rosenthal, D. I.; Glatstein, E. *Drugs* **1999**, *57*, 725-734.
(51) Hamblin, M. R.; Hasan, T. *Opt. Photonics News* **1996**, *7*, 16-21.
(52) Matsumura, Y.; Maeda, H. *Cancer Res.* **1986**, *46*, 6387-6392.
(53) Henderson, B. W.; Bellnier, D. A.; Greco, W. R.; Sharma, A.; Pandey, R. K.; Vaughan, L. A.; Weishaupt, K. R.; Dougherty, T. J. *Cancer Res.* **1997**, *57*, 4000-4007.
(54) Pandey, R. K.; Sumlin, A. B.; Constantine, S.; Aoudla, M.; Potter, W. R.; Bellnier, D. A.; Henderson, B. W.; Rodgers, M. A.; Smith, K. M.; Dougherty, T. J. *Photochem. Photobiol.* **1996**, *64*, 194-204.
(55) Moan, J.; Rimington, C.; Western, A. *Int. J. Biochem* **1988**, *20*, 1401-1404.
(56) Cairns, R. A.; Harris, I. S.; Mak, T. W. *Nat. Rev. Cancer* **2011**, *11*, 85-95.
(57) Wike-Hooley, J. L.; Haveman, J.; S., R. H. *Radiother. Oncol.* **1984**, *2*, 343-366.
(58) Thomas, J. P.; Girotti, A. W. *Photochem. Photobiol.* **1989**, *49*, 241-247.
(59) Moan, J.; Ma, L. W.; Bjørklund, E. *J Photochem Photobiol B.* **1999**, *50*, 94-98.
(60) Henderson, B. W.; Waldow, S. M.; Mang, T. S.; Potter, W. R.; Malone, P. B.; J., D. T. *Cancer Res.* **1985**, *45*, 572-576.
(61) Korbelik, M.; Krosl, G. *Br. J. Cancer* **1994**, *70*, 604-610.
(62) Messmann, H.; Mlkvy, P.; Buonaccorsi, G.; Davies, C. L.; MacRobert, A. J.; Bown, S. G. *Br. J. Cancer* **1995**, *72*, 589-594.
(63) Pogue, B. W.; Hasan, T. *Radiat. Res.* **1997**, *147*, 551-559.
(64) Fingar, V. H.; Wieman, T. J.; Haydon, P. S. *Photochem. Photobiol.* **1997**, *66*, 513-517.
(65) Fingar, V. H.; Kik, P. K.; Haydon, P. S.; Cerrito, P. B.; Tseng, M.; Abang, E.; Wieman, T. J. *Br. J. Cancer* **1999**, *79*, 1702-1708.
(66) Dolmans, D. E.; Kadambi, A.; Hill, J. S.; Waters, C. A.; Robinson, B. C.; Walker, J. P.; Fukumura, D.; Jain, R. K. *Cancer Res.* **2002**, *62*, 2151-2156.
(67) Henderson, B. W.; Fingar, V. H. *Cancer Res.* **1987**, *47*, 3110-3114.
(68) Chen, Q.; Chen, H.; Hetzel, F. W. *Photochem. Photobiol.* **1996**, *63*, 128-131.
(69) Carmeliet, P.; Jain, R. K. *Nature* **2000**, *407*, 249-257.
(70) Jain, R. K.; Carmeliet, P. F. *Sci. Am.* **2001**, *285*, 38-45.
(71) Henderson, B. W.; Fingar, V. H. *Photochem. Photobiol.* **1989**, *49*, 299-304.
(72) Ferrario, A.; von Tiehl, K.; Wong, S.; Luna, M.; Gomer, C. J. *Cancer Res.* **2002**, *62*, 3956-3961.
(73) Gollnick, S. O.; Liu, X.; Owczarczak, B.; Musser, D. A.; Henderson, B. W. *Cancer Res.* **1997**, *57*, 3904-3909.
(74) Shumaker, B. P.; Hetzel, F. W. *Photochem. Photobiol.* **1987**, *46*, 899-901.
(75) Korbelik, M.; Krosl, G.; Krosl, J.; Dougherty, G. J. *Cancer Res.* **1996**, *56*, 5647-5652.
(76) Castano, A. P.; Mroz, P.; Hamblin, M. R. *Nature Reviews Cancer* **2006**, *6*, 535-545.
(77) Dewhirst, M. W.; Kimura, H.; Rehmus, S. W.; Braun, R. D.; Papahadjopoulos, D.; Hong, K.; Secomb, T. W. *Br. J. Cancer Suppl.* **1996**, 247-251.
(78) Tromberg, B. J.; Orenstein, A.; Kimel, S.; Barker, S. J.; Hyatt, J.; Nelson, J. S.; Berns, M. W. *Photochem. Photobiol.* **1990**, *52*, 375-385.
(79) Kerr, J. F.; Wyllie, A. H.; Currie, A. R. *Br J. Cancer* **1972**, *26*, 239-257.

(80) Castano, A. P.; Demidova, T. N.; Hamblin, M. R. *Photodiagnosis and photodynamic therapy* **2005**, *2*, 123-146.
(81) Agostinis, P.; Buytaert, E.; Breyssens, H.; Hendrickx, N. *Photochem. Photobiol. Sci.* **2004**, *3*, 721-729.
(82) Moor, A. C. *Photochem. Photobiol.* **2000**, *57*, 1-13.
(83) Plaetzer, K.; Kiesslich, T.; Oberdanner, C. B.; Krammer, B. *Curr. Pharm. Des.* **2005**, *11*, 1151-1165.
(84) Kaneko, T.; Chiba, H.; Yasuda, T.; Kusama, K. *Oral Oncol.* **2004**, *40*, 787-792.
(85) Lilge, L.; Portnoy, M.; Wilson, B. C. *Br J. Cancer* **2000**, *83*, 1110-1117.
(86) Castedo, M.; Perfettini, J. L.; Roumier, T.; Andreau, K.; Medema, R.; Kroemer, G. *Oncogene* **2004**, *23*, 2825-2837.
(87) Bizik, J.; Kankuri, E.; Ristimaki, A.; Taieb, A.; Vapaatalo, H.; Lubitz, W. *Cell Death Differ.* **2004**, *11*, 183-195.
(88) Yu, L.; Lenardo, M. J.; Baehrecke, E. H. *Cell Cycle* **2004**, *3*, 1124-1126.
(89) Oleinick, N. L.; Morris, R. L.; Belichenko, I. *Photochem. Photobiol. Sci.* **2002**, 1-21.
(90) Xue, L. Y.; Chiu, S. M.; Oleinick, N. L. *Exp. Cell Res.* **2001**, *263*, 145-155.
(91) Morton, C. A. *Br. J. Dermatol.* **2001**, *145*, 1-2.
(92) Bonnett, R. *Chemical Aspects of Photodynamic Therapy*; Gordon and Breach Science Publishers: Amsterdam, 2000; Vol. 1.
(93) Milgrom, L. R. *The Colours of Life: An Introduction to the Chemistry of Porphyrins and Related Compounds*; Oxford University Press, 1997.
(94) Foote, C. S. *Acc. Chem. Res.* **1968**, *1*, 104-110.
(95) Jacques, S. L. *Phys. Med. Biol.* **2013**, *58*, 37-61.
(96) Bonnett, R.; Martinez, G. *Tetrahedron* **2001**, *57*, 9513-9547.
(97) Symposium., C. F. *John Wiley & Sons Ltd. Chichester, U.K.* **1989**, *146*.
(98) Bilski, P.; Motten, A. G.; Bilska, M.; Chignell, C. F. *Photochem. Photobiol.* **1993**, *58*, 11-18.
(99) Bonnett, R.; Martinez, G. *Org. Lett.* **2002**, *4*, 2013-2016.
(100) Dougherty, T. J. *Photochem. Photobiol.* **1993**, *58*, 895-900.
(101) G., J. *Photochem. Photobiol. A* **1992**, *62*, 371-378.
(102) Kessel, D.; Thompson, P.; Muselman, B.; Chang, C. K. *Cancer Res.* **1987**, *47*, 4642-4645.
(103) Bonnett, R. *Chem. Soc. Rev.* **1995**, *24*, 19-33.
(104) Boyle, R. W.; Dolphin, D. *Photochemistry and photobiology* **1996**, *64*, 469-485.
(105) Pandey, R. K., Zheng, G. K. In *The Porphyrin Handbook*; Kadish, K. M., Smith, K. M.,Guilard, R., Ed.; Academic Press: San Diego, 2000; Vol. 6, p 157-230.
(106) Senge, M. O.; Brandt, J. C. *Photochemistry and photobiology* **2011**, *87*, 1240-1296.
(107) Bonnett, R.; Charlesworth, P.; Djelal, B. D.; Foley, S.; McGarvey, D. J.; Truscott, T. G. J. *J. Chem. Soc. Perkin Trans. 2* **1999**, 325-328.
(108) Kessel, D. *Int. J. Clin. Pract.* **1999**, *53*, 263-267.
(109) Ball, D. J.; Vernon, D. I.; Brown, S. B. *Photochem. Photobiol.* **1999**, *69*, 360-363.
(110) Sasnouski, S.; Kachatkou, D.; Zorin, V.; Guillemin, F.; Bezdetnaya, L. *Photochem. Photobiol.* **2006**, *5*, 770-777.
(111) Castano, A. P.; Demidova, T. N.; Hamblin, M. R. *Photodiagnosis and photodynamic therapy* **2004**, *1*, 279-293.
(112) Bryce, R. *BMJ* **2000**, *320*, 1731.
(113) Rezzoug, H.; Bezdetnaya, L.; A'amar, O.; Merlin, J. L.; Guillemin, F. *Lasers Med. Sci.* **1998**, *13*, 119-125.
(114) Ris, H. B.; Altermatt, H. J.; Nachbur, B.; Stewart, J. C. M.; Wang, Q.; Lim, C. K.; Bonnett, R.; Althaus, U. *Int. J. Cancer* **1993**, *53*, 141-146.
(115) Ris, H. B.; Altermatt, H. J.; Stewart, C. M.; Schaffner, T.; Wang, Q.; Lim, C. K.; Bonnett, R.; Althaus, U. *Int. J. Cancer* **1993**, *55*, 245-249.
(116) Veenhuizen, R. B.; Ruevekamp-Helmers, M. C.; Helmerhorst, T. J. M.; Kenemans, P.; Mooi, W. J.; Marunissen, J. P. A.; Stewart, F. A. *Int. J. Cancer* **1994**, *59*, 830-836.

(117) Howe, L.; Sucheta, A.; Einarsdottir, O.; Zhang, J. Z. *Photochem. Photobiol.* **1999**, *69*, 617-623.
(118) Bonnett, R. *Rev. Contemp. Pharmacother.* **1999**, *10*, 1-17.
(119) Brown, S. B.; Truscott, T. G. *Chem. Br.* **1993**, 955-958.
(120) Sternberg, E. D.; Dolphin, D.; Brückner, C. *Tetrahedron* **1998**, *54*, 4151-4202.
(121) Milgrom, L.; MacRobert, S. *Chem. Br.* **1998**, *34*, 45-50.
(122) Pandey, R. K.; Herman, C. K. *Chem. Ind.* **1998**, *London*, 739-743.
(123) Rosenkranz, A. A.; Jans, D. A.; Sobolev, A. S. *Immunol. Cell Biol.* **2000**, *78*, 452-464.
(124) Dogutan, D. K.; Zaidi, S. H. H.; Thamyongkit, P.; Lindsey, J. S. *The Journal of Organic Chemistry* **2007**, *72*, 7701-7714.
(125) Lindsey, J. S.; Hsu, H. C.; Schreiman, I. C. *Tetrahedron letters* **1986**, *27*, 4969-4970.
(126) Rao, P. D.; Dhanalekshmi, S.; Littler, B. J.; Lindsey, J. S. *The Journal of Organic Chemistry* **2000**, *65*, 7323-7344.
(127) Geier, G. R.; Lindsey, J. S. *Tetrahedron* **2004**, *60*, 11435-11444.
(128) Ryppa, C.; Senge, M. O.; Hatscher, S. S.; Kleinpeter, E.; Wacker, P.; Schilde, U.; Wiehe, A. *Chemistry– A European Journal* **2005**, *11*, 3427-3442.
(129) Senge, M. O. *Chemical Communications* **2011**, *47*, 1943-1960.
(130) Feng, X.; Bischoff, I.; Senge, M. O. *Journal of Organic Chemistry* **2001**, *66*, 8693-8700.
(131) Feng, X.; Senge, M. O. *Journal of the Chemical Society, Perkin Transactions 1* **2001**, 1030-1038.
(132) Senge, M. O. *Accounts Chemical Research* **2005**, *38*, 733-743.
(133) Senge, M. O.; Kalisch, W. W.; Bischoff, I. *Chemistry- A European Journal* **2000**, *6*, 2721-2738.
(134) Wallace, D. M.; Leung, S. H.; Senge, M. O.; Smith, K. M. *J. Org. Chem.* **1993**, *58*, 7245-7257.
(135) Dogutan, D. K.; Lindsey, J. S. *The Journal of Organic Chemistry* **2008**, *73*, 6728-6742.
(136) Littler, B. J.; Ciringh, Y.; Lindsey, J. S. *The Journal of Organic Chemistry* **1999**, *64*, 2864-2872.
(137) Senge, M. O.; Runge, S.; Speck, M.; Ruhlandt-Senge, K. *Tetrahedron* **2000**, *56*, 8927-8932.
(138) Runge, S.; Senge, M. O. *Z. Naturforsch. B: Chem. Sci.* **1998**, *53*, 1021-1030.
(139) Kalisch, W. W.; Senge, M. O. *Angewandte Chemie International Edition* **1998**, *37*, 1107-1109.
(140) Hofmann, A. F.; Borgström, B. *J. Clin. Invest.* **1964**, *43*, 247-257.
(141) Fiorucci, S.; Mencarelli, A.; Palladino, G.; Cipriani, S. *Trends Pharmacol. Sci.* **2009**, *30*, 570-580.
(142) Kralova, J.; Koivukorpi, J.; Kejik, Z.; Pouckova, P.; Sievaenen, E.; Kolehmainen, E.; Kral, V. *Org. Biomol. Chem.* **2008**, *6*, 1548-1552.
(143) Koivukorpi, J.; Sievanen, E.; Kolehmainen, E.; Kral, V. *Molecules* **2007**, *12*, 13-24.
(144) Sharma, R.; Majer, F.; Peta, V. K.; Wang, J.; Keaveney, R.; Kelleher, D.; Long, A.; Gilmer, J. F. *Bioorg. Med. Chem. Lett.* **2010**, *18*, 6886-6895.
(145) Kessel, D.; Poretz, R. D. *Photochem. Photobiol.* **2000**, *71*, 94-96.
(146) Kessel, D.; Caruso, J. A.; Reiners, J. J. *Cancer Res.* **2000**, *60*, 6985-6988.
(147) Sharma, R.; Long, A.; Gilmer, J. F. *Curr. Med. Chem* **2011**, *18*, 4029-4052.
(148) Majer, F.; Sharma, R.; Mullins, C.; Keogh, L.; Phipps, S.; Duggan, S.; Kelleher, D.; Keely, S.; Long, A.; Radics, G.; Wang, J.; Gilmer, J. F. *Bioorg. Med. Chem. Lett.* **2014**, *22*, 256-268.
(149) Heindl, C. C.; Corral, A.; Senge, M. O. *Eur. J. Org. Chem.* **2010**.
(150) Cavaleiro, J. A. S.; Tomé, J. P. C.; Faustino, M. A. F. *Top. Heterocycyl. Chem.* **2007**, *7*, 179-248.
(151) Moylan, C.; Senge, M. O. *Unpublished Results*.
(152) Pavlopoulos, T. G.; Boyer, J. H.; Shah, M.; Thangaraj, K.; Soong, M. L. *Appl. Opt.* **1990**, *29*, 3885-3886.

(153) Shah, M.; Thangaraj, K.; Soong, M. L.; Wolford, L. T.; Boyer, J. H.; Politzer, I. R.; Pavlopoulos, T. G. *Heteroat. Chem.* **1990**, *1*, 389-399.
(154) Yogo, T.; Urano, Y.; Ishitsuka, Y.; Maniwa, F.; Nagano, T. *J. Am. Chem. Soc.* **2005**, *127*, 12162-12163.
(155) Rieth, R. D.; Mankad, N. P.; Calimano, E.; Sadighi, J. P. *Org. Lett.* **2004**, *6*, 3981-3983.
(156) Loudet, A.; Burgess, K. *Chemical reviews* **2007**, *107*, 4891-4932.
(157) Ulrich, G.; Ziessel, R.; Harriman, A. *Angewandte Chemie (International ed. in English)* **2008**, *47*, 1184-1201.
(158) Murtagh, J.; Frimannsson, D. O.; O'Shea, D. F. *Organic letters* **2009**, *11*, 5386-5389.
(159) Palma, A.; McDonnell, S. O.; Hall, M. J.; O'Shea, D. F. *Organic letters* **2008**, *10*, 4771-4774.
(160) Jensen, T. J.; Vicente, M. G.; Luguya, R.; Norton, J.; Fronczek, F. R.; Smith, K. M. *Photochem. Photobiol. B* **2010**, *100*, 100-111.
(161) Picard, N.; Ali, H.; van Lier, J. E.; Klarskov, K.; Paquette, B. *Photochem. Photobiol. Sci.* **2009**, *8*, 224-232.
(162) Silva, J. N.; Galmiche, A.; Tomé, J. P.; Boullier, A.; Neves, M. G.; Silva, E. M.; Capiod, J.-C. C.; Cavaleiro, J. A.; Santus, R.; Mazière, J.-C. C.; Filipe, P.; Morlière, P. *Biochem.Pharmacol.* **2010**, *80*, 1373-1385.
(163) Dai, T.; Huang, Y.-Y. Y.; Hamblin, M. R. *Photodiagn. Photodyn. Ther.* **2009**, *6*, 170-188.
(164) Kranz, S.; Guellmar, A.; Völpel, A.; Gitter, B.; Albrecht, V.; Sigusch, B. W. *Lasers Surg. Med.* **2011**, *43*, 241-248.
(165) Wainwright, M. *J. Antimicrob. Chemother.* **1998**, *42*, 13-28.
(166) Bakleh, M. E.; Sol, V.; Estieu-Gionnet, K.; Granet, R.; Déléris, G.; Krausz, P. *Tetrahedron* **2009**, *65*, 7385-7392.
(167) Bell, A.; Roberts, D. J. H.; Brown, S. B.; Vernon, D. I. *Photochem. Photobiol. Sci.* **2008**, *7*, 290-298.
(168) Srivatsan, A.; Ethirajan, M.; Pandey, S. K.; Dubey, S.; Zheng, X.; Liu, T.-H. H.; Shibata, M.; Missert, J.; Morgan, J.; Pandey, R. K. *Mol. Pharm.* **2011**, *8*, 1186-1197.
(169) Thomas, N.; Tirand, L.; Chatelut, E.; Plénat, F.; Frochot, C.; Dodeller, M.; Guillemin, F.; Barberi-Heyob, M. *Photochem. Photobiol. Sci.* **2008**, *7*, 433-441.
(170) Camerin, M.; Magaraggia, M.; Soncin, M.; Jori, G.; Moreno, M.; Chambrier, I.; Cook, M. J.; Russell, D. A. *Eur. J. Cancer* **2010**, *46*, 1910-1918.
(171) Chatterjee, D. K.; Fong, L. S.; Zhang, Y. *Adv. Drug Deliv. Rev.* **2008**, *60*, 1627-1637.
(172) Shcherbakov, A. B.; Usatenko, A. V.; Kholin, V. V. *Exp. Oncol.* **2010**, *31*, 44-47.
(173) Battogtokh, G.; Liu, H.-B. B.; Bae, S.-M. M.; Chaturvedi, P. K.; Kim, Y.-W. W.; Kim, I.-W. W.; Ahn, W. S. *Photochem. Photobiol. B* **2012**, *110*, 50-57.
(174) Gederaas, O. A.; Schønberg, S. A.; Ramstad, S.; Berg, K.; Johnsson, A.; Krokan, H. E. *Photochem. Photobiol. Sci.* **2005**, *4*, 383-389.
(175) Bullous, A. J.; Alonso, C. M. A.; Boyle, R. W. *Photochem. Photobiol. Sci.* **2011**, *10*, 721-750.
(176) Scarf, A. M.; Kassiou, M. *J. Nucl. Med.* **2011**, *52*, 677-680.
(177) Rupprecht, R.; Papadopoulos, V.; Rammes, G. *Nat. Rev. Drug Discov.* **2010**, *9*, 971-988.
(178) Verma, A.; Nye, J. S.; Snyder, S. H. *Proc. Natl. Acad. Sci. USA* **1987**, *84*, 2256-2260.
(179) Mantione, C. R.; Weissman, B. A.; Goldman, M. E.; Paul, S. M.; Skolnick, P. *FEBS Lett.* **1984**, *176*, 69-74.
(180) Schoemaker, H.; Boles, R. G.; Horst, W. D.; Yamamura, H. I. *J. Pharmacol. Exp. Ther.* **1983**, *225*, 61-69.
(181) Ritsner, M.; Modai, I.; Gibel, A. *J. Psychiatr. Res.* **2003**, *37*, 549-556.
(182) Becker, D. M.; Kramer, S. *Medicine* **1977**, *56*, 411-423.
(183) Veenman, L.; Papadopoulos, V.; Gavish, M. *Curr. Pharm. Des.* **2007**, *13*, 2385-2405.
(184) Rosenberg, N.; Rosenberg, O.; Weizman, A.; Veenman, L.; Gavish, M. *J. Bioener. Biomembr.* **2013**, *45*, 333-341.
(185) Barman, S.; Ana, J.; Garg, O. B.; Venkatesan, K.; Berke, H. *Chemical communications (Cambridge, England)* **2012**, *48*, 11127-11129.

(186) Dahms, K.; Senge, M. O. *Tet. Lett.* **2008**, *49*, 5397-5399.
(187) Hilton, C. L.; Jamison, C. R.; Zane, H. K.; King, B. T. *J. Org. Chem.* **2009**, *74*, 405-407.
(188) Mondal, S.; Chakraborty, S.; Bhowmick, S.; Das, N. *J. Am. Chem. Soc.* **2013**, *46*, 6824-6831.
(189) Bartlett, P. D.; Ryan, M. J.; Cohen, S. G. *J. Am. Chem. Soc.* **1942**, *64*, 2649-2653.
(190) Craig, A. C.; Wilcox, C. F. *J. Org. Chem.* **1959**, *24*, 1619.
(191) Chen, C. F.; Ma, Y. *Springer: London, New York, 2013.*
(192) Wittig, G. *Org. Synth.* **1959**, *39*, 75-77.
(193) Bruce, H.; Perkins, K.; Perkins, W. *J. Org. Chem.* **1968**, *34*, 630-633.
(194) Kornfeld, E. C.; Barney, P.; Blankley, J.; Faul, W. *J. Med. Chem* **1965**, *8*, 342-347.
(195) Jiang, Y.; Chen, C. F. *Eur. J. Org. Chem.* **2011**, 6377-6403.
(196) Rogers, M. E.; Averill, B. A. *J. Org. Chem.* **1986**, *51*, 3308-3314.
(197) Zhang, C.; Chen, C. F. F. *J. Org. Chem.* **2006**, *71*, 6626-6629.
(198) Finnigan, E. M.; Rein, R.; Solladié, N.; Dahms, K.; Götz, D. C. G.; Bringmann, G.; Senge, M. O. *Tetrahedron* **2011**, *67*, 1126-1134.
(199) Barber, J. *Chem Soc. Rev* **2009**, *38*, 185-196.
(200) Scholes, G. D.; Fleming, G. R.; Olaya-Castro, A.; van Grondelle, R. *Nat Chem* **2011**, *3*, 763-774.
(201) Harriman, A.; Sauvage, J. P. *Chem. Soc. Rev.* **1996**, *25*, 41-48.
(202) Huber, R. *Angew. Chem. Int. Ed. Engl.* **1989**, *28*, 848-869.
(203) Balaban, T. S. *Acc. Chem. Res.* **2005**, *38*, 612-623.
(204) Marek, P. L.; Hahn, H.; Balaban, T. S. *Energy Environ. Sci.* **2011**, *4*, 2366-2378.
(205) Miyatake, T.; Tamiaki, H. *J. Photochem. Photobiol. C: Photochem. Rev.* **2005**, *6*, 89-107.
(206) Wasielewski, M. R. *Acc. Chem. Res.* **2009**, *42*, 1910-1921.
(207) Terazono, Y.; Kodis, G.; Bhushan, K.; Zaks, J.; Madden, C.; Moore, A. L.; Moore, T. A.; Fleming, G. R.; Gust, D. *J. Am. Chem. Soc.* **2011**, *133*, 2916-2922.
(208) Maeda, C.; Kim, P.; Cho, S.; Park, J. K.; Lim, J. M.; Kim, D.; Vura-Weis, J.; Wasielewski, M. R.; Shinokubo, H.; Osuka, A. *Chem. Eur. J.* **2010**, *16*, 5052-5061.
(209) Tan, J.; A., C. J. *Biochemistry* **1991**, *30*, 8910-8917.
(210) Adams, M. W. W.; Mortenson, L. E. *Molybdenum Enzymes* **1985**, *Wiley-Interscience, New York*, 519-593.
(211) Wikstrom, M.; Krab, K.; Saraste, M.; Academic Press, London, 1981.
(212) *Copper Proteins and Copper Enzymes*; CRC, Boca Raton, Fl, USA, 1984; Vol. III.
(213) Wieghardt, K. *Angew. Chem.* **1989**, *101*, 1179-1198.
(214) Wieghardt, K. *Angew. Chem. Int. Ed. Engl.* **1989**, *28*, 1153-1172.
(215) Debus, R. *Biochim. Biophys. Acta* **1992**, *1102*, 269-352.
(216) Thorneley, R. N. F.; Lowe, D. J. In *Molybdenum Enzymes*; Spiro, T. G., Ed.; Wiley-Interscience: New York, 1985, p 221-341.
(217) W., A. M. W. *Biochim. Biophys. Acta* **1990**, *1020*, 115-145.
(218) Malmstrom, B. G. *Chem. Rev.* **1990**, *90*, 1247-1260.
(219) Schwarz, F. P.; Gouterman, M.; Muljiani, Z.; Dolphin, D. *Bioinorg. Chem.* **1972**, *2*, 1-32.
(220) Collman, J. P.; Elliott, C. M.; Halbert, T. R.; Tovrog, B. S. *Proc. Natl. Acad. Sci. USA* **1977**, *74*, 18-22.
(221) Ogoshi, H.; Sugimoto, H.; Yoshida, Z. I. *Tet. Lett.* **1977**, *2*, 169-172.
(222) Kagan, N. E.; Mauzerall, D.; Merrifield, R. B. *J. Am. Chem. Soc.* **1977**, *99*, 5484-5486.
(223) James, P. C.; Paul, S. W.; James, E. H. *Angewandte Chemie International Edition in English* **1994**, *33*, 1537-1554.
(224) Griffith, J. S. *Proc. Roy. Soc. Ser A.* **1956**, *235*, 23.
(225) Pauling, L. *Stanford Med. Bull.* **1948**, *6*, 215.
(226) Weiss, J. J. *Nature* **1964**, *202*, 83.
(227) Dickerson, R. E.; Geis, I. *The Structure and Action of Proteins*; Harper and Row: New York, 1969.
(228) Nobbs, C. L.; Watson, H. C.; Kendrew, J. C. *Nature* **1966**, *209*, 339-341.

(229) Collman, J. P.; Gagne, R. R.; Reed, C.; Halbert, T. R.; Lang, G.; Robinson, W. T. *J. Am. Chem. Soc.* **1975**, *97*, 1427-1439.
(230) Collman, J. P.; Gagne, R. R.; Halbert, T. R.; Marchon, J. C.; Reed, C. A. *J. Am. Chem. Soc.* **1973**, *95*, 7868-7870.
(231) Collman, J. P.; Gagne, R. R.; Gray, H. B.; Hare, J. *J. Am. Chem. Soc.* **1974**, *96*, 6522-6524.
(232) Collman, J. P.; Gagne, R. R.; Reed, C. A.; Robinson, W. T.; Rodley, G. A. *Proc. Natl. Acad. Sci. USA* **1974**, *71*, 1326-1329.
(233) Diekmann, H.; Chang, C. K.; Traylor, T. G. *J. Am. Chem. Soc.* **1971**, *93*, 4068-4070.
(234) Gottwald, L. K.; Ullman, E. F. *Tet. Lett.* **1969**, *36*, 3071.
(235) Wang, Z.; Chen, G.; Ding, K. *Chem. Rev.* **2009**, *109*, 322-359.
(236) Li, J. R.; Kuppler, R. J.; Zhou, H. C. *Chem Soc. Rev* **2009**, *38*, 1477-1504.
(237) Kuppler, R. J.; Timmons, D. J.; Fang, Q. R.; Li, J. R.; Makal, T. A.; Young, M. D.; Yuan, D.; Zhao, D.; Zhuang, W.; Zhou, H. C. *Coord. Chem. Rev.* **2009**, *253*.
(238) Ockwig, N. W.; Delgado-Friedrichs, O.; O'Keeffe, M.; Yaghi, O. M. *Acc. Chem. Res.* **2005**, *38*, 176-182.
(239) Furukawa, H.; Cordova, K. E.; O'Keeffe, M.; Yaghi, O. M. *Science* **2013**, *341*, 974-998.
(240) Horcajada, P.; Serre, C.; Maurin, G.; Ramsahye, N. A.; Balas, F.; Vallet-Regi, M.; Sebban, M.; Taulelle, F.; Férey, G. *J. Am. Chem. Soc.* **2008**, *130*, 6774-6780.
(241) Rothemund, P. *Journal of the American Chemical Society* **1935**, *57*, 2010-2011.
(242) Rothemund, P. *Journal of the American Chemical Society* **1936**, *58*, 625-627.
(243) Lindsey, J. S.; Schreiman, I. C.; Hsu, H. C.; Kearney, P. C.; Marguerettaz, A. M. *The Journal of Organic Chemistry* **1987**, *52*, 827-836.
(244) Dolmans, D.; Fukumura, D.; Jain, R. K. *Nat. Rev. Cancer* **2003**, *3*, 380-387.
(245) Kadish, K. M.; Guo, N.; Van, C. E.; Paolesse, R.; Monti, D.; Tagliatesta, P. *Journal of Porphyrins and Phthalocyanines* **1998**, *2*, 439-450.
(246) Notaras, E. G.; Fazekas, M.; Doyle, J. J.; Blau, W. J.; Senge, M. O. *Chem Commun (Camb)* **2007**, 2166-2168.
(247) Senge, M. O.; Fazekas, M.; Notaras, E. G. A.; Blau, W. J.; Zawadzka, M.; Locos, O. B.; Ni Mhuircheartaigh, E. M. *Advanced Materials* **2007**, *19*, 2737-2774.
(248) Zawadzka, M.; Wang, J.; Blau, W. J.; Senge, M. O. *Chemical Physics Letters* **2009**, *477*, 330-335.
(249) Mhuircheartaigh, E. M. N.; Giordani, S.; MacKernan, D.; King, S. M.; Rickard, D.; Val, V. L. M.; Senge, M. O.; Blau, W. J. *J. Nanotechnol.* **2011**, 745202, 745212 pp.
(250) Nocera, D. G. *Accounts of Chemical Research* **1995**, *28*, 209-217.
(251) Yongqi, D.; Christopher, J. C.; Daniel, G. N. *Journal of the American Chemical Society* **2000**, *122*, 410-411.
(252) Robert, E. B.; David, M. T.; James, B.; Gary, W. B.; Graham, F.; Maria, G.; Gunner, M. R.; Wolfgang, J.; David, M. K.; Anastasios, M.; Thomas, A. M.; Christopher, C. M.; Daniel, G. N.; Arthur, J. N.; Donald, R. O.; William, W. P.; Roger, C. P.; Richard, T. S. *Science* **2011**, *332*, 805-809.
(253) Tomohiro, Y.; Satake, A.; Kobuke, Y. *J. Org. Chem.* **2001**, *66*, 8442-8446.
(254) Lindsey, J. S. *Accounts of Chemical Research* **2009**, *43*, 300-311.
(255) Lindsey, J. S.; Prathapan, S.; Johnson, T. E.; Wagner, R. W. *Tetrahedron* **1994**, *50*, 8941-8968.
(256) Sharman, W. M.; Van, L. J. E. *J. Porphyrins Phthalocyanines* **2000**, *4*, 441-453.
(257) Baudouy, R. P. *Tetrahedron* **1989**, *45*, 2067-2074.
(258) Rogers, L.; Majer, F.; Sergeeva, N. N.; Paszko, E.; Gilmer, J. F.; Senge, M. O. *Bioorganic & medicinal chemistry letters* **2013**, *23*, 2495-2499.
(259) Neises, B.; Steglich, W. *Angew. Chem. Int. Ed. Engl.* **1978**, *17*, 522-524.
(260) Ryan, A. A.; Senge, M. O. *Unpublished Results* **2014**.
(261) Mu, Y. Q.; Gibbs, R. A. *Tetrahedron Lett.* **1995**, *36*, 5669-5672.
(262) Molander, G. A.; Ito, T. *Org. Lett.* **2001**, *3*, 393-396.
(263) Guram, A. S.; Buchwald, S. L. *J. Am. Chem. Soc.* **1994**, *116*, 7901-7902.
(264) Paul, F.; Patt, J.; Hartwig, J. F. *J. Am. Chem. Soc.* **1994**, *116*, 5969-5970.

(265) Ullmann, F.; Sponagel, P. *Ber. Dtsch. Chem. Ges.* **1905**, *38*, 2211-2212.
(266) Qiao, J. X.; Lam, P. Y. S. *Synthesis* **2011**, 829-856.
(267) Nascimento, B. F. O.; Pineiro, M.; Gonsalves, A. M. d. A. R.; Silva, M. R.; Beja, A. M.; Paixao, J. A. *J. Porphyrins Phthalocyanines* **2007**, *11*, 77-84.
(268) Buchler, J. W. In *The Porphyrins*; Dolphin, D., Ed.; Academic: London, 1978; Vol. 1, p 389-483.
(269) Lennoxa, A. J. J.; Lloyd-Jones, G. C. *Chem. Soc. Rev.* **2014**, *43*, 412-443.
(270) Sessler, J. L.; Jayawickramarajah, J.; Gouloumis, A.; Torres, T.; Guldi, D. M.; Maldonado, S.; Stevenson, K. J. *Chem. Commun.* **2005**, *14*, 1892-1894.
(271) Callot, H. J. *Tetrahedron letters* **1973**, 4987-4990.
(272) Arnold, D. P.; Bott, R. C.; Eldridge, H.; Elms, F. M.; Smith, G.; Zojaji, M. *Australian Journal of Chemistry* **1997**, *50*, 495-504.
(273) Chumakov, D. E.; Khoroshutin, A. V.; Anisimov, A. V.; Kobrakov, K. I. *Chemistry of Heterocyclic Compounds* **2009**, *45*, 259-283.
(274) Arnold, D. P.; Bott, R. C.; Eldridge, H.; Elms, F. M.; Smith, G.; Zojaji, M. *Australian Journal of Chemistry* **1997**, *50*, 495-503.
(275) Shanmugathasan, S.; Johnson, C. K.; Edwards, C.; Matthews, E. K.; Dolphin, D.; Boyle, R. W. *Journal of Porphyrins and Phthalocyanines* **2000**, *4*, 228-232.
(276) Nayak, S. K.; Kadam, S. M.; Banerji, A. *Synlett* **1993**, *1993*, 581-582.
(277) Choi, M.-S.; Yamazaki, T.; Yamazaki, I.; Aida, T. *Angewandte Chemie International Edition* **2004**, *43*, 150-158.
(278) Manas, K. P.; Kalliopi, L.; Athanassios, G. C. *Coordination Chemistry Reviews* **2012**, *256*, 2601-2627.
(279) Collman, J. P.; Gagne, R. R.; Reed, C. *Journal of the American Chemical Society* **1975**, *97*, 1427-1439.
(280) Collman, J. P.; Brauman, J. I.; Iverson, B. L. *Journal of the American Chemical Society* **1983**, *105*, 3052-3064.
(281) Smeets, S.; Roex, H.; Dehaen, W. *ARKIVOC* **2003**, *83*, 83-92.
(282) Collman, J. P.; Denisevich, P.; Konai, Y.; Marrocco, M.; Koval, C.; Anson, F. C. *Journal of the American Chemical Society* **1980**, *102*, 6027-6036.
(283) Harvey, P. D.; Stern, C.; Gros, C. P.; Guilard, R. *Coord. Chem. Rev.* **2007**, *251*, 401-428.
(284) Beletskaya, I.; Tyurin, V. S.; Tsivadze, A. Y.; Guilard, R.; Stern, C. *Chemical reviews* **2009**, *109*, 1659-1713.
(285) Zhang, J.; Li, Y.; Yang, W.; Lai, S. W.; Zhou, C.; Liu, H.; Che, C. M.; Li, Y. *Chem. Commun.* **2012**, *48*, 3602-3604.
(286) Gilday, L. C.; White, N. G.; Beer, P. D. *Dalton Trans.* **2012**, *41*, 7092-7097.
(287) Rogers, L.; Burke-Murphy, E.; Senge, M. O. *Eur. J. Org. Chem.* **2014**, *2014*, 4283-4294.
(288) Huisgen, R. *Angew. Chem.* **1963**, *7*, 604-637.
(289) Locos, O. B.; Heindl, C. C.; Corral, A.; Senge, M. O.; Scanlan, E. M. *European Journal of Organic Chemistry* **2010**, 1026-1028, S1026/1021-S1026/1018.
(290) Guillaume, G.; Delphine, N.-M.; Danièle, C.; Alain, C.; Philippe, M. *Tetrahedron* **2011**, *67*, 4924-4932.
(291) Arsenault, G. P.; Bullock, E.; MacDonald, S. F. *Journal of the American Chemical Society* **1960**, *82*, 4384-4389.
(292) Manka, J. S.; Lawrence, D. S. *Tetrahedron letters* **1989**, *30*, 6989-6992.
(293) Bruckner, C.; Posakony, J. J.; Johnson, C. K.; Boyle, R. W.; James, B. R.; Dolphin, D. *Journal of Porphyrins and Phthalocyanines* **1998**, *2*, 455-465.
(294) Wiehe, A.; Ryppa, C.; Senge, M. O. *Organic letters* **2002**, *4*, 3807-3809.
(295) Osuka, A.; Marumo, S.; Mataga, N.; Taniguchi, S.; Okada, T.; Yamazaki, I.; Nishimura, Y.; Ohno, T.; Nozaki, K. *Journal of the American Chemical Society* **1996**, *118*, 155-168.
(296) Adler, A. D.; Longo, F. R.; Finarelli, J. D.; Goldmacher, J.; Assour, J.; Korsakoff, L. *The Journal of Organic Chemistry* **1967**, *32*, 476-476.
(297) Senge, M. O.; Kalisch, W. W. *Inorg Chem* **1997**, *36*, 6103-6116.
(298) Krattinger, B.; Callot, H. J. *Tetrahedron letters* **1996**, *37*, 7699-7702.

(299) Krattinger, B.; Callot, H. J. *European Journal of Organic Chemistry* **1999**, 1857-1867.
(300) Senge, M. O.; Feng, X. *Journal of the Chemical Society, Perkin Transactions 1* **2000**, 3615-3621.
(301) Horn, S.; Senge, M. O. *European Journal of Organic Chemistry* **2008**, *2008*, 4881-4890.
(302) Senge, M. O.; Shaker, Y. M.; Pintea, M.; Ryppa, C.; Hatscher, S. S.; Ryan, A.; Sergeeva, Y. *European Journal of Organic Chemistry* **2010**, *2010*, 207-207.
(303) Balaban, T. S.; Goddard, R.; Linke-Schaetzel, M.; Lehn, J.-M. *Journal of the American Chemical Society* **2003**, *125*, 4233-4239.
(304) Buchler, J. W. In *Porphyrins and metalloporphyrins*; Smith, K. M., Ed.; Elsevier: Amsterdam, 1975, p 157-231.
(305) Pavani, C.; Uchoa, A. F.; Oliveira, C. S.; Iamamoto, Y.; Baptista, M. S. *Photochemical & Photobiological Sciences* **2009**, *8*, 233-240.
(306) Vaz, G. M. F.; Paszko, E.; Davies, A. M.; Senge, M. O. *PLOS ONE* **2013**, *8*, e70653.
(307) Berenbaum, M. C.; Akande, S. L.; Bonnett, R. *British Journal of Cancer* **1986**, *54*, 717-725.
(308) Ormond, A. B.; Freeman, H. S. *Dyes Pigments* **2013**, *96*, 440-448.
(309) Aucagne, V.; Hänni, K. D.; Leigh, D. A.; Lusby, P. J.; Walker, D. B. *J. Am. Chem. Soc.* **2006**, *128*, 2186-2187.
(310) Bonnett, R.; Djelal, B. D.; Hawkes, G. E. *J. Chem. Soc. Perkin Trans. 2* **1994**.
(311) Peng, X.; Sternberg, E.; Dolphin, D. *Electrophoresis* **2005**, *26*, 3861-3868.
(312) Cory, A. H.; Owen, T. C.; Barltrop, J. A.; Cory, J. G. *Cancer Comm.* **1991**, *3*, 207-212.
(313) Sergeeva, N. N.; Donnier-Marechal, E.; Vaz, G. M.; Davies, A. M.; Senge, M. O.; *Bioorg. Med. Chem. Lett.* **2011**, *21*, 4385-4388.
(314) Gorman, A.; Killoran, J.; O'Shea, C.; Kenna, T.; Gallager, W. M.; O'Shea, D. F. *J. Am. Chem. Soc.* **2004**, *126*, 10619-10631.
(315) Kolb, H. C.; Finn, M. G.; Sharpless, K. B. *Angew. Chem. Int. Ed. Engl.* **2001**, *40*, 2004-2021.
(316) Douglas, P.; Thomas, J. D.; Strohm, H.; Winscom, C.; Clarke, D.; Garley, M. S. *Photochem. Photobiol. Sci.* **2003**, *2*, 563-568.
(317) Kessel, D.; Dougherty, T. J. *Rev. Contemp. Pharmacother.* **1999**, *10*, 19-24.
(318) Nyman, E. S.; Hynninen, P. H. *Journal of photochemistry and photobiology. B, Biology* **2004**, *73*, 1-28.
(319) Gomer, C. J.; Ferrario, A.; Luna, M.; Rucker, N.; Wong, S.; Bozkulak, O.; Xu, F. In *Handbook of Porphyrin Science*; Kadish, K. M., Smith, K. M., Guilard, R., Eds.; World Scientific: Singapore, 2011; Vol. 4, p 425-441.
(320) Li, W.; Lu, W.; Fan, Z.; Zhu, X.; Reed, A.; Newton, B.; Zhang, Y.; Courtney, S.; Tiyyagura, P. T.; Li, S.; Butler, E.; Yu, H.; Ray, P. C.; Gao, R. *Journal of materials chemistry* **2012**, *22*, 12701-12708.
(321) Senge, M. O. *Photodiagnosis and photodynamic therapy* **2012**, *9*, 170-179.
(322) Ferrario, A.; Chantrain, C. F.; von Tiehl, K. F.; Buckley, S.; Rucker, N.; Shalinsky, D. R.; Shimada, H.; DeClerck, Y. A.; Gomer, C. J. *Cancer Res.* **2004**, *64*, 2328-2332.
(323) Ferrario, A.; F., v. T. K.; Rucker, N.; Schwarz, M. A.; Gill, P. S.; Gomer, C. J. *Cancer Res.* **2000**, *60*, 4066-4069.
(324) Ferrario, A.; Fisher, A. M.; Rucker, N.; Gomer, C. J. *Cancer Res.* **2005**, *65*, 9473-9478.
(325) Luna, M.; Wong, S.; Ferrario, A.; Gomer, C. J. *Photochem. Photobiol.* **2008**, *84*, 509-514.
(326) Song, J.; Chen, Q.; Xing, D. *Experimental cell research* **2013**, *319*, 1491-1504.
(327) Dubois, R. W.; Melmed, G. Y.; Henning, J. M.; Bernal, M. *J. Clin. Rheumatol.* **2004**, *10*, 178-189.
(328) Ferrario, A.; Lim, S.; Xu, F.; Luna, M.; Gaffney, K. J.; Petasis, N. A.; Schönthal, A. H.; Gomer, C. J. *Cancer letters* **2011**, *304*, 33-40.
(329) Burke, A.; Smyth, E.; Fitzgerald, G. A. In *Goodman and Gilman's the pharmacological basis of therapeutics*; 11 ed.; McGraw-Hill: New York, 2006, p 671-716.
(330) Mc Connan, T. *J. Am. Chem. Soc.* **1906**, *89*, 1331-1332.
(331) Riegel, W. *J. Am. Chem. Soc.* **1942**, *64*, 1486-1487.

(332) Williams, A.; Ibrahim, I. T. *Chem. Rev.* **1991**, *81*, 589-636.
(333) Bakar, M. B.; Oelgemöller, M.; Senge, M. O. *Tetrahedron* **2009**, *65*, 7064-7078.
(334) Newman, M. S.; Boden, H. *J. Org. Chem.* **1961**, *26*, 2525-2528.
(335) Peroni, G.; Pescitelli, G.; Huang, X.; Nakanishi, K.; Berova, N. *J. Am. Chem. Soc.* **2003**, *126*, 12914-12927.
(336) Adams, S. S.; Cobb, R. *Prog. Med. Chem.* **1967**, *5*, 59-138.
(337) Bauman, D. R.; Rudnick, S. I.; Szewczuk, L. M.; Jin, Y.; Gopishetty, S.; Penning, T. M. *Mol. Pharmacol.* **2005**, *67*, 60-68.
(338) Salmann, A. R. *Am. J. Med.* **1986**, *40*, 29-33.
(339) Montecucco, F.; Quercioli, A.; Dallegri, F.; Viviani, G. L.; Mach, F. *Expert Rev. Cardiovasc. Ther.* **2010**, *8*, 1457-1467.
(340) Bannwarth, B.; Labat, L.; Moride, Y.; Schaeverbeke, T. *Drugs* **1994**, *47*, 25-50.
(341) Rogers, L.; Sergeeva, N. N.; Senge, M. O. *PLOS ONE* **2014**, *Submitted*.
(342) Kay, E. R.; Leigh, D. A.; Zerbetto, F. *Angew. Chem. Int. Ed. Engl.* **2007**, *46*, 72-191.
(343) Burrell, A. K.; Officer, D. L.; Plieger, P. G.; Reid, D. C. W. *Chem. Rev.* **2001**, *101*, 2751-2796.
(344) Kinbara, K.; Aida, T. *Chemical reviews* **2005**, *105*, 1377-1400.
(345) McDermott, G.; Prince, S. M.; Freer, A. A.; Hawthornthwaitelawless, A. M.; Papiz, M. Z.; Gogdell, R. J.; Isaacs, N. W. *Nature* **1995**, *374*, 517-521.
(346) Yamamoto, G. *Pure Appl. Chem* **1990**, *62*, 569-574.
(347) Shaker, Y. M.; Senge, M. O. *Unpublished Results* **2013**.
(348) Li, P.-F. F.; Chen, C.-F. F. *The Journal of Organic Chemistry* **2012**, *77*, 9250-9259.
(349) Crane, A. K.; Patrick, B. O.; MacLachlan, M., J. *Dalton transactions (Cambridge, England : 2003)* **2013**, *42*, 8026-8033.
(350) James, S. L. *Chemical Society Reviews* **2003**, *32*, 276-288.
(351) Hong-Cai, Z.; Jeffrey, R. L.; Omar, M. Y. *Chemical reviews* **2012**, *112*, 673-674.
(352) Furukawa, H.; Ko, N.; Go, Y. B.; Aratani, N.; Choi, S. B.; Choi, E.; Yaghi, O. M. *Science* **2010**, *329*, 424-428.
(353) Ryan, A.; Tuffy, B.; Horn, S.; Blau, W. J.; Senge, M. O. *Tetrahedron* **2011**, *67*, 8248-8254.
(354) DiMagno, S. G.; Lin, V. S. Y.; Therien, M. J. *The Journal of Organic Chemistry* **1993**, *58*, 5983-5993.
(355) Sonogashira, K.; Tohda, Y.; Hagihara, N. *Tetrahedron letters* **1975**, 4467-4470.
(356) Sonogashira, K. *Handbook of Organopalladium Chemistry for Organic Synthesis* Wiley-Interscience: New York, 2002.
(357) ; Sonogashira, K., Ed.; John Wiley and Sons: New York, 2002; Vol. 1.
(358) Chinchilla, R.; Nájera, C. *Chemical reviews* **2007**, *107*, 874-922.
(359) Chinchilla, R.; Najera, C. *Chem Soc. Rev* **2011**, *40*, 5084-5121.
(360) Zheng, S. L.; Reid, S.; Lin, N.; Wang, B. H. T. *Tetrahedron Lett.* **2006**, *47*, 2331-2335.
(361) Muraoka, T.; Kinbara, K.; Aida, T. *Journal of the American Chemical Society* **2006**, *128*, 11600-11605.
(362) Tougerti, A.; Negri, S.; Jutand, A. *Chemistry – A European Journal* **2007**, *13*, 666-676.
(363) Plunkett, S.; Dahms, K.; Senge, M. O. *European Journal of Organic Chemistry* **2013**, 1566-1579.
(364) Ryan, A.; Gehrold, A.; Perusitti, R.; Pintea, M.; Fazekas, M.; Locos, O. B.; Blaikie, F.; Senge, M. O. *European Journal of Organic Chemistry* **2011**, 5817-5844.
(365) Murata, M.; Watanabe, S.; Masuda, Y. *The Journal of Organic Chemistry* **1997**, *62*, 6458-6459.
(366) Moreno-Mañas, M.; Pérez, M.; Pleixats, R. *The Journal of Organic Chemistry* **1996**, *61*, 2346-2351.
(367) Wuertz, S.; Glorius, F. *Accounts of Chemical Research* **2008**, *41*, 1523-1533.
(368) O'Brien, C. J.; Kantchev, E. A. B.; Valente, C.; Hadei, N.; Chass, G. A.; Lough, A.; Hopkinson, A. C.; Organ, M. G. *Chemistry-a European Journal* **2006**, *12*, 4743-4748.
(369) Nasielski, J.; Hadei, N.; Achonduh, G.; Kantchev, E. A. B.; O'Brien, C. J.; Lough, A.; Organ, M. G. *Chem. Eur. J.* **2010**, *16*, 10844-10853.

(370) Wolfe, J. P.; Singer, R. A.; Yang, B. H.; Buchwald, S. L. *J. Am. Chem. Soc.* **1999**, *121*, 9550-9561.
(371) Hashimoto, L.; Shudo, O. *Tetrahedron Lett.* **1983**, *24*, 1523-1526.
(372) Gust, D.; Moore, T. A.; Moore, A. L.; Gao, F.; Luttrull, D.; DeGraziano, J. M.; Ma, X. C.; Makings, L. R.; Lee, S.-J.; Trier, T. T.; Bittersmann, E.; Seely, G. R.; Woodward, S.; Bensasson, R. V.; Rougee, M. D. S., F. C.; Van Der Auweraer, M. *J. Am. Chem. Soc.* **1991**, *113*, 2628-2647.
(373) Faustino, M. A. F.; Neves, M. G. P. M. S.; Vicente, M. G. H.; Cavaleiro, J. A. S.; Neumann, M.; Brauer, H. D.; Jori, G. *Photochem. Photobiol.* **1997**, *66*, 405-412.
(374) Nekongo, E. E.; Popik, V. V. *J. Org. Chem.* **2014**, *79*, 7665-7671.
(375) Goldfinger, M. B.; Crawford, K. B.; Swager, T. M. *J. Am. Chem. Soc.* **1997**, *119*, 4578-4593.
(376) Barluenga, J.; González, J. M.; Garcıa-Martın, M. A.; Campos, P. J.; Asensio, G. *J. Org. Chem.* **1993**, *58*, 2058-2061.
(377) Milne, J. E.; Jarowicki, K.; Kocienski, P. J. *Synlett* **2002**, 607-609.
(378) Lindley, J. *Tetrahedron* **1984**, *40*, 1433-1456.
(379) Braestrup, C.; Squires, R. F. *Proc. Natl. Acad. Sci. USA* **1977**, *74*, 3805-3809.
(380) Lambert, J. J.; Belelli, D.; Hillvenning, C.; Peters, J. A. *Trends Pharmacol. Sci.* **1995**, *16*, 295-303.
(381) Papadopoulos, V.; Baraldi, M.; Guilarte, T. R. *Trends Pharmacol. Sci.* **2006**, *27*, 402-409.
(382) Fan, J.; Lindemann, P.; Feuilloley, M. G.; Papadopoulos, V. *Curr. Mol. Med.* **2012**, *12*, 369-386.
(383) Hanahan, D.; Weinberg, R. A. *Cell* **2000**, *100*, 57-70.
(384) Fulda S. . Int. J. Cancer 124 *Int. J. Cancer* **2009**, *124*, 511-515.
(385) Kroemer, G.; Galluzzi, L.; Brenner, C. *Physiol. Rev.* **2007**, *87*, 99-163.
(386) Kroemer, G.; Pouyssegur, J. *Cancer Cell* **2008**, *13*, 472-482.
(387) Galluzzi, L.; Larochette, N.; Zamzami, N.; Kroemer, G. *Oncogene* **2006**, *25*, 4812-4830.
(388) Okaro, A. C.; Fennell, D. A.; Corbo, M.; Davidson, B. R.; Cotter, F. E. *Gut* **2002**, *51*, 556-561.
(389) Decaudin, D.; Castedo, M.; Nemati, F. *Cancer Res.* **2002**, *62*, 1388-1393.
(390) Fulda, S.; Galluzzi, L.; Kroemer, G. *Nat. Rev. Drug Discov.* **2010**, *9*, 447-464.
(391) Shoshan-Barmatz, V.; Israelson, A.; Brdiczka, D.; Sheu, S. S. *Curr. Pharm. Des.* **2006**, *12*, 2249-2270.
(392) Batarseh, A.; Papadopoulos, V. *Mol. Cell. Endocrinol.* **2010**, *7*, 1-12.
(393) Chen, M. K.; Guilarte, T. R. *Pharmacol. Ther.* **2008**, *118*, 1-17.
(394) Papadopoulos, V.; Amri, H.; Boujrad, N. *Steroids* **1997**, *62*, 21-28.
(395) Liu, J.; Rone, M. B.; Papadopoulos, V. *J. Biol. Chem.* **2006**, *15*, 38879-38893.
(396) Kugler, W.; Veenman, L.; Shandalov, Y. *Cell Oncol.* **2008**, *30*, 435-450.
(397) Carmel, I.; Fares, F. A.; Leschiner, S.; Scherubl, H.; Weisinger, G.; M., G. *Biochem.Pharmacol.* **1999**, *58*, 273-278.
(398) Batra, S.; Alenfall, J. *Prostate* **1994**, *24*, 269-278.
(399) Batra, S.; Iosif, C. S. *Anticancer Res.* **2000**, *20*, 463-466.
(400) Katz, Y.; Eitan, A.; Gavish, M. *Oncology* **1990**, *47*, 139-142.
(401) Katz, Y.; Ben-Baruch, G.; Kloog, Y.; Menczer, J.; Gavish, M. *Clin. Sci.* **1990**, *78*, 155-158.
(402) Sakai, M.; Ferraz-de-Paula, V.; Pinheiro, M. L. *Eur. J. Pharmacol* **2010**, *626*, 131-138.
(403) Parker, M. A.; Bazan, H. E.; Marcheselli, V.; Rodriguez de Turco, E. B.; Bazan, N. G. *J. Neurosci. Res.* **2002**, *69*, 39-50.
(404) De Rosa, A.; Naviglio, D.; Di Luccia, A. *Curr. Cancer Ther. Rev.* **2011**, *14*, 234-247.
(405) Scarf, A. M.; Ittner, L. M.; Kassiou, M. *J. Med. Chem* **2009**, *52*.
(406) Korkhov, V. M.; Sachse, C.; Short, J. M.; Tate, C. G. *Structure* **2010**, *18*, 677-687.
(407) Luus, C.; Hanani, R.; Reynolds, A.; Kassiou, M. *J. Label Compd. Radiopharm.* **2010**, *53*, 501-510.
(408) Sprengel, R.; Werner, P.; Seeburg, P. H. *J. Biol. Chem.* **1989**, *264*, 20415-20421.
(409) Fujimura, Y.; Ikoma, Y.; Yasuno, F. *J. Nucl. Med.* **2006**, *47*, 43-50.

(410) Zhang, M.; Maeda, J.; Ogawa, M. *J. Med. Chem.* **2004**, *47*, 2228-2235.
(411) Okuyama, S.; Chaki, S.; Yoshikawa, R. *Life Sci.* **1999**, *64*, 1455-1464.
(412) Vas, A.; Shchukin, Y.; Karrenbauer, V. D. *J. Neurol. Sci.* **2008**, *264*, 9-17.
(413) Kita, A.; Kohayakawa, H.; Kinoshita, T. *Br. J. Pharmacol.* **2004**, *142*, 1059-1072.
(414) Amitani, M.; Zhang, M. R.; Noguchi, J. *Nucl. Med. Biol.* **2006**, *2006*, 971-975.
(415) Margiotta, N.; Denora, N.; Ostuni, R. *J. Med. Chem* **2010**, *53*, 5144-5154.
(416) Piccinonna, S.; Margiotta, N.; Denora, N. *Dalton Trans.* **2013**, *42*, 10112-10115.
(417) Denora, N.; Laquintana, V.; Pisu, M. G. *J. Med. Chem.* **2008**, *51*, 6876-6888.
(418) Fujimura, Y.; Ikoma, Y.; Yasuno, F. *J. Nucl. Med.* **2006**, *47*, 43-50.
(419) Farges, R.; Joseph-Liauzun, E.; Shire, D.; Caput, D.; Le Fur, G.; Ferrara, P. *Mol. Pharmacol.* **1994**, *46*, 1160-1167.
(420) Lin, D.; Chang, Y. J.; Strauss, J. F.; Miller, W. L. *Genomics* **1993**, *18*, 643-650.
(421) Venneti, S.; Lopresti, B. J.; Wiley, C. A. *Prog. Neurobiol.* **2006**, *80*, 308-322.
(422) Camsonne, R.; Crouzel, C.; Comar, D. *J. Label Compd. Radiopharm.* **1984**, *21*, 985-991.
(423) Bergström, M.; Mosskin, M.; Ericson, K. *Acta. Radiol. Suppl.* **1986**, *369*, 409-411.
(424) Deane, N. G.; Manning, H. C.; Foutch, A. C. *Mol. Cancer. Res.* **2007**, *5*, 341-349.
(425) Wyatt, S. K.; Manning, H. C.; Bai, M. *Mol. Imaging Biol.* **2010**, *12*, 349-358.
(426) Tang, D.; Hight, M. R.; McKinley, E. T. *J. Nucl. Med.* **2012**, *53*, 287-294.
(427) Buck, J. R.; McKinley, E. T.; Hight, M. R. *J. Nucl. Med.* **2011**, *52*, 107-114.
(428) James, M. L.; Fulton, R. R.; Vercoullie, J. *J. Nucl. Med.* **2008**, *49*, 814-822.
(429) Tang, D.; McKinley, E. T.; Hight, M. R. *J. Med. Chem* **2013**, *56*, 3429-3433.
(430) Reddi, E.; Zhou, C.; Biolo, R.; Menegaldo, E.; Jori, G. *Br. J. Cancer* **1990**, *61*, 407-411.
(431) Paszko, E.; Ehrhardt, C.; Senge, M. O.; Kelleher, D. P.; Reynolds, J. V. *Photodiagnosis Photodyn Ther* **2011**, *8*, 14-29.
(432) Taketani, S.; Kohno, H.; Furukawa, T.; Tokunaga, R. *J. Biochem.* **1995**, *117*, 875-880.
(433) Roberts, W. G.; Berns, M. W. *Lasers Surg. Med.* **1989**, *9*, 90-101.
(434) Perlin, D. S.; Murant, R. S.; Gibson, S. L.; Hilf, R. *Cancer Res.* **1985**, *45*, 653-658.
(435) Ortel, B.; Chen, N.; Brissette, J.; Dotto, G. P.; Maytin, E.; Hasan, T. *Br. J. Cancer* **1998**, *77*, 1744-1751.
(436) Furre, I. E.; Shahzidi, S.; Luksiene, Z. *Cancer Res.* **2005**, *65*, 11051-11060.
(437) Dailey, H. A. *Biochem. Soc. Trans.* **2002**, *30*, 590-595.
(438) Kinnally, K.; Zorov, D. B.; Antonenko, Y. N.; Snyder, S. H.; McEnery, M. W.; Tedeschi, H. *Proc. Natl. Acad. Sci. USA* **1993**, *90*, 1374-1378.
(439) Kessel, D.; Antolovich, M.; Smith, K. M. *Photochem. Photobiol.* **2001**, *74*, 346-349.
(440) Ben-Dror, S.; Bronshtein, I.; Wiehe, A.; Roder, B.; Senge, M. O.; Ehrenberg, B. *Photochem Photobiol* **2006**, *82*, 695-701.
(441) Mojzisova, H.; Bonneau, S.; Brault, D. *Eur. Biophys. J.* **2007**, *36*, 943-953.
(442) Helmlinger, G.; Sckell, A.; Dellian, M.; Forbes, N. S.; Jain, R. K. *Clin. Cancer Res.* **2002**, *8*, 1284-1291.
(443) Bombalska, A.; Graczyk, A. *Photdiagn. Photodyn. Ther.* **2009**, *6*, 46-51.
(444) Senge, M. O.; Forsyth, T. P.; Nguyen, L. T.; Smith, K. M. *Angew. Chem. Int. Ed. Engl.* **1995**, *33*, 2485-2487.
(445) Senge, M. O. *Chemical Communications* **2006**, 243-256.
(446) Sinclair, R. S.; Tait, D.; Truscott, T. G. *J. Chem. Soc., Faraday Trans.* **1980**, *76*, 417-425.
(447) Senge, M. O.; Medforth, C. J.; Forsyth, T. P.; Lee, D. A.; Olmstead, M. M.; Jentzen, W.; Pandey, R. K.; Shelnutt, J. A.; Smith, K. M. *Inorg Chem* **1997**, *36*, 1149-1163.
(448) Bombalska, A.; Graczyk, A. J. *Photochem. Photobiol., B:Biol* **2009**, *94*, 138-142.
(449) Chen, Y.; Potter, W. R.; Missert, J. R.; Morgan, J.; Pandey, R. K. *Bioconjugate chem.* **2007**, *18*, 1460-1473.
(450) Pandey, S. K.; Gryshuk, A. L.; Sajjad, M.; Zheng, X.; Chen, Y.; Abouzeid, M. M.; Morgan, J.; Charamisinau, I.; Nabi, H. A.; Oseroff, A.; Pandey, R. K. *J. Med. Chem.* **2005**, *48*, 6286-6295.
(451) Chen, Y.; Graham, A.; Potter, W.; Morgan, J.; Vaughan, L.; Bellnier, D. A.; Henderson, B. W.; Oseroff, A.; Dougherty, T. J.; Pandey, R. K. *J. Med. Chem.* **2002**, *45*, 255-258.

(452) Morris, R. L.; Varnes, M. E.; Kenney, M. E. *Photochem. Photobiol.* **2002**, *75*, 652-661.
(453) Massoud, T. F.; Gambhir, S. S. *Genes Dev.* **2003**, *17*, 545-580.
(454) Rudin, M.; Weissleder, R. *Nat. Rev. Drug Discov.* **2003**, *2*, 123-131.
(455) Verel, I.; Vissser, G. W.; van Dongen, G. A. *J. Nucl. Med.* **2005**, *46*, 164-171.
(456) Koziorowski, J.; Henssen, C.; Weinreich, R. *Appl. Radiat. Isot* **1998**, *49*, 955-959.
(457) Verel, I.; Visser, G. W.; Vosjan, M. J.; Finn, R.; Boellaard, R.; van Dongen, G. A. *J. Nucl. Med. Mol. Imaging* **2004**, *31*, 1645-1652.
(458) Chen, Y.; Sajjad, M.; Wang, Y.; Batt, C.; Nabi, H. A.; Pandey, R. K. *Med. Chem. Lett.* **2011**, *2*, 136-141.
(459) Holten, D.; Bocian, D. F.; Lindsey, J. S. *Accounts of Chemical Research* **2002**, *35*, 57-69.
(460) Chen, Y.; Zheng, X.; Dobhal, M. P.; Gryshuk, A.; Morgan, J.; Dougherty, T. J.; Oseroff, A.; Pandey, R. K. *J. Med. Chem* **2005**, *48*, 3692–3695.
(461) Chen, Y. H.; Li, G. L.; Pandey, R. K. *Curr. Org. Chem* **2004**, *8*, 1105-1134.
(462) Li, G.; Graham, A.; Chen, Y.; Pandey, R. K. *J. Med. Chem.* **2003**, *46*, 5349-5359.
(463) Graham, A.; Li, G.; Chen, Y.; Morgan, J.; Oseroff, A.; Dougherty, T. J.; Pandey, R. K. *Photochemistry and photobiology* **2003**, *77*, 561-566.
(464) Wendler, G.; Lindemann, P.; Lacapere, J. J.; Papdopoulos, V. *Biochem. Biophys. Res. Commun.* **2003**, *311*, 847-852.
(465) Kessel, D. *Cancer Lett.* **1988**, *39*, 193-198.
(466) Verma, A.; Snyder, S. H. *Mol. Pharmacol.* **1988**, *34*, 800-805.
(467) Hirsch, J. D.; Beyer, C. F.; Malkowitz, L.; Loullis, C. C.; Blume, A. J. *Mol. Pharmacol.* **1989**, *35*, 164-172.
(468) Verma, A.; Facchina, S. L.; Hirsch, D. J.; Song, S. Y.; Dillahey, L. F.; Williams, J. R.; Snyder, S. H. *Mol. Med.* **1998**, *4*, 40-45.
(469) Joseph-Liazun, E.; Farges, R.; Delmas, P.; Ferrara, P.; Loison, G. *J. Biol. Chem.* **1997**, *272*, 28102-28106.
(470) Li, H.; Papadopoulos, V. *Endocrinology* **1998**, *139*, 4991-4997.
(471) Yeliseev, A. A.; Kaplan, S. *J. Biol. Chem.* **1995**, *270*, 21167-21175.
(472) Yeliseev, A. A.; Kaplan, S. *J. Biol. Chem.* **2000**, *275*, 5657-5667.
(473) Goldman, B. S.; Beck, D. L.; Monika, E. M.; Kranz, R. G. *Proc. Natl. Acad. Sci. USA* **1998**, *95*, 5003-5008.
(474) Joseph-Liauzun, E.; Delmas, P.; Shire, D.; Ferrara, P. *J. Biol. Chem.* **1998**, *273*, 2146-2152.
(475) Yeliseev, A. A.; Krueger, K. E.; Kaplan, S. *Proc. Natl. Acad. Sci. USA* **1997**, *94*, 5101-5106.
(476) Li, F.; Xia, Y.; Meiler, J.; Ferguson-Miller, S. *Biochemistry* **2013**, *52*, 5884-5899.
(477) Baker, M. E.; Fanestil, D. D. *Cell* **1991**, *65*, 721-722.
(478) Yeliseev, A. A.; Kaplan, S. *J. Biol. Chem.* **1999**, *274*, 21234-21243.
(479) Guillaumot, D.; Guillon, S.; De´planque, T. *Plant J.* **2009**, *60*, 242-256.
(480) Lindemann, P.; Koch, A.; Degenhardt, B.; Hause, G.; Grimm, B.; Papadopoulos, V. *Plant Cell Physiol.* **2004**, *45*, 723-733.
(481) Frank, W.; Baar, K. M.; Qudeimat, E. *Plant J.* **2007**, *51*, 1004-1018.
(482) Avallone, R.; Cosenza, F.; Farina, F.; Baraldi, C.; Baraldi, M. *Fitoterapia* **2002**, *73*, 390-396.
(483) Kurumaji, A.; Wakai, T.; Toru, M. *J. Neural Transm.* **1997**, *104*, 1361-1370.
(484) Scarf, A. M.; Auman, K. M.; Kassiou, M. *Curr. Mol. Med.* **2012**, *12*, 387-397.
(485) Scarf, A. M.; Luus, C.; Da Pozzo, E. *Curr. Mol. Med.* **2012**, *12*, 488-493.
(486) Gonzalez-Polo, R. A.; Carvalho, G.; Braun, T. *Oncogene* **2005**, *24*, 7503-7513.
(487) Meisel, P.; Kocher, T. *Journal of Photochemistry and Photobiology B-Biology* **2005**, *79*, 159-170.
(488) Littler, B. J.; Miller, M. A.; Hung, C.-H.; Wagner, R. W.; O'Shea, D. F.; Boyle, P. D.; Lindsey, J. S. *Journal of Organic Chemistry* **1999**, *64*, 1391-1396.
(489) Wiehe, A.; Ryppa, C.; Senge, M. O. *Org Lett* **2002**, *4*, 3807-3809.
(490) Sergeeva, N. N.; Donnier-Marechal, M.; Vaz, G. M.; Davies, A. M.; Senge, M. O. *Bioorg Med Chem Lett* **2011**, *21*, 4385-4388.

(491) Habermeyer, B.; Takai, A.; Gros, C. P.; El Ojaimi, M.; Barbe, J. M.; Fukuzumi, S. *Chem. Eur. J.* **2011**, *17*, 10670-10681.

(492) Achelle, S.; Saettel, N.; Baldeck, P.; Fichou, M. P. T.; Maillard, P. *J. Porphyrins Phthalocyanines* **2010**, *14*, 877-884.

(493) Finnigan, E. M.; Rein, R.; Solladie, N.; Dahms, K.; Goetz, D. C. G.; Bringmann, G.; Senge, M. O. *Tetrahedron* **2011**, *67*, 1126-1134.

(494) More, K. M.; Sawant, B. M.; Eaton, G. R.; Eaton, S. S. *Inorg. Chem* **1981**, *20*.